

AD-A055 758

PURDUE UNIV LAFAYETTE IND SCHOOL OF ELECTRICAL ENGI--ETC F/G 17/9
SPACE-TIME SIGNAL PROCESSING OF RADAR RETURNS.(U)
APR 78 G R COPPER, C D MCGILLEM

UNCLASSIFIED

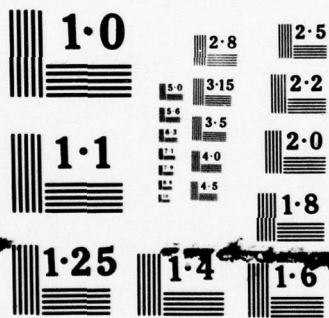
RADC-TR-78-89

F30602-75-C-0082

NL

1 OF 2
ADA
065758





NATIONAL BUREAU OF STANDARDS
MICROCOPY RESOLUTION TEST CHART

FOR FURTHER TRAN

2

2

RADC-TR-78-89
Phase Report
April 1978



SPACE-TIME SIGNAL PROCESSING OF RADAR RETURNS

Purdue University



Approved for public release; distribution unlimited.

ROME AIR DEVELOPMENT CENTER
Air Force Systems Command
Griffiss Air Force Base, New York 13441

78 06 26 014

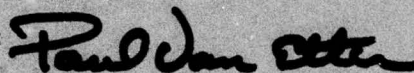
AD No. _____
DDC FILE COPY
AD A055758

SPACE-TIME SIGNAL PROCESSING OF RADAR RETURNS

This report has been reviewed by the RADC Information Office (OI) and is releasable to the National Technical Information Service (NTIS). At NTIS it will be releasable to the general public, including foreign nations.

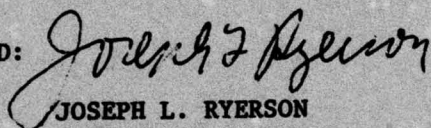
RADC-TR-78-89 has been reviewed and is approved for publication.

APPROVED:



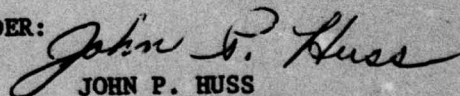
PAUL VAN ETEN
Project Engineer

APPROVED:



JOSEPH L. RYERSON
Technical Director
Surveillance Division

FOR THE COMMANDER:



JOHN P. HUSS
Acting Chief, Plans Office

If your address has changed or if you wish to be removed from the RADC mailing list, or if the addressee is no longer employed by your organization, please notify RADC (OCTS) Griffiss AFB NY 13441. This will assist us in maintaining a current mailing list.

Do not return this copy. Retain or destroy.

UNCLASSIFIED

SECURITY CLASSIFICATION OF THIS PAGE (When Data Entered)

| REPORT DOCUMENTATION PAGE | | READ INSTRUCTIONS BEFORE COMPLETING FORM |
|--|-----------------------|---|
| 1. REPORT NUMBER RADC-TR-78-89 | 2. GOVT ACCESSION NO. | 3. RECIPIENT'S CATALOG NUMBER |
| 4. TITLE (and Subtitle) SPACE-TIME SIGNAL PROCESSING OF RADAR RETURNS. | | 5. TYPE OF REPORT & PERIOD COVERED Phase Report 1 May 77 - 30 Nov 77 |
| 6. AUTHOR(s) George R. Cooper Clare D. McGillem | | 6. PERFORMING ORG. REPORT NUMBER N/A |
| 7. PERFORMING ORGANIZATION NAME AND ADDRESS Purdue University School of Electrical Engineering W. Lafayette IN 47907 | | 8. CONTRACT OR GRANT NUMBER(s) F30602-75-C-0082 |
| 9. CONTROLLING OFFICE NAME AND ADDRESS Rome Air Development Center (OCTS) Griffiss AFB NY 13441 | | 10. PROGRAM ELEMENT, PROJECT, TASK AREA & WORK UNIT NUMBERS 62702F 95670015 |
| 11. MONITORING AGENCY NAME & ADDRESS (if different from Controlling Office) Rome Air Development Center (OCTS) Griffiss AFB NY 13441 | | 12. REPORT DATE Apr 78 |
| 13. DISTRIBUTION STATEMENT (of this Report) Approved for public release; distribution unlimited. | | 13. NUMBER OF PAGES 141 |
| 14. DISTRIBUTION STATEMENT (of the abstract entered in Block 20, if different from Report) Same | | 15. SECURITY CLASS. (of this report) UNCLASSIFIED |
| 15. SUPPLEMENTARY NOTES RADC Project Engineer: Paul VanEtten (OCTS) | | 15a. DECLASSIFICATION/DOWNGRADING SCHEDULE N/A |
| 16. KEY WORDS (Continue on reverse side if necessary and identify by block number) Target Cross Section Signal Processing | | |
| 17. ABSTRACT (Continue on reverse side if necessary and identify by block number) Radar returns from complex targets that are large compared to the wavelength of the radar signal are composed of reflections from a number of scattering points on the surface of the target. Although the target may contain a large number of scattering points, experience indicates that at any particular instant of time the major portion of the returned signal energy comes from only a few such points. These predominant reflections combine at the receiving point with phases that are random because the range differences between reflecting | | |

DD FORM 1 JAN 73 1473

EDITION OF 1 NOV 65 IS OBSOLETE

UNCLASSIFIED

SECURITY CLASSIFICATION OF THIS PAGE (When Data Entered)

78 06 26 014 CL
292000

UNCLASSIFIED

SECURITY CLASSIFICATION OF THIS PAGE(When Data Entered)

points are random and critically dependent upon the aspect angle of the target. As a consequence of the random phase differences, the total signal power observed by the receiver is also random and fluctuates drastically around some average value as a result of changes in target attitude. The average value of power is simply the sum of the powers from the individual reflecting points, and this situation is referred to here as noncoherent signal summation.

If the return signal from each of the predominant reflecting points had the same phase as all the other signals, then the voltages in the receiver would add rather than the powers. The resulting received signal power is then proportional to the square of the sum of the voltages and will always be larger than the average power obtained by noncoherent signal summation. The factor by which the coherent signal power exceeds the average noncoherent signal power may be as large as the number of predominate reflecting points.

The problem that is addressed in this research is that of finding a form for the transmitted radar signal such that coherent signal summation occurs at the receiving point.

| | |
|---------------------------------|-------------------------------------|
| ACCESSION FOR | |
| NTIS | <input checked="" type="checkbox"/> |
| DDC | <input type="checkbox"/> |
| UNANNOUNCED | <input type="checkbox"/> |
| JUSTIFICATION | <input type="checkbox"/> |
| BY | |
| DISTRIBUTION/AVAILABILITY CODES | |
| Dist. | AVAIL. |
| A | |

UNCLASSIFIED

SECURITY CLASSIFICATION OF THIS PAGE(When Data Entered)

TABLE OF CONTENTS

SPACE-TIME SIGNAL PROCESSING OF RADAR TARGET RETURNS

| | Page |
|---|------------|
| 1. INTRODUCTION | |
| 1.1. OVERVIEW OF PROGRAM | |
| 1.1.1. Problem Definition | 1 |
| 1.1.2. Objectives of the Investigation. | 2 |
| 1.1.3. Brief Summary of the Results and Conclusions | 3 |
| 1.2. PRESENTATION OF SELECTED RESULTS | |
| 1.2.1. General Target Model | 7 |
| 1.2.2. CW Signal: Two-Point Target. | 9 |
| 1.2.3. CW Signal: Ten-Point Target. | 10 |
| 1.2.4. Time-Limited Signal: Two-Point Target. | 19 |
| 1.2.5. Time-Limited Signal: Ten-Point Target. | 19 |
| 1.2.6. Optimum Orthonormal Signal Expansion: Ten-Point Target | 31 |
| 1.2.7. Variation of Optimum Frequency with Incidence Angle. | 35 |
| 2. TECHNICAL PRESENTATION | |
| 2.1. MATHEMATICAL ANALYSIS | |
| 2.1.1. Problem Definition in Mathematical Form. | 37 |
| 2.1.2. General Formulation. | 38 |
| 2.1.3. Optimization With No Time Constraint: Frequency-Domain Solution. | 39 |
| 2.1.4. Optimization With No Time Constraint: Time-Domain Solution. | 41 |
| 2.1.5. Optimization With Time-Limited Signals | 44 |
| 2.1.6. Sub-Optimum Signals: Pulsed Sinusoids. | 48 |
| 2.1.7. Sub-Optimum Signals: Multiple-Frequency Pulsed Sinusoids. | 50 |
| 2.1.8. Optimum Orthonormal Signal Expansion | 51 |
| 2.2. COMPUTATIONAL RESULTS | |
| 2.2.1. Computation Methods. | 55 |
| 2.2.2. CW Signals | 57 |
| 2.2.3. Bistatic CW Signals. | 109 |
| 2.2.4. Pulse and Matched Filter Signals | 109 |
| 2.2.5. RF Pulse Signals | 123 |
| 2.2.6. Simultaneous Angle and Frequency Variations. | 123 |
| 2.2.7. Comparison of Optimum and Non-Optimum Frequencies. | 136 |
| 3. CONCLUSIONS AND RECOMMENDATIONS | |
| 3.1. CONCLUSIONS. | 139 |
| 3.2. RECOMMENDATIONS. | 141 |

1.1. OVERVIEW OF PROGRAM

1.1.1. Problem Definition

Radar returns from complex targets that are large compared to the wavelength of the radar signal are composed of reflections from a number of scattering points on the surface of the target. Although the target may contain a large number of scattering points, experience indicates that at any particular instant of time the major portion of the returned signal energy comes from only a few such points. These predominant reflections combine at the receiving point with phases that are random because the range differences between reflecting points are random and critically dependent upon the aspect angle of the target. As a consequence of the random phase differences, the total signal power observed by the receiver is also random and fluctuates drastically around some average value as a result of changes in target attitude. The average value of power is simply the sum of the powers from the individual reflecting points, and this situation is referred to here as noncoherent signal summation.

If the return signal from each of the predominant reflecting points had the same phase as all the other signals, then the voltages in the receiver would add rather than the powers. The resulting received signal power is then proportional to the square of the sum of the voltages and will always be larger than the average power obtained by noncoherent signal summation. This situation is referred to here as coherent signal summation. The factor by which the coherent signal power exceeds the average noncoherent signal power may be as large as the number of predominate reflecting points.

The problem that is addressed in this research is that of finding a form for the transmitted radar signal such that coherent signal summation occurs at the receiving point. It is assumed in this investigation that the predominant reflecting points are known in regard to both location and

radar cross-section. The only restriction imposed on the transmitted radar signal is that it contain finite energy.

Since the target reflecting points are assumed known, the target may be modeled mathematically in terms of its impulse response. The model assumed here is that the impulse response consists of a set of delta functions, each having an appropriate magnitude factor that is related to the radar cross section of one of the reflecting points and each having a delay factor that is related to the relative time delay of the signal reflected from that reflecting point. This model and the mathematical analysis that results from it are discussed in more detail in a subsequent section. The mathematical problem may be defined as that of finding the signal form that maximizes the ratio of the signal energy at the output of the target model to the signal energy at the input to the target model.

1.1.2. Objectives of the Investigation

The investigation pursued here has three major objectives. They are:

- 1) To provide a mathematical analysis that will define the optimum signal waveform for maximizing coherent signal summation and to determine theoretical limits on the amount of improvement that can be obtained by using this signal waveform.
- 2) To perform a computer study in which optimum and sub-optimum signal waveforms are determined for a specified target model and to evaluate the response of the target model to the derived waveforms in a variety of monostatic and bistatic situations with various target aspect angles.
- 3) To compare the computed results with those predicted by the mathematical theory and to draw some conclusions with regard to the advantages and disadvantages of using optimum radar waveforms to enhance returned signal energy, and also to make recommendations regarding the feasibility of extending this approach to consider unknown targets by means of adaptive signal processing.

All three of these objectives have been achieved. The next subsection gives a brief summary of the major theoretical results and conclusions, and Section 1.2 presents some selected computational results and their significance. This is done on a non-mathematical basis in order to emphasize the physical

aspects of the situation. The detailed mathematical analysis and the bulk of the computational results are presented in Chapter 2 and conclusions and recommendations for further work are in Chapter 3.

1.1.3. Brief Summary of Results and Conclusions

Mathematical Analysis. The mathematical analysis contains three principal parts. The first part considers signals that are not time-limited, but are constrained to have a finite energy. This analysis indicates that the optimum signal waveform is a steady-state sinusoid with vanishingly small amplitude and having a frequency such that the power transfer function of the target model is a maximum. In some cases there may be many such frequencies. Although an optimum frequency is difficult to determine analytically, they can always be determined by computation. The physical significance of such a frequency is that it corresponds to a wavelength such that all delay differences from the various reflecting points on the target are integral multiples of the wavelength. Thus, a coherent wave impinging on the target will result in reflections that add in phase and the maximum signal voltage is achieved. Since the delay differences can have any value, some combinations will result in the lowest optimum frequency being very high -- perhaps outside of the range of practical interest. There will be lower frequencies, however, at which the reflections almost add in phase and these will yield local maxima that may be very close to the theoretical absolute maximum. This phenomenon is clearly exhibited in some of the results that follow.

The second phase of the mathematical analysis considers time-limited signals that are also constrained to have a finite energy. The analysis in this case reveals that the energy ratio that is being maximized depends only upon the time-ambiguity function of the transmitted signal. The optimum signal is one for which the time-ambiguity function has its largest values at delay values corresponding to the delay differences for the target

model. A sub-optimum approach to achieving such a waveform is to use a time-limited sinusoid whose duration is several times the duration of the target impulse response and whose frequency is one of the optimum frequencies that exist for the non-time-limited signal. The computational results reveal that this waveform will usually yield results that are within a fraction of a dB of the theoretical absolute maximum.

The third phase of the mathematical analysis is to seek a truly optimum signal waveform by representing the transmitted signal by the weighted sum of orthonormal basis functions and selecting the coefficients multiplying these basis functions so as to maximize the desired energy ratio. If the basis functions form a complete orthonormal set, then such an approach will yield an optimum waveform. The computational results reveal that as the duration of the time-limited signal becomes long compared to the duration of the target impulse response, the optimum waveform approaches a constant amplitude sinusoid having one of the optimum frequencies previously noted.

Computational Results. Computations have been made for two different target models. One model assumed only two reflecting points with equal reflection coefficients. This model was employed primarily as a check on the computer program since it is relatively easy to evaluate selected points analytically with a model this simple. The second model assumed ten reflecting points distributed in an area roughly 12 meters by 18 meters. In most cases the reflection coefficients were the same for all reflecting points since this represents a worst-case situation so far as variation in the return signal is concerned.

For the case of non-time-limited signals (CW case), calculations were made of the squared magnitude of the target transfer function, $|H(f)|^2$, at a variety of incidence angles, reflection angles, and frequencies. Since $|H(f)|^2$ is equal to the desired ratio of reflected signal energy to

incident signal energy, the maxima of this function are exactly the information sought. Selected computations are displayed in the next section and reveal two significant items:

- 1) At some angles there are many frequencies at which the theoretical maximum response is achieved. In general, these frequencies are harmonically related (as would be expected from the physical interpretation above).
- 2) At some angles there is no frequency at which the theoretical maximum response is achieved within the range of frequencies searched (1 GHz to 10 GHz). In most such cases, however, there are one or more frequencies for which the maximum response is very close to the theoretical maximum.

In the case of time-limited signals the actual ratio of reflected signal energy to incident signal energy is calculated. This calculation is made in terms of the time-ambiguity function of the signal rather than the signal itself, since this approach reduces computer time. Computations have been made for signals composed of video pulses and signals composed of a single RF pulse with a rectangular envelope. The video pulse corresponds to using a zero frequency carrier and zero frequency is always an optimum frequency. The RF pulse case was evaluated for both arbitrarily selected frequencies and for frequencies that had been shown to be optimum in the CW case. In all cases a variety of incident and reflection angles were used. Selected results are displayed in the next section and reveal the following:

- 1) Video pulses having durations about 4 times the duration of the target impulse response yield results that are very near the theoretical maximum. This suggests that RF pulses of the same duration and at the optimum frequency should do equally well.
- 2) RF pulses of long duration yielded results that were essentially the same as those for the CW case.
- 3) RF pulses of shorter duration yielded results that were essentially similar to the video pulse case when the frequency was at one of the optimum CW frequencies.
- 4) As would be expected, the variation in response with aspect angle becomes much more rapid as the carrier frequency goes up. Thus, if one attempts to achieve more nearly optimum results by going to higher frequencies, the angular sensitivity of the response becomes more of a problem.

Computations were also made using a signal defined by the optimum orthonormal expansion and evaluating 10 or 12 terms of this expansion. The results of this phase of the computational study clearly indicate that for signals much longer in duration than the target impulse response, the RF pulse at an optimum frequency and having a rectangular envelope is the signal that is approached in the limit. The justification for this statement is pursued in more detail in a subsequent section.

Major Conclusions. A brief summary of the major conclusions is given here in order that this section may serve as a self-contained summary of the overall report. The justification for these conclusions, and an elaboration on them, are presented in detail in Chapters 2 and 3. The conclusions may be summarized as follows:

- 1) The received signal energy may be increased over that obtained with noncoherent signal summation by a factor that is at most equal to the number of dominant reflecting points.
- 2) The theoretical maximum improvement can be very nearly achieved with an RF pulse having a duration that is long compared to the duration of the target impulse response and a frequency that is one of those for which the target transfer function is a maximum.
- 3) At some aspect angles, the lowest optimum or near-optimum frequency may lie above the range of frequencies that can be used.
- 4) The change in optimum frequency with aspect angle is rapid and discontinuous.
- 5) Complex waveforms that are more nearly optimum than simple RF pulses can be determined theoretically, and may provide improved performance over constant amplitude pulses.

1.2. PRESENTATION OF SELECTED COMPUTATIONAL RESULTS

This section presents a few selected computational results as a means of summarizing the scope of the study and revealing its salient features. A more complete documentation of the computational results appears in Chapter 2.

1.2.1. General Target Model

A complex radar target may be modeled as a collection of M reflecting points, each having a radar cross-section of σ_i , $i = 1, 2, \dots, M$. Although the actual cross-section of any one reflecting point depends upon the angle of incidence and the angle of reflection, this aspect is not considered here and all reflecting points are assumed to be omnidirectional.

From the radar equation the returned signal voltage (defined as the square root of the instantaneous power) from the i th reflecting point is

$$v_{Ri}(t) = \frac{\sqrt{G_T G_R} \lambda_0}{(4\pi)^{3/2} R_{Ti} R_{Ri}} \sqrt{\sigma_i} v_T(t - \frac{R_{Ti} + R_{Ri}}{c}) \quad (1-1)$$

where

G_T = transmitting antenna power gain

G_R = receiving antenna power gain

λ_0 = wavelength

R_{Ti} = range from the transmitter to the i th reflecting point

R_{Ri} = range from the receiver to the i th reflecting point

$v_T(t)$ = transmitted voltage

Since all of the reflecting points are very nearly at the same range, it is convenient to define a common amplitude factor for all reflecting points as

$$K = \frac{\sqrt{G_T G_R} \lambda_0}{(4\pi)^{3/2} R_T R_R}, \text{ all } i \quad (1-2)$$

Thus,

$$v_{Ri}(t) = K\sqrt{\sigma_i} v_T(t - \frac{R_{Ti} + R_{Ri}}{c}) \quad (1-3)$$

and the total voltage at the receiving point is

$$\begin{aligned} v_R(t) &= \sum_{i=1}^M v_{Ri}(t) \\ &= K \sum_{i=1}^M \sqrt{\sigma_i} v_T(t - \frac{R_{Ti} + R_{Ri}}{c}) \end{aligned} \quad (1-4)$$

It is convenient to compare the power or energy in the returned signal with that of the incident signal without considering the effects of range and antenna gain. For this purpose define the incident voltage at the i th reflecting point as

$$e(t) = \frac{\sqrt{G_T}}{\sqrt{4\pi} R_T} \sqrt{A} v_T(t) \quad (1-5)$$

where A is an arbitrary reference area. Similarly, define a reflected signal, $d_i(t)$, such that

$$v_{Ri}(t) = \frac{\sqrt{G_R} \lambda_0}{4\pi R_R} d_i(t) \quad (1-6)$$

Upon comparing (1-5) and (1-6) with (1-1), it is clear that letting

$$d_i(t) = a_i e(t - \frac{R_{Ti} + R_{Ri}}{c}) \quad (1-7)$$

where

$$a_i = \frac{\sigma_i}{A}$$

will lead directly to (1-1).

The total received voltage may now be expressed as

$$v_R(t) = K\sqrt{A} \sum_{i=1}^M d_i(t) = K\sqrt{A} d(t) \quad (1-8)$$

where

$$d(t) = \sum_{i=1}^M a_i e(t - \frac{R_{Ti} + R_{Ri}}{c}) \quad (1-9)$$

Since $d(t)$ contains all of the relevant information about the target structure, it is sufficient to compare the power or energy of $d(t)$ with that of $e(t)$. It is this comparison that is used in the computational and analytical results presented in this report.

1.2.2. CW Signal: Two-Point Target

The notation and geometry associated with the target having two reflecting points are shown in Figure 1-1.

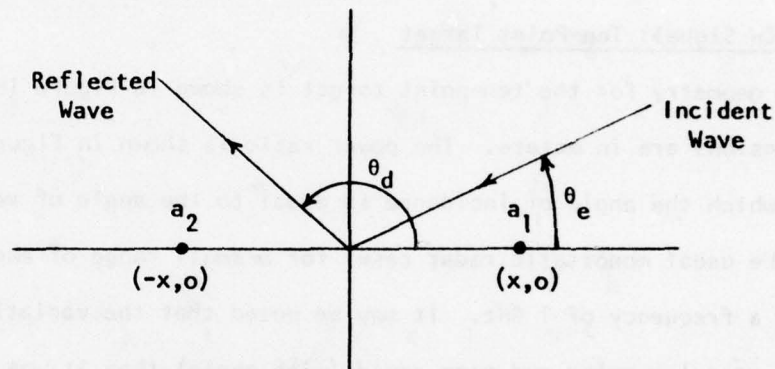


Figure 1-1. Geometry for the two-point target. The a_i are reflection coefficients.

The basic assumption in this case, and all others considered here, is that the radar transmitter and receiver are far enough away from the target that both incident and reflected wavefronts may be considered plane. Thus, the angle of incidence, θ_e , is measured from the abscissa to the normal to the incident wavefront and the angle of reflection, θ_d , is measured to the normal to the reflected wavefront.

The incident signal is described by

$$e(t) = \cos \omega_0 t \quad (1-10)$$

and the reflected signal by

$$d(t) = D \cos (\omega_0 t + \theta) \quad (1-11)$$

The magnitude parameter D relates the average power in the reflected signal to that in the incident signal, the ratio of these two powers being D^2 . Thus, $10 \log D^2$ is the power ratio expressed in dB. This quantity is shown in Figures 1-2 and 1-3 for two different angles of incidence and all angles of reflection. It is apparent that although the maximum ratio is 6 dB, as it should be for two identical reflecting points, there is a great deal of variation in the response for even this very simple target configuration.

1.2.3. CW Signal: Ten-Point Target

The geometry for the ten-point target is shown in Figure 1-4, in which all dimensions are in meters. The power ratio is shown in Figure 1-5 for a case in which the angle of incidence is equal to the angle of reflection (i.e., the usual monostatic radar case) for a small range of angles (70° to 80°) and a frequency of 1 GHz. It may be noted that the variation in power ratio is more irregular and more rapid (with angle) than it was for the two-point case. Furthermore, there is no angle at which the power ratio reaches its theoretical maximum value of 20 dB at this frequency.

A similar plot, for the same set of angles, is shown in Figure 1-6 for a frequency of 10 GHz. In this case the variation has become much more irregular and rapid and there is one angle at which the theoretical maximum of 20 dB is reached for all practical purposes.

In order to determine the optimum frequencies for the ten-point target, plots of the magnitude squared of the target transfer function, $|H(f)|^2$, have been made for all frequencies between 1 and 10 GHz for a variety of angles of incidence. Three such plots are shown here for the frequency range between 4 and 5 GHz and angles of incidence equal to 30° , 45° , and 60° . These are displayed in Figures 1-7, 1-8, and 1-9. It is of interest to note that the theoretical maximum of 100 is achieved at numerous frequencies for the 45° case, but is not achieved at any frequency (in this

D VS THETA D, THETA E = 0 DEGREES
 FREQUENCY = 1 GHz
 2 REFLECTING POINTS

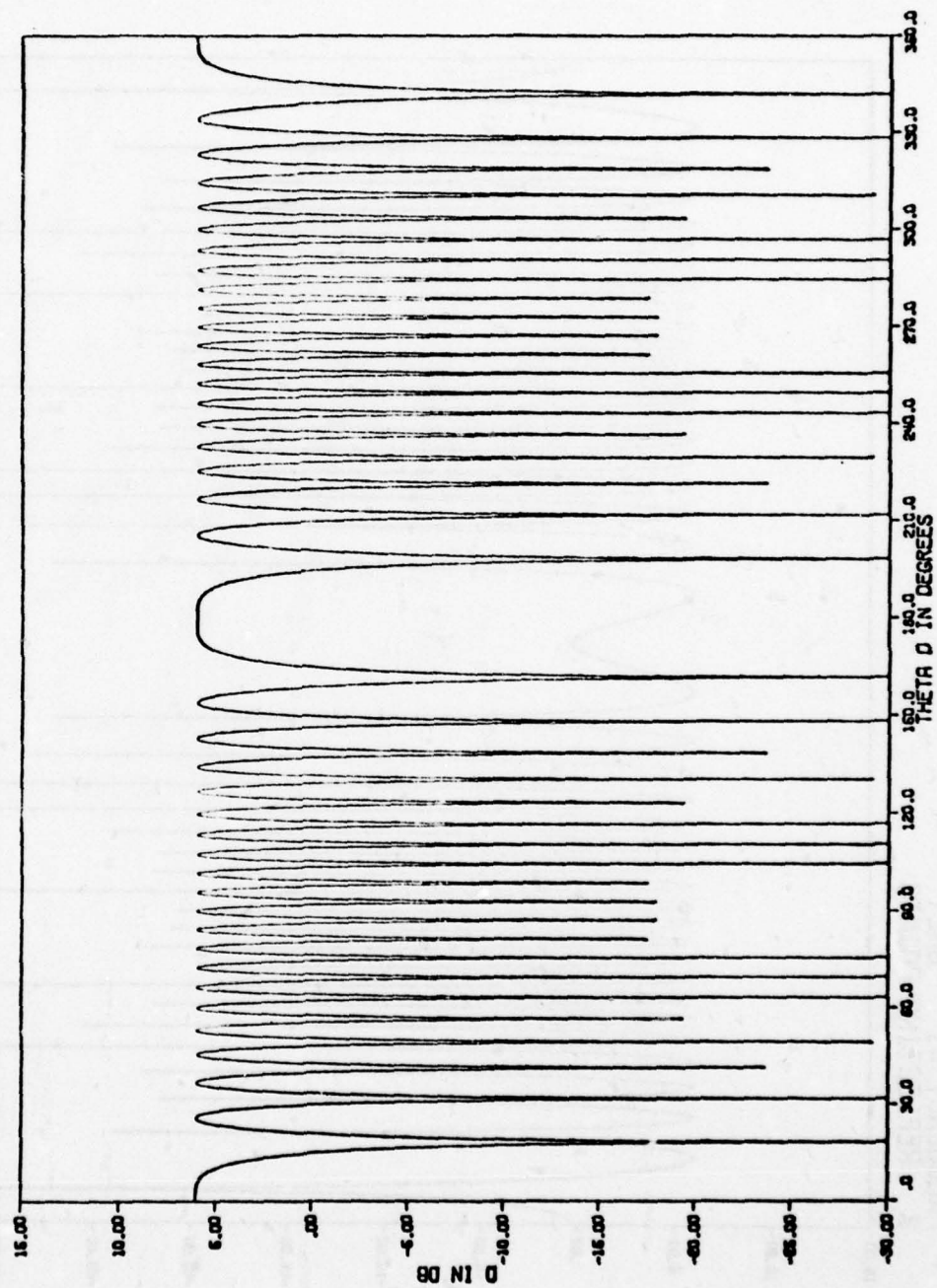


Figure 1-2. Power ratio for two points separated by 10 wavelengths. $a_1 = a_2 = 1$.

D VS THETA D. THETA E = 30 DEGREES
 FREQUENCY = 1 GHZ
 2 REFLECTING POINTS

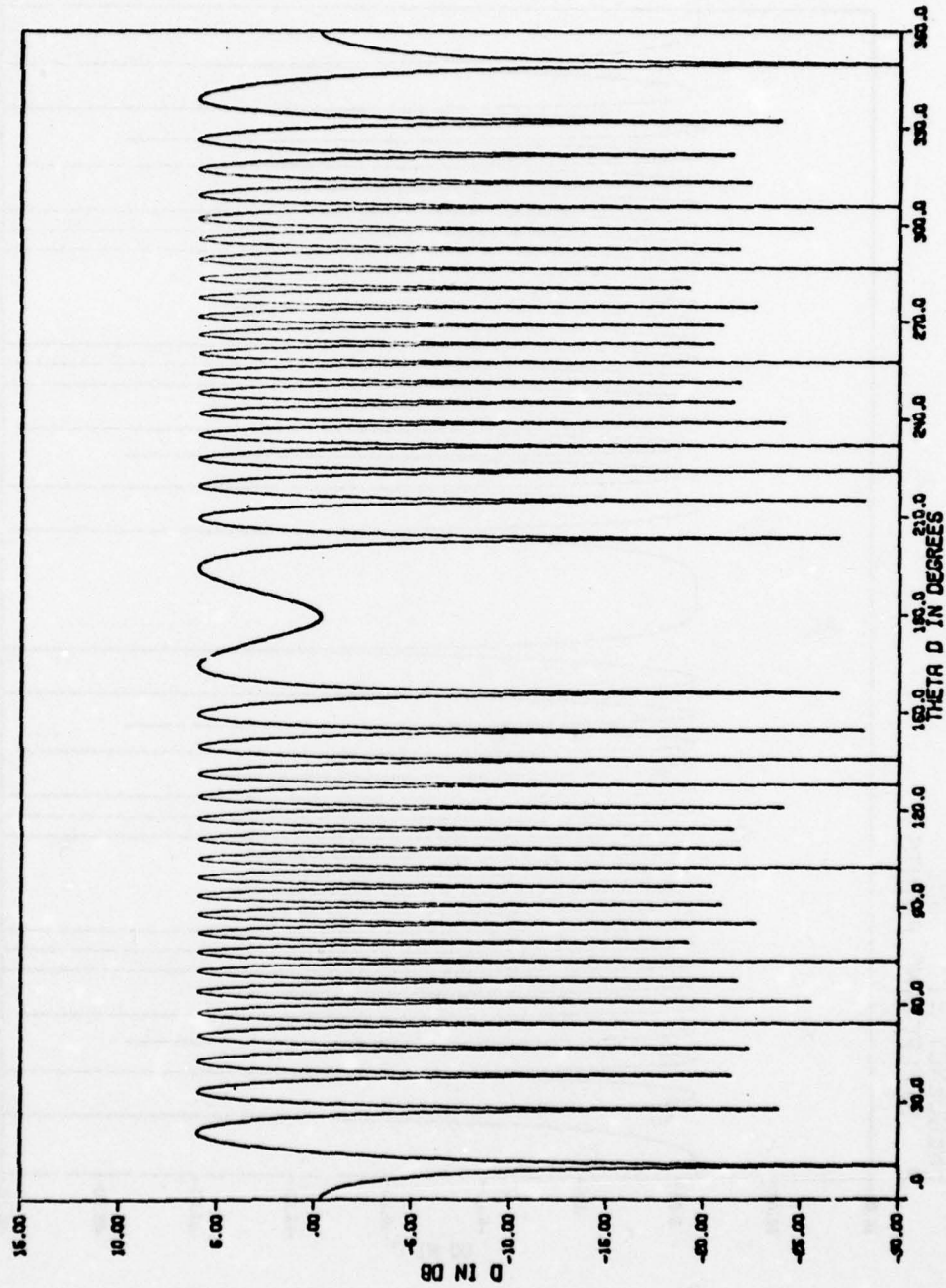


Figure 1-3. Power ratio for two points separated by 10 wavelengths. $a_1 = a_2 = 1$.

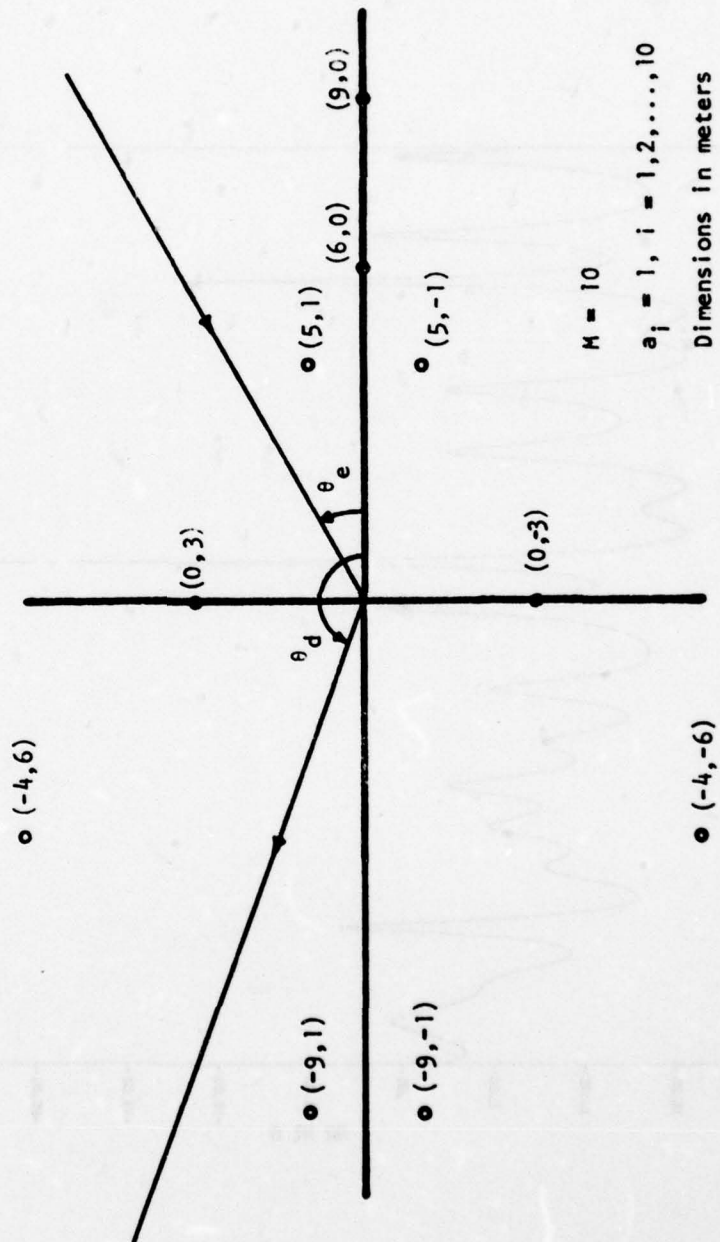


Fig. 1-4. Geometry for the ten-point target

D VS THETA D. THETA E = THETA D
FREQUENCY = 1 GHZ
10 REFLECTING POINTS

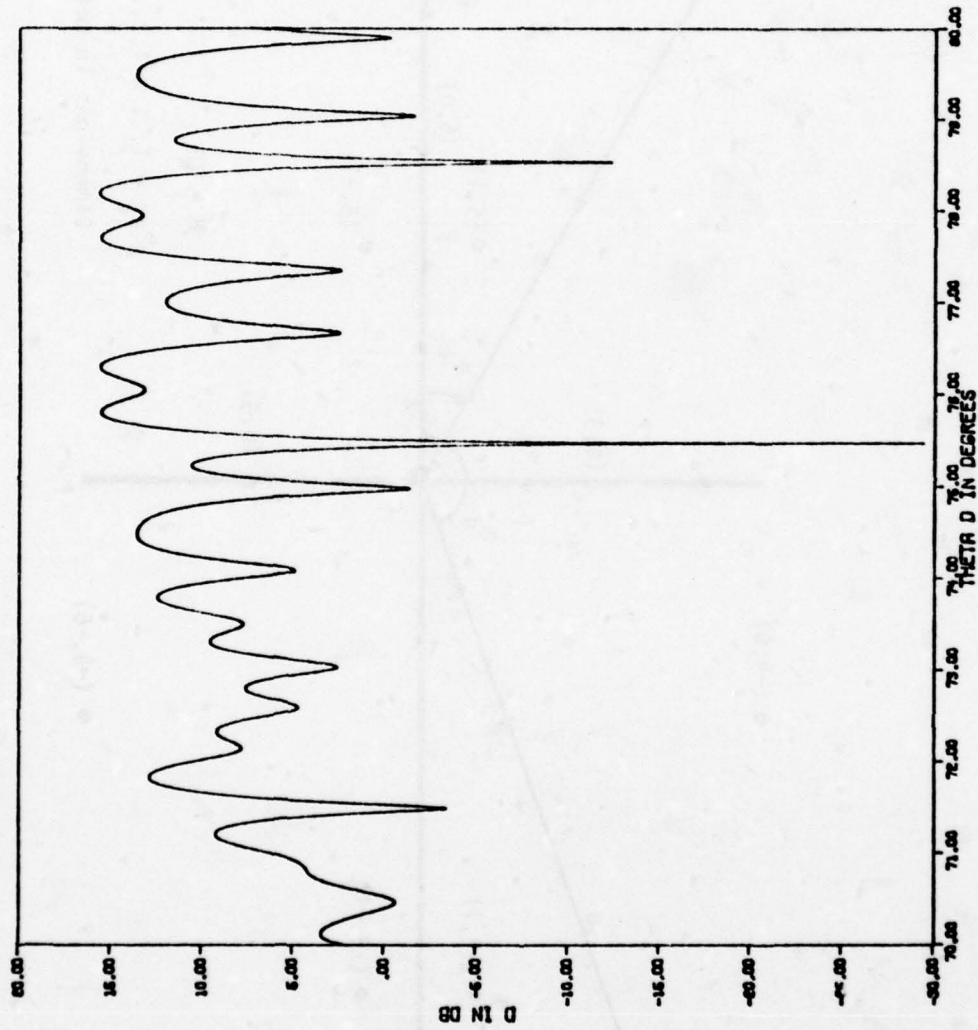


Figure 1-5. Power ratio for the ten-point target at 1 GHz.

D VS THETA D. THETA E = THETA D
FREQUENCY = 10 GHZ
10 REFLECTING POINTS

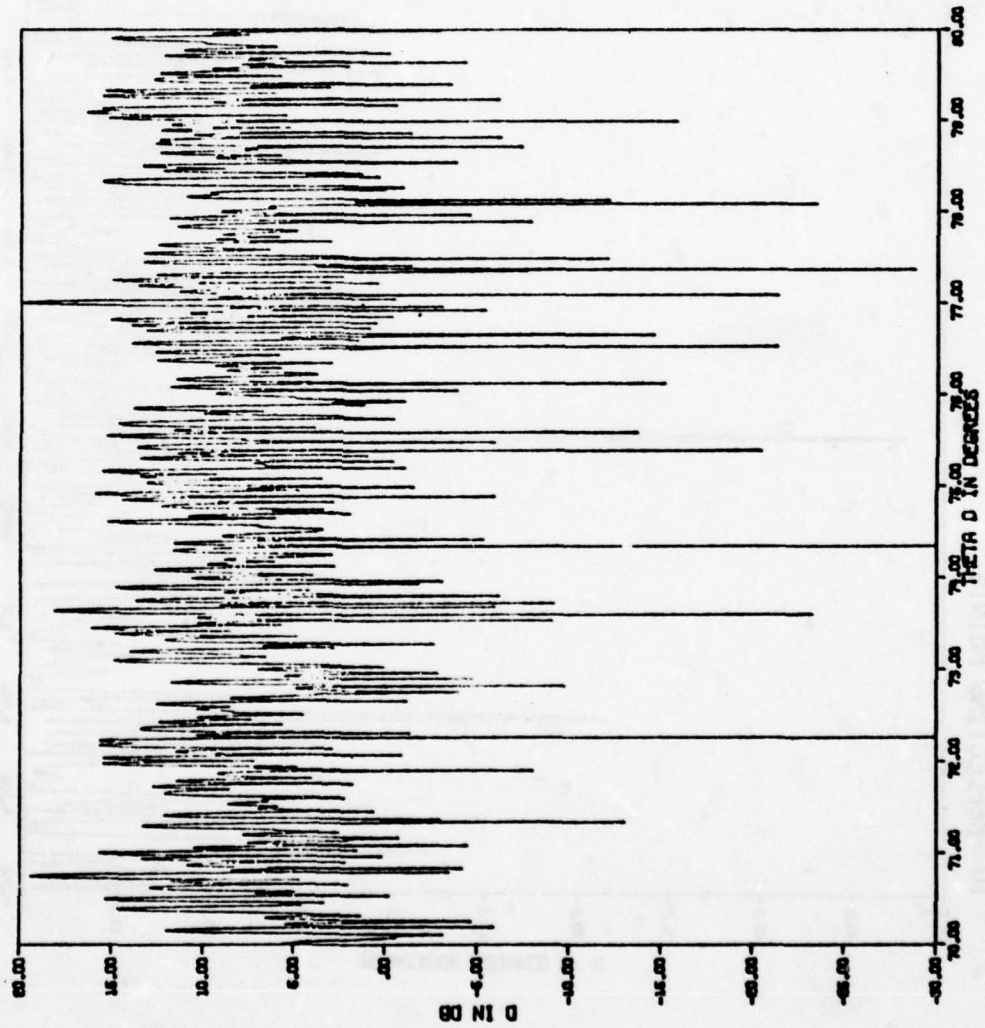


Figure 1-6. Power ratio for the ten-point target at 10 GHz.

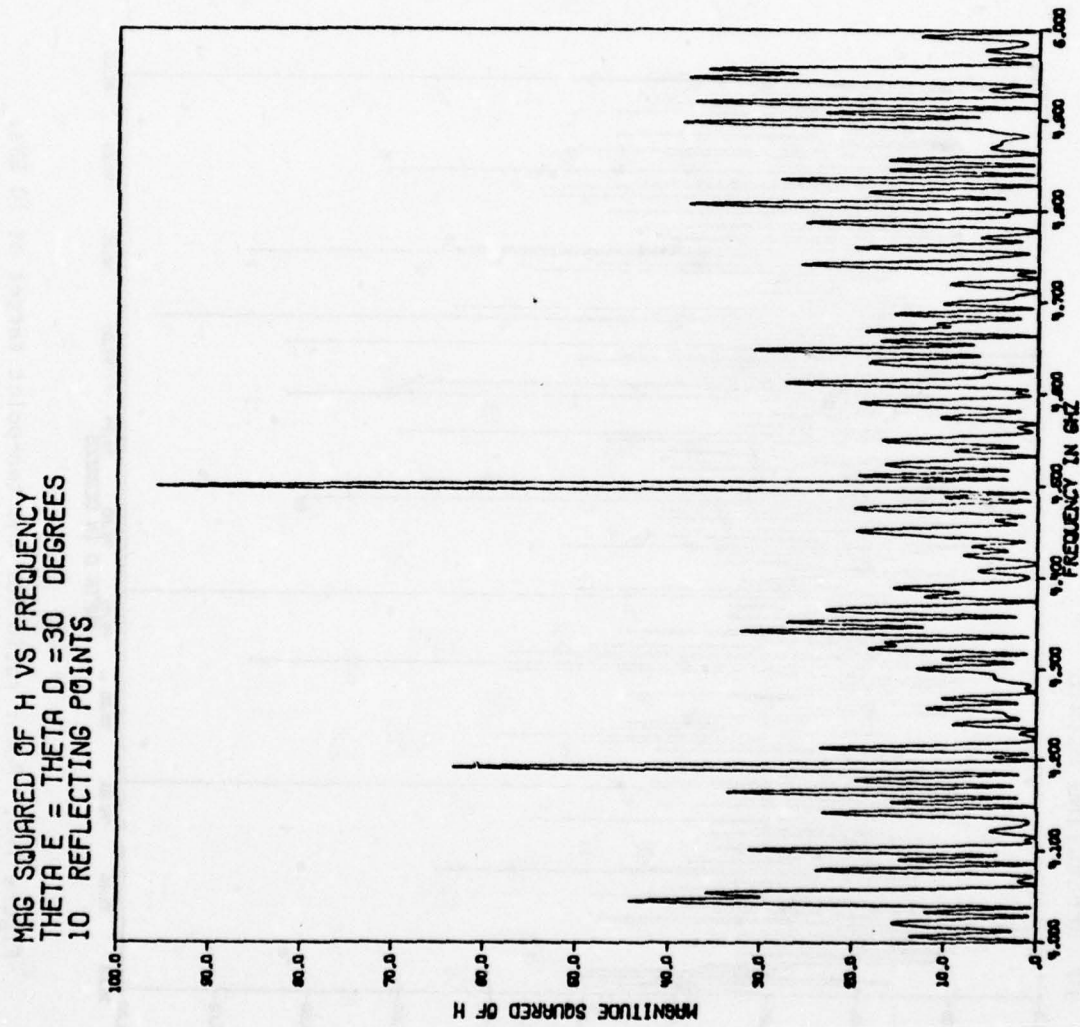


Figure 1-7. Magnitude squared of the ten-point target transfer function. $\theta_e = \theta_d = 30^\circ$.

MAG SQUARED OF H VS FREQUENCY
 THETA E = THETA D = 45 DEGREES
 10 REFLECTING POINTS

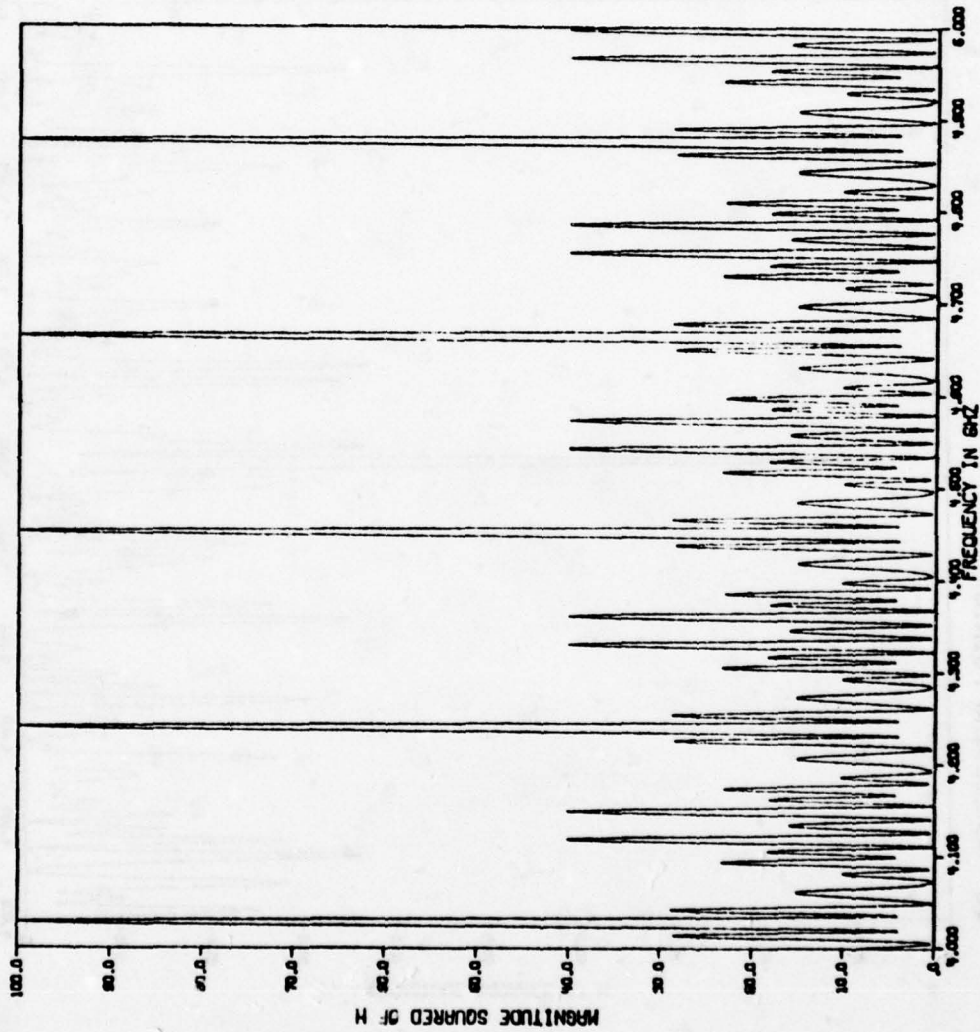


Figure 1-8. Magnitude squared of the ten-point target transfer function. $\theta = \theta_D = 45^\circ$.

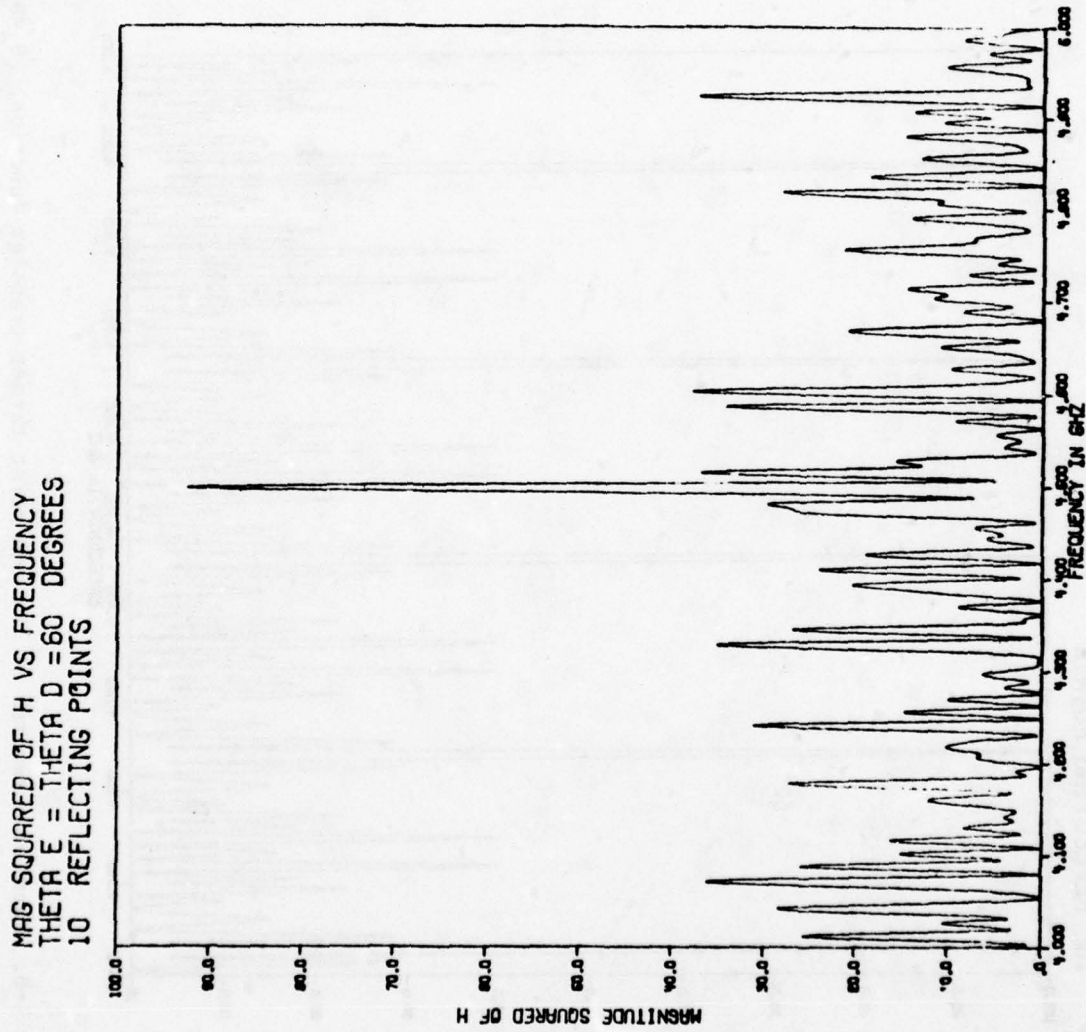


Figure 1-9. Magnitude squared of the ten-point target transfer function. $\theta_e = \theta_d = 60^\circ$.

range or in the range from 1 to 10 GHz) at angles of 30° and 60°. However, there are frequencies for both of these angles at which $|H(f)|^2$ exceeds 90 and, hence, comes within 0.5 dB of achieving the theoretical maximum. A similar statement can be made for every other angle that was tried and, hence, is probably true in general.

1.2.4. Time-Limited Signal: Two-Point Target

For purposes of checking the computer program with some simple signals and targets, the two-point target was tested with a sequence of five rectangular video pulses as shown in Figure 1-10. Typical results are shown in Figures 1-11, 1-12, and 1-13 for two reflecting points separated by 15 meters. These results display the ratio (in dB) of the energy of reflected signal to the energy of the incident signal for three different angles of incidence and all angles of reflection. In all cases the theoretical maximum of 6 dB is achieved at some angle.

1.2.5. Time-Limited Signal: Ten-Point Target

Three classes of signals were tried with the ten-point target. These included:

- 1) Single rectangular video pulse.
- 2) "Matched filter signal" video pulses.
- 3) RF pulse with rectangular envelope.

Examples of all three are included here.

Figure 1-14 shows the energy ratio for a single rectangular video pulse having a duration of 120 ns and with $\theta_e = \theta_d$. (This is approximately the maximum duration of the target impulse response). Although the theoretical maximum is not achieved anywhere (because of the relatively short signal duration), the response is within 1 dB of this maximum at some angles and within 2 dB of the maximum almost everywhere.

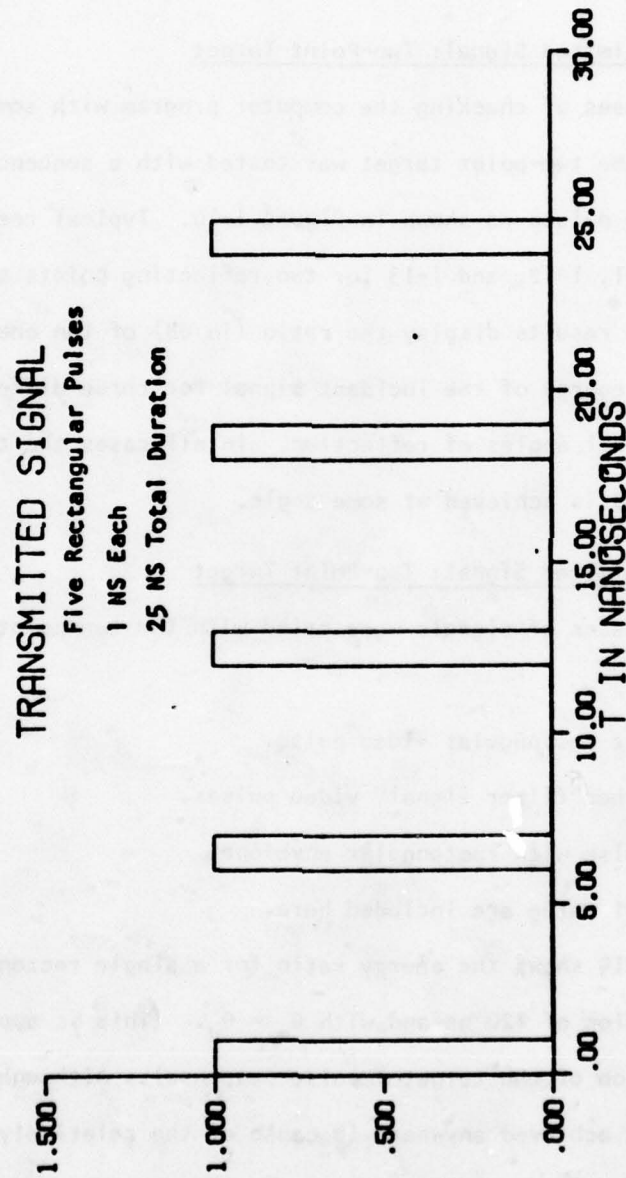


Figure 1-10. Pulse sequence used for testing the computer program

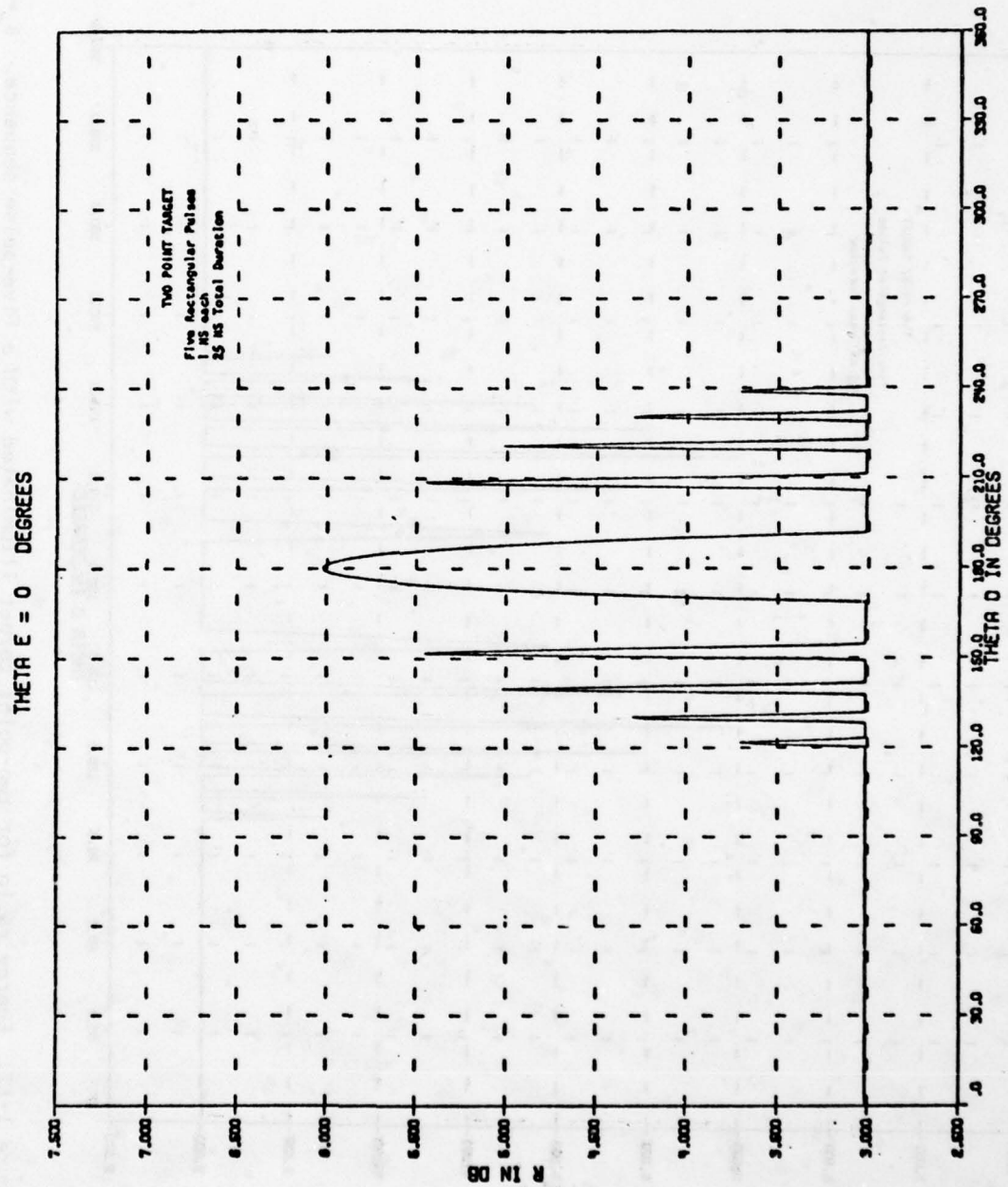


Figure 1-11. Energy ratio for two-point target illuminated with a five-pulse sequence. $\theta_e = 0^\circ$.

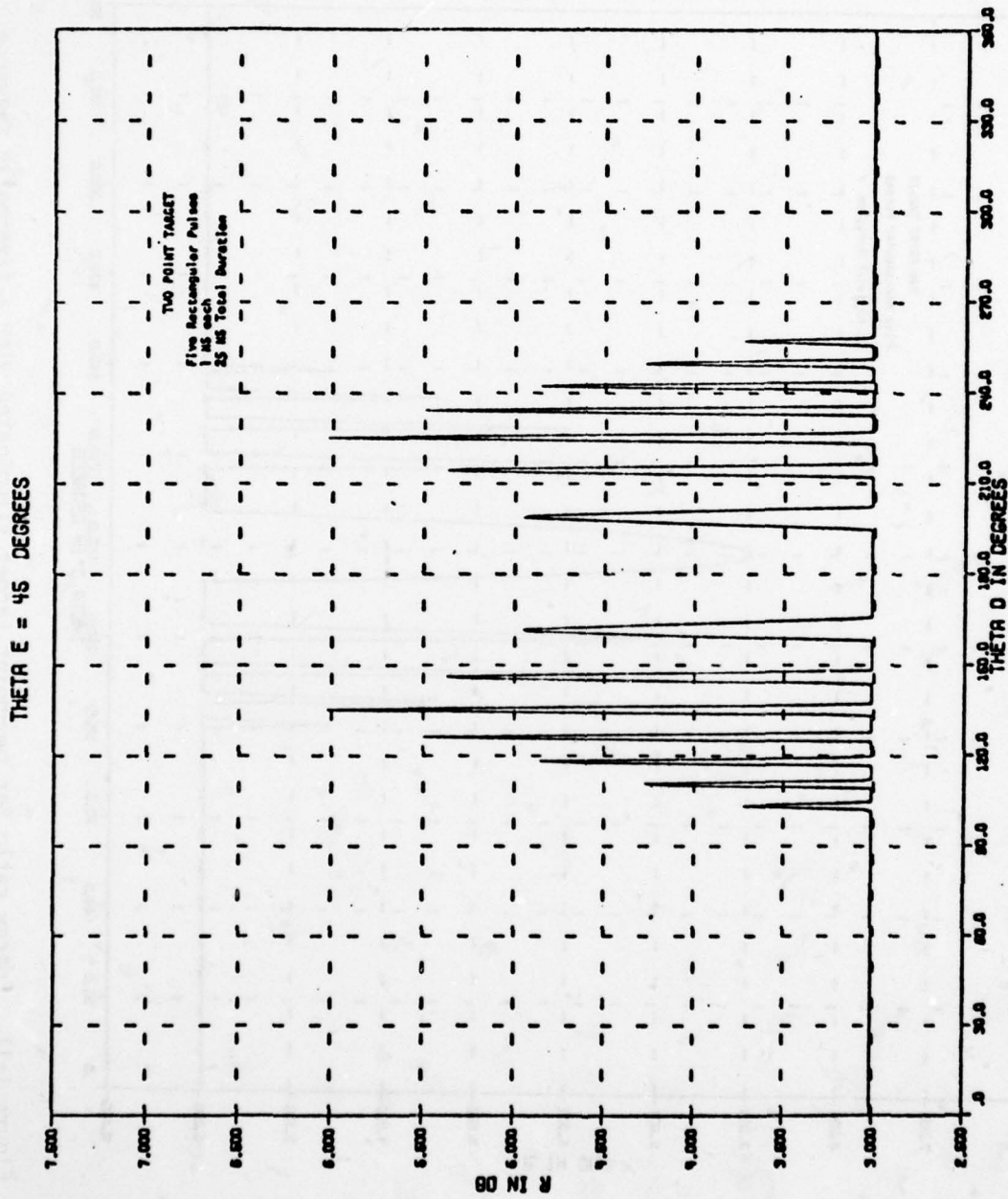


Figure 1-12. Energy ratio for two-point target illuminated with a five-pulse sequence. $\theta_e = 45^\circ$.

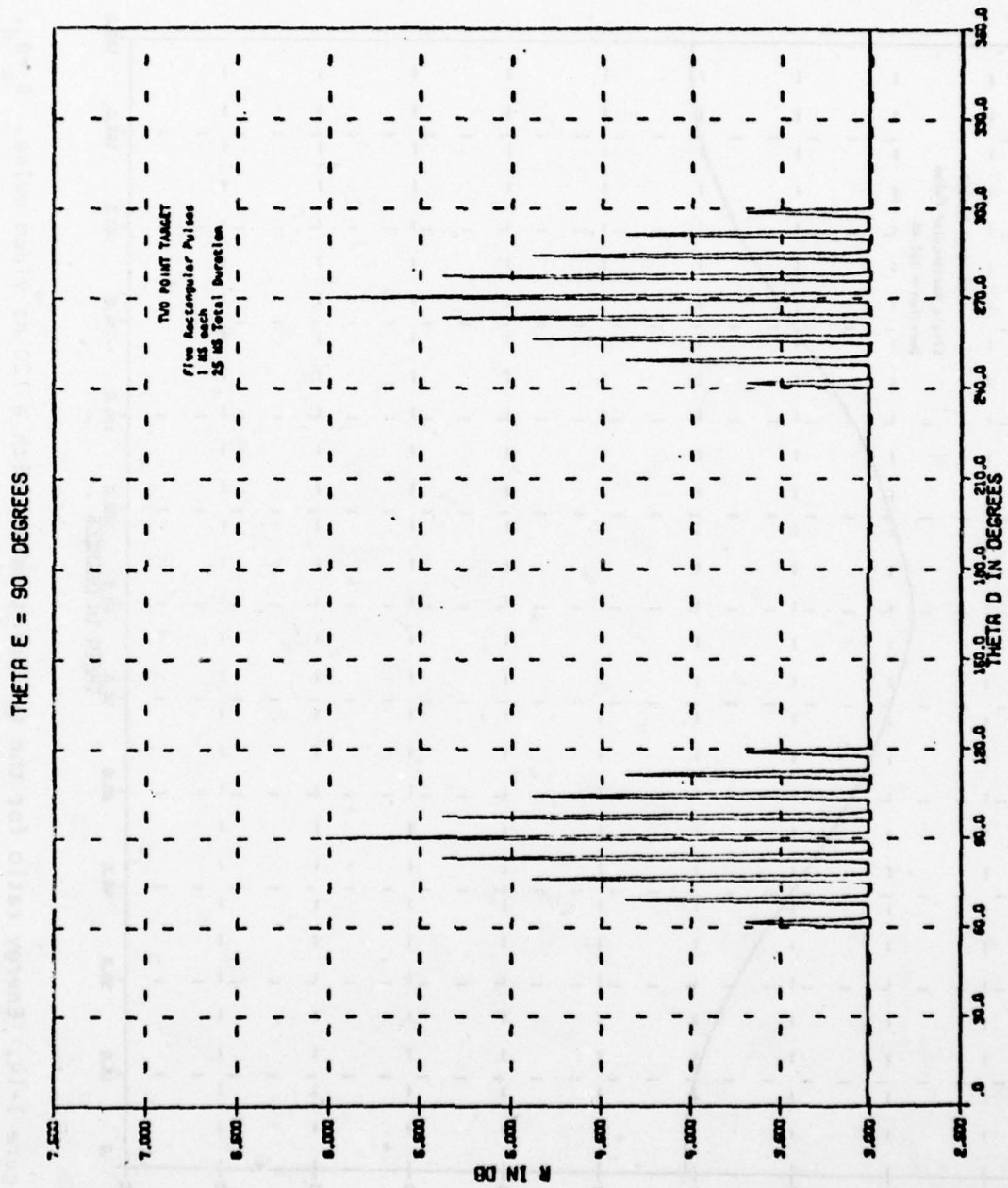


Figure 1-13. Energy ratio for two-point target illuminated by a five-pulse sequence. $\theta_e = 90^\circ$.

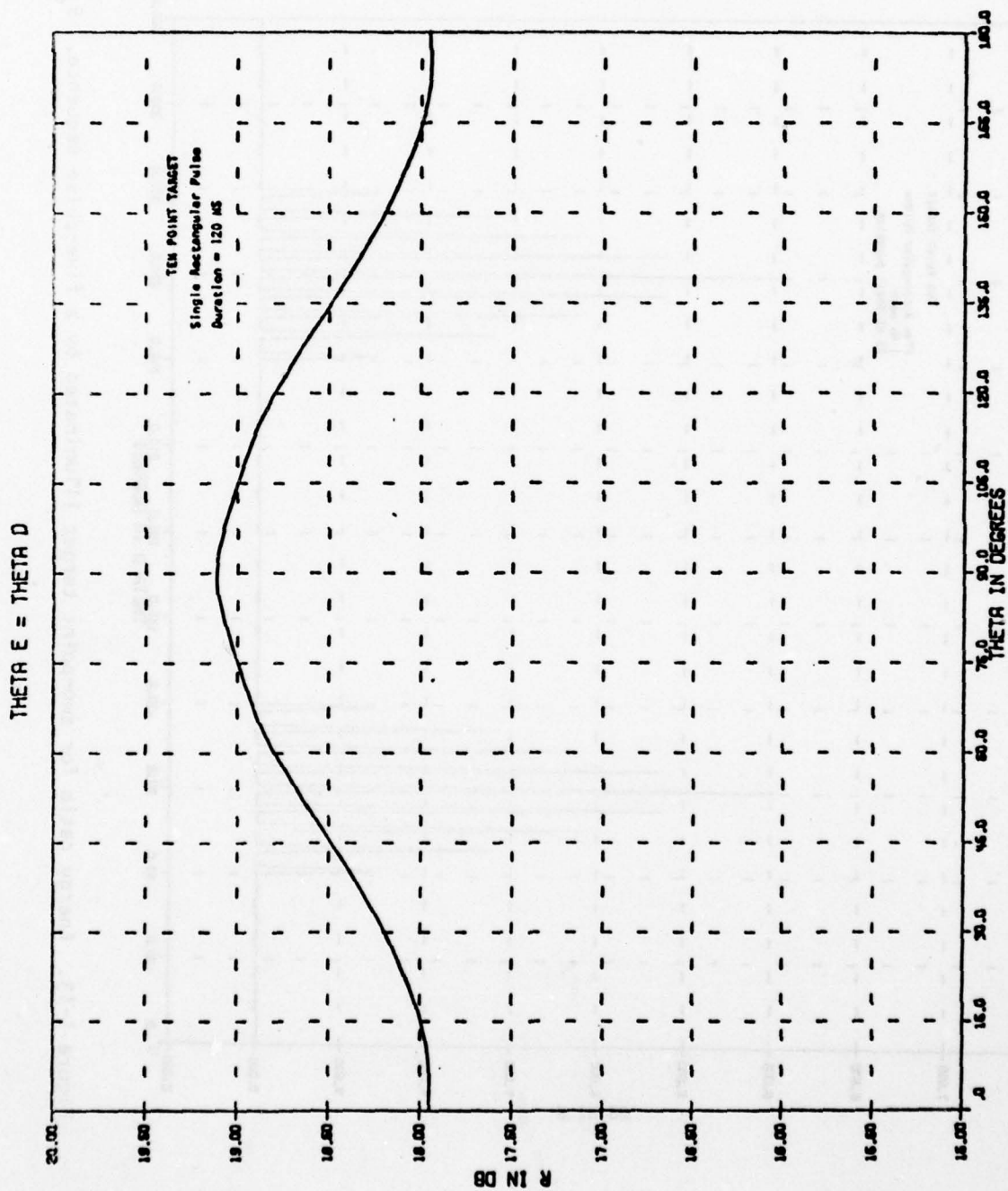


Figure 1-14. Energy ratio for the ten-point target with a 120 ns video pulse. $\theta = \theta_D$.

Figure 1-15 shows a similar result in which the video pulse duration has been made 10 times the duration of the target impulse response at each angle. The energy ratio in this case is within 0.4 dB of the theoretical maximum at all angles.

It should be recalled that the video pulse, although not a practical signal for transmission, corresponds to using a carrier frequency of zero, and that zero frequency is always one at which coherent signal summation occurs.

The "matched filter signal" is defined to be a sequence of video pulses having separations that are the time inverse of the delays in the target impulse response. Thus, this is the signal for which the target impulse response is the matched filter. It might be thought that this should be an optimum type of waveform, but the mathematical analysis in Chapter 2 reveals why this is not the case. The matched filter signal depends upon the target aspect angle and is shown in Figure 1-16 for the case in which $\theta_e = \theta_d = 60^\circ$. The response to this waveform is shown for all angles in Figure 1-17. Although the response does peak at 60° (and its complement) the maximum response is almost 7 dB below the theoretical maximum. It is clear that this form of signal is not as good as the single long pulse.

Two examples of the RF pulse with a rectangular envelope are shown in Figures 1-18 and 1-19 for angles between 55° and 65° and for a pulse duration that is about four times the maximum duration of the target impulse response. In the first figure the frequency is picked arbitrarily to be 1 GHz. The maximum response in this case occurs at an angle of about 63.3° . The second figure uses a frequency that is the closest optimum frequency above 1 GHz for the 60° case. It is of interest to note that although this frequency yields the highest response at 60° of any frequency in this range, there is an angle close to 60° for which the response is still higher. In both figures, however, the maximum response is about 2.5 dB

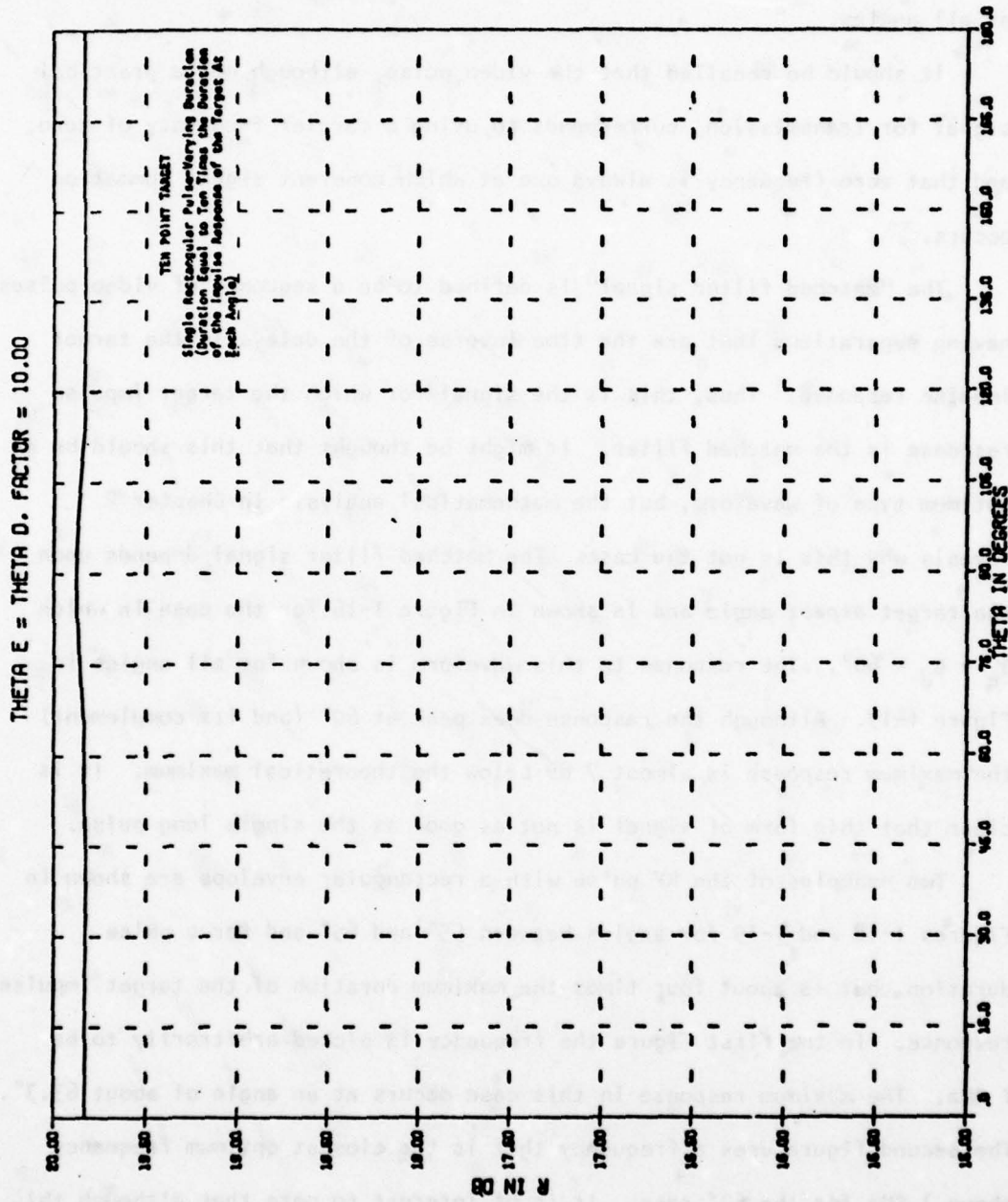


Figure 1-15. Energy ratio for the ten-point target with a long video pulse. $\theta_e = \theta_d$.

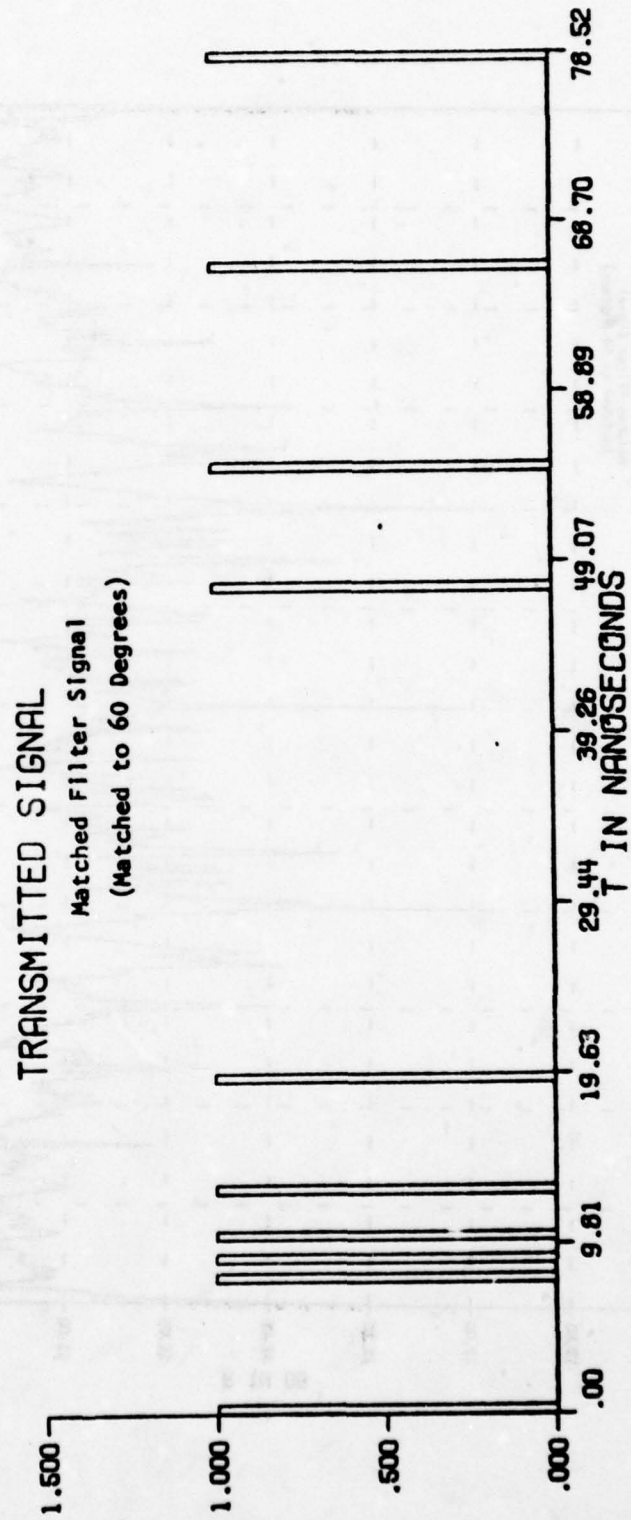


Figure 1-16. "Matched filter signal" for the ten-point target at 60°.

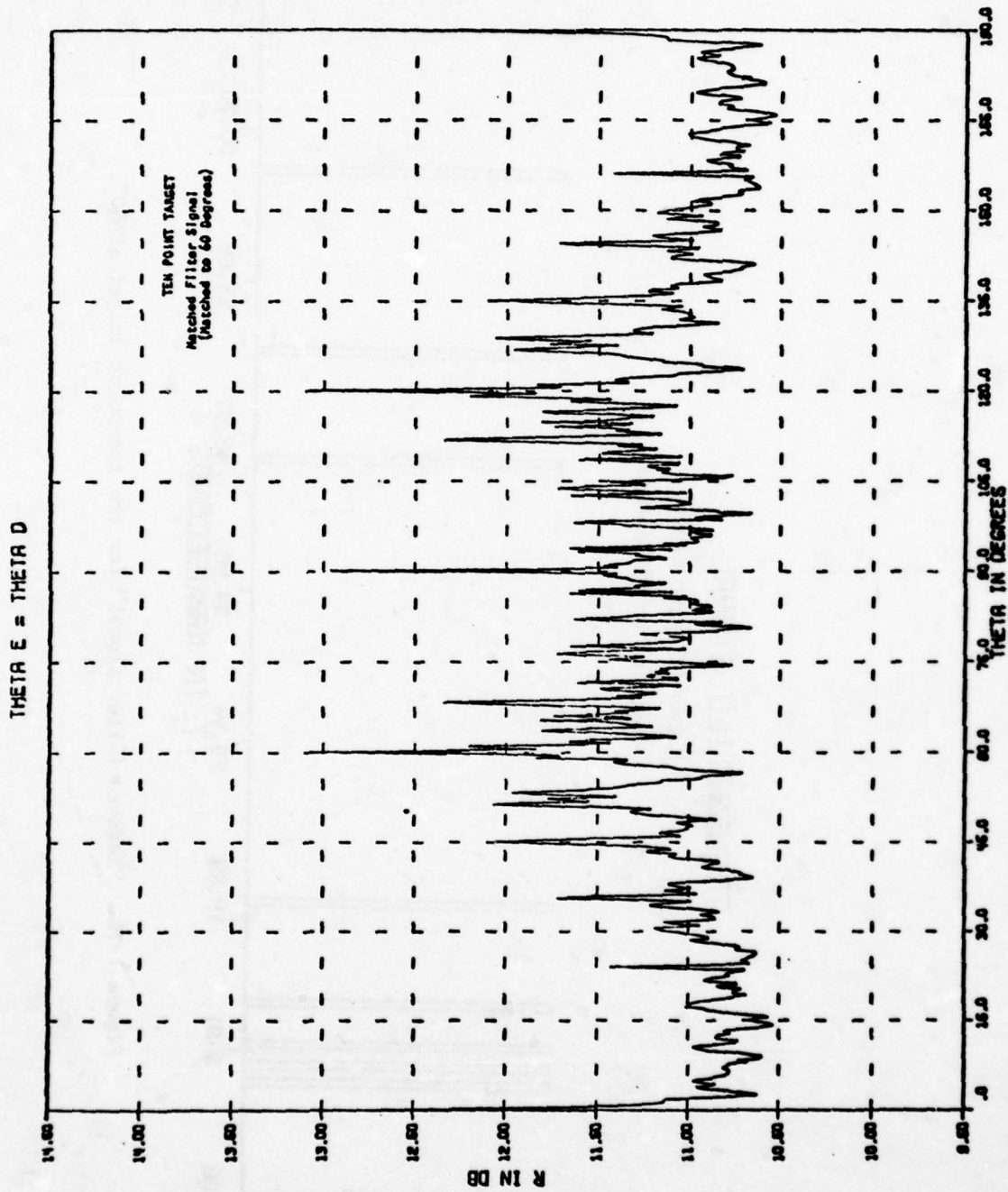


Figure 1-17. Energy ratio for the ten-point target with a matched filter signal.

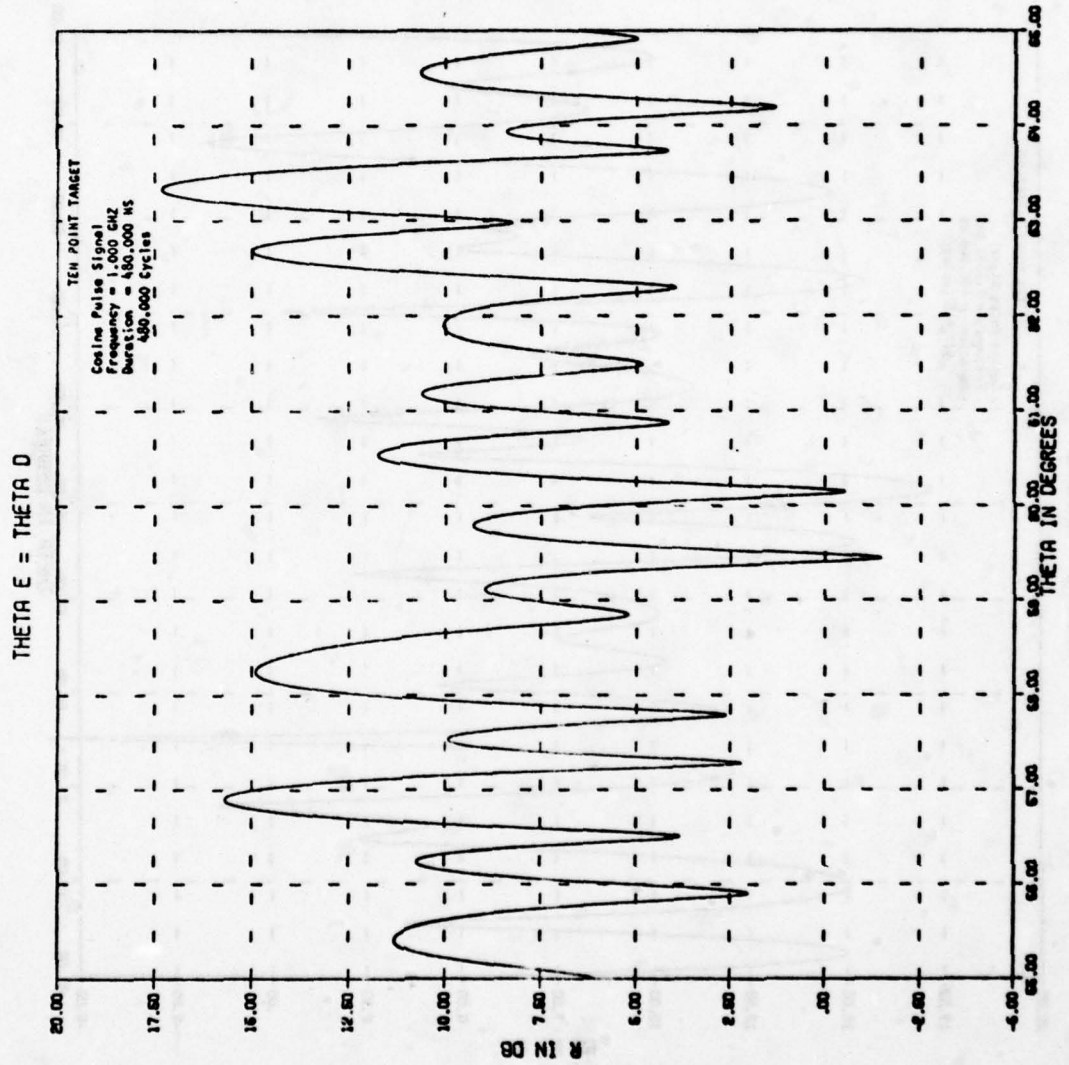


Figure 1-18. Energy ratio for the ten-point target with an RF pulse at 1 GHz.

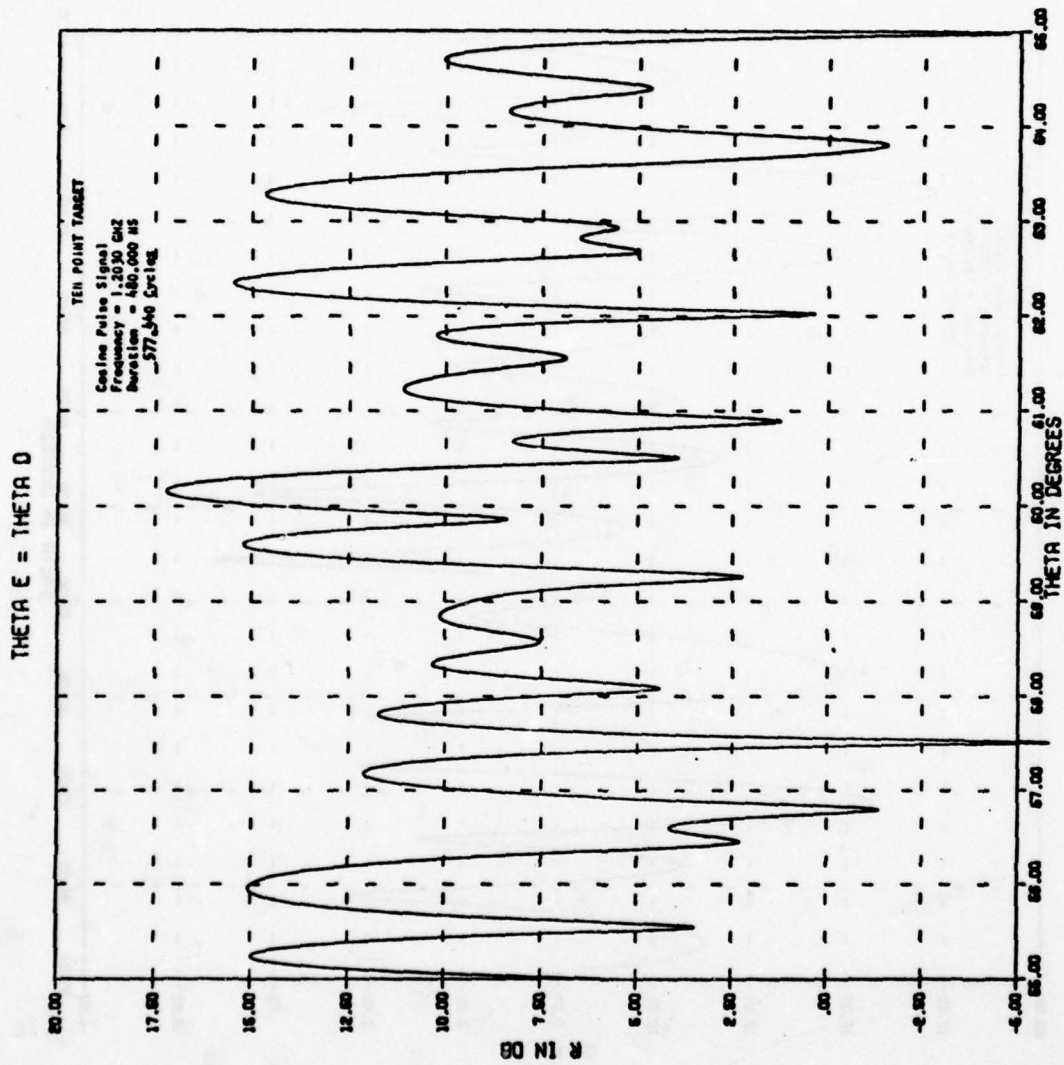


Figure 1-19. Energy ratio for the ten-point target with an RF pulse at the optimum frequency closest to 1 GHz.

below the theoretical maximum. In order to achieve better results, one would have to go to a frequency of about 4.5 GHz. The response for this optimum frequency is shown in Figure 1-20, in which it is evident that the maximum response is less than 1 dB below the theoretical maximum.

1.2.6. Optimum Orthonormal Signal Expansion: Ten-Point Target

An optimum signal waveform can be found by representing the signal in terms of orthonormal basis functions and finding the coefficients that maximize the energy ratio. The mathematical details of this technique are presented in a subsequent section.

A computational approach to this method was performed by using twenty mutually orthogonal sinusoids to amplitude modulate a carrier and adjusting the relative amplitudes of the sinusoids in accordance with the mathematical relations. Thus, the general form of the transmitted signal is that of a carrier and twenty pairs of sidebands.

Without dwelling on the mathematical details at this point, two computed examples serve to show the nature of the result. The first case is one in which the carrier frequency is selected to be one of the optimum frequencies for an incidence angle of 45° and the pulse duration is very long (10s) compared to the target impulse response. (See Figure 1-8 and observe that the theoretical maximum is achieved at $f_o = 4.451650$ GHz, as well as at other frequencies). This carrier is then modulated with 20 harmonically related sinusoids and the amplitudes of these modulation signals adjusted to maximize the desired energy ratio. The resulting optimum amplitudes are displayed in Table 1. It is evident from the table that essentially all of the transmitted signal energy is assigned to the carrier frequency (which is the optimum frequency) and very little of it to the other frequency components. This waveform gives an energy ratio of 100 which is the same as that of the single frequency sinusoid. The envelope is shown in Figure 1-21a and is seen to be of a generally rectangular shape.

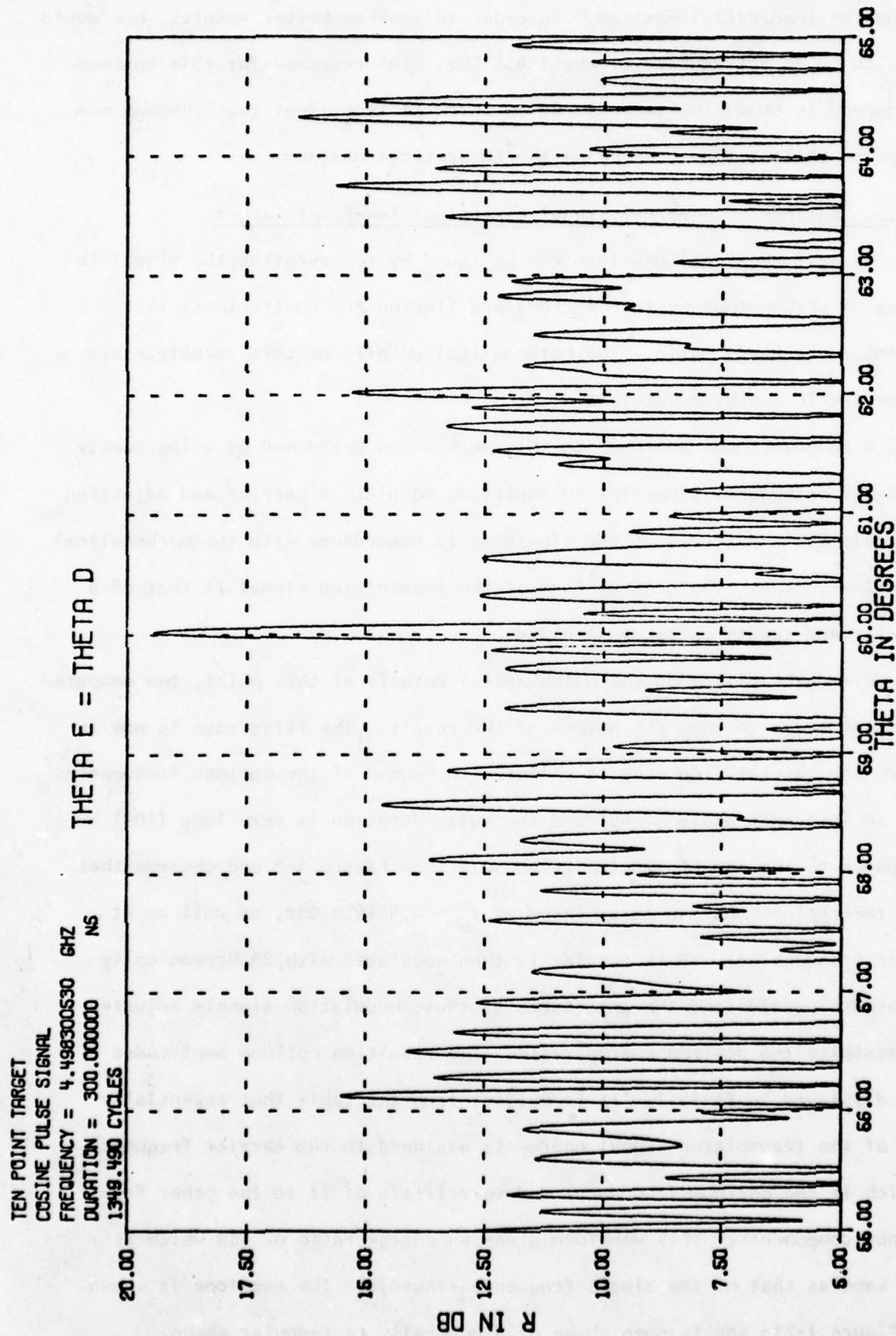
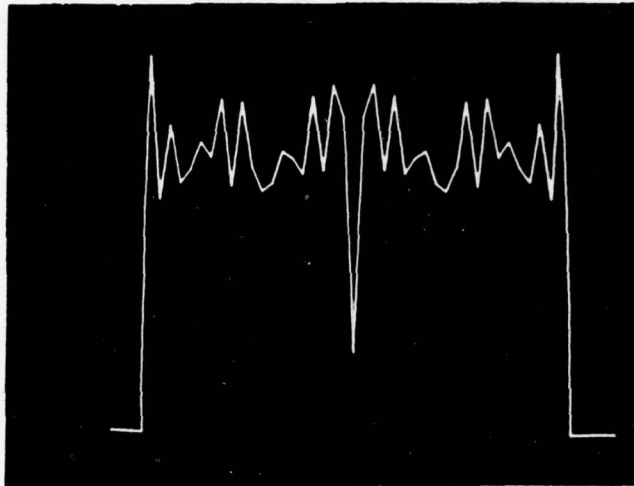
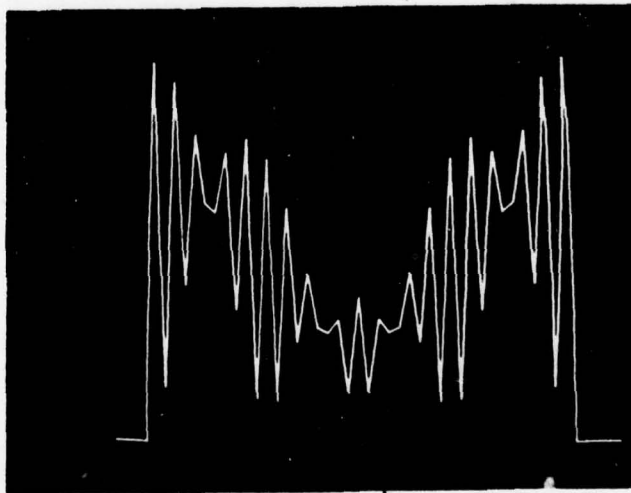


Figure 1-20. Energy ratio for the ten-point target with an RF pulse at the optimum frequency near 4.5 GHz.



(a) Signal duration of 10^{10} ns



(b) Signal duration of 300 ns

Figure 1-21. Envelope of optimum waveform for 10-point target ($f_0 = 4.5$ GHz and $\theta = 60.1^\circ$).

Table I. Optimum Amplitude Modulated Signal

$$\theta_e = 45^\circ, f_o = 4.451650 \text{ GHz}$$

| <u>Harmonic</u> | <u>Amplitude</u> | <u>Harmonic</u> | <u>Amplitude</u> |
|-----------------|------------------|-----------------|------------------|
| 0 | .9708 | 10 | -.0498 |
| 1 | -.0085 | 11 | -.0238 |
| 2 | .0107 | 12 | -.0224 |
| 3 | .0138 | 13 | -.0941 |
| 4 | -.0241 | 14 | -.0727 |
| 5 | -.0854 | 15 | -.0663 |
| 6 | -.0138 | 16 | -.0309 |
| 7 | -.0421 | 17 | -.1177 |
| 8 | -.0336 | 18 | .0672 |
| 9 | -.0031 | 19 | -.0298 |

In the second example the carrier frequency is set arbitrarily at 4.50 GHz, the pulse duration at 300 ns and the optimum amplitudes determined for an incidence angle of 60.1° . The results are shown in Table II. The energy ratio for this waveform is 14.3 as compared to 6.5 for a rectangular RF pulse of the same duration.

Table II. Optimum Amplitude Modulated Signal

$$\theta_e = 60.1^\circ, f_o = 4.500 \text{ GHz}$$

| <u>Harmonic</u> | <u>Amplitude</u> | <u>Harmonic</u> | <u>Amplitude</u> |
|-----------------|------------------|-----------------|------------------|
| 0 | -.003 | 10 | .280 |
| 1 | -.004 | 11 | .053 |
| 2 | -.005 | 12 | .019 |
| 3 | -.012 | 13 | .010 |
| 4 | -.014 | 14 | .006 |
| 5 | -.011 | 15 | .002 |
| 6 | -.004 | 16 | -.002 |
| 7 | .014 | 17 | -.002 |
| 8 | .130 | 18 | .002 |
| 9 | -.949 | 19 | .001 |

It is seen from Table II that the maximum amplitude component is the 9th harmonic of the fundamental. This corresponds to side bands at 4.5 ± 0.03 GHz and calculation reveals that these sidebands fall nearest to the peaks of the CW power transfer function. In this case however, the other components are of sufficient amplitude to significantly alter the shape of the envelope from that of a rectangular pulse. The envelope is shown in Figure 1-22b. More study will be required before the full significance of optimizing the envelope of the waveform can be determined. However, it appears that a rectangular pulse at the optimum frequency gives results comparable to the optimum waveform.

1.2.7. Variation of Optimum Frequency With Incidence Angle

This phase of the study attempted to determine how the optimum frequency varies with the angle of incidence and, in particular, if this variation was a continuous one. This question is motivated by the desire to consider automatic techniques for tracking the optimum frequency as the target changes its aspect angle.

This aspect is investigated by producing three-dimensional plots of the target response as a function of both frequency and angle of incidence. Such a plot is displayed in Figure 1-22. Note that the angular range covered by this plot is extremely small. Consideration of this plot reveals that a continuous frequency tracking operation is not feasible because the optimum frequency jumps abruptly from one value to another whenever the amplitude of one ridge in the plot drops below the amplitude of an adjacent ridge. This conclusion indicates the need for a more extensive study of this phenomenon if adaptive space-time signal processing is contemplated.

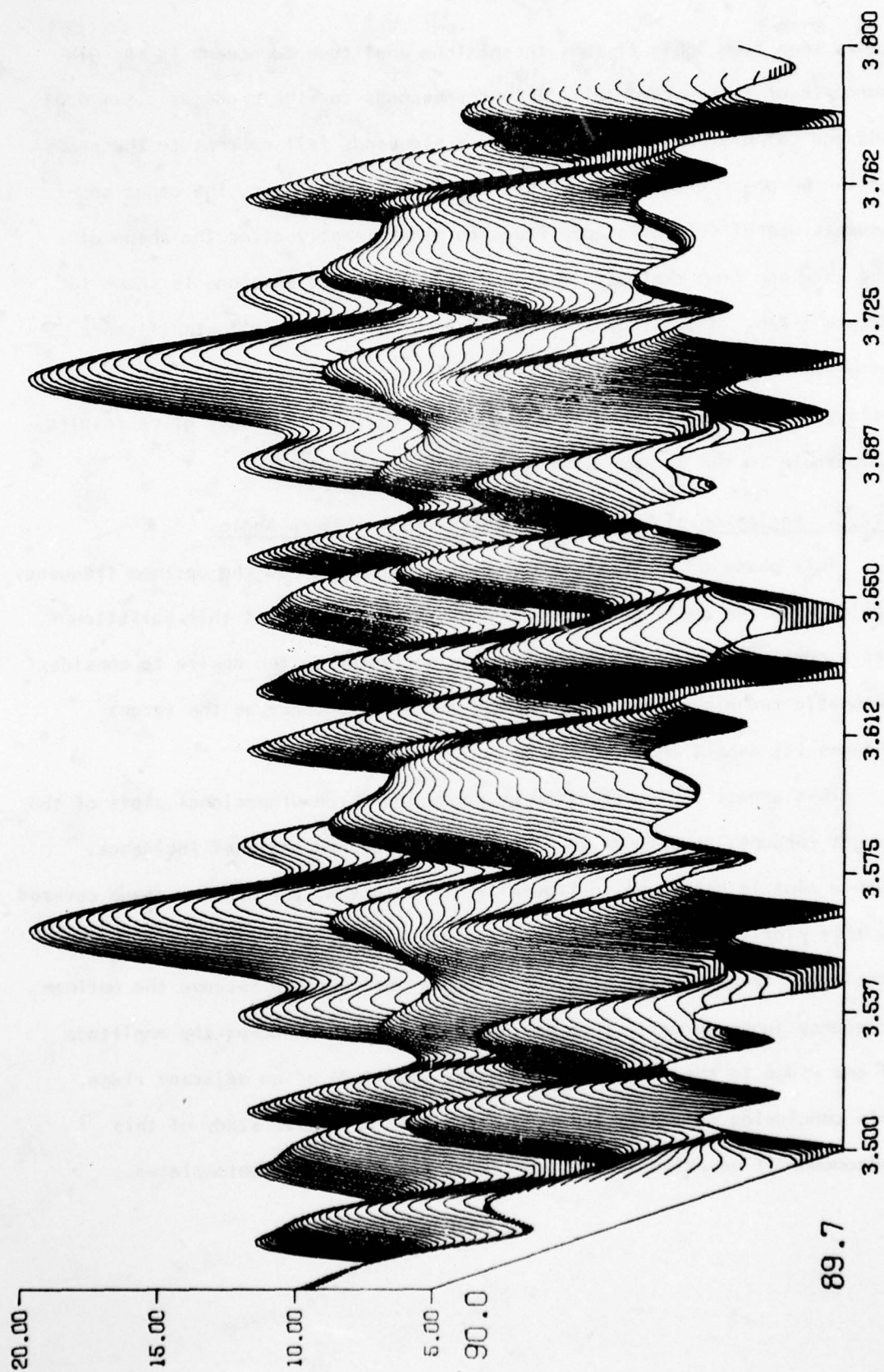


Figure 1-22. Variation with frequency in GHz, angles in degrees

2.1. MATHEMATICAL ANALYSIS

In this chapter the physical problem described in Section 1.1.1 is restated in mathematical terms and solved to the extent that an analytical solution is possible. Since the target is to be modeled in terms of its impulse response, the problem becomes one of linear system analysis and the discussion that follows is placed in that context.

2.1.1. Problem Definition in Mathematical Form

The system under consideration is shown in Figure 2-1.

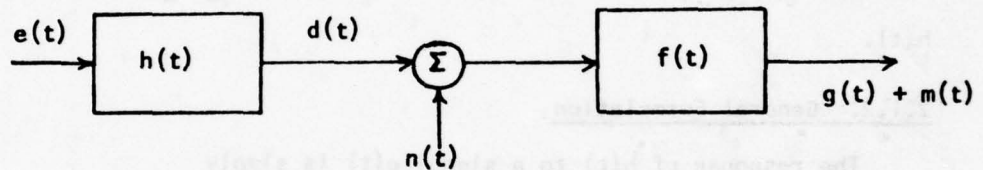


Figure 2-1. Block diagram of system under consideration.

It is desired to find the form of $e(t)$ that will maximize the output signal-to-noise ratio at any specified time t_0 under the following assumptions:

- The impulse response $h(t)$ is known.
- The noise $n(t)$ is white with a one-sided spectral density of N_0 .
- The energy of $e(t)$ is constrained to be a fixed value, E_0 .
- The filter impulse response $f(t)$ is causal.

The output signal-to-noise ratio is defined to be

$$(S/N)_0 = \frac{g^2(t_0)}{E[m^2(t)]} \quad (2-1)$$

When the noise is white it is well known that this signal-to-noise ratio is maximized by using the matched filter; that is when

$$\begin{aligned} f(t) &= d(t_0 - t), & t &\geq 0 \\ &= 0, & t &< 0 \end{aligned} \quad (2-2)$$

and that the maximum signal-to-noise ratio is

$$\text{Max}(S/N)_0 = \frac{2}{N_0} \int_{-\infty}^{t_0} d^2(t) dt = \frac{2 E_d(t_0)}{N_0} \quad (2-3)$$

where $E_d(t_0)$ is the energy in $d(t)$ up to the time t_0 . If $d(t)$ is time limited, then t_0 can be selected large enough to include all of the energy of $d(t)$.

Thus, in this case

$$E_d(t_0) = E_d$$

It is clear that maximizing E_d , subject to the constraint on E_0 , will satisfy the conditions of the problem. Thus, the problem may be stated as finding the form of $e(t)$ that maximizes the ratio E_d/E_0 for any specified $h(t)$.

2.1.2. General Formulation

The response of $h(t)$ to a signal $e(t)$ is simply

$$d(t) = \int_{-\infty}^{\infty} e(u) h(t-u) du \quad (2-4)$$

and the energy of this response is

$$E_d = \int_{-\infty}^{\infty} d^2(t) dt \quad (2-5)$$

Likewise, the energy of $e(t)$ is

$$E_0 = \int_{-\infty}^{\infty} e^2(t) dt \quad (2-6)$$

The ratio to be maximized is

$$R = \frac{E_d}{E_0} = \frac{\int_{-\infty}^{\infty} \left[\int_{-\infty}^{\infty} e(u) h(t-u) du \right]^2 dt}{\int_{-\infty}^{\infty} e^2(t) dt} \quad (2-7)$$

An alternative formulation is to maximize the parameter

$$J = \int_{-\infty}^{\infty} \left[\int_{-\infty}^{\infty} e(u) h(t-u) du \right]^2 dt - \lambda \int_{-\infty}^{\infty} e^2(t) dt \quad (2-8)$$

where λ is the Lagrangian multiplier and is adjusted to satisfy (2-6).

The problem can also be formulated in the frequency domain by noting that the Fourier transform of $d(t)$ is simply

$$D(f) = E(f) H(f) \quad (2-9)$$

where $E(f)$ is the Fourier transform of $e(t)$ and $H(f)$ is the Fourier transform of $h(t)$. Furthermore, the energy of $d(t)$ is

$$E_d = \int_{-\infty}^{\infty} |D(f)|^2 df \quad (2-10)$$

while that of $e(t)$ is

$$E_o = \int_{-\infty}^{\infty} |E(f)|^2 df \quad (2-11)$$

Thus, (2-7) and (2-8) become

$$R = \frac{\int_{-\infty}^{\infty} |E(f)|^2 |H(f)|^2 df}{\int_{-\infty}^{\infty} |E(f)|^2 df} \quad (2-12)$$

and

$$J = \int_{-\infty}^{\infty} |E(f)|^2 |H(f)|^2 df - \lambda \int_{-\infty}^{\infty} |E(f)|^2 df \quad (2-13)$$

2.1.3. Optimization With No Time Constraint: Frequency-Domain Solution

When $e(t)$ is not constrained to have a finite time duration, the optimization is most conveniently carried out in the frequency domain. Equation (2-13) may be written as

$$J = \int_{-\infty}^{\infty} [|H(f)|^2 - \lambda] |E(f)|^2 df \quad (2-14)$$

It is apparent by inspection that J can be maximized by having all of the energy of $e(t)$ concentrated at a single frequency and letting that frequency be the frequency at which $|H(f)|^2$ is a maximum.

To express this conclusion more precisely, let

$$E(t) = \begin{cases} \lim_{T \rightarrow \infty} \frac{E_o}{T} \cos 2\pi f_o t, & |t| \leq T \\ 0, & |t| > T \end{cases} \quad (2-15)$$

where f_0 is a frequency at which $|H(f)|^2$ has a global maximum. Note that the signal amplitude becomes vanishingly small in the limit. This is a consequence of maintaining a finite energy over an infinite time duration. (There may be more than one such frequency.) It is then straightforward to show that in the limit

$$|E(f)|^2 = \frac{E_0}{2} [\delta(f-f_0) + \delta(f+f_0)] \quad (2-16)$$

The desired ratio then becomes

$$\begin{aligned} \text{Max}(R) &= \frac{\int_{-\infty}^{\infty} \frac{E_0}{2} [\delta(f-f_0) + \delta(f+f_0)] |H(f)|^2 df}{\int_{-\infty}^{\infty} \frac{E_0}{2} [\delta(f-f_0) + \delta(f+f_0)] df} \\ &= \frac{1}{2} [|H(f_0)|^2 + |H(-f_0)|^2] = |H(f_0)|^2 \end{aligned} \quad (2-17)$$

A case of particular interest is that in which the impulse response $h(t)$ can be represented as a set of δ functions. Thus, let

$$h(t) = \sum_{i=1}^M a_i \delta(t-\tau_i), \quad 0 \leq a_i \leq 1 \quad (2-18)$$

from which

$$H(f) = \sum_{i=1}^M a_i e^{-j2\pi f \tau_i} \quad (2-19)$$

Then,

$$|H(f)|^2 = \sum_{i=1}^M \sum_{j=1}^M a_i a_j e^{-j2\pi f (\tau_i - \tau_j)} \quad (2-20)$$

The frequency f_0 may be obtained from

$$\frac{d|H(f)|^2}{df} = 0$$

which leads to the transcendental equation

$$\sum_{i=1}^M \sum_{j=1}^M 2\pi a_i a_j (\tau_i - \tau_j) \sin 2\pi f (\tau_i - \tau_j) = 0$$

This can be further reduced, by using symmetry, to

$$\sum_{i=2}^M \sum_{j=1}^{i-1} a_i a_j (\tau_i - \tau_j) \sin 2\pi f(\tau_i - \tau_j) = 0 \quad (2-21)$$

The desired f_0 is among the solutions of (2-21) but it may be necessary to check all of the solutions in (2-20) in order to determine which one is the global maximum.

Although an explicit result for the maximum value of $|H(f)|^2$ is not possible, it is possible to establish a bound on this quantity. From the evenness of the cosine and the oddness of the sine, (2-20) can be written as

$$|H(f)|^2 = \sum_{i=1}^M \sum_{j=1}^M a_i a_j \cos 2\pi f(\tau_i - \tau_j) \quad (2-22)$$

This clearly will have its greatest possible value if all of the cosine terms are equal to unity. Thus,

$$|H(f)|^2 \leq \left[\sum_{i=1}^M a_i \right]^2 \quad (2-23)$$

In some cases this bound can be achieved (e.g., when the a_i are all equal and the τ_i are equally spaced, or at $f = 0$) but in the more general case it cannot. Thus, it appears that computational evaluation of the maximum is necessary in general.

2.1.4. Optimization With No Time Constraint: Time-Domain Solution

Although the frequency-domain solution given above is adequate to solve the problem when there is no time constraint, some additional insight can be gained by looking at a time-domain solution. Referring to (2-8)

$$J = \int_{-\infty}^{\infty} \left[\int_{-\infty}^{\infty} e(u) h(t-u) du \right]^2 dt - \lambda \int_{-\infty}^{\infty} e^2(t) dt \quad (2-8)$$

the procedure is to replace $e(u)$ by $e(u) + \epsilon \eta(u)$ where $\eta(u)$ is any variation that vanishes at $\pm \infty$. Thus,

$$J = \int_{-\infty}^{\infty} \left\{ \int_{-\infty}^{\infty} [e(u) + \epsilon n(u)] h(t-u) du \right\}^2 dt - \lambda \int_{-\infty}^{\infty} [e(t) + \epsilon n(t)]^2 dt \quad (2-24)$$

and

$$\left. \frac{\partial J}{\partial \epsilon} \right|_{\epsilon=0} = \int_{-\infty}^{\infty} \left[\int_{-\infty}^{\infty} e(u) h(t-u) du \right] \left[\int_{-\infty}^{\infty} n(u) h(t-u) du \right] dt - \lambda \int_{-\infty}^{\infty} e(t) n(t) dt = 0 \quad (2-25)$$

Writing this as an iterated integral and rearranging the sequence of integration leads to

$$\int_{-\infty}^{\infty} n(v) dv \int_{-\infty}^{\infty} \int_{-\infty}^{\infty} e(u) h(t-u) h(t-v) du dt - \lambda \int_{-\infty}^{\infty} n(v) e(v) dv = 0$$

or

$$\int_{-\infty}^{\infty} n(v) \left[\int_{-\infty}^{\infty} \int_{-\infty}^{\infty} e(u) h(t-u) h(t-v) du dt - \lambda e(v) \right] dv = 0 \quad (2-26)$$

For this to be true for any variation $n(v)$ requires that

$$\int_{-\infty}^{\infty} \int_{-\infty}^{\infty} e(u) h(t-u) h(t-v) du dt - \lambda e(v) = 0, \quad -\infty < v < \infty \quad (2-27)$$

Equation (2-27) can be written in simpler form by defining the time-ambiguity function of $h(t)$ as

$$R_h(\tau) = \int_{-\infty}^{\infty} h(t) h(t+\tau) dt$$

Substituting into (2-27) leads to

$$\int_{-\infty}^{\infty} e(u) R_h(u-v) du - \lambda e(v) = 0, \quad -\infty < v < \infty \quad (2-28)$$

This is a homogeneous Fredholm integral equation for which there are well-known solutions.

The easiest approach is to Fourier transform (2-28) to obtain

$$E(f) S_h(f) - \lambda E(f) = 0 \quad (2-29)$$

where $S_h(f)$ is the Fourier transform of $R_h(\tau)$. Non-trivial solutions of (2-29) exist for every value of λ for which

$$S_h(f) - \lambda = 0 \quad (2-30)$$

For every value of λ there are a set of solutions corresponding to all values of f that satisfy (2-30). Since these solutions must have Fourier transforms that satisfy (2-29) for discrete values of f , they must be sinusoids. Thus, the general solution may be represented as

$$e(t) = \sum_{k=1}^K c_k \cos(2\pi f_k t + \theta_k) \quad (2-31)$$

where the f_k are the discrete solutions of (2-30), the c_k are selected to satisfy the energy constraint on $e(t)$, and K is the total number discrete solutions of (2-30).

When λ is chosen to be equal to the maximum value of $S_h(f)$ then there is just one value of f_k and the solution becomes identical to that in the previous section since it is apparent from the definition of $R_h(\tau)$ that its Fourier transform is

$$S_h(f) = |H(f)|^2$$

However, other solutions can also be obtained by selecting smaller values of λ . The details of such solutions are tedious and are not pursued here. The main point to be learned from the time-domain approach is that there appears to be an infinite number of possible solutions.

For the particular case in which

$$h(t) = \sum_{i=1}^M a_i \delta(t - \tau_i) \quad , \quad 0 \leq a_i \leq 1$$

the time-ambiguity function becomes

$$R_h(\tau) = \sum_{i=1}^M \sum_{j=1}^M a_i a_j \delta(\tau + \tau_i - \tau_j) \quad (2-32)$$

Using this form in the integral equation reduces (2-28) to

$$\sum_{i=1}^M \sum_{j=1}^M a_i a_j e(v + \tau_i - \tau_j) = \lambda e(v) \quad , \quad -\infty < v < \infty \quad (2-33)$$

If

$$\lambda = \text{Max} |H(f)|^2$$

and if f_0 is a frequency at which a global maximum occurs, then

$$e(t) = c_0 \cos 2\pi f_0 t \quad (2-34)$$

Using this and (2-22) in (2-33) yields

$$\sum_{i=1}^M \sum_{j=1}^M a_i a_j c_0 \cos 2\pi f_0 (v + \tau_i - \tau_j) = \sum_{i=1}^M \sum_{j=1}^M a_i a_j c_0 \cos 2\pi f_0 (\tau_i - \tau_j) \cos 2\pi f_0 v$$

The left side of (2-33) may be rewritten as

$$\begin{aligned} \sum_{i=1}^M \sum_{j=1}^M a_i a_j c_0 [\cos 2\pi f_0 v \cos 2\pi f_0 (\tau_i - \tau_j) - \sin 2\pi f_0 v \sin 2\pi f_0 (\tau_i - \tau_j)] \\ = \sum_{i=1}^M \sum_{j=1}^M a_i a_j c_0 \cos 2\pi f_0 v \cos 2\pi f_0 (\tau_i - \tau_j) \end{aligned} \quad (2-35)$$

In which the sine terms cancel because of the oddness of the sine function.

Thus, (2-34) is a solution to (2-33).

The solution discussed above is artificial in the sense that the finite signal energy over an infinite time duration forces the signal amplitude to become vanishingly small. However, they can be interpreted in a practical sense as representing a near-optimum solution when long pulses are employed. In order to avoid the problem of vanishing signals it is possible to impose a constraint on the time duration of the signals. This is done in the following section of this report.

2.1.5. Optimization With Time-Limited Signals

A time constraint is imposed by stipulating that $e(t)$ be zero outside of a finite time interval, say, $-T$ to T . The response of $h(t)$ to this time-limited signal is simply

$$d(t) = \int_{-T}^T e(u) h(t-u) du \quad (2-36)$$

and is not necessarily time limited. The energy in $d(t)$ may be expressed as

$$\begin{aligned}
 E_d &= \int_{-\infty}^{\infty} \left[\int_{-T}^T e(u) h(t-u) du \right]^2 dt \\
 &= \int_{-\infty}^{\infty} \int_{-T}^T \int_{-T}^T e(u) e(v) h(t-u) h(t-v) du dv dt
 \end{aligned} \tag{2-37}$$

Upon employing the definition of the time-ambiguity function, this can be written as

$$E_d = \int_{-T}^T \int_{-T}^T e(u) e(v) R_h(u-v) du dv \tag{2-38}$$

The above expression can be written in more convenient form by letting $\tau = u-v$ and expressing the double integral as

$$\int_{-T}^T \int_{-T}^T () du dv = \int_0^{2T} d\tau \int_{-T}^{T-\tau} () dv + \int_{-2T}^0 d\tau \int_{-T}^{T+\tau} () du \tag{2-39}$$

If τ is replaced by $-\tau$ in the second integral, it becomes the same as the first since $R_h(-\tau) = R_h(\tau)$. Thus,

$$E_d = \int_{-2T}^{2T} d\tau \int_{-T}^{T-\tau} e(v) e(v+\tau) R_h(\tau) dv \tag{2-40}$$

Consider next the integral over v in (2-40). This is sketched in Figure 2-2. It is clear from this sketch that the integral is zero outside of

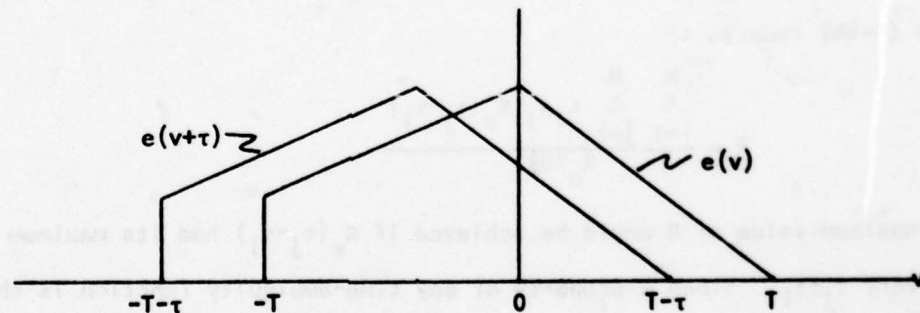


Figure 2-2. Integrand of the signal integral.

$-T \leq v \leq T-\tau$. Thus, the integral over v is just the time-ambiguity function for $e(v)$. That is,

$$R_e(\tau) = \int_{-T}^{T-\tau} e(v) e(v+\tau) dv \tag{2-41}$$

and (2-40) becomes

$$E_d = \int_{-2T}^{2T} R_e(\tau) R_h(\tau) d\tau \quad (2-42)$$

The energy of the incident signal is

$$E_o = \int_{-T}^T e^2(t) dt = R_e(0) \quad (2-43)$$

Hence, the energy ratio that is to be maximized is

$$R = \frac{E_d}{E_o} = \frac{\int_{-2T}^{2T} R_e(\tau) R_h(\tau) d\tau}{R_e(0)} \quad (2-44)$$

An interesting conclusion that can be drawn from this result is that R depends only upon the time-ambiguity function of $e(t)$ and not upon the actual time function. This suggests that there may be many solutions, all of which are equally good.

When the target's impulse response is modeled by a set of delta functions so that

$$R_h(\tau) = \sum_{k=1}^M \sum_{j=1}^M a_i a_j \delta(T + \tau_i - \tau_j)$$

then (2-44) reduces to

$$R = \frac{\sum_{i=1}^M \sum_{j=1}^M a_i a_j R_e(\tau_j - \tau_i)}{R_e(0)} \quad (2-45)$$

The maximum value of R would be achieved if $R_e(\tau_j - \tau_i)$ had its maximum value at every $\tau_j - \tau_i$. Since a property of any time-ambiguity function is that

$$R_e(\tau) \leq R_e(0)$$

it follows that an upper bound on (2-45) is

$$R \leq \sum_{i=1}^M \sum_{j=1}^M a_i a_j = \left[\sum_{i=1}^M a_i \right]^2 \leq M^2 \quad (2-46)$$

The problem of finding the form of $e(t)$ that maximizes R still remains, however. A straightforward approach is to express $R_e(\cdot)$ in (2-45) in integral form and proceed in the same manner as was done in Section 2.1.4 with no time constraint. Since the only change from the previous analysis is the finite limits, this procedure is not repeated here. By analogy, however, the resulting integral equation that must be solved is

$$\int_{-T}^T e(u) R_h(u-v) du - \lambda e(v) = 0, \quad -T \leq v \leq T \quad (2-47)$$

which follows directly from (2-28). When the impulse response is a set of delta functions, (2-47) becomes

$$\sum_{i=1}^M \sum_{j=1}^M a_i a_j e(v + \tau_i - \tau_j) = \lambda e(v), \quad -T \leq v \leq T \quad (2-48)$$

Any solution of this equation will be an optimum signal waveform.

Explicit solutions to (2-48) have not been found and it is conjectured that none exist, although this has not been proven either. Since this conclusion is somewhat unusual, several comments are in order:

- 1) Since the τ_i may have any value (within a specified range), (2-48) implies that the sum of M arbitrary translations of $e(v)$ must be proportional to $e(v)$. Since some of the translations will result in $|v + \tau_i - \tau_j| > T$, these terms will be zero and will not contribute to the sum for some values of v . Thus, it appears that the only function that will satisfy (2-48) is $e(v) = 0$ and this, of course, is a trivial one.
- 2) The fact that there are no solutions to (2-48) does not imply that there are no optimum waveforms. Clearly, some waveforms are better than others and there must be one or more waveforms that are better than all others. What is implied by this conclusion is that the best waveforms cannot be identified by this standard optimization procedure.
- 3) If the standard optimization procedures do not work in this case, there are two possible ways to proceed. One is to consider some sub-optimum waveforms and investigate them in a systematic fashion. The second approach is to define signal waveforms in terms of some sort of orthogonal expansion and attempt to optimize the coefficients of this expansion. Both of these approaches are considered in the following sections.

2.1.6. Sub-Optimum Signals: Pulsed Sinusoids

Since the optimum signal when there is no time constraint is a steady-state sinusoid at some optimum frequency, it is reasonable to assume that a sinusoid with a finite duration will be close to optimum if it has the same frequency. In particular, if the duration of the sinusoidal pulse is made long compared to the duration of the impulse response, the resulting performance should be very nearly optimum. This conclusion is strengthened by noting that the theoretical maximum value of R is identical in both the time-limited and non-time-limited cases.

Thus, define the signal as

$$e(t) = \begin{cases} \frac{E_0}{T} \cos \omega_0 t & , \quad |t| \leq T \\ 0 & , \quad |t| > T \end{cases} \quad (2-49)$$

which is sketched in Figure 2-3. The time-ambiguity function for this is

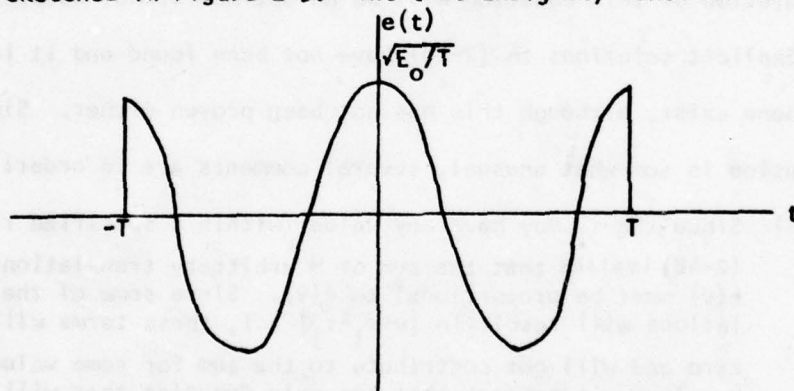


Figure 2-3. The sinusoidal RF pulse.

defined by

$$R_e(\tau) = \int_{-T}^{T-\tau} \frac{E_0}{T} \cos \omega_0 t \cos \omega_0 (t+\tau) dt \quad , \quad \tau > 0 \quad (2-50)$$

Straightforward evaluation of this integral yields

$$R_e(\tau) = \frac{E_0}{1 + \frac{\sin 2\omega_0 T}{2\omega_0 T}} \left[\left(1 - \frac{|\tau|}{2T}\right) \cos \omega_0 \tau + \frac{\sin \omega_0 (2T - |\tau|)}{2\omega_0 T} \right] \quad , \quad |\tau| \leq 2T$$

$$= 0 \quad , \quad |\tau| > 2T \quad (2-51)$$

in which the form for $\tau < 0$ is determined by utilizing the symmetry of $R_e(\tau)$; i.e., $R_e(-\tau) = R_e(\tau)$. This time-ambiguity function is sketched in Figure 2-4.

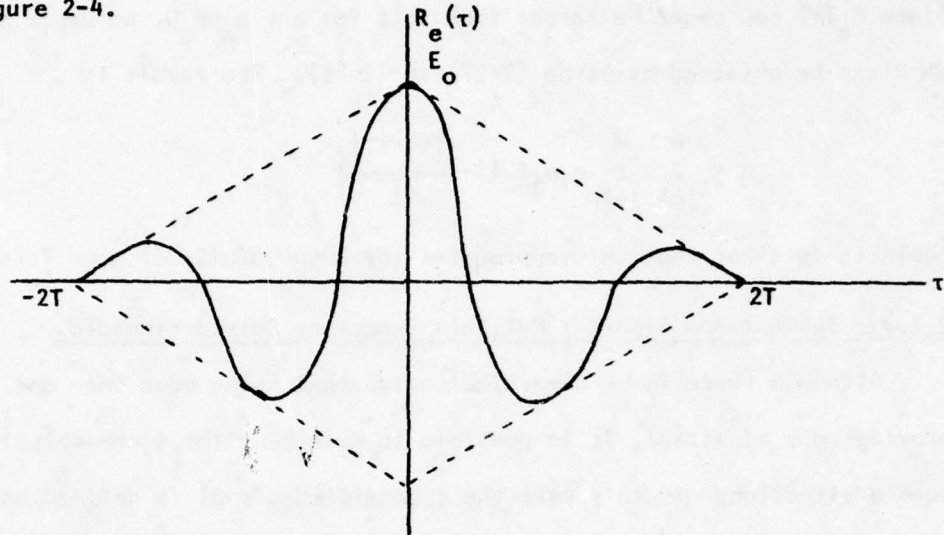


Figure 2-4. Time-ambiguity function for the sinusoidal RF pulse.

It is noted in the previous section that a condition for an optimum signal is that $R_e(\tau_j - \tau_i)$ be as large as possible for all τ_i and τ_j . Since the peaks of $R_e(\tau)$ occur at multiples of the period $2\pi/\omega_0$, the criterion for selecting ω_0 is exactly the same as it was in the non-time-limited case; that is, pick a frequency such that all $(\tau_j - \tau_i)$ are as close to being multiples of the period as possible.

The extent to which the time-limited RF pulse will be inferior to the steady state sinusoid depends upon the duration of the impulse response. If the largest value of $|\tau_j - \tau_i|$ is small compared to $2T$, then all values of $R_e(\tau_j - \tau_i)$ that occur near peaks will be close to E_0 and a nearly optimum result will occur. Thus, if the frequency is correct, improved results will always be obtained by making T larger.

An upper bound on the performance that can be achieved with an RF pulse is obtained by letting the frequency of the sinusoid go to zero. In this case

$$R_e(\tau) = E_0 \left[1 - \frac{|\tau|}{2T} \right], \quad |\tau| \leq 2T, \quad \omega_0 = 0$$

$$= 0, \quad |\tau| > 2T \quad (2-52)$$

Since $R_e(\tau)$ can never be larger than this for any $\omega_0 \neq 0$, an upper bound on R can be obtained by using (2-52) in (2-45). The result is

$$R \leq \sum_{i=1}^M \sum_{j=1}^M a_i a_j \left(1 - \frac{|\tau_i - \tau_j|}{2T} \right) \quad (2-53)$$

Again it is clear that this approaches the bound of (2-46) when T is large.

2.1.7. Sub-Optimum Signals: Multiple-Frequency Pulsed Sinusoids

Although there is no clear indication that using more than one frequency provides any advantage, it is possible to determine the time-ambiguity for such a situation. In this case the transmitted signal is defined as

$$e(t) = \sum_{\ell=1}^N c_{\ell} \cos \omega_{\ell} t, \quad |t| \leq T$$

$$= 0, \quad |t| > T \quad (2-54)$$

in which there are N different frequencies with different amplitudes. The time-ambiguity function for this signal may be written as

$$R_e(\tau) = \int_{-T}^{T-\tau} \sum_{\ell=1}^N \sum_{k=1}^N c_{\ell} c_k \cos \omega_{\ell} t \cos \omega_k (t+\tau) dt \quad (2-55)$$

There is an additional constraint on the amplitude of the coefficients to meet the signal energy requirements. Namely,

$$R_e(0) = E_0 \quad (2-56)$$

Evaluation of (2-55) yields

$$R_e(\tau) = T \sum_{\ell=1}^N \sum_{k=1}^N c_{\ell} c_k \left\{ \frac{\sin[(\omega_{\ell} + \omega_k)(T - \frac{|\tau|}{2})]}{(\omega_{\ell} + \omega_k)T} \cos \frac{1}{2} (\omega_{\ell} - \omega_k) \tau \right.$$

$$\left. + \frac{\sin[(\omega_{\ell} - \omega_k)(T - \frac{|\tau|}{2})]}{(\omega_{\ell} - \omega_k)T} \cos \frac{1}{2} (\omega_{\ell} + \omega_k) \tau \right\} \quad (2-57)$$

and the condition of (2-56) becomes

$$T \sum_{\ell=1}^N \sum_{k=1}^N c_{\ell} c_k \left\{ \frac{\sin(\omega_{\ell} + \omega_k)T}{(\omega_{\ell} + \omega_k)T} + \frac{\sin(\omega_{\ell} - \omega_k)T}{(\omega_{\ell} - \omega_k)T} \right\} = E_0 \quad (2-58)$$

Several computations were performed for the case in which $N = 2$ but no results were found that were superior, or even equal, to the single frequency sinusoidal pulse.

2.1.8. Optimum Orthonormal Signal Expansion

The failure of the fundamental optimizing equation, (2-48), to yield explicit solutions emphasizes the need to consider an alternative approach to seeking optimum signal waveforms. The approach considered here is both elegant and powerful but somewhat limited in its usefulness because of computational constraints. Nevertheless, it is worthy of consideration because the computational results that have been obtained suggest that the rectangular envelope sinusoidal pulse is very nearly optimum as discussed in a previous section.

In this formulation the transmitted signal is represented by means of the expansion

$$\begin{aligned} e(t) &= \sum_{n=1}^{\infty} c_n \phi_n(t) \quad , \quad |t| \leq T \\ &= 0 \quad , \quad |t| > T \end{aligned} \quad (2-59)$$

where the $\phi_n(t)$ are orthonormal on the interval $[-T, T]$. That is

$$\begin{aligned} \int_{-T}^T \phi_n(t) \phi_m(t) dt &= 1 \quad , \quad n = m \\ &= 0 \quad , \quad n \neq m \end{aligned} \quad (2-60)$$

Thus, the time-ambiguity function can be written as

$$R_e(\tau) = \sum_{n=1}^{\infty} \sum_{m=1}^{\infty} c_n c_m \int_{-\infty}^{\infty} \phi_n(t) \phi_m(t+\tau) dt \quad (2-61)$$

in which it is specified that $\phi_m(t) = 0$, $|t| > T$.

This can be expressed in matrix form by defining

$$\gamma_{nm}(\tau) = \int_{-\infty}^{\infty} \phi_n(t) \phi_m(t+\tau) dt \quad (2-62)$$

as the (n,m) element of an infinite-order square matrix

$$\underline{\Gamma}(\tau) = \begin{bmatrix} \gamma_{11}(\tau) & \gamma_{12}(\tau) & \dots \\ \gamma_{21}(\tau) & \gamma_{22}(\tau) & \dots \\ \vdots & \vdots & \ddots \end{bmatrix} \quad (2-63)$$

Note that because of the orthonormality, $\gamma_{nm}(0) = \delta_{nm}$, the Kronecker delta, and $\underline{\Gamma}(0) = \underline{I}$, an infinite-order identity matrix. Also define the coefficient vector as

$$\underline{c} = \begin{bmatrix} c_1 \\ c_2 \\ \vdots \end{bmatrix} \quad (2-64)$$

Hence, (2-61) becomes

$$R_e(\tau) = \underline{c}^T \underline{\Gamma}(\tau) \underline{c} \quad (2-65)$$

The optimization problem may now be stated as the requirement to maximize the quantity

$$\sum_{i=1}^M \sum_{j=1}^M a_i a_j R_e(\tau_j - \tau_i)$$

subject to the constraint $R_e(0) = E_0$. Thus, the energy ratio is

$$R = \frac{\sum_{i=1}^M \sum_{j=1}^M a_i a_j \underline{c}^T \underline{\Gamma}(\tau_j - \tau_i) \underline{c}}{\underline{c}^T \underline{\Gamma}(0) \underline{c}} = \frac{\underline{c}^T \underline{A} \underline{c}}{\underline{c}^T \underline{\Gamma}(0) \underline{c}} \quad (2-66)$$

where

$$\underline{A} = \sum_{i=1}^M \sum_{j=1}^M a_i a_j \underline{\Gamma}(\tau_j - \tau_i)$$

Note that once the orthonormal basis functions are defined, \underline{A} becomes completely known.

Maximizing a ratio of quadratic forms, as in (2-66), is a well-known eigenvalue problem whose solution is yielded by the Rayleigh-Ritz criterion. Specifically:

- 1) The maximum value of R is equal to the largest eigenvalue of $\underline{\Gamma}^{-1}(0) \underline{A}$. Since $\underline{\Gamma}(0) = \underline{I}$, this reduces to finding the largest eigenvalue of \underline{A} .
- 2) The optimum coefficient vector \underline{C} , that will yield the maximum value of R , is the eigenvector of \underline{A} corresponding to the largest eigenvalue.

The obvious difficulty in applying the above elegant result to a practical situation is the impossibility of manipulating infinite-order matrices. The practical solution to this difficulty is to limit the number of basis functions to a finite quantity. Constraints imposed by standard computer programs for finding eigenvalues and eigenvectors set this limit at about 100, although it could certainly be increased by special programming.

A modification of this approach is to assume that $e(t)$ is an amplitude modulated carrier of the form

$$\begin{aligned} e(t) &= \sum_{n=1}^{\infty} c_n \phi_n(t) \cos \omega_0 t, & |t| < T \\ &= 0, & |t| > 0 \end{aligned} \quad (2-67)$$

If T is picked to be an integral number of cycles of ω_0 , the time-ambiguity function can be expressed as

$$R_e(\tau) = \frac{1}{2} \cos \omega_0 \tau \underline{C}^T \underline{\Gamma}(\tau) \underline{C} \quad (2-68)$$

The energy ratio R can once more be expressed as

$$R = \frac{\underline{C}^T \underline{B} \underline{C}}{\underline{C}^T \underline{\Gamma}(0) \underline{C}} \quad (2-69)$$

$$\text{where } \underline{B} = \sum_{i=1}^M \sum_{j=1}^M a_i a_j \Gamma(\tau_j - \tau_i) \cos \omega_0(\tau_j - \tau_i).$$

Since \underline{B} is again completely known, the previously stated solution still applies. Namely:

- 1) The maximum value of R is the largest eigenvalue of \underline{B} .
- 2) The optimum \underline{c} is the corresponding eigenvector of \underline{B} .

Since this modified form results in basis functions having a smaller center frequency (the carrier term does not have to be included in the basis function), it is somewhat easier to compute than the more general form. In fact, it is this form that is used to provide the computational results discussed previously.

2.2. COMPUTATIONAL RESULTS

This chapter presents the results of extensive computation in somewhat more complete form. The selected results of Chapter 1.2 are repeated here along with additional computations of the same type.

2.2.1. Computational Methods

It is shown in Chapter 2.1 that all of the analytical results depend only upon the differences in delays corresponding to all pairs of reflecting points. This being the case it is not necessary to calculate absolute delay values. Instead, the delay associated with any reflecting point can be referred to an arbitrary reference point. A convenient reference point is the origin of the coordinate system used to describe the location of the target reflecting points.

The coordinate system and an arbitrary reflecting point are shown in Figure 2.5. The i th reflecting point is located at (x_i, y_i) and its delay,

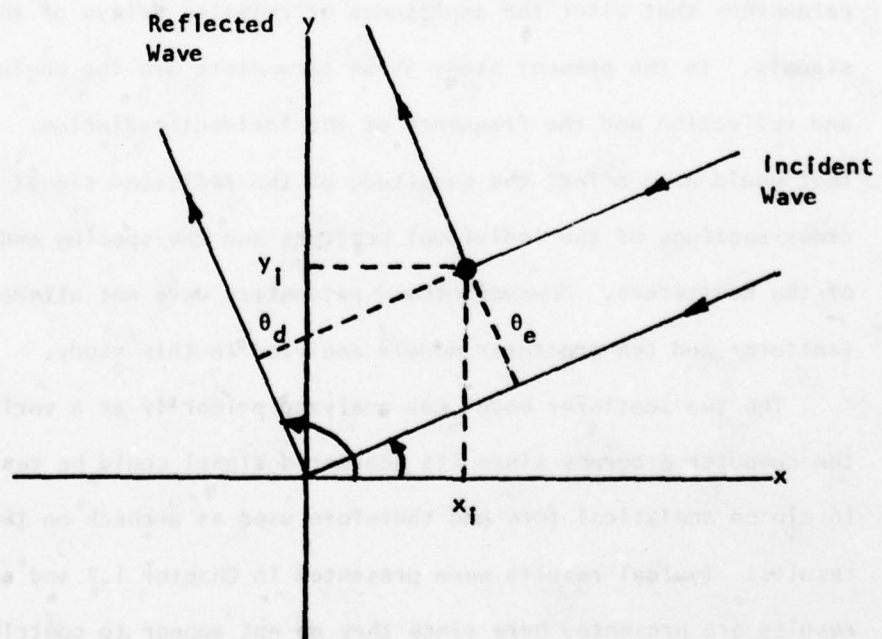


Figure 2.5. Illustrating the computation of delay values.

relative to the origin, is clearly given by the sum of its projections on the incident and reflected rays passing through the origin. The projection on the incident ray is $(x_i \cos \theta_e + y_i \sin \theta_e)$ while the projection on the reflected ray is $(x_i \cos \theta_d + y_i \sin \theta_d)$. Thus, the delay τ_i is

$$\tau_i = -\frac{1}{c} [x_i (\cos \theta_e + \cos \theta_d) + y_i (\sin \theta_e + \sin \theta_d)] \quad (2-70)$$

The fact that some delays are negative relative to the origin is of no consequence since only delay differences are required.

Once the τ_i are determined for given angles of incidence and reflection, the remaining calculations are straightforward. The only practical problem that arises is a consequence of the very rapid variations that occur with very small changes in angle or frequency. This rapid variation requires that computations be performed for many very closely spaced conditions in order to be able to plot the results.

The magnitude of the reflected signal is affected by variation of any parameters that alter the amplitudes or relative delays of the scattered signals. In the present study these parameters are the angles of incidence and reflection and the frequency of the incident radiation. Other parameters that would also affect the magnitude of the reflected signal are the radar cross-sections of the individual scatters and the spacing and configuration of the scatterers. However, these parameters were not altered in the two scatterer and ten scatterer models analyzed in this study.

The two scatterer model was analyzed primarily as a verification of the computer programs since its scattered signal could be readily expressed in closed analytical form and therefore used as a check on the computed results. Typical results were presented in Chapter 1.2 and no additional results are presented here since they do not appear to contribute significantly to the problem under study.

Many combinations of the parameters for the 10-point target were analyzed and a number of them are presented here as a supplement to the results given in Chapter 1.2. In all cases the ordinate of the graphs is a quantitative measure of the reflection properties of the target. The three quantities used are: D , the ratio of reflected to incident radiation (expressed in dB) for the CW case; R , the ratio of reflected energy to incident energy (expressed in dB) for the finite energy case; and $|H(f)|^2$, the squared magnitude of the target power transfer function at frequency f .

2.2.2. CW Signals

Figures 2-6a through o show the squared magnitude of the power transfer function of the 10-point target as a function of frequency for various viewing angles. The frequency ranges from 1 to 10 GHz and the viewing angles range from 0° to 90° . The spacings and amplitude of the maxima of $|H(f)|^2$ are clearly a function of the target viewing angle and vary over wide ranges.

Figure 2-7 shows $|H(f)|^2$ as a function of viewing angle for one of the frequencies at which a maximum at $\theta_0 = 0$ was found in Figure 2-6; viz., 1.04926419 GHz. It is evident that the maximum is very short and is not repeated in the 90° viewing angle shown.

Figure 2-8 shows $|H(f)|^2$ as a function of frequency using an expanded frequency scale to illustrate more clearly the fine structure of the power transfer function of the 10-point target. In this frequency interval $|H(f)|^2$ reaches about 70% (-1.5 dB) of its theoretical maximum of 100.

Figures 2-9a through q and 2-10a through q are plots of the power ratio versus viewing angle for the 10-point target at 1 GHz and 10 GHz respectively. The angular segments from 70° - 80° for these two figures are presented in Chapter 1.2 as Figures 1-5 and 1-6 respectively. The rapid variation in the magnitude of the backscattered power with viewing angle is clearly evident in these figures with the excursions being more rapid and of generally larger magnitude for the shorter wavelength radiation. Only occasionally

MAG SQUARED OF H VS FREQUENCY
THETA E = THETA D = 0 DEGREES
10 REFLECTING POINTS

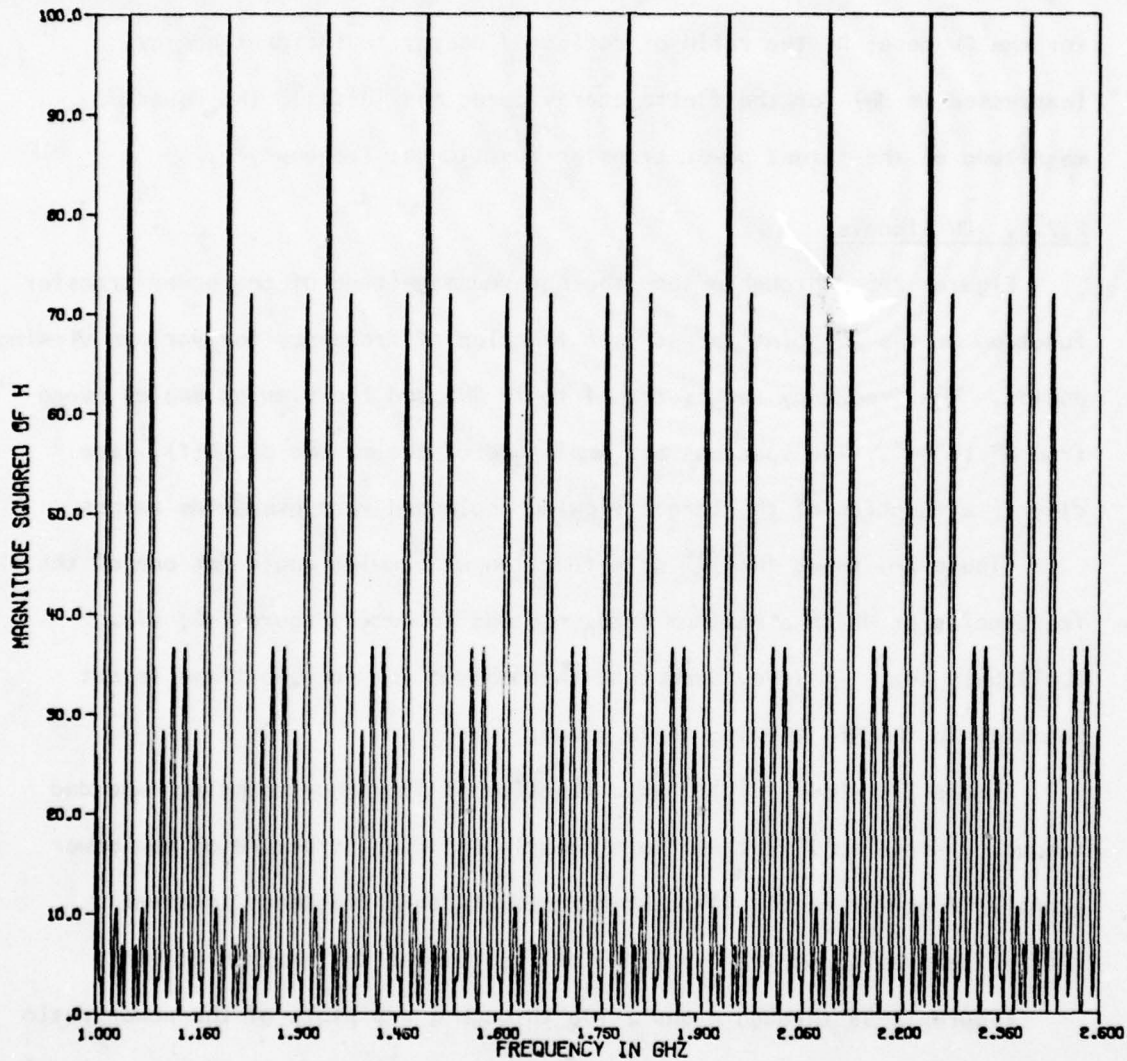


Figure 2-6a. $|H(f)|^2$ versus frequency for the 10-point target.

MAG SQUARED OF H VS FREQUENCY
THETA E = THETA D = 30 DEGREES
10 REFLECTING POINTS

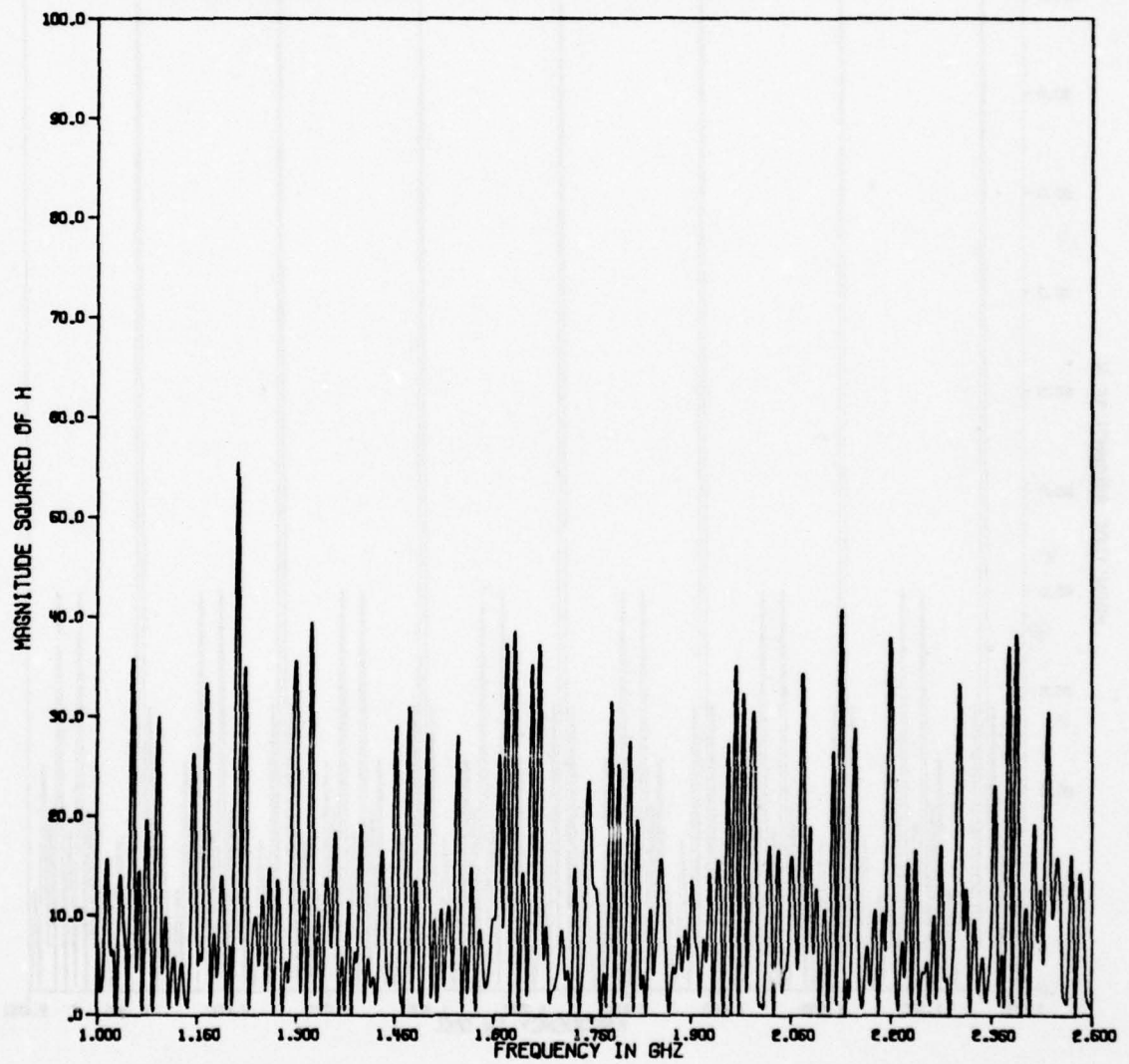


Figure 2-6b. $|H(f)|^2$ versus frequency for the 10-point target.

MAG SQUARED OF H VS FREQUENCY
THETA E = THETA D = 45 DEGREES
10 REFLECTING POINTS

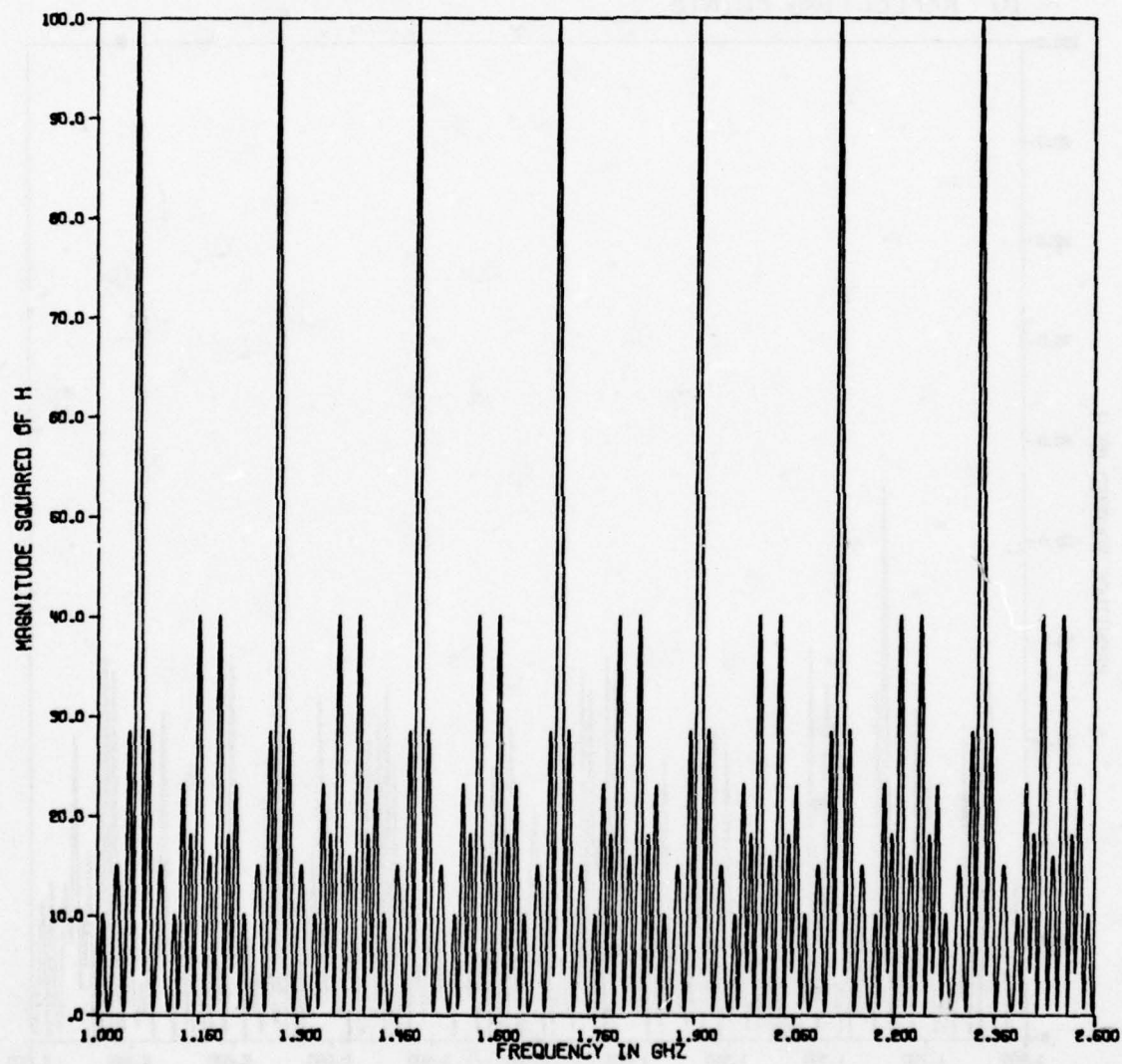


Figure 2.6c. $|H(f)|^2$ versus frequency for the 10-point target.

MAG SQUARED OF H VS FREQUENCY
THETA E = THETA D = 60 DEGREES
10 REFLECTING POINTS

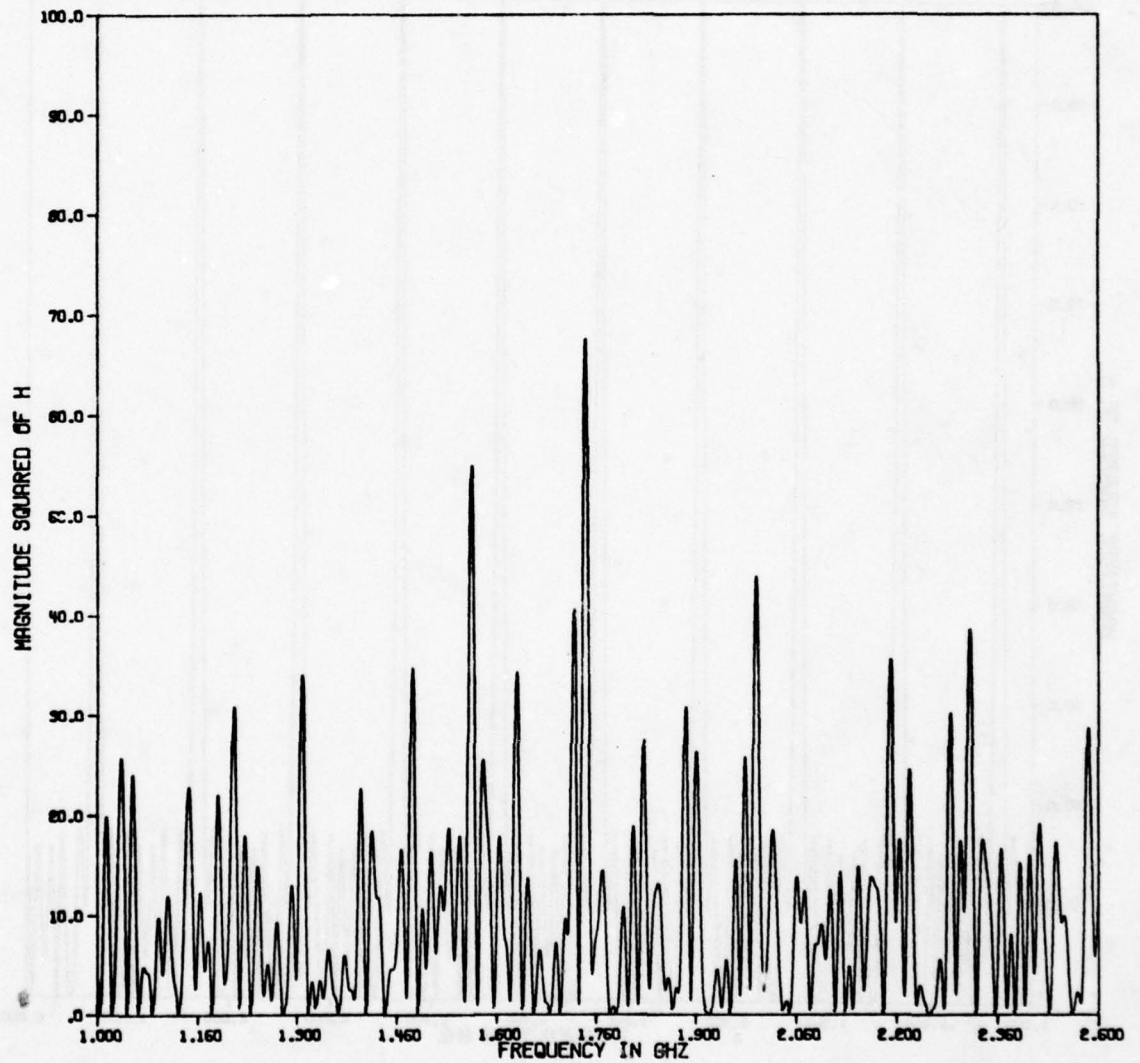


Figure 2-6d. $|H(f)|^2$ versus frequency for the 10-point target.

MAG SQUARED OF H VS FREQUENCY
THETA E = THETA D = 90 DEGREES
10 REFLECTING POINTS

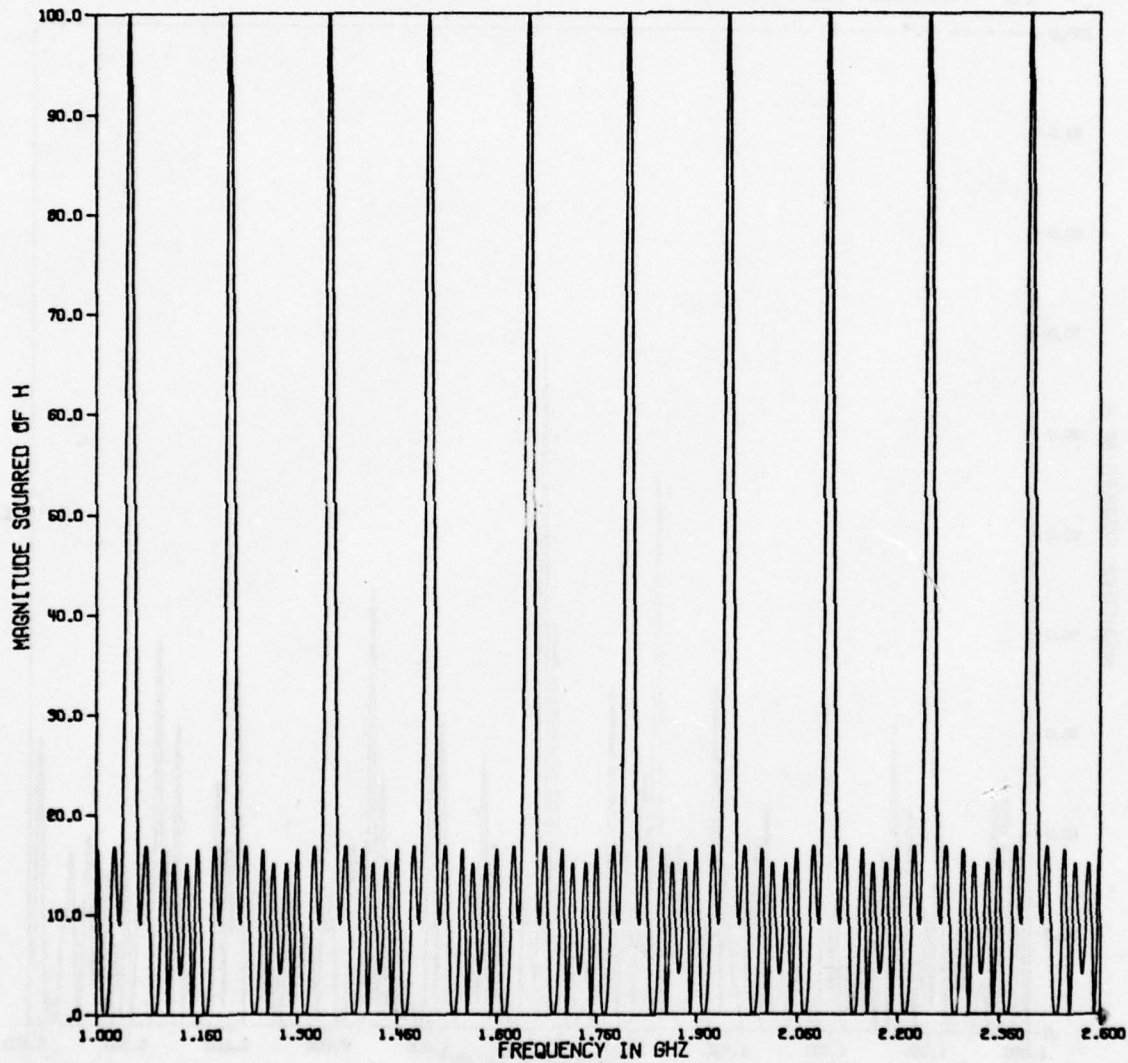


Figure 2-6e. $|H(f)|^2$ versus frequency for the 10-point target.

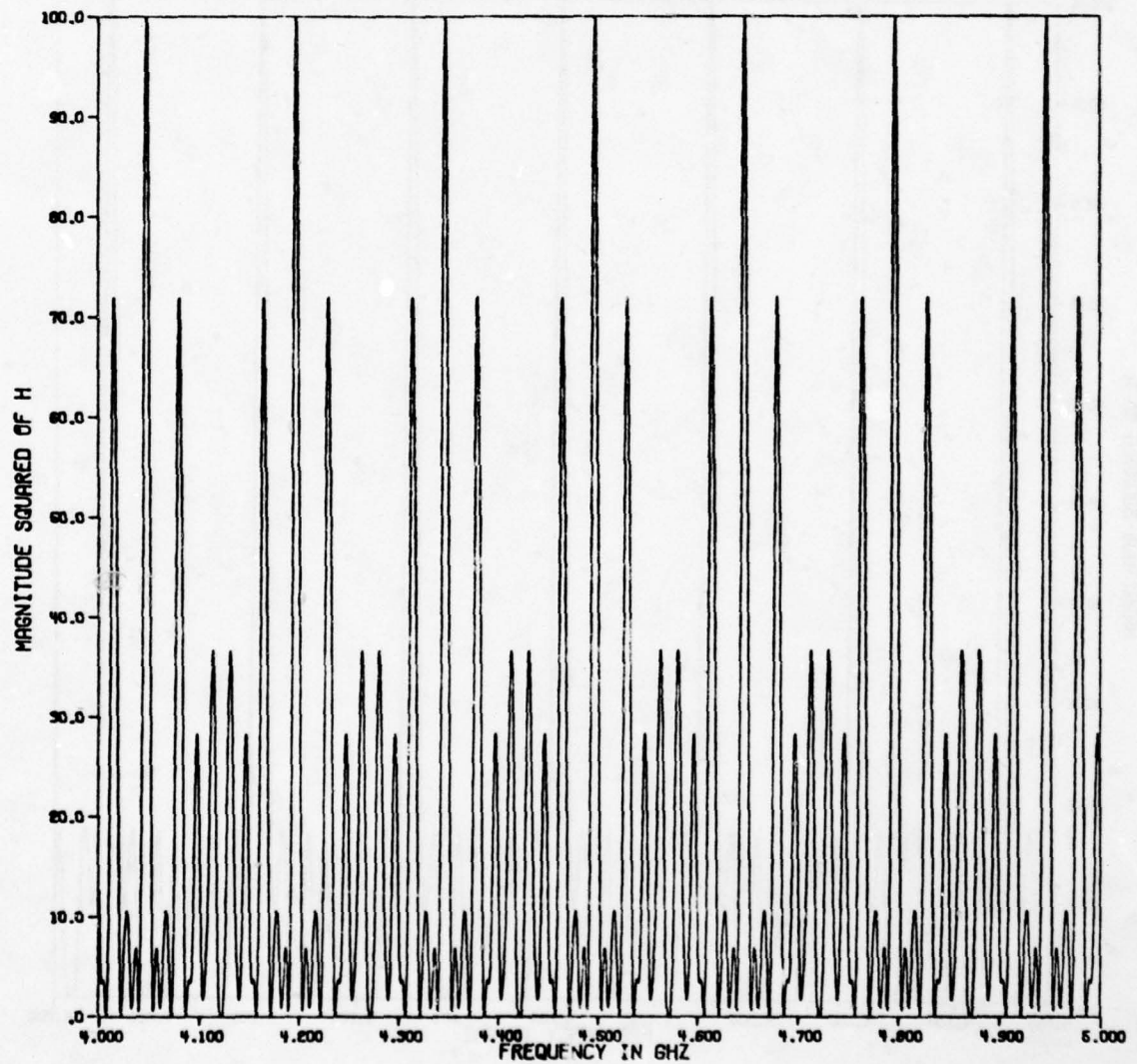


Figure 2-6f. $|H(f)|^2$ versus frequency for the 10-point target.

MAG SQUARED OF H VS FREQUENCY
THETA E = THETA D = 90 DEGREES
10 REFLECTING POINTS

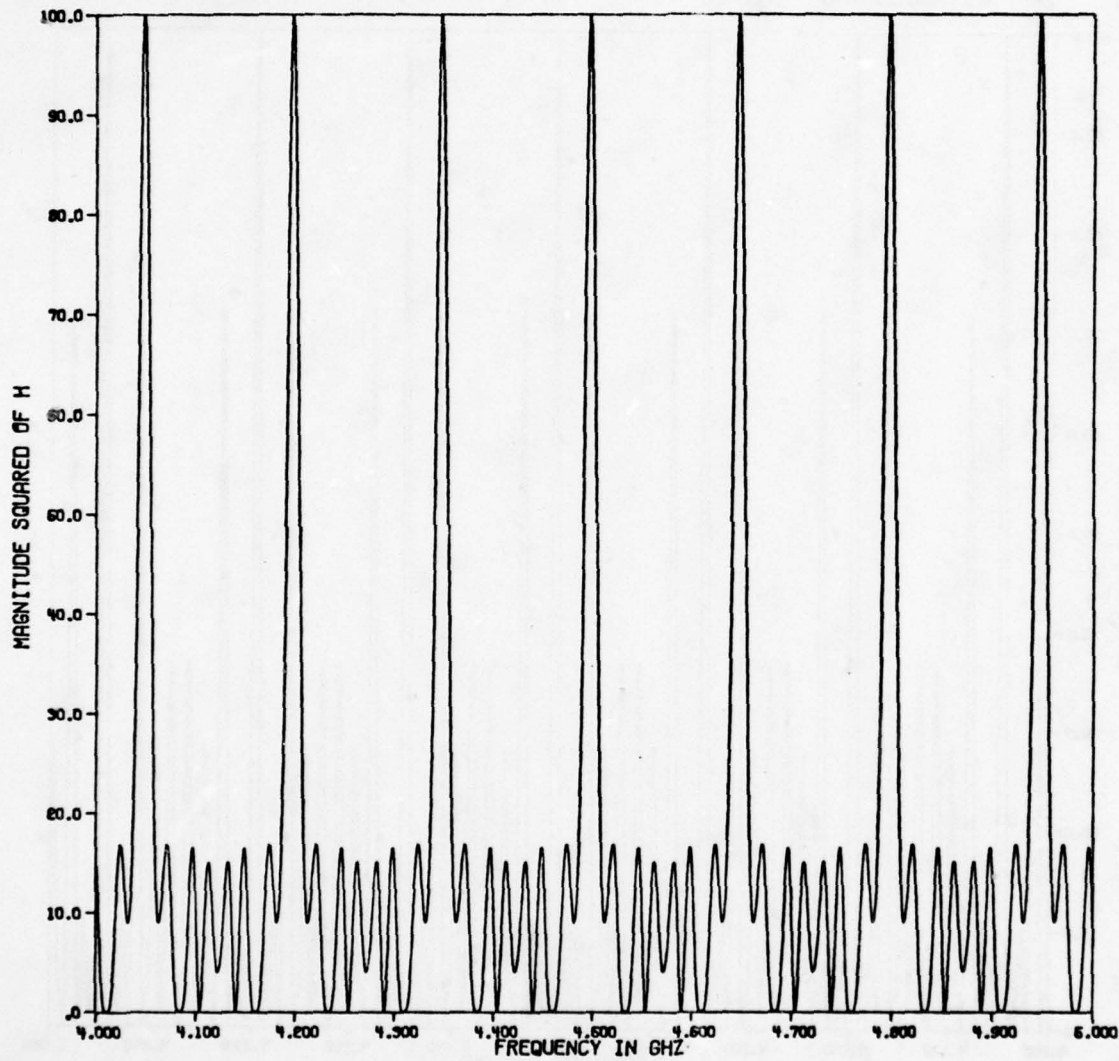


Figure 2-6g. $|H(f)|^2$ versus frequency for the 10-point target.

MAG SQUARED OF H VS FREQUENCY
THETA E = THETA D = 0 DEGREES
10 REFLECTING POINTS

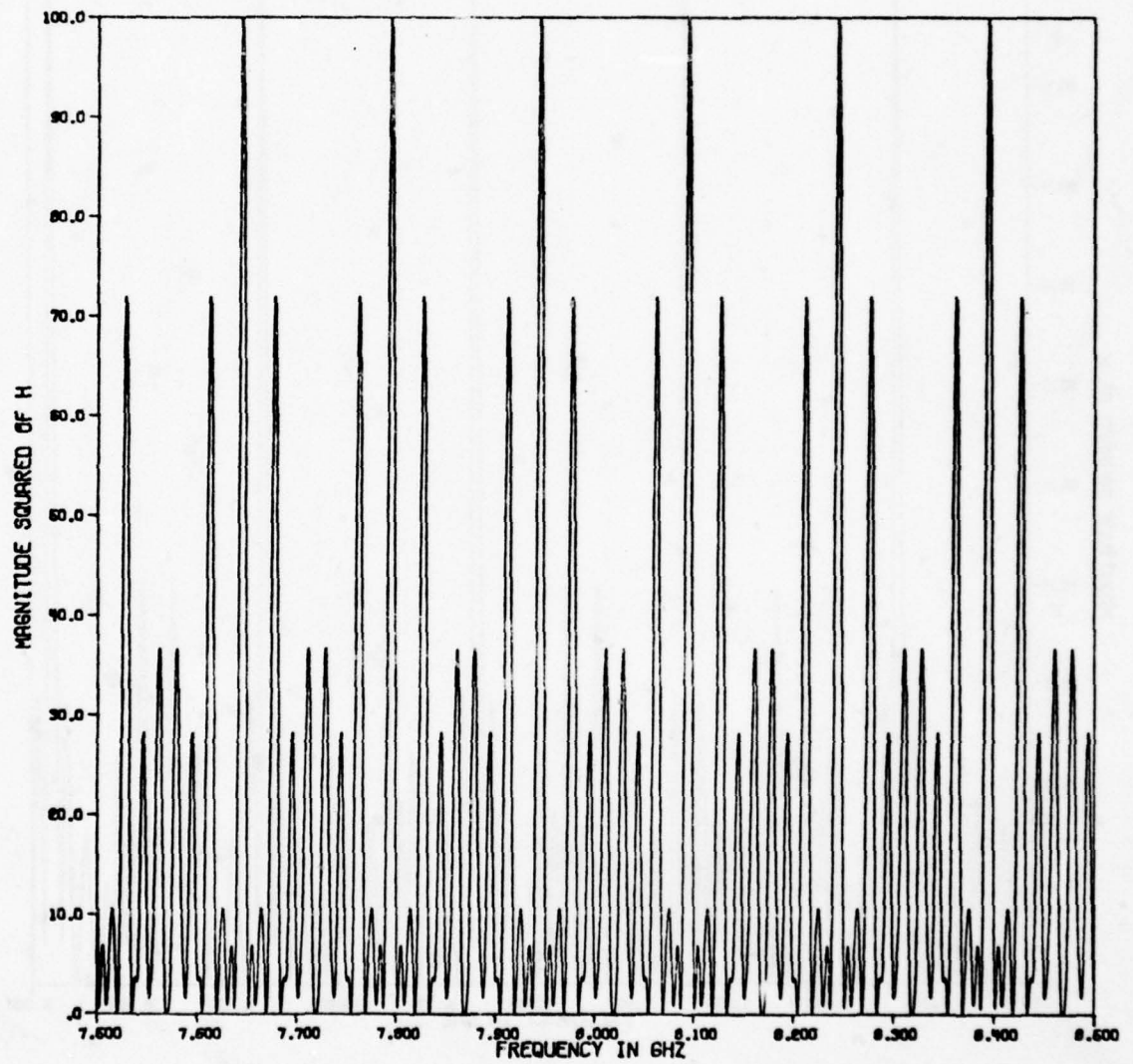


Figure 2-6h. $|H(f)|^2$ versus frequency for the 10-point target.

MAG SQUARED OF H VS FREQUENCY
THETA E = THETA D = 45 DEGREES
10 REFLECTING POINTS

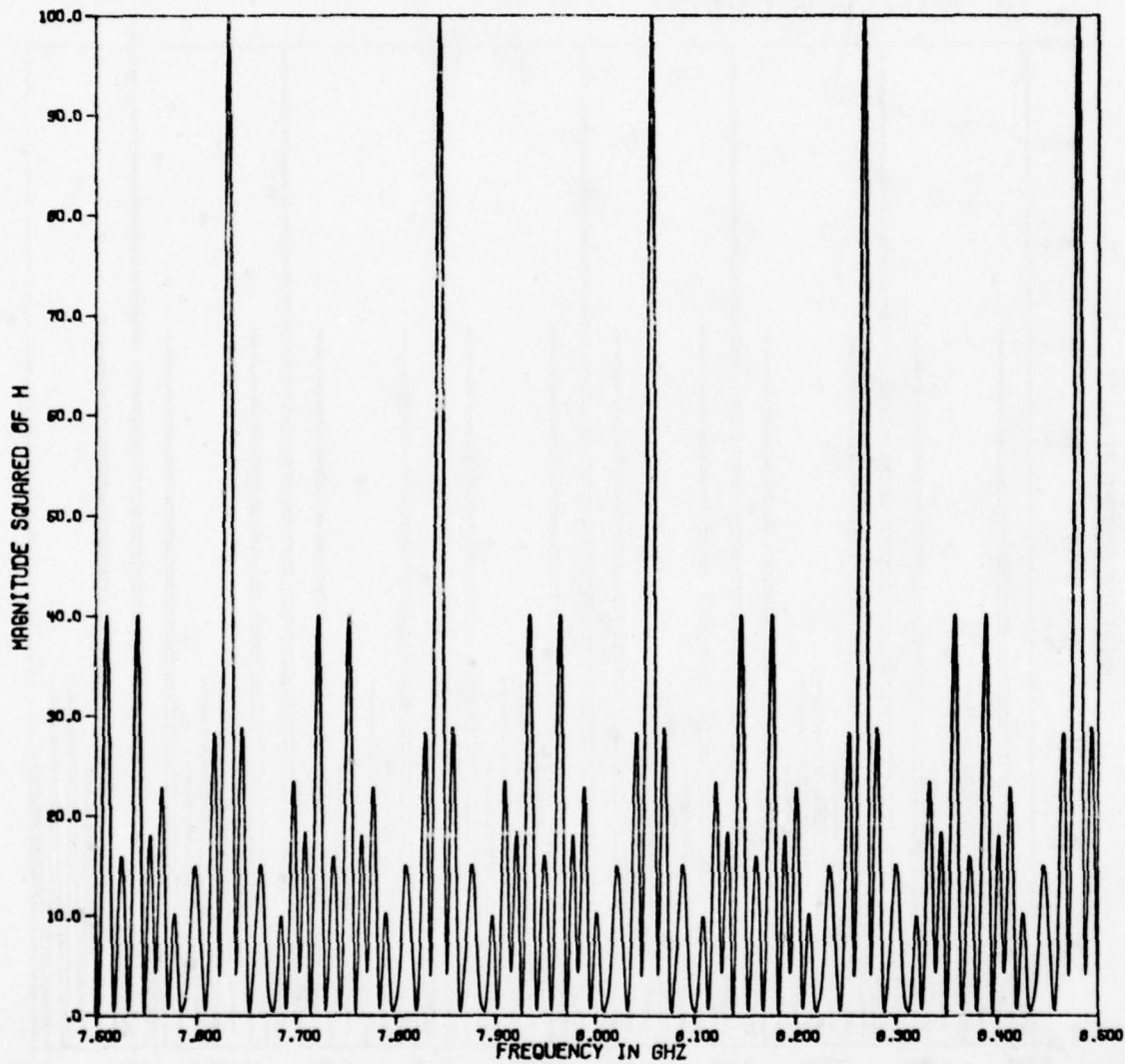


Figure 2-61. $|H(f)|^2$ versus frequency for the 10-point target.

MAG SQUARED OF H VS FREQUENCY
THETA E = THETA D = 90 DEGREES
10 REFLECTING POINTS

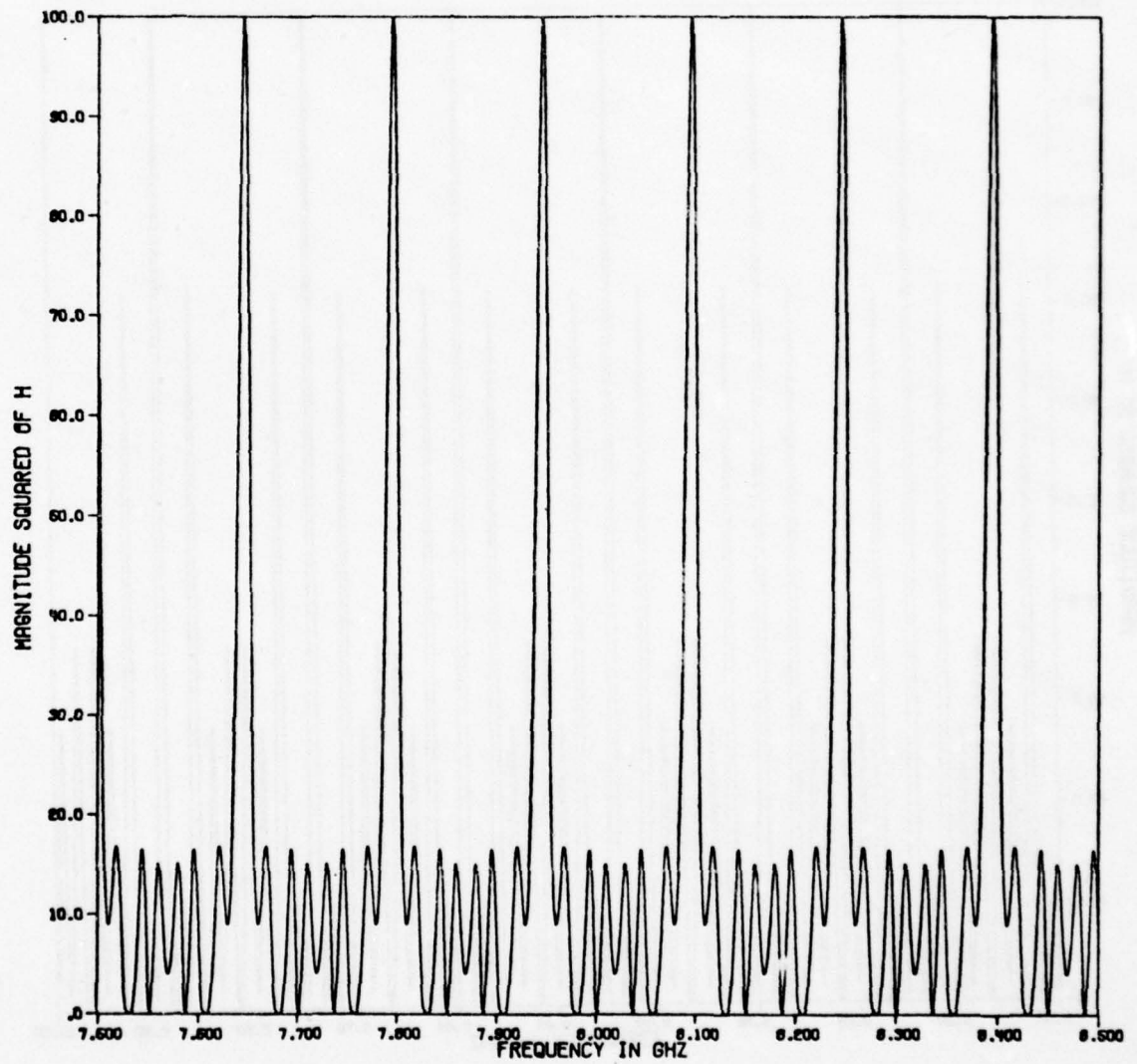


Figure 2-6j. $|H(f)|^2$ versus frequency for the 10-point target.

MAG SQUARED OF H VS FREQUENCY
THETA E = THETA D = 0 DEGREES
10 REFLECTING POINTS

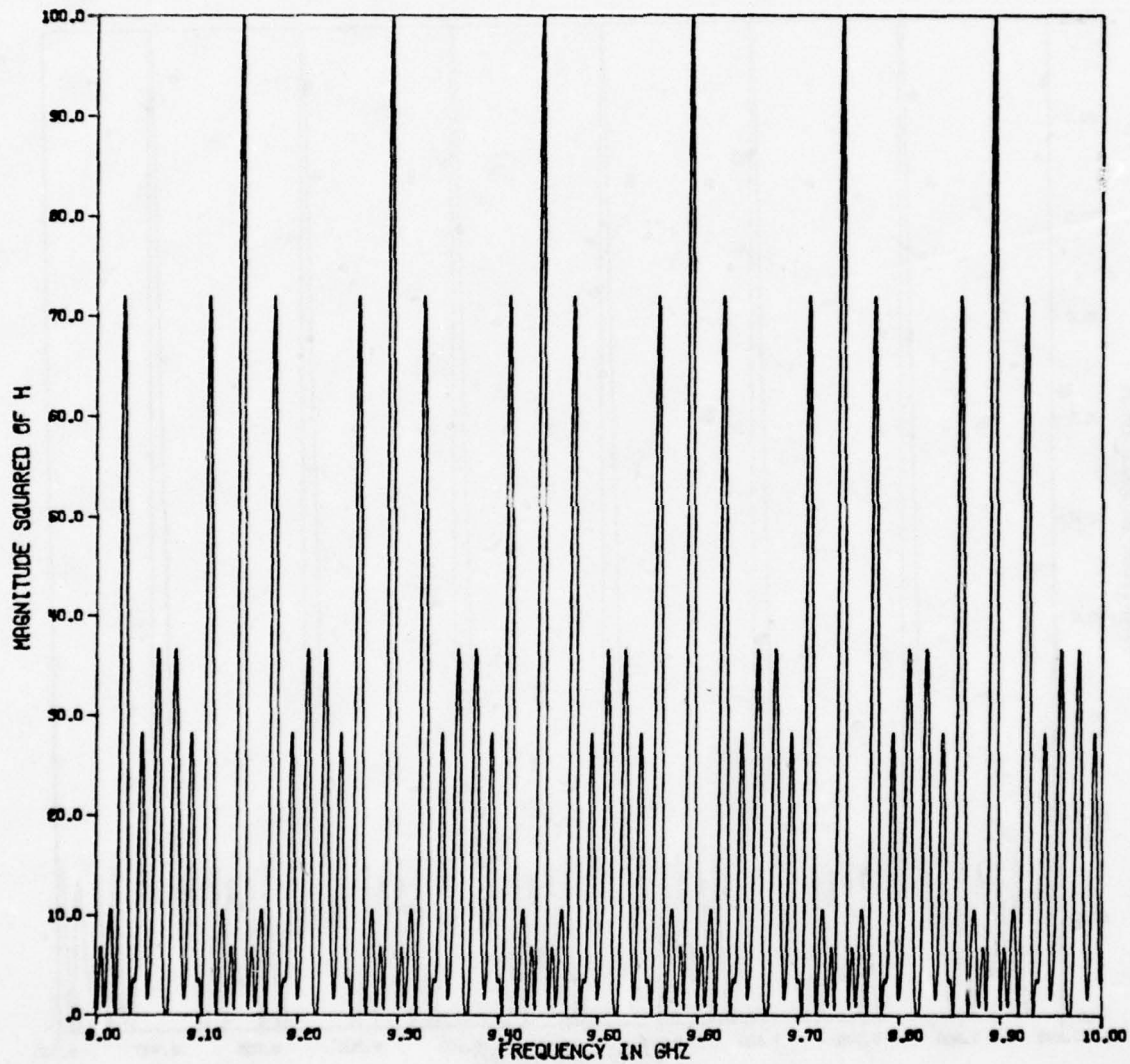


Figure 2-6k. $|H(f)|^2$ versus frequency for the 10-point target.

MAG SQUARED OF H VS FREQUENCY
THETA E = THETA D = 30 DEGREES
10 REFLECTING POINTS

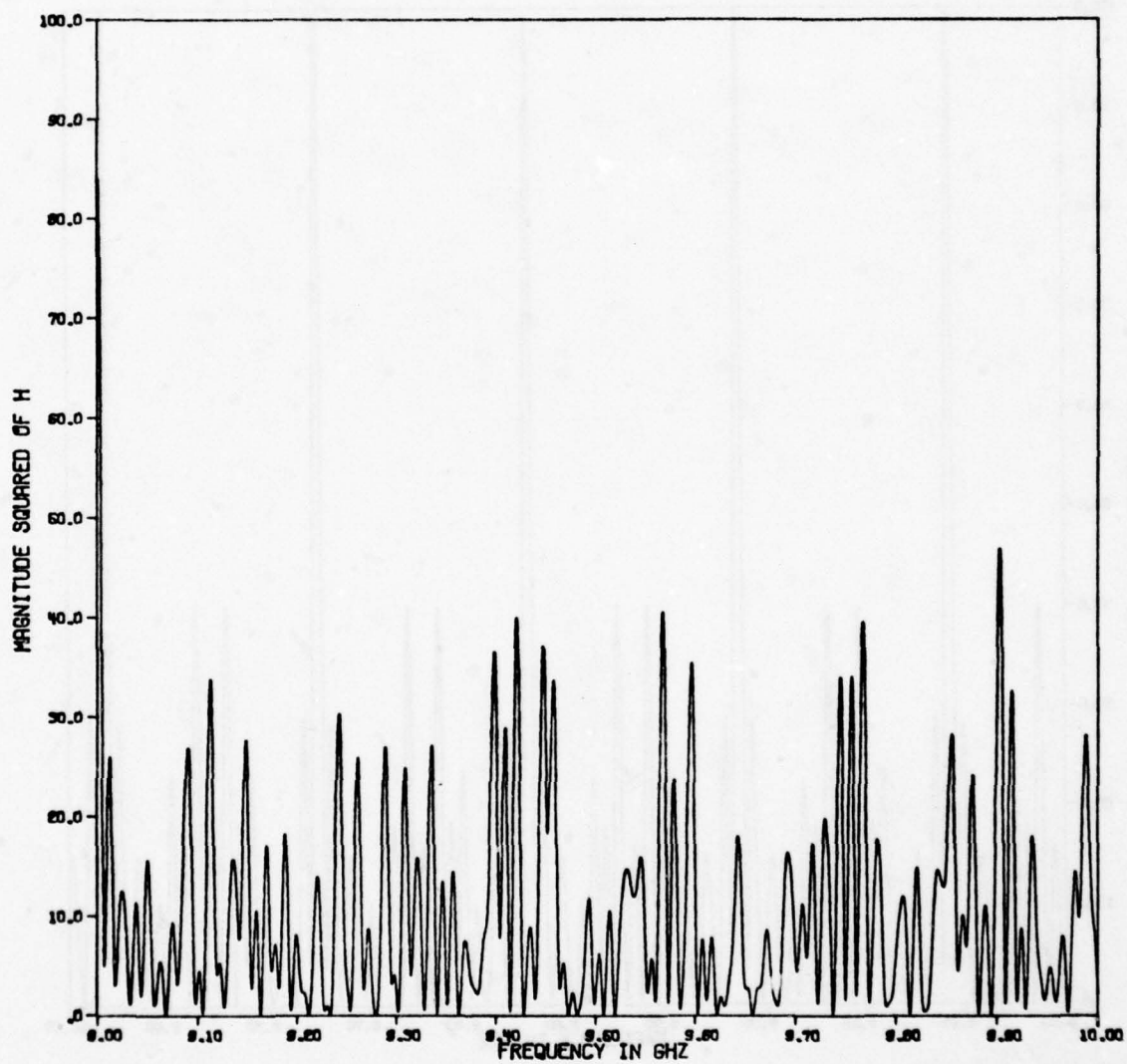


Figure 2-61. $|H(f)|^2$ versus frequency for the 10-point target.

MAG SQUARED OF H VS FREQUENCY
THETA E = THETA D = 45 DEGREES
10 REFLECTING POINTS

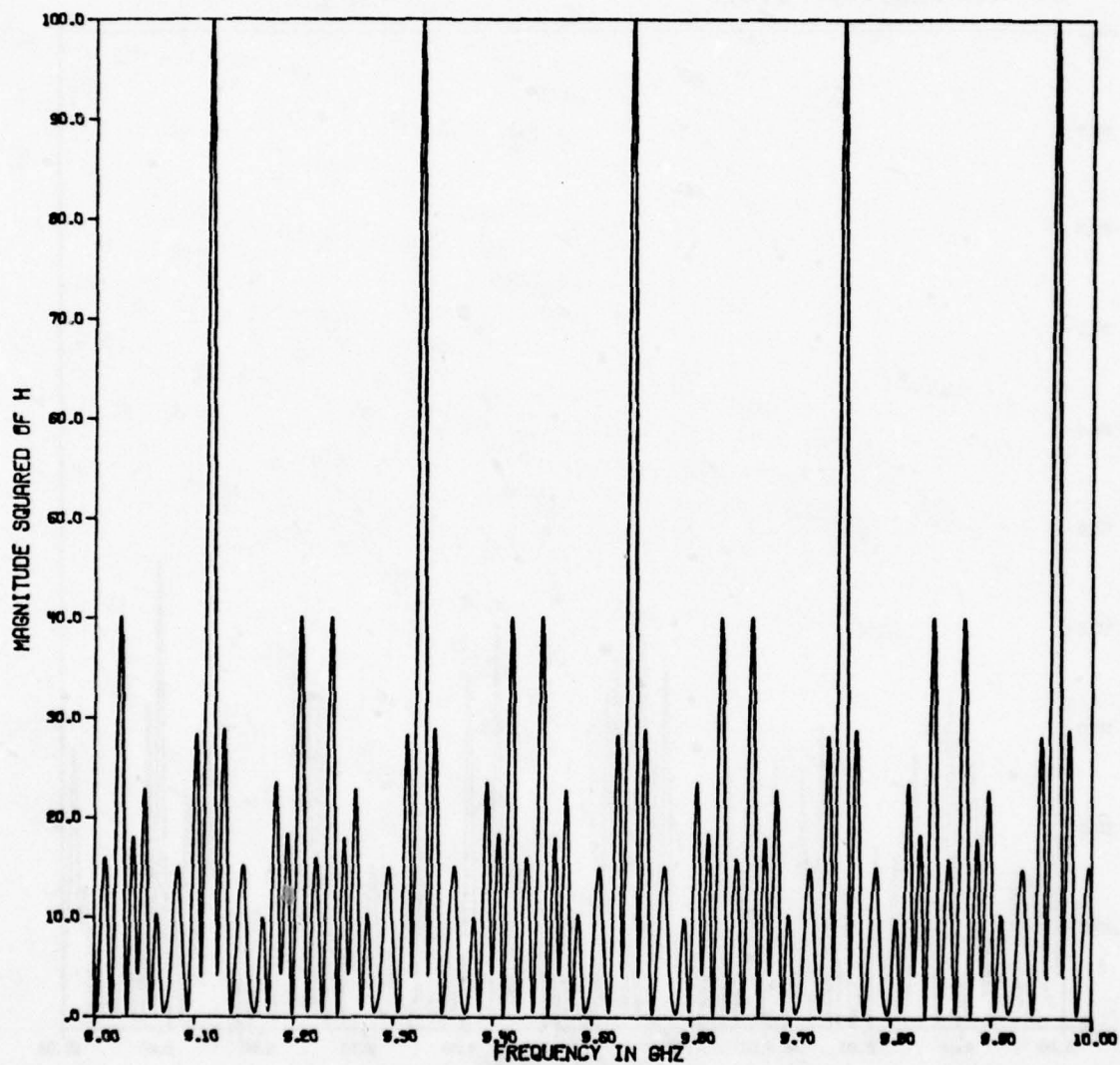


Figure 2-6m. $|H(f)|^2$ versus frequency for the 10-point target.

MAG SQUARED OF H VS FREQUENCY
THETA E = THETA D = 60 DEGREES
10 REFLECTING POINTS

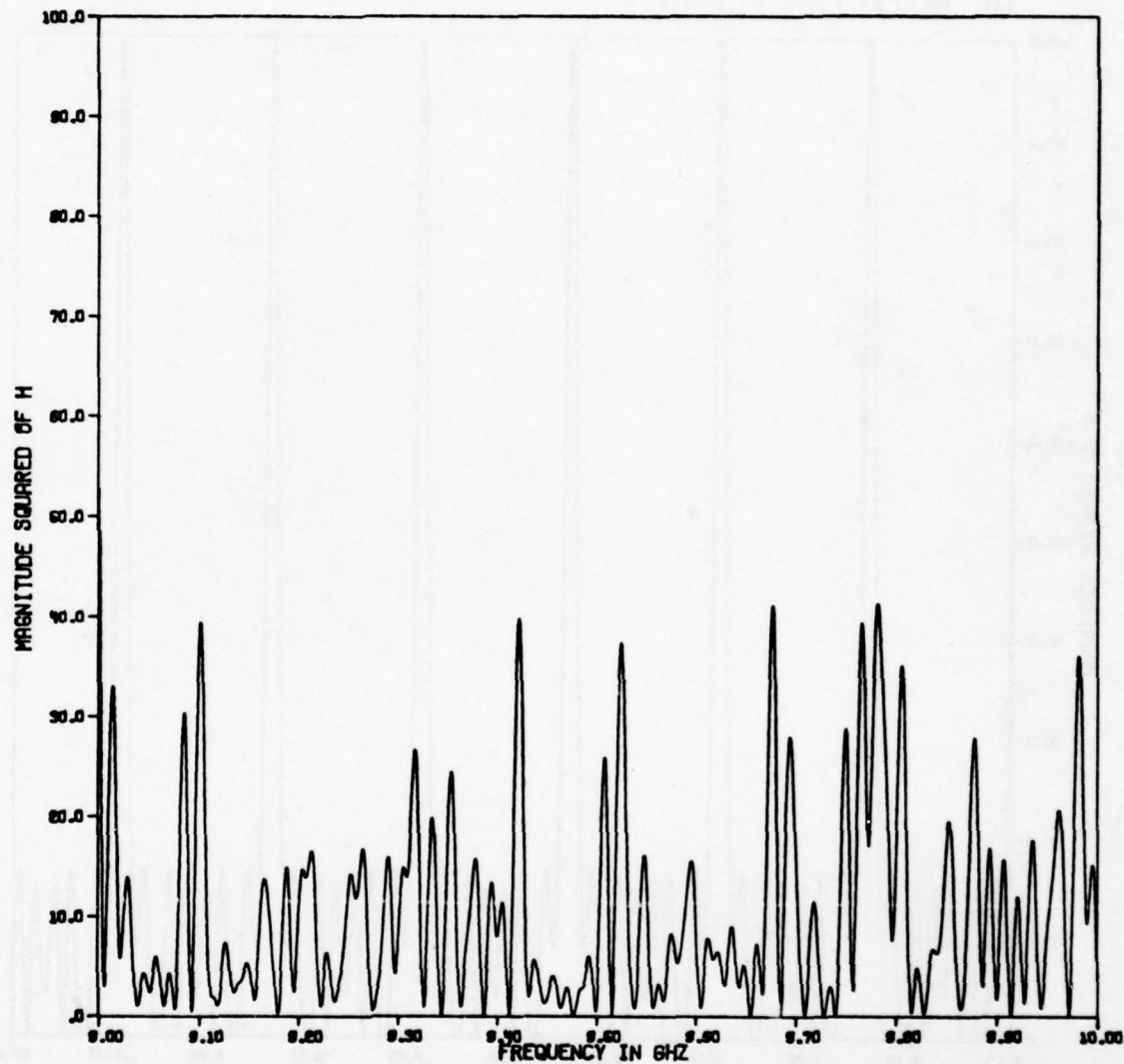


Figure 2-6n. $|H(f)|^2$ versus frequency for the 10-point target.

MAG SQUARED OF H VS FREQUENCY
THETA E = THETA D = 90 DEGREES
10 REFLECTING POINTS

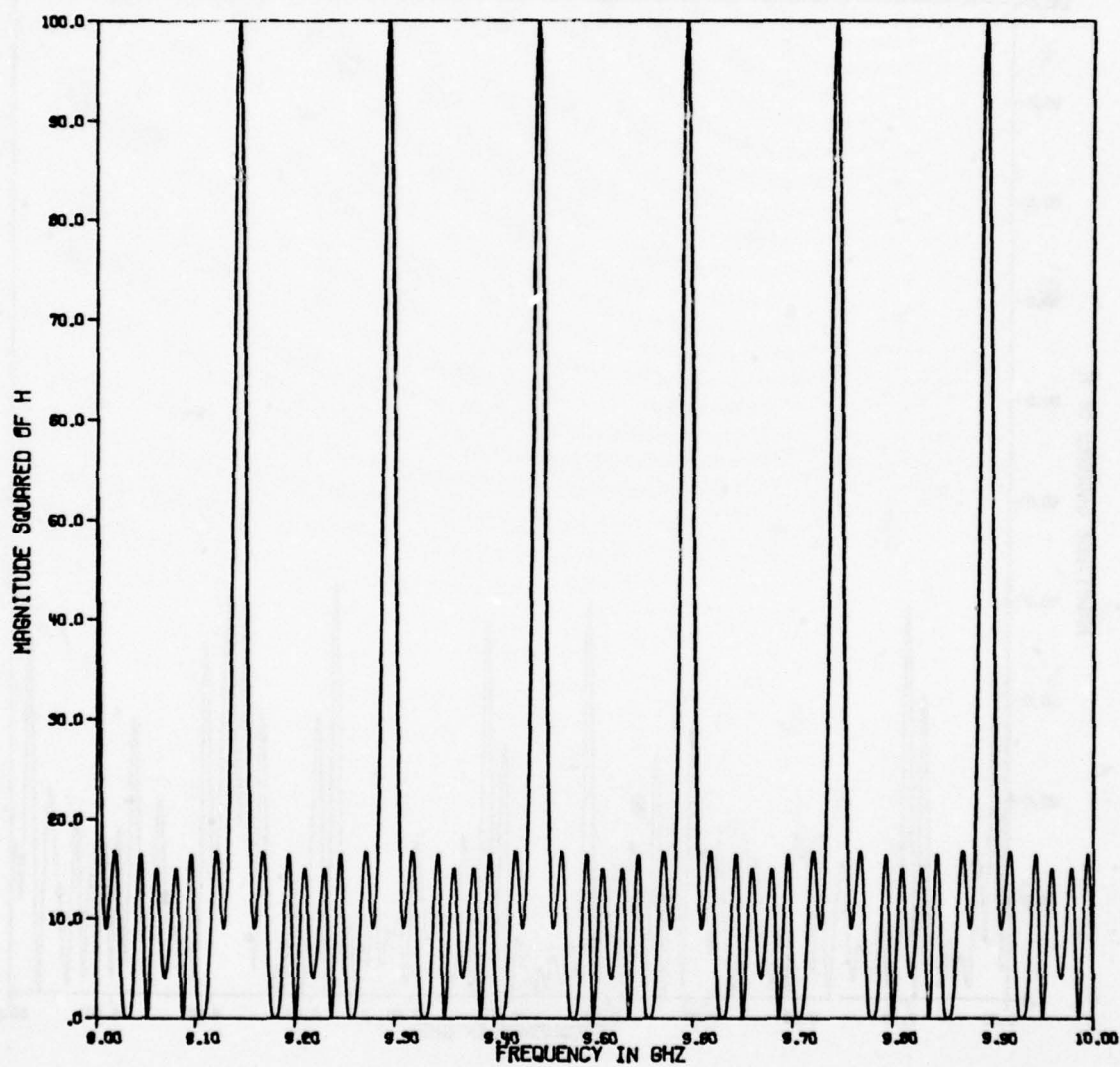


Figure 2-60. $|H(f)|^2$ versus frequency for the 10-point target.

MAG SQUARED OF H VS DETECTOR ANGLE
THETA E = 0 DEGREES
FREQUENCY = 1.04926419 GHZ
10 REFLECTING POINTS

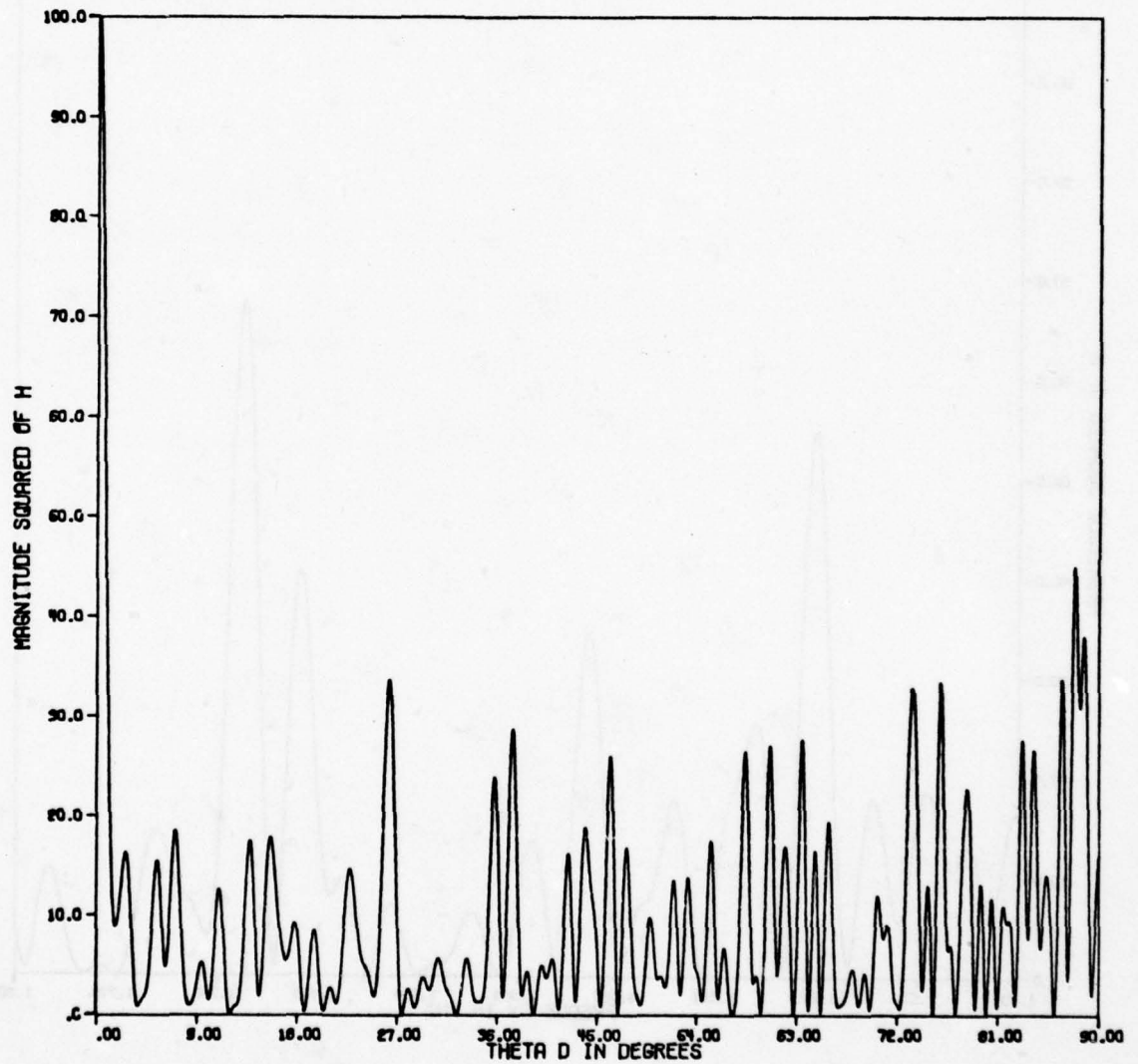


Figure 2-7. $|H(f)|^2$ versus viewing angle for 10-point target.

MAG SQUARED OF H VS FREQUENCY
THETA E = THETA D = 60 DEGREES
10 REFLECTING POINTS

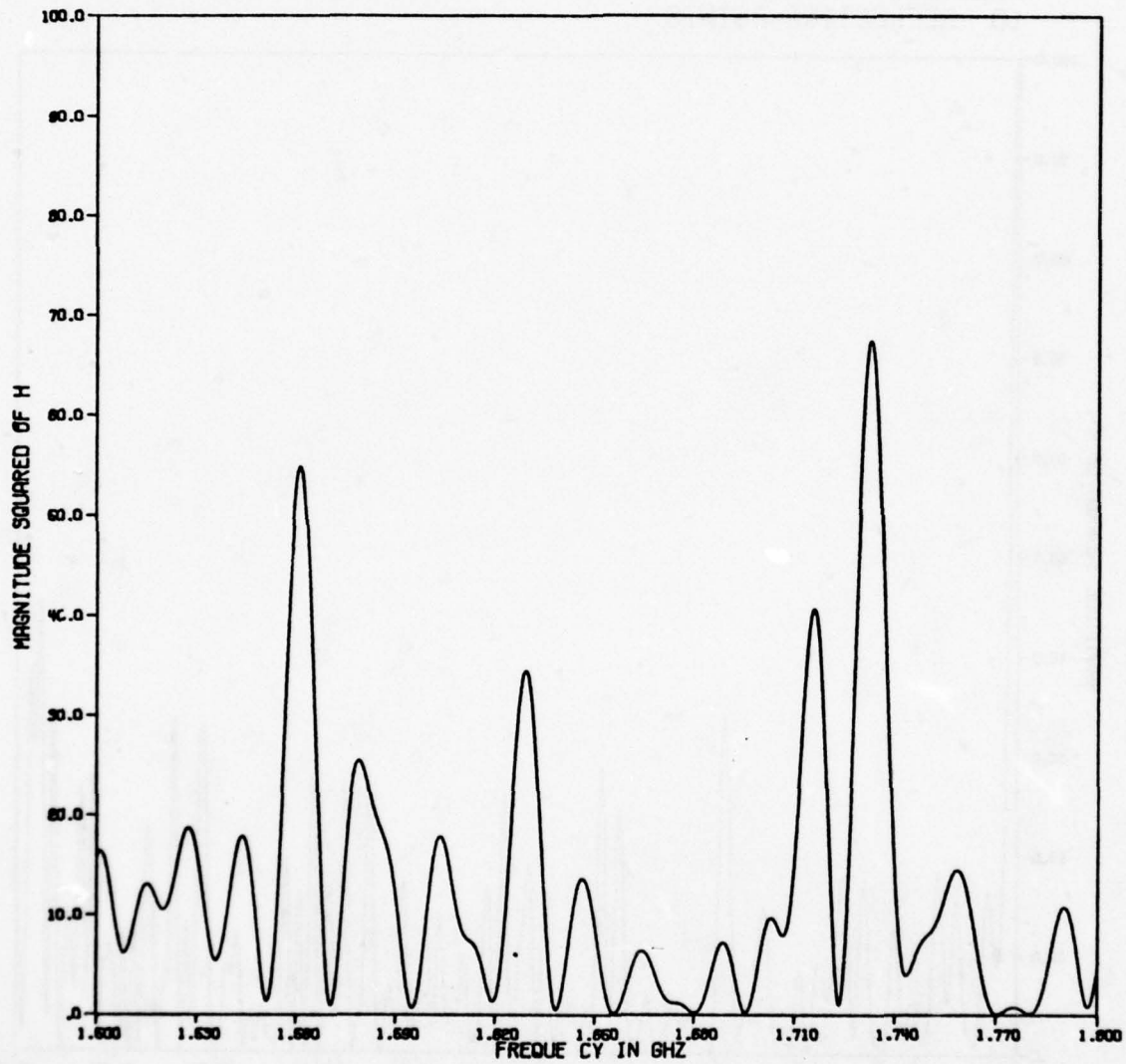


Figure 2-8. $|H(f)|^2$ versus viewing angle for 10-point target.

D VS THETA D, THETA E = THETA D
FREQUENCY = 1 GHZ
10 REFLECTING POINTS

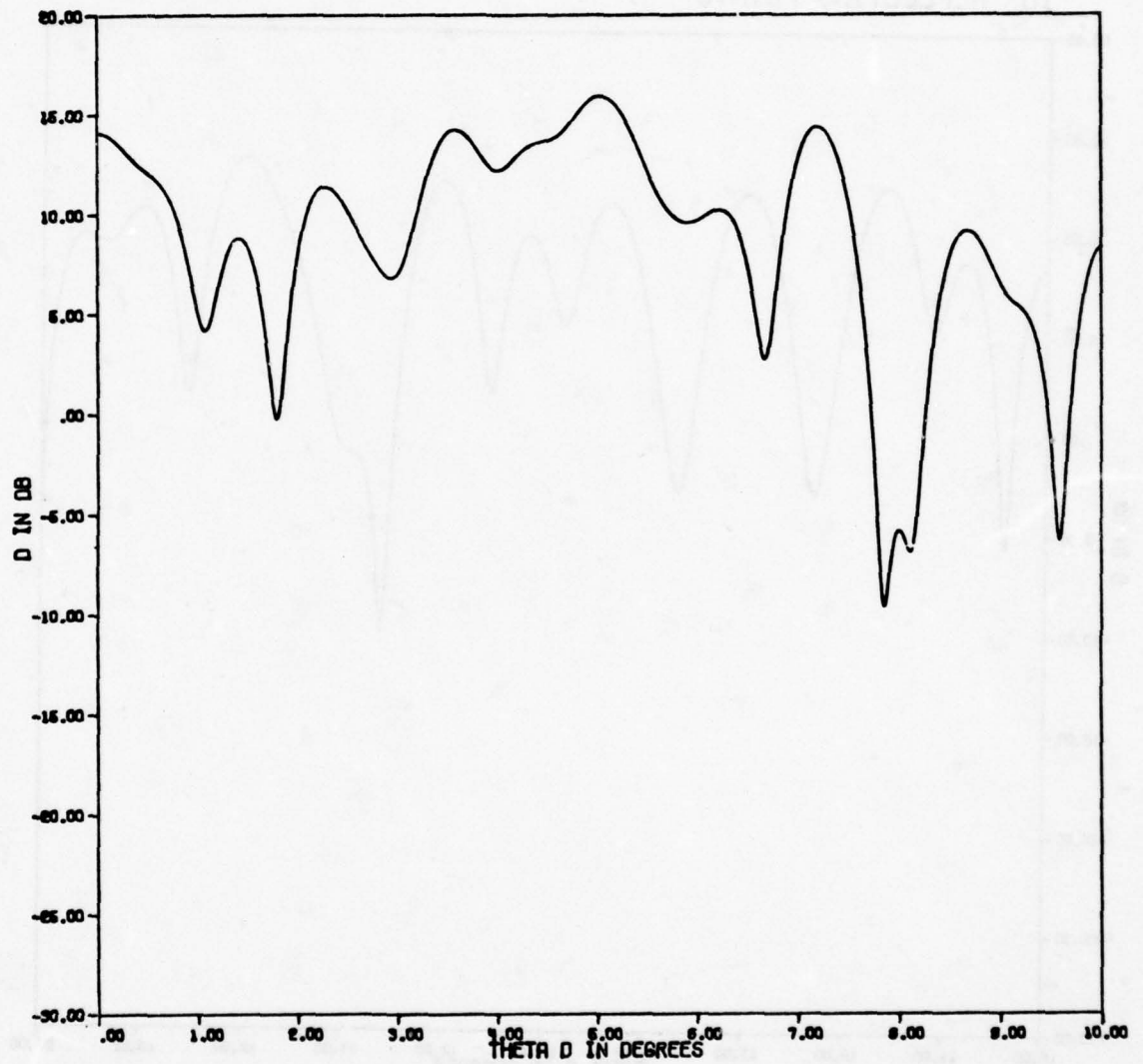


Figure 2-9a. Power ratio versus viewing angle for 10-point target.

D VS THETA D. THETA E = THETA D
FREQUENCY = 1 GHZ
10 REFLECTING POINTS

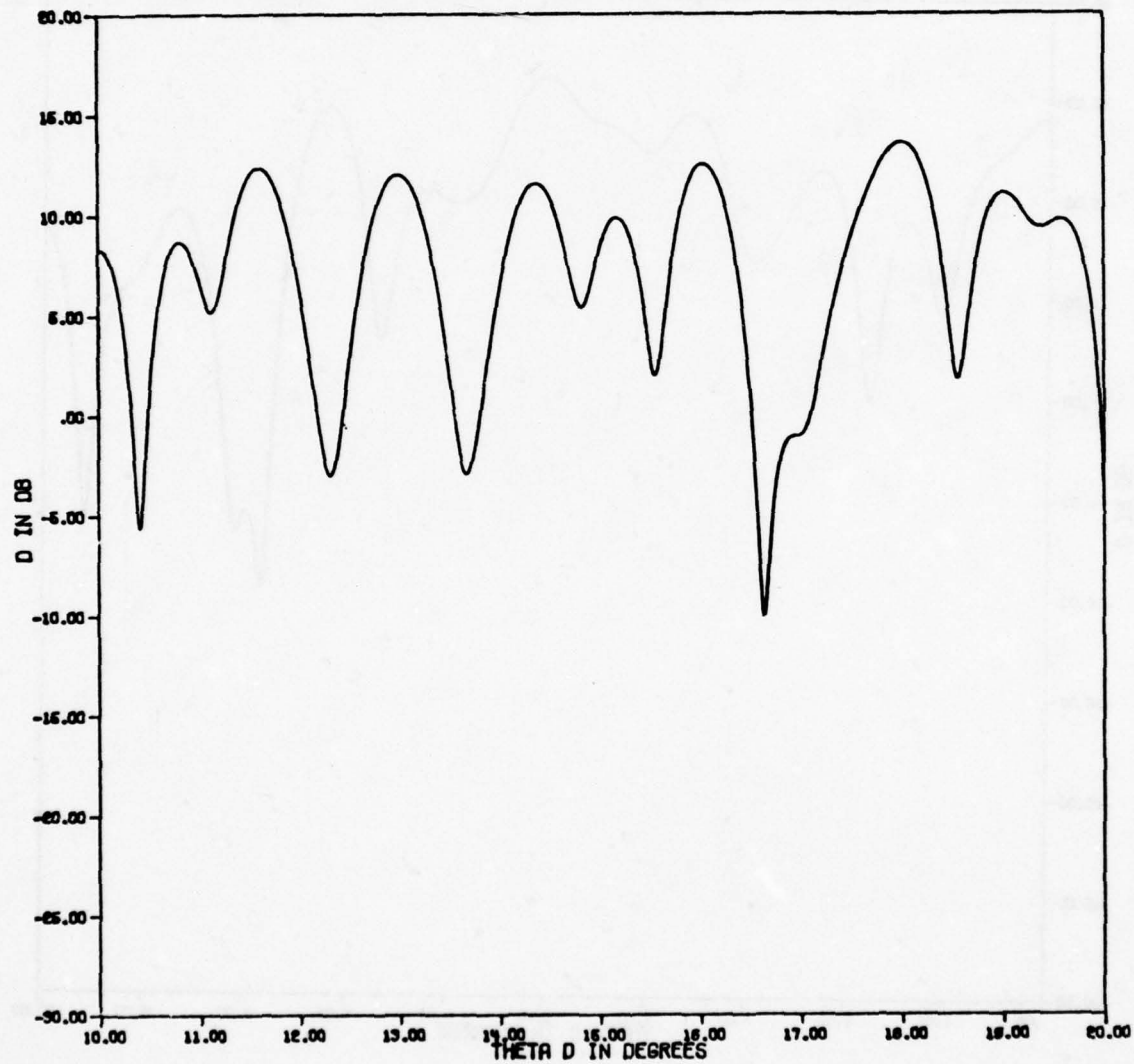


Figure 2-9b. Power ratio versus viewing angle for 10-point target.

D VS THETA D, THETA E = THETA D
FREQUENCY = 1 GHZ
10 REFLECTING POINTS

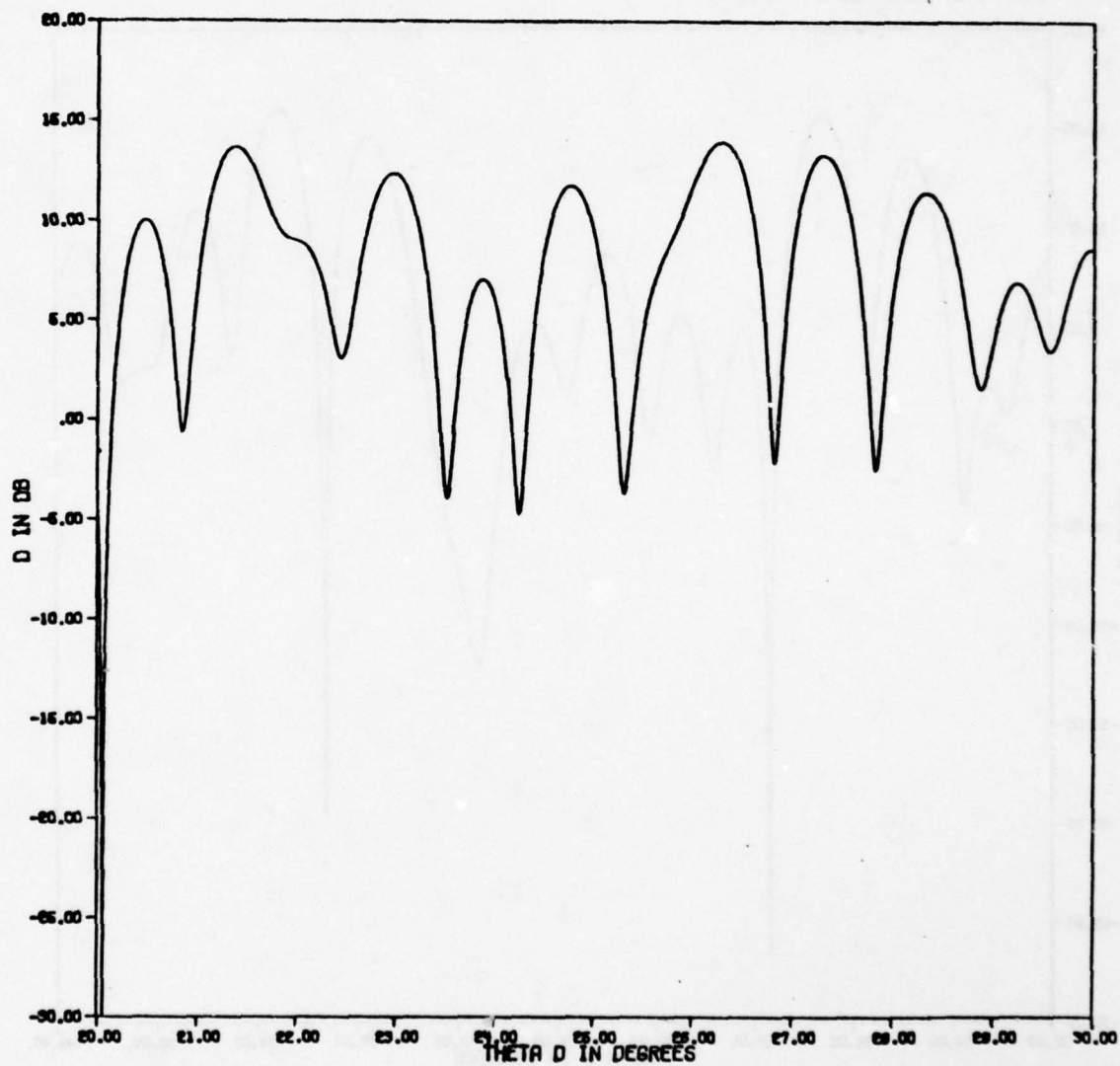


Figure 2-9c. Power ratio versus viewing angle for 10-point target.

D VS THETA D, THETA E = THETA D
FREQUENCY = 1 GHZ
10 REFLECTING POINTS

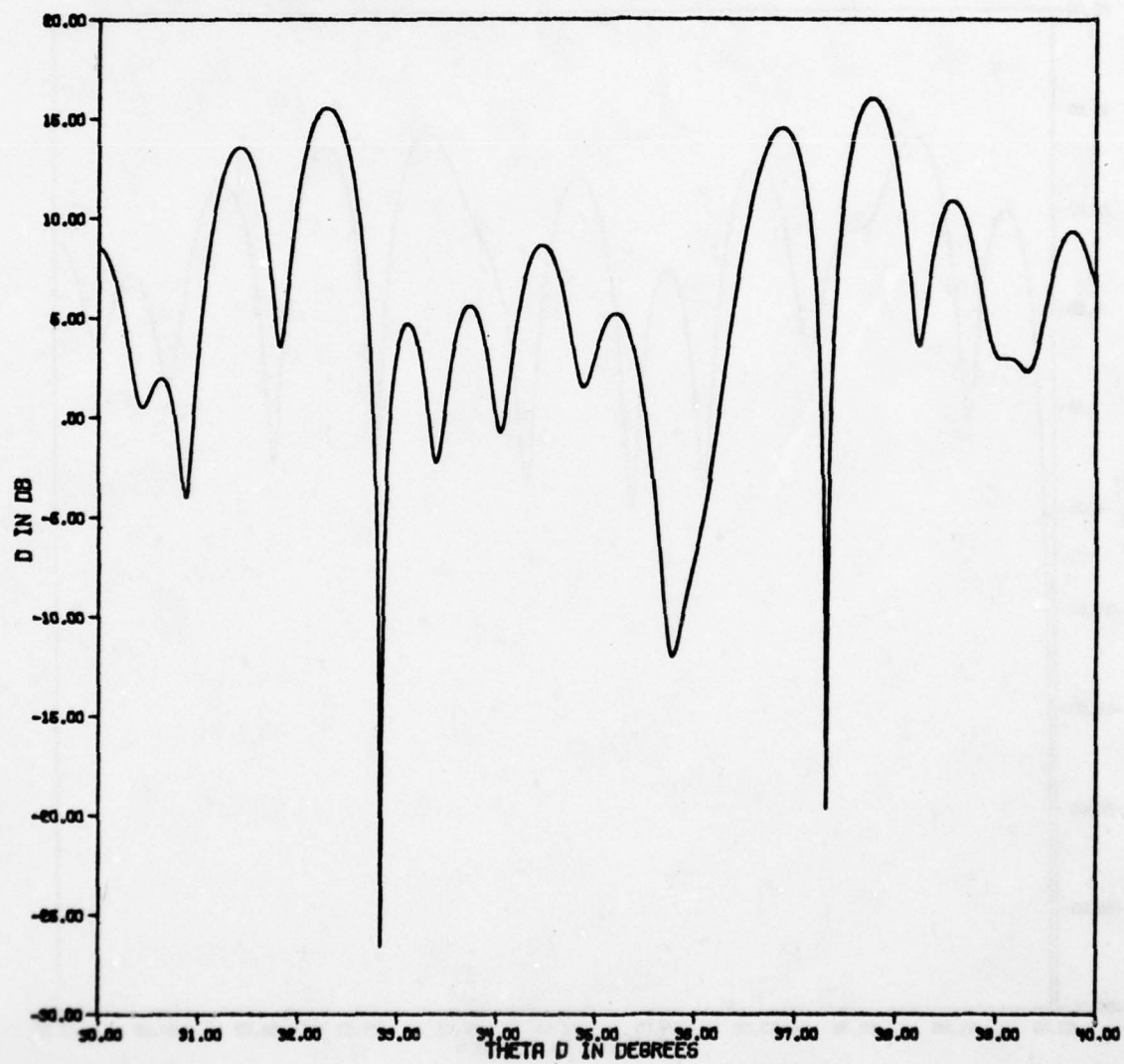


Figure 2-9d. Power ratio versus viewing angle for 10-point target.

D VS THETA D. THETA E = THETA D
FREQUENCY = 1 GHZ
10 REFLECTING POINTS

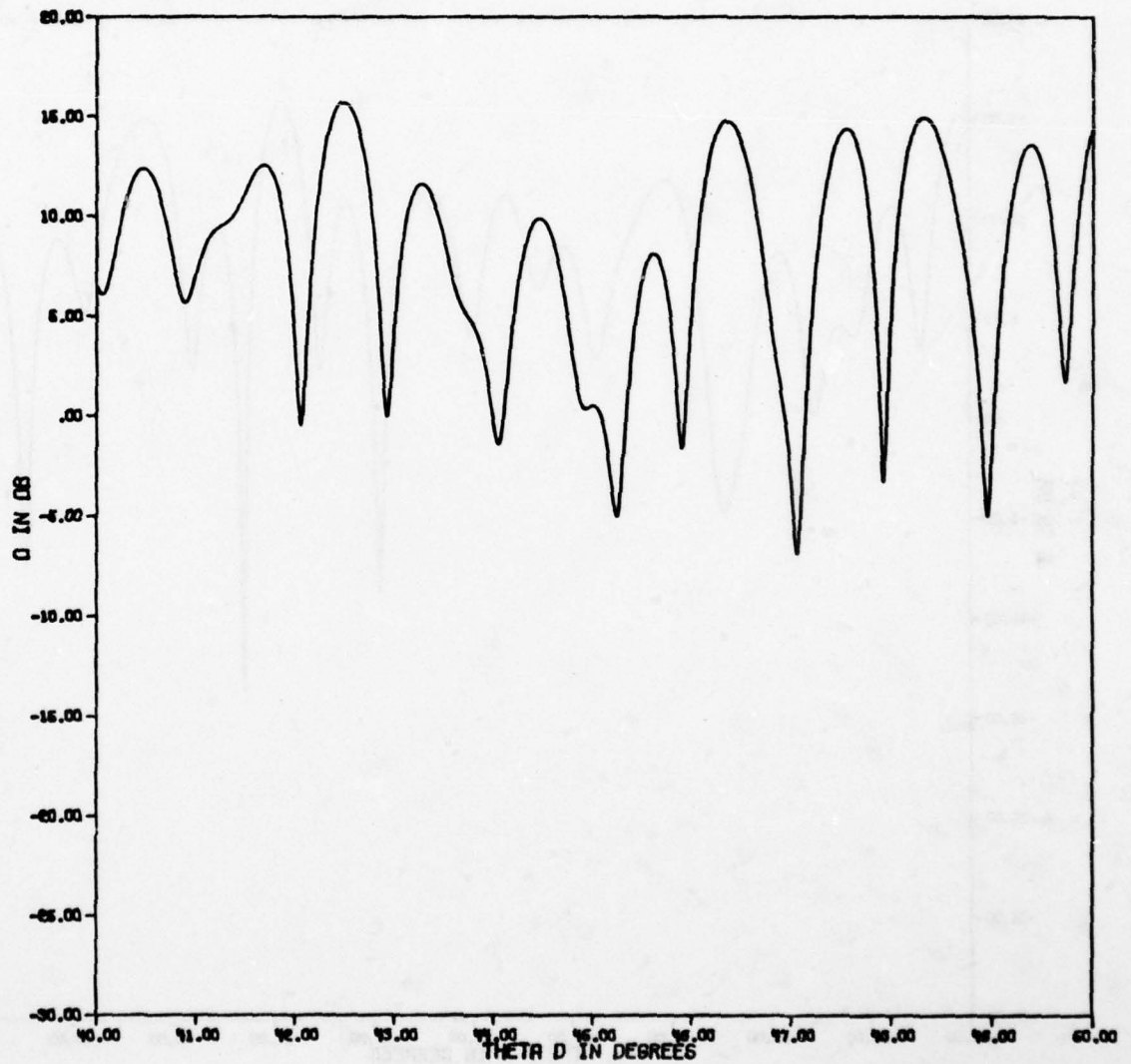


Figure 2-9e. Power ratio versus viewing angle for 10-point target.

D VS THETA D. THETA E = THETA D
FREQUENCY = 1 GHZ
10 REFLECTING POINTS

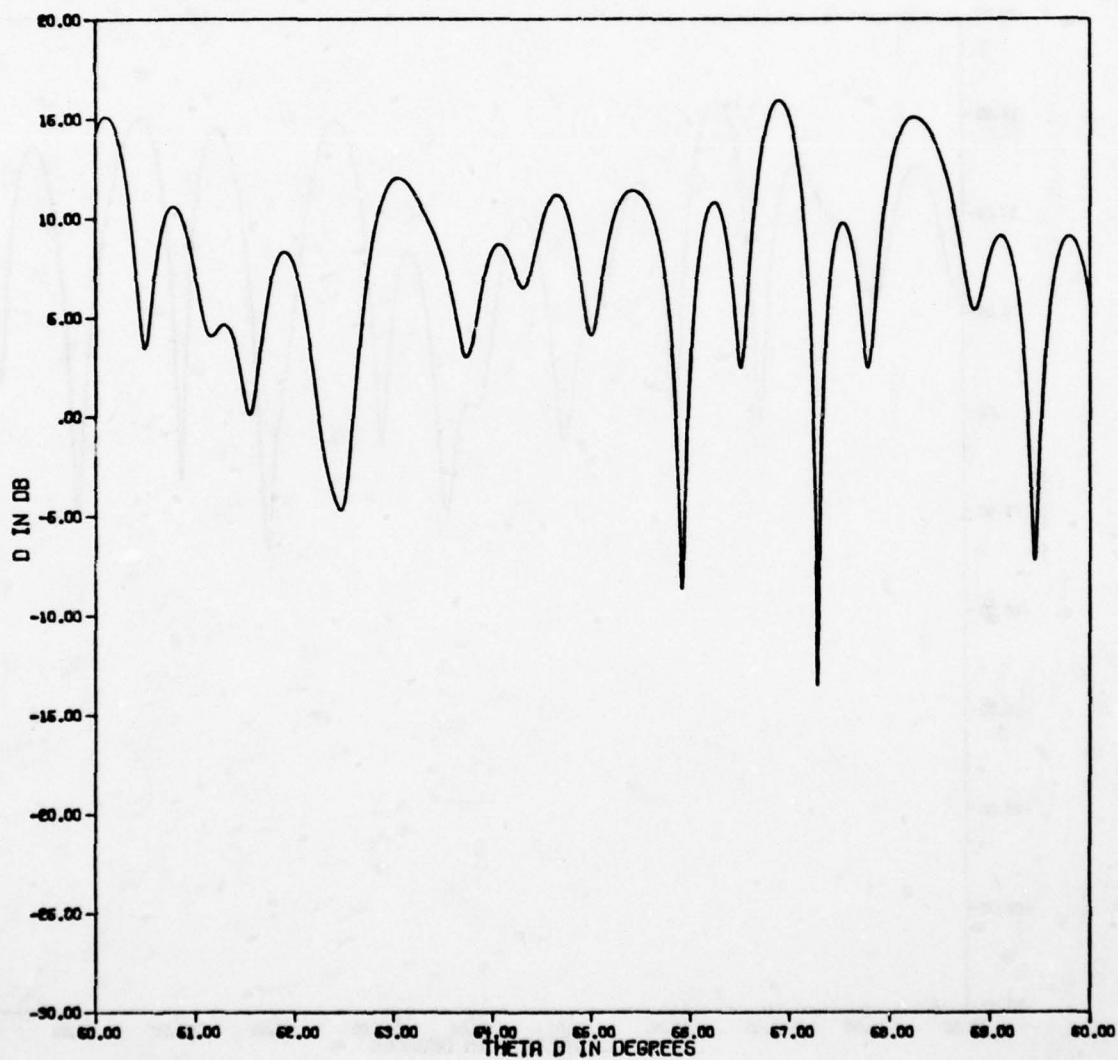


Figure 2-9f. Power ratio versus viewing angle for 10-point target.

D VS THETA D. THETA E = THETA D
FREQUENCY = 1 GHZ
10 REFLECTING POINTS

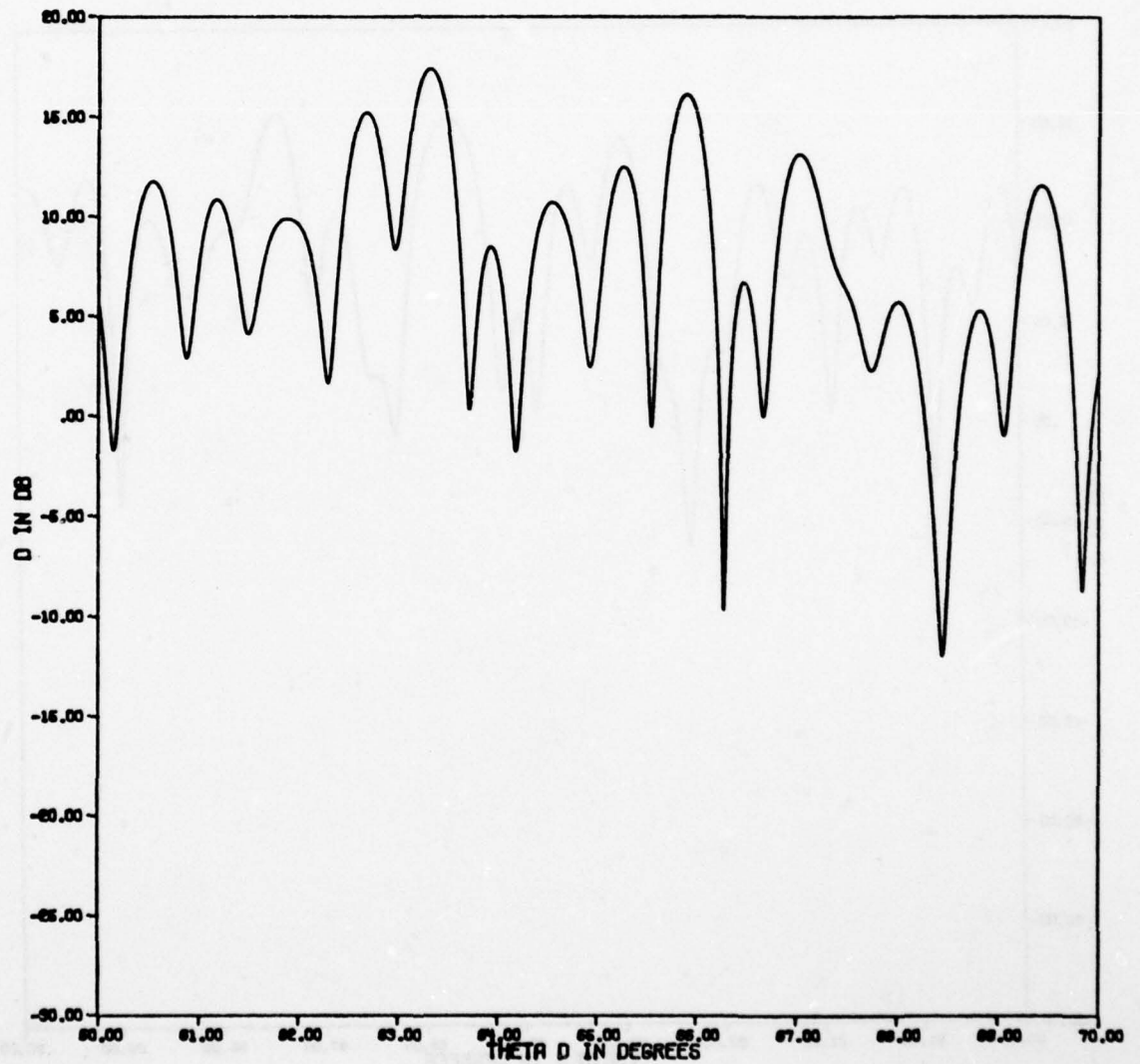


Figure 2-9g. Power ratio versus viewing angle for 10-point target.

D VS THETA D. THETA E = THETA D
FREQUENCY = 1 GHZ
10 REFLECTING POINTS

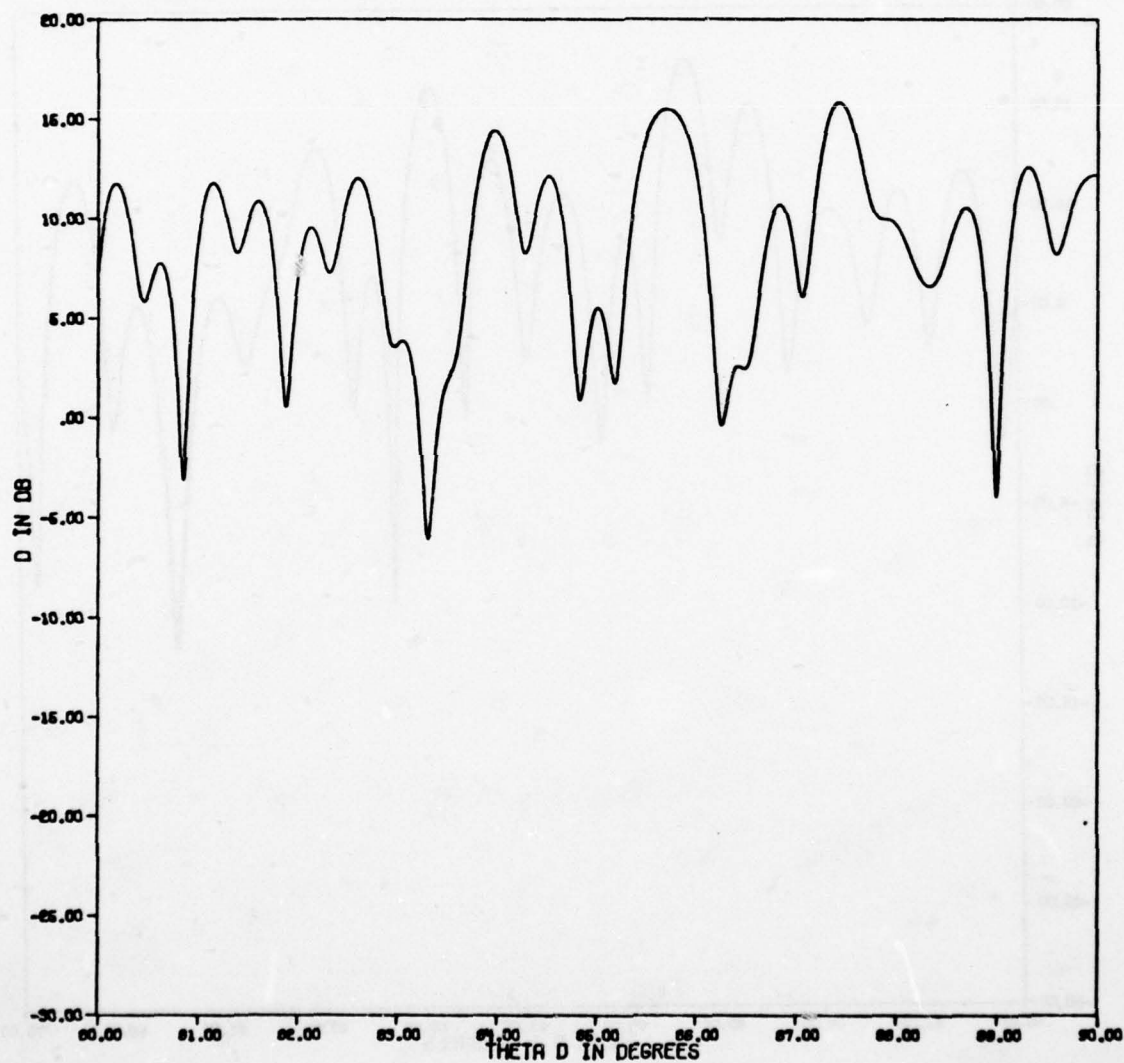


Figure 2-9h. Power ratio versus viewing angle for 10-point target.

D VS THETA D. THETA E = THETA D
FREQUENCY = 1 GHZ
10 REFLECTING POINTS

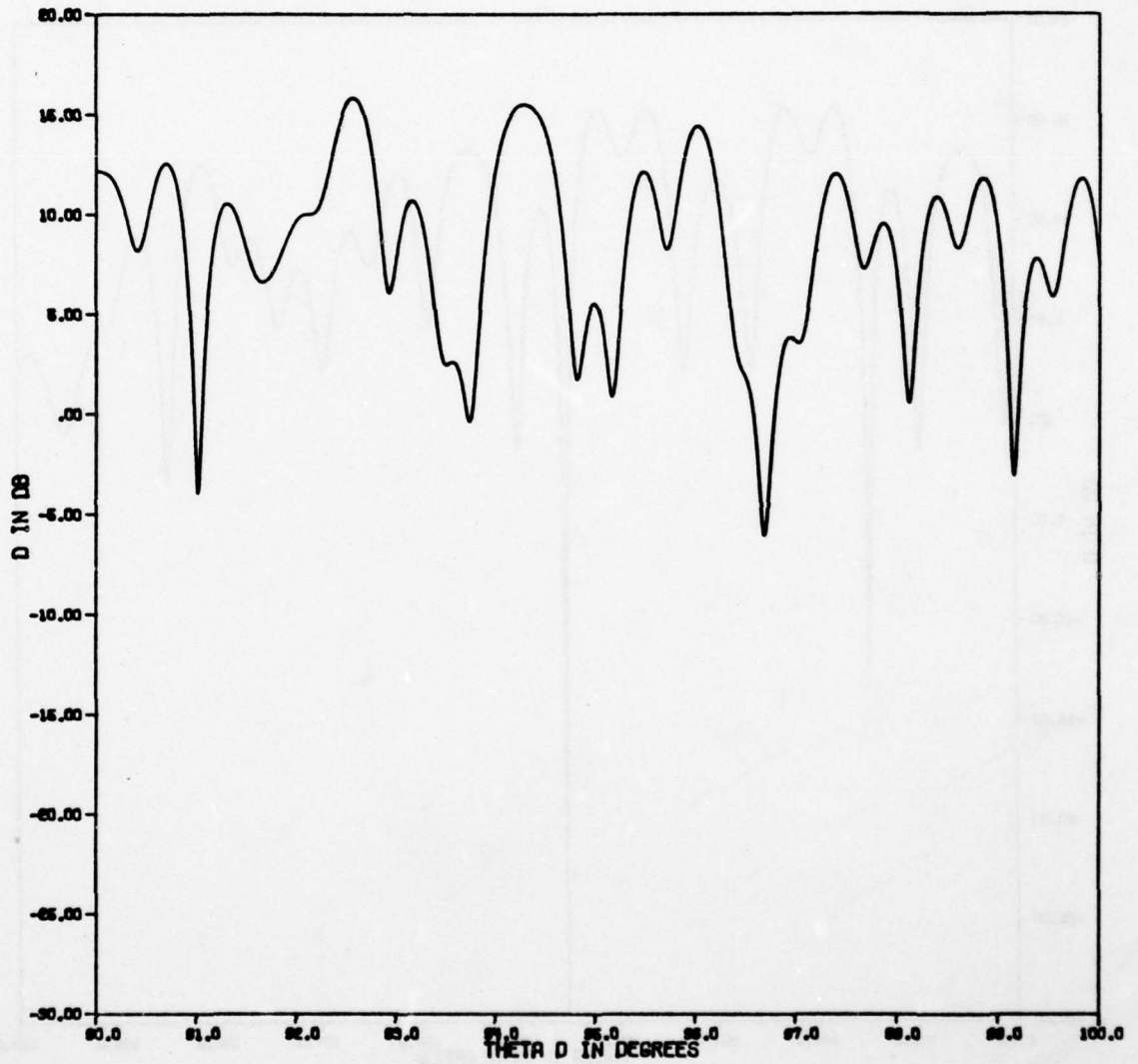


Figure 2-91. Power ratio versus viewing angle for 10-point target.

D VS THETA D. THETA E = THETA D
FREQUENCY = 1 GHZ
10 REFLECTING POINTS

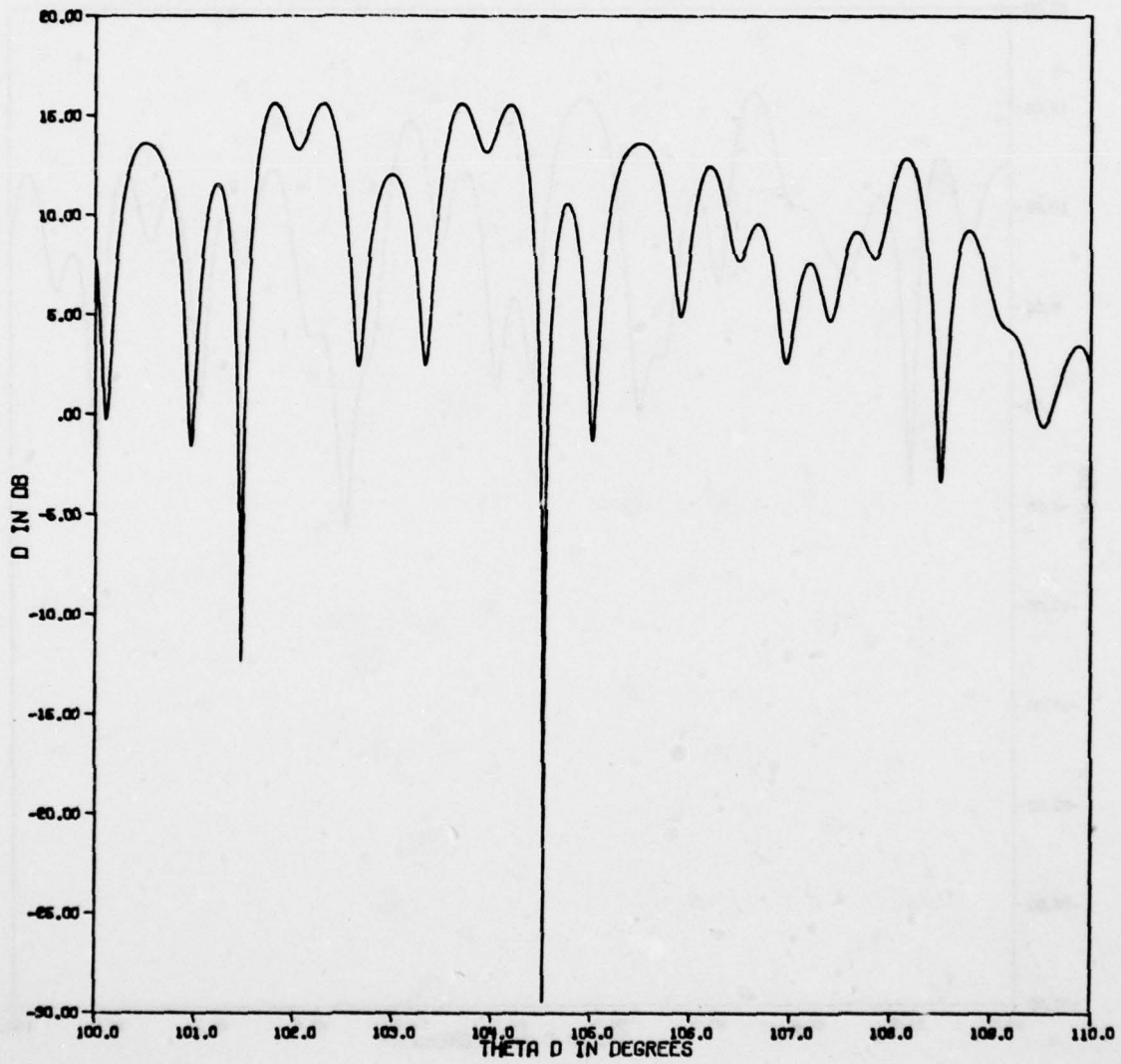


Figure 2-9j. Power ratio versus viewing angle for 10-point target.

D VS THETA D, THETA E = THETA D
FREQUENCY = 1 GHZ
10 REFLECTING POINTS

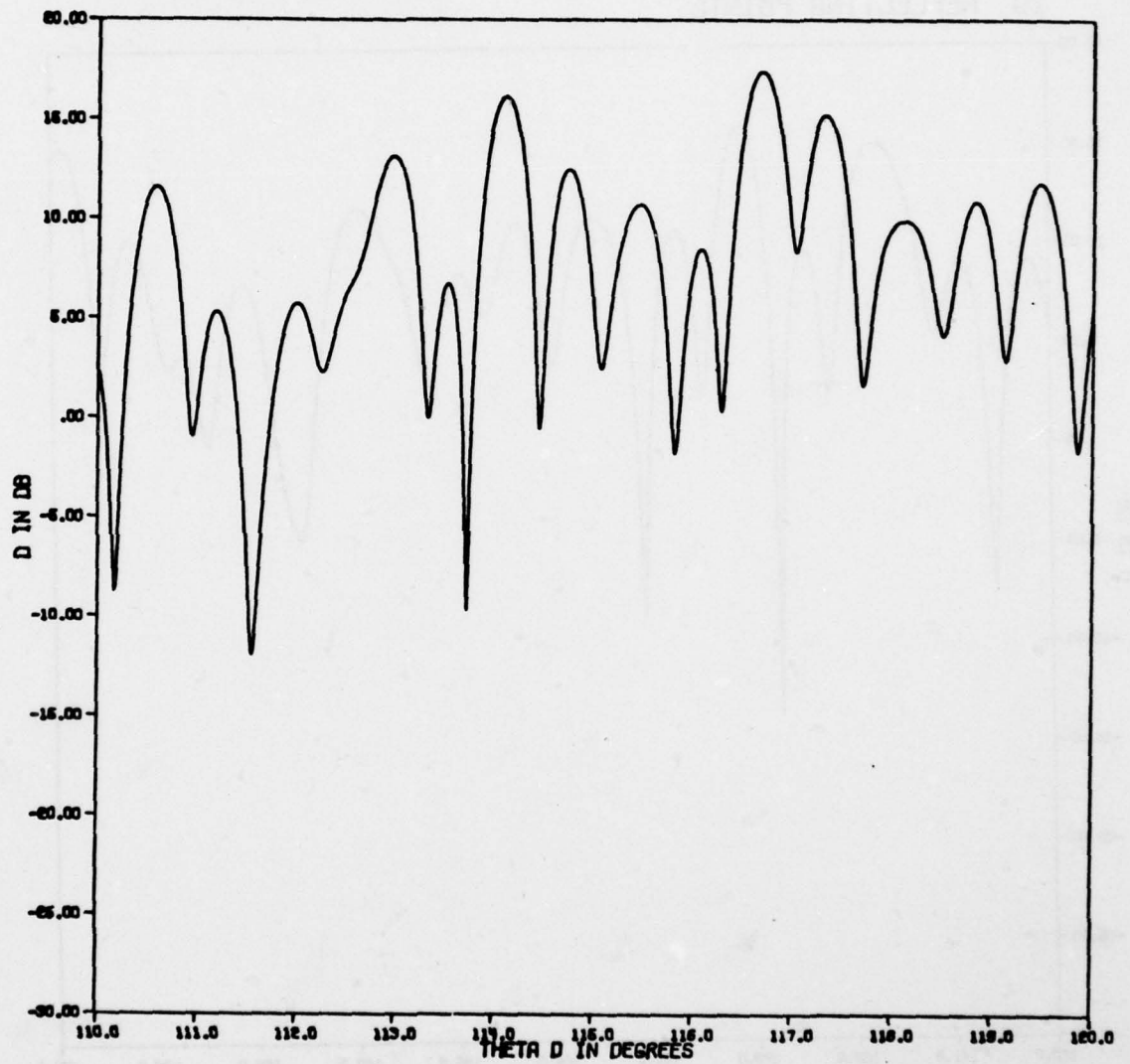


Figure 2-9k. Power ratio versus viewing angle for 10-point target.

D VS THETA D. THETA E = THETA D
FREQUENCY = 1 GHZ
10 REFLECTING POINTS

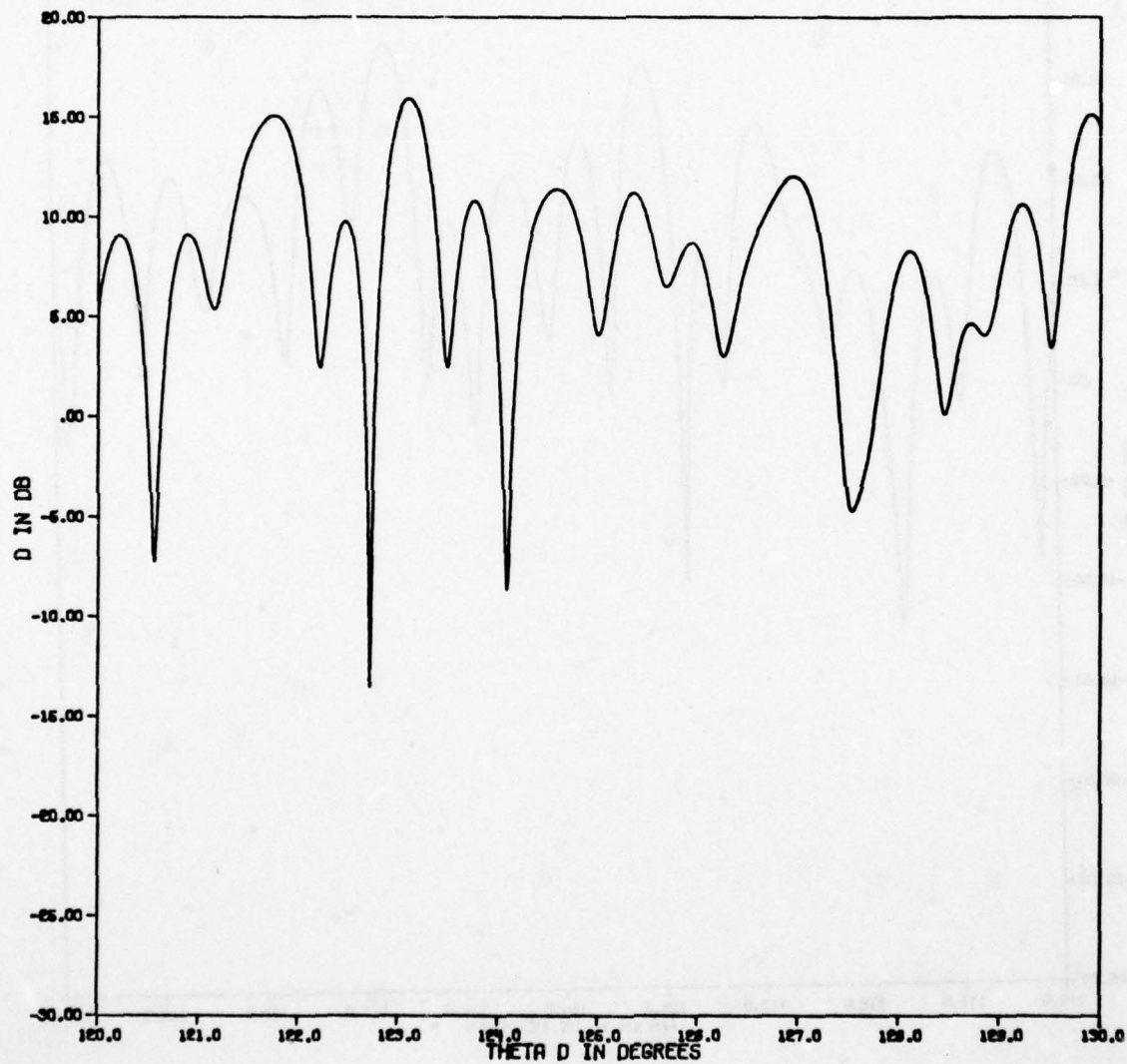


Figure 2-91. Power ratio versus viewing angle for 10-point target.

D VS THETA D. THETA E = THETA D
FREQUENCY = 1 GHZ
10 REFLECTING POINTS

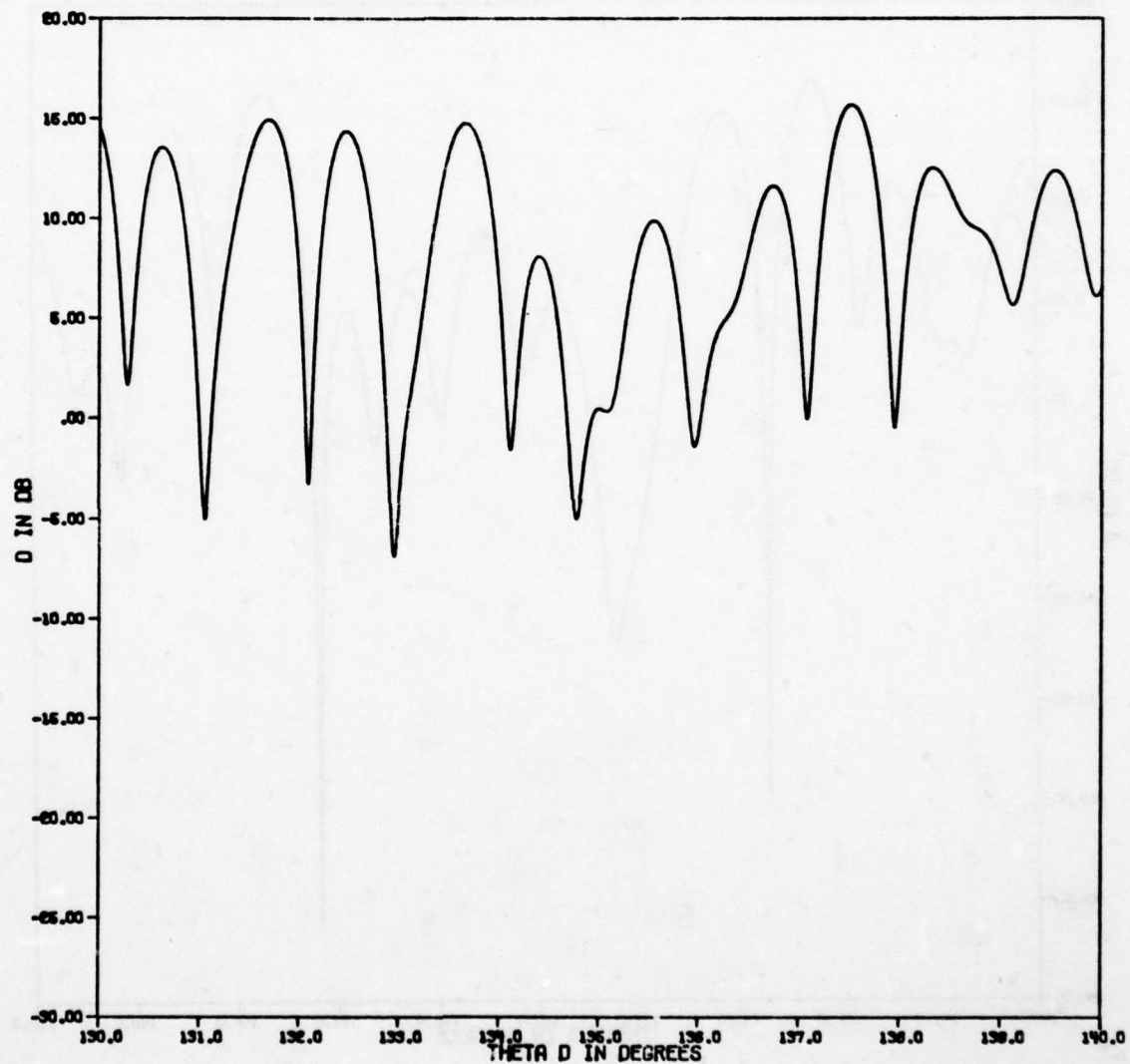


Figure 2-9m. Power ratio versus viewing angle for 10-point target.

D VS THETA D, THETA E = THETA D
FREQUENCY = 1 GHZ
10 REFLECTING POINTS

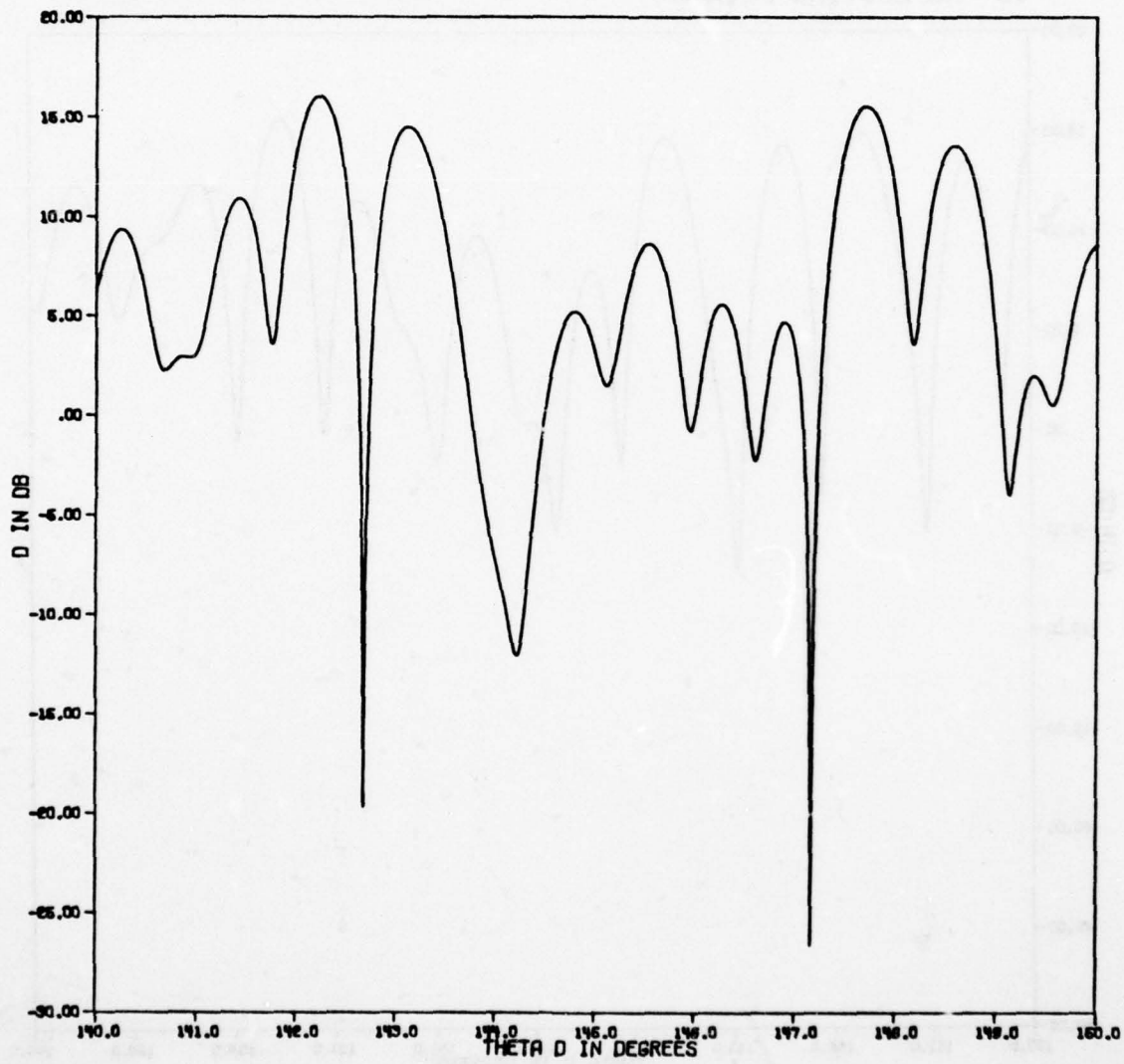


Figure 2-9n. Power ratio versus viewing angle for 10-point target.

D VS THETA D. THETA E = THETA D
FREQUENCY = 1 GHZ
10 REFLECTING POINTS

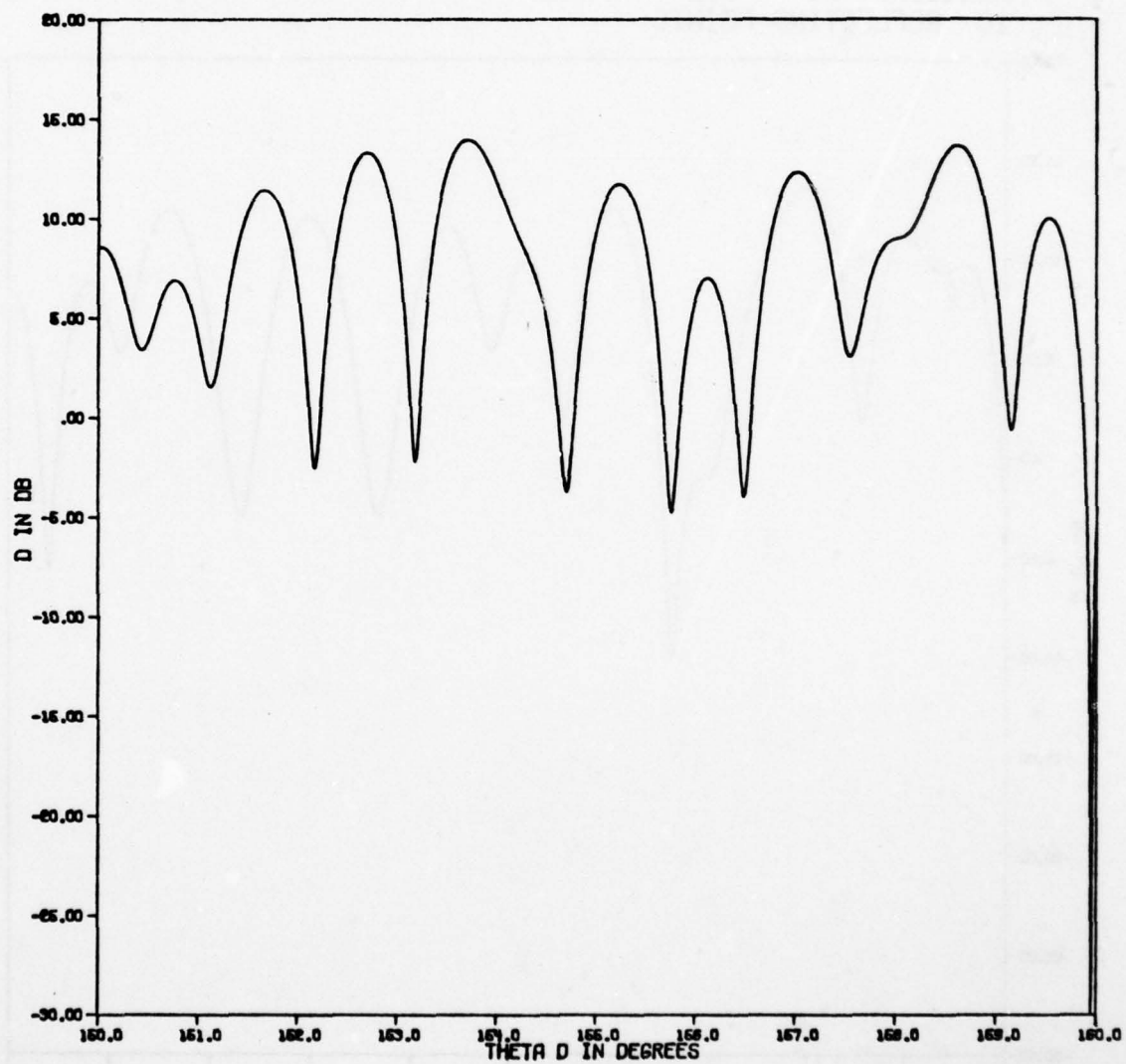


Figure 2-90. Power ratio versus viewing angle for 10-point target.

D VS THETA D. THETA E = THETA D
FREQUENCY = 1 GHZ
10 REFLECTING POINTS

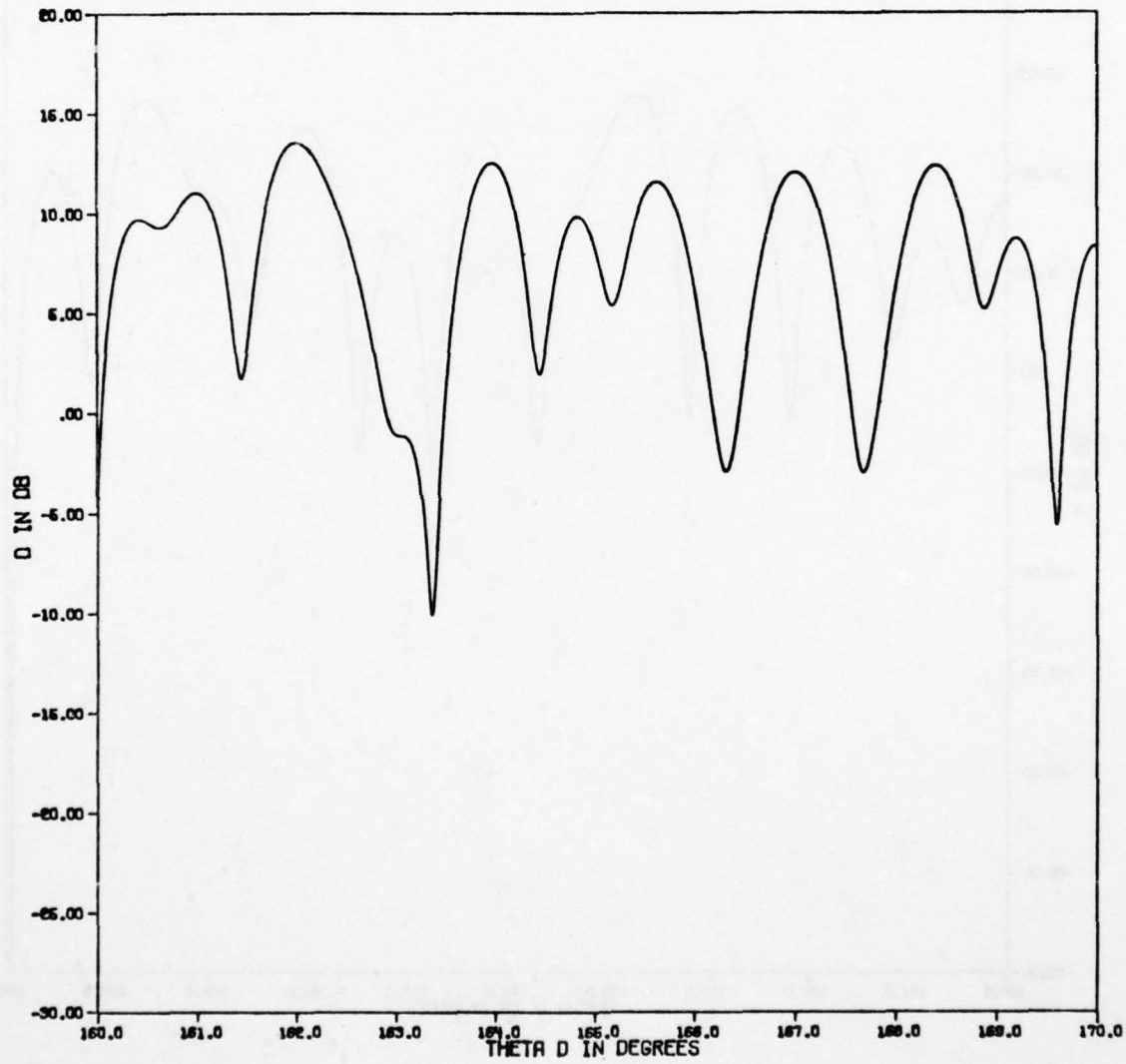


Figure 2-9p. Power ratio versus viewing angle for 10-point target.

D VS THETA D, THETA E = THETA D
FREQUENCY = 1 GHZ
10 REFLECTING POINTS

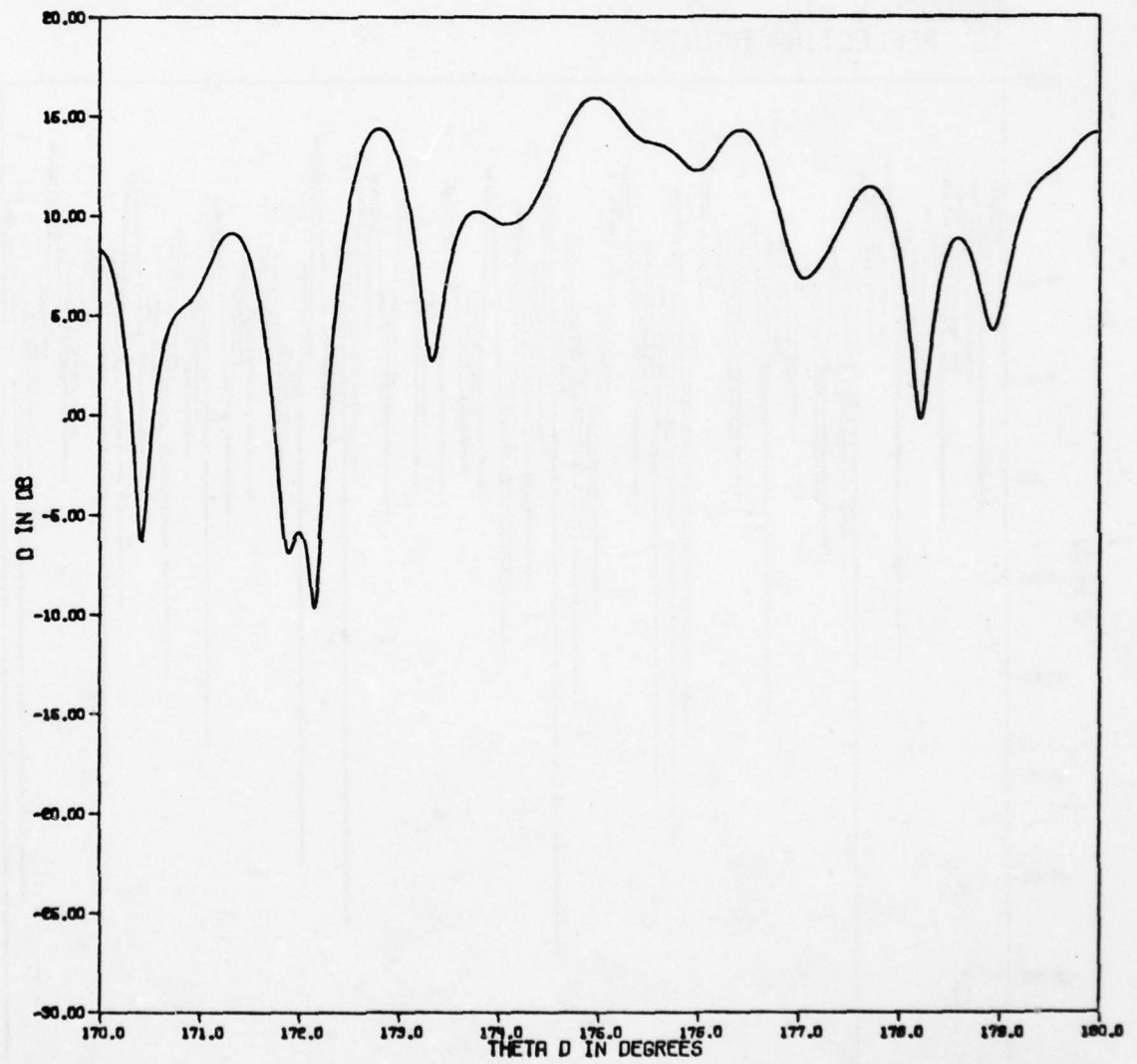


Figure 2-9q. Power ratio versus viewing angle for 10-point target.

AD-A055 758

PURDUE UNIV LAFAYETTE IND SCHOOL OF ELECTRICAL ENGI--ETC F/G 17/9
SPACE-TIME SIGNAL PROCESSING OF RADAR RETURNS.(U)
APR 78 G R COPPER, C D MCGILLEM

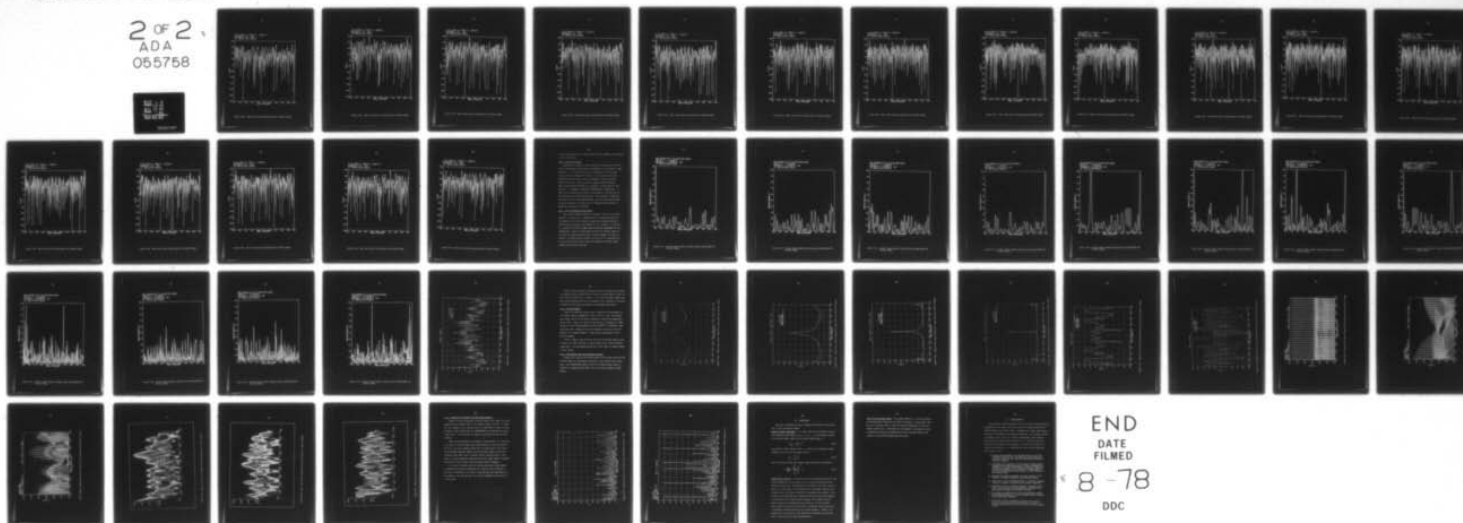
F30602-75-C-0082

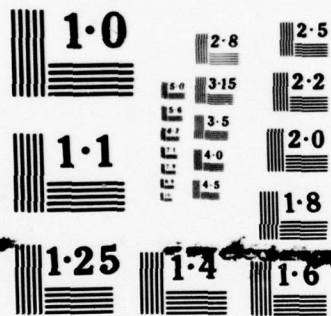
UNCLASSIFIED

RADC-TR-78-89

NL

2 OF 2
ADA
055758





NATIONAL BUREAU OF STANDARDS
MICROCOPY RESOLUTION TEST CHART

D VS THETA D. THETA E = THETA D
FREQUENCY = 10 GHZ
10 REFLECTING POINTS

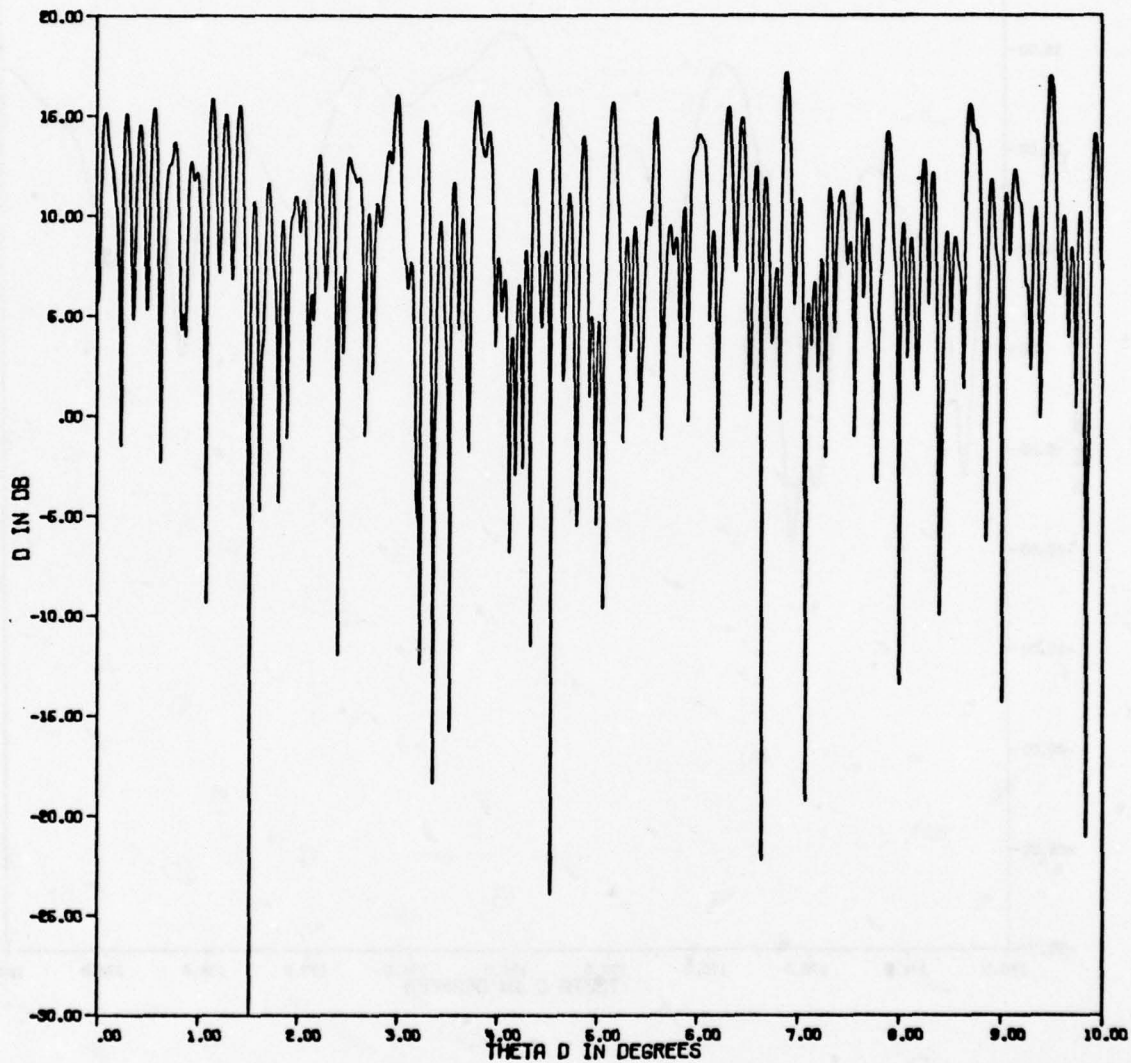


Figure 2-10a. Power ratio versus viewing angle for 10-point target.

D VS THETA D. THETA E = THETA D
FREQUENCY = 10 GHZ
10 REFLECTING POINTS

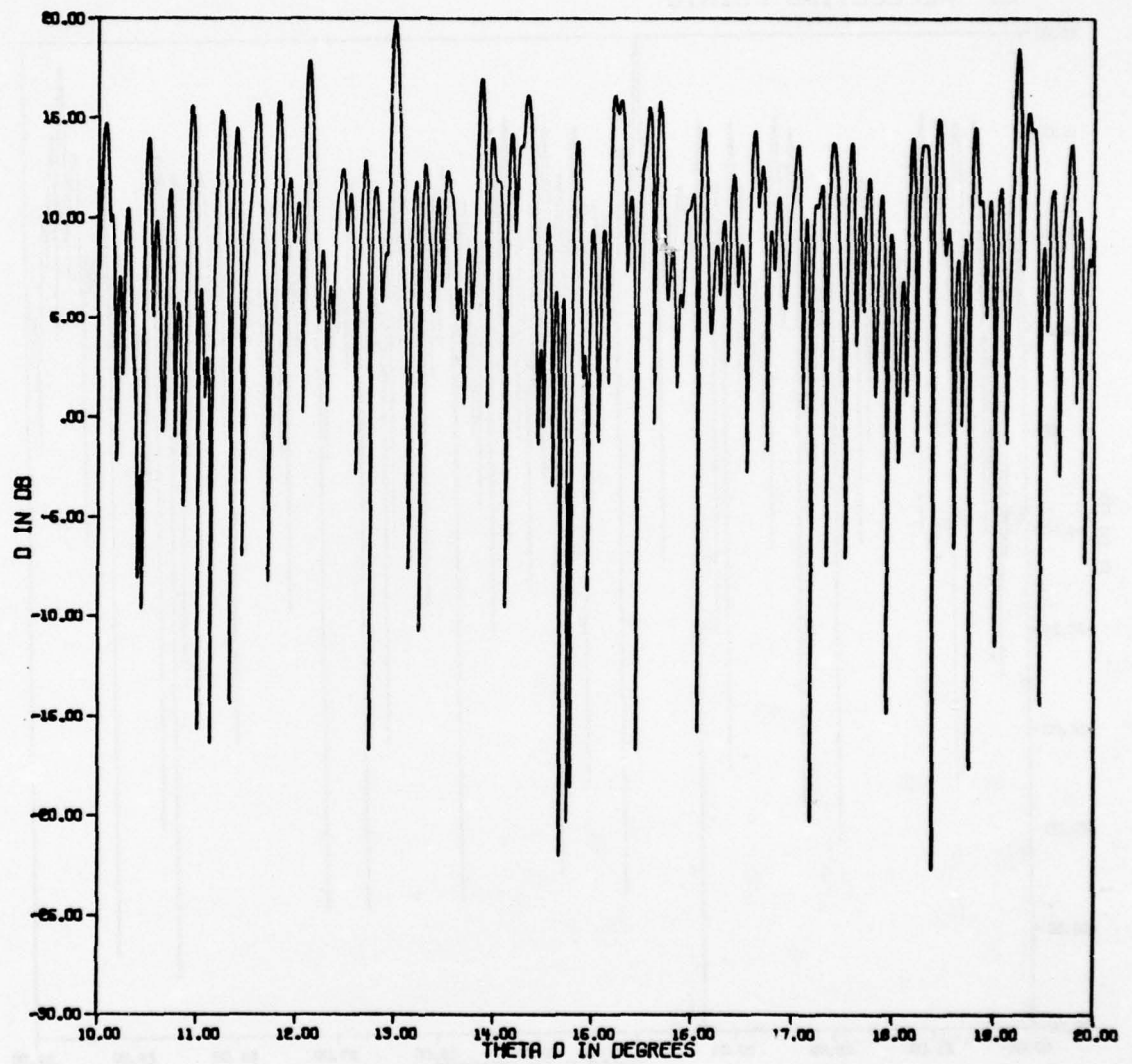


Figure 2-10b. Power ratio versus viewing angle for 10-point target.

D VS THETA D. THETA E = THETA D
FREQUENCY = 10 GHZ
10 REFLECTING POINTS

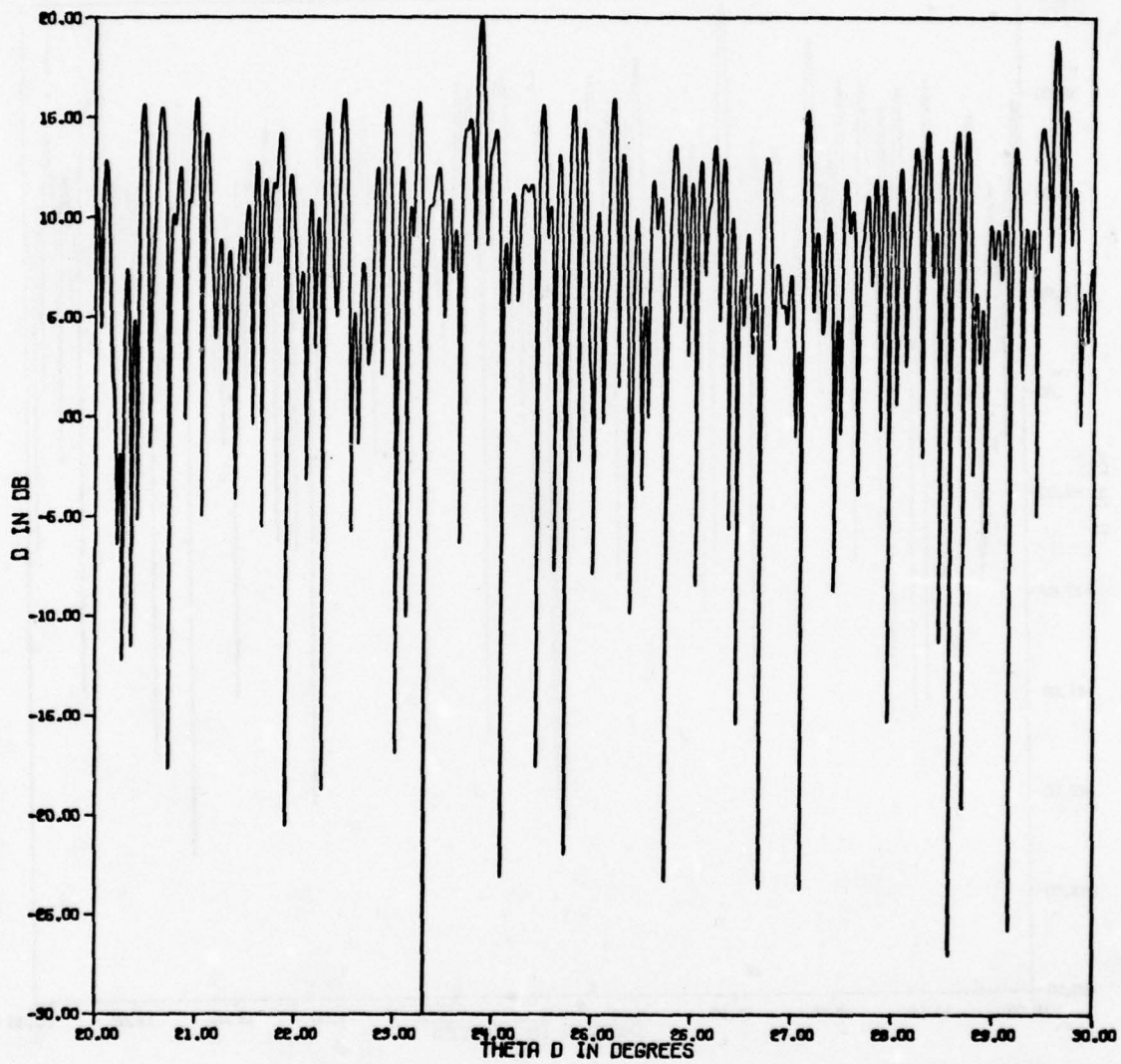


Figure 2-10c. Power ratio versus viewing angle for 10-point target.

D VS THETA D. THETA E = THETA D
FREQUENCY = 10 GHz
10 REFLECTING POINTS

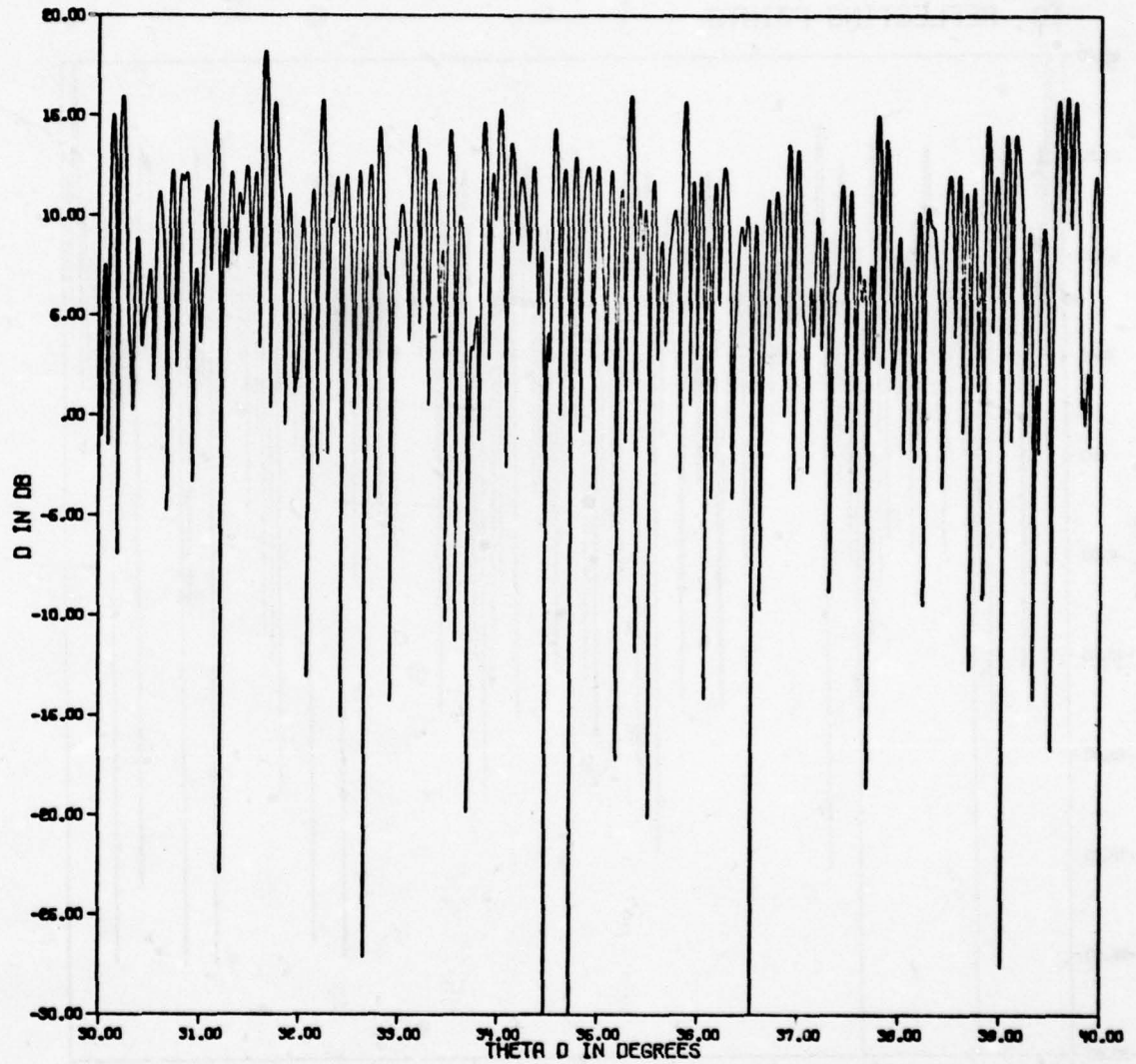


Figure 2-10d. Power ratio versus viewing angle for 10-point target.

D VS THETA D. THETA E = THETA D
FREQUENCY = 10 GHZ
10 REFLECTING POINTS

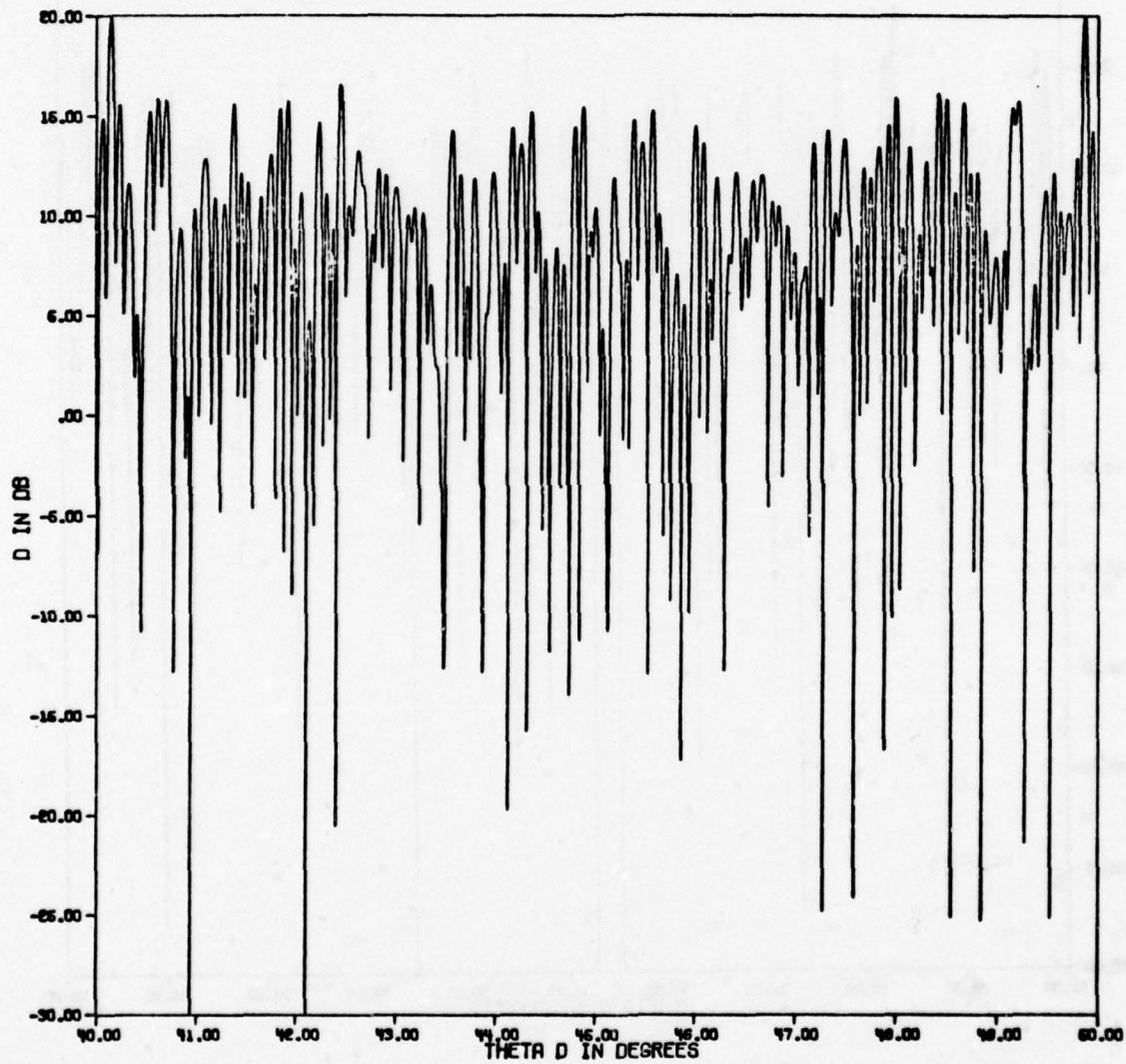


Figure 2-10e. Power ratio versus viewing angle for 10-point target.

D VS THETA D, THETA E = THETA D
FREQUENCY = 10 GHZ
10 REFLECTING POINTS

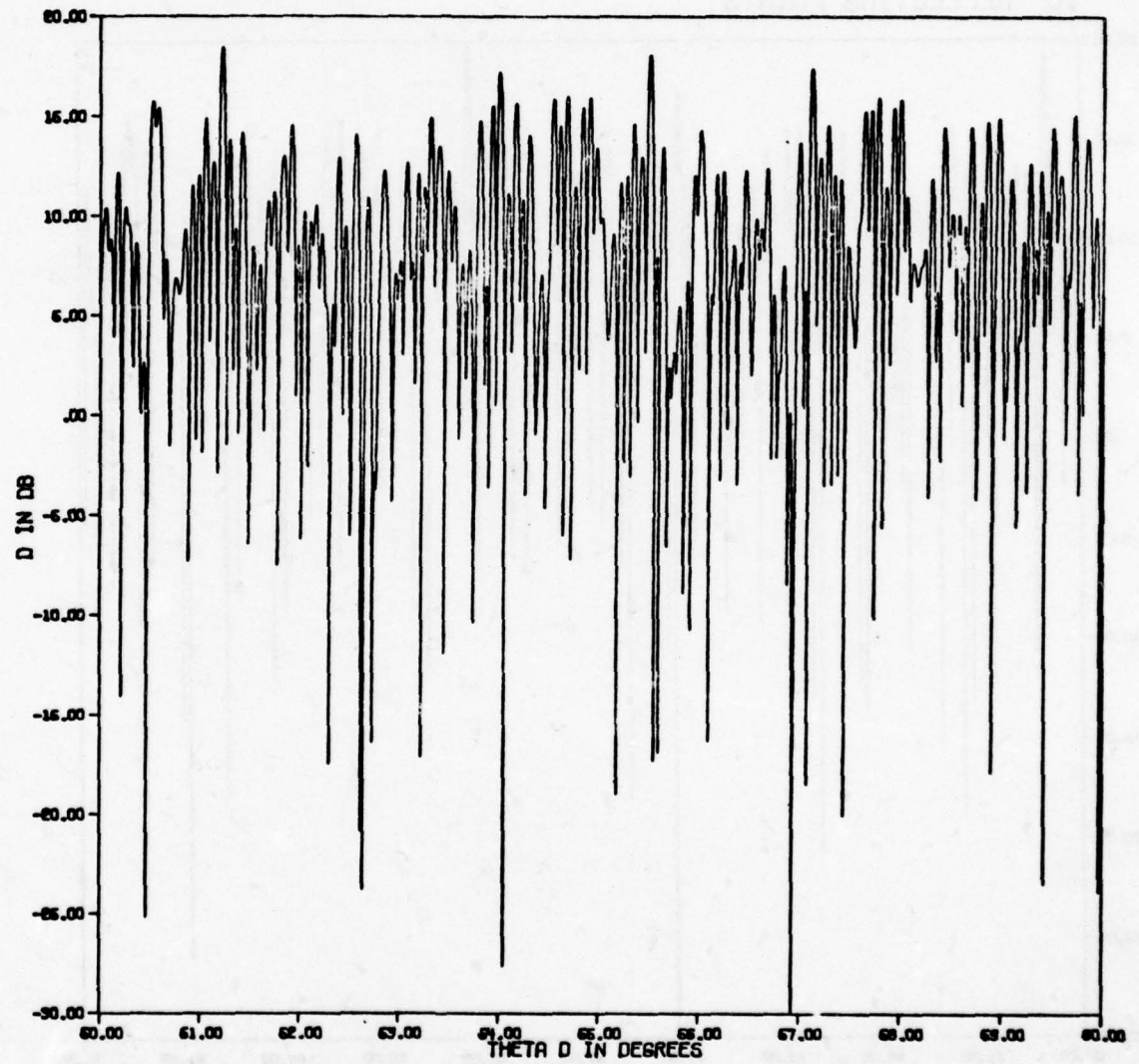


Figure 2-10f. Power ratio versus viewing angle for 10-point target.

D VS THETA D, THETA E = THETA D
FREQUENCY = 10 GHZ
10 REFLECTING POINTS

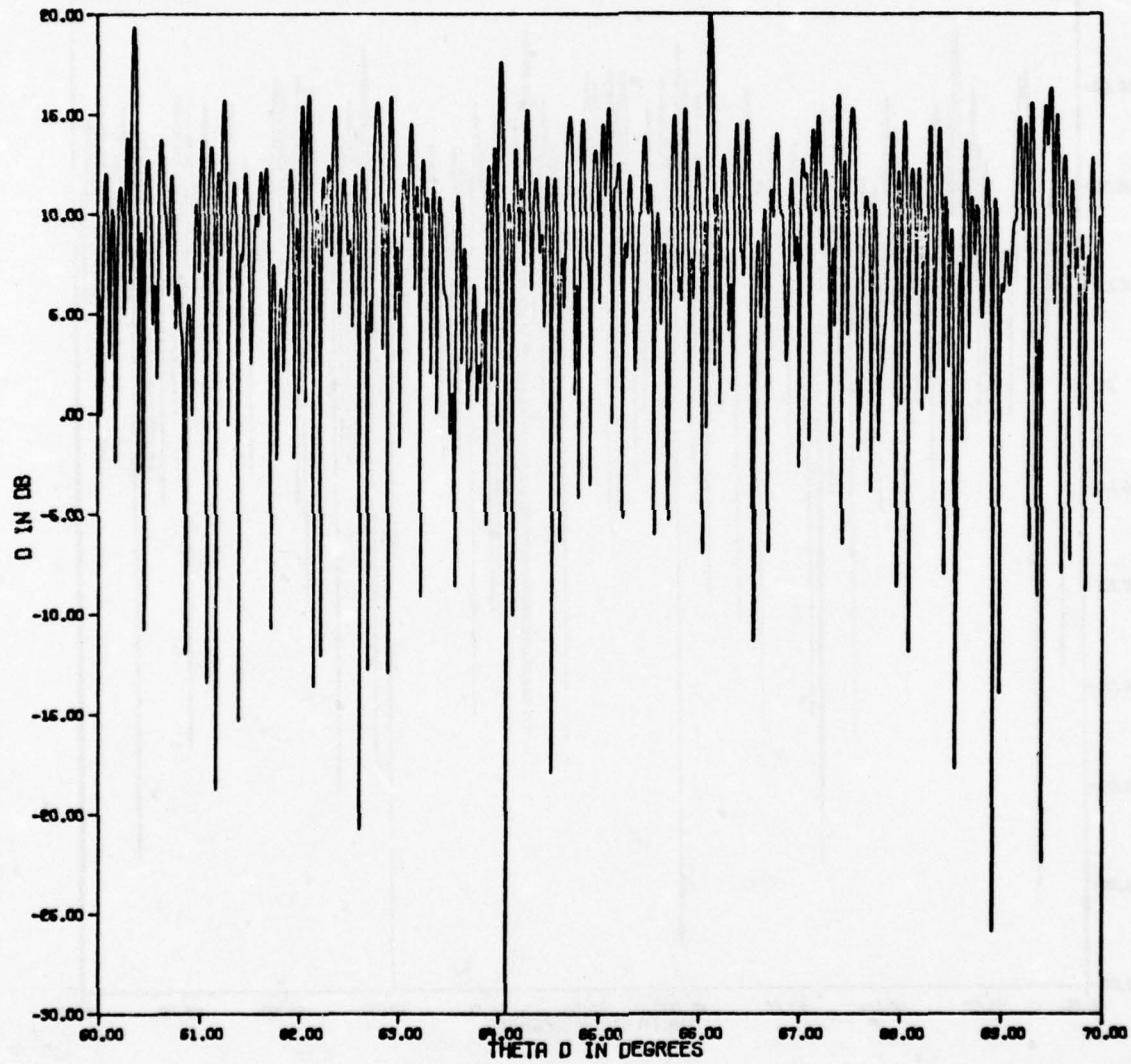


Figure 2-10g. Power ratio versus viewing angle for 10-point target.

D VS THETA D. THETA E = THETA D
FREQUENCY = 10 GHZ
10 REFLECTING POINTS

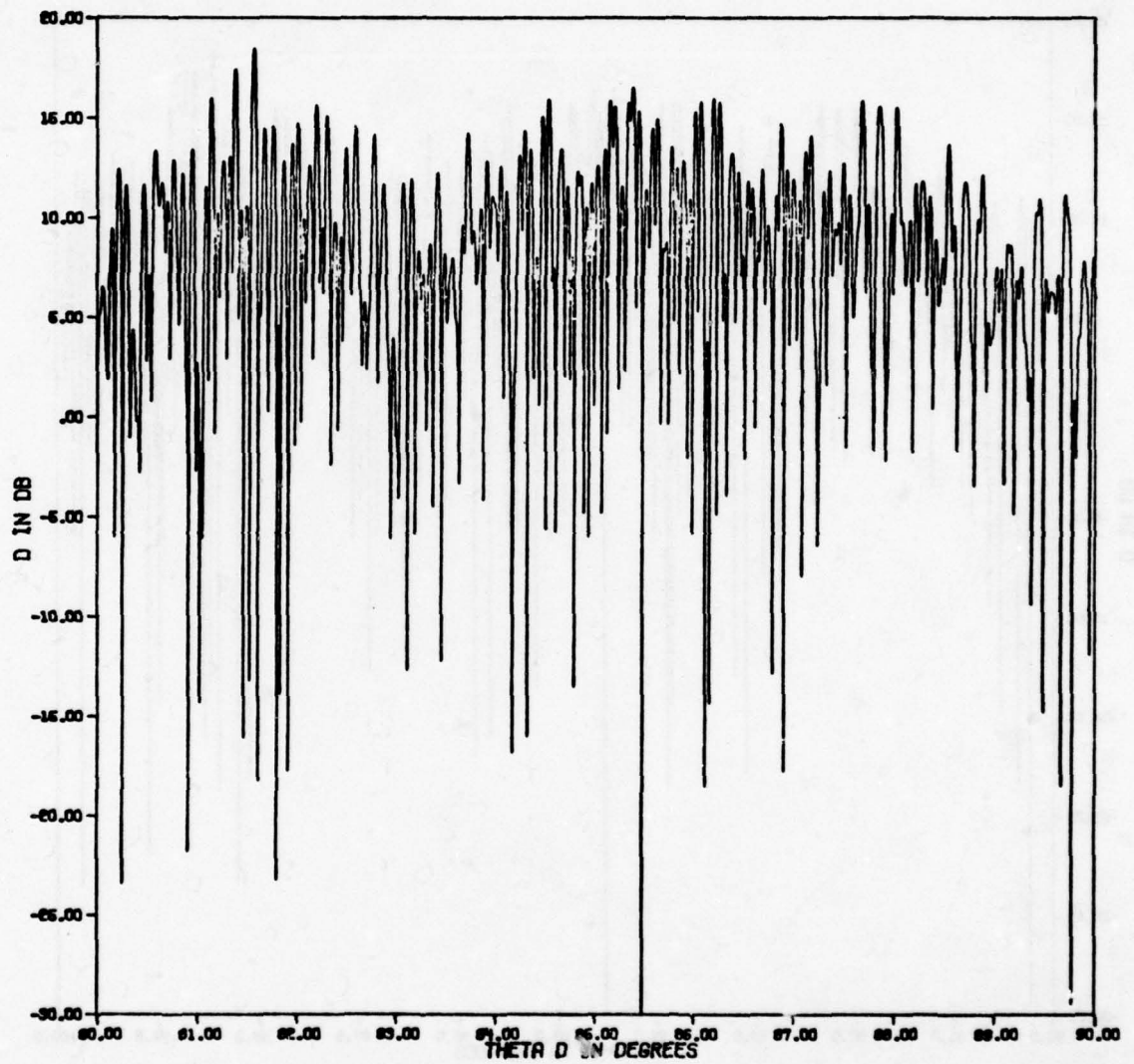


Figure 2-10h. Power ratio versus viewing angle for 10-point target.

D VS THETA D. THETA E = THETA D
FREQUENCY = 10 GHZ
10 REFLECTING POINTS

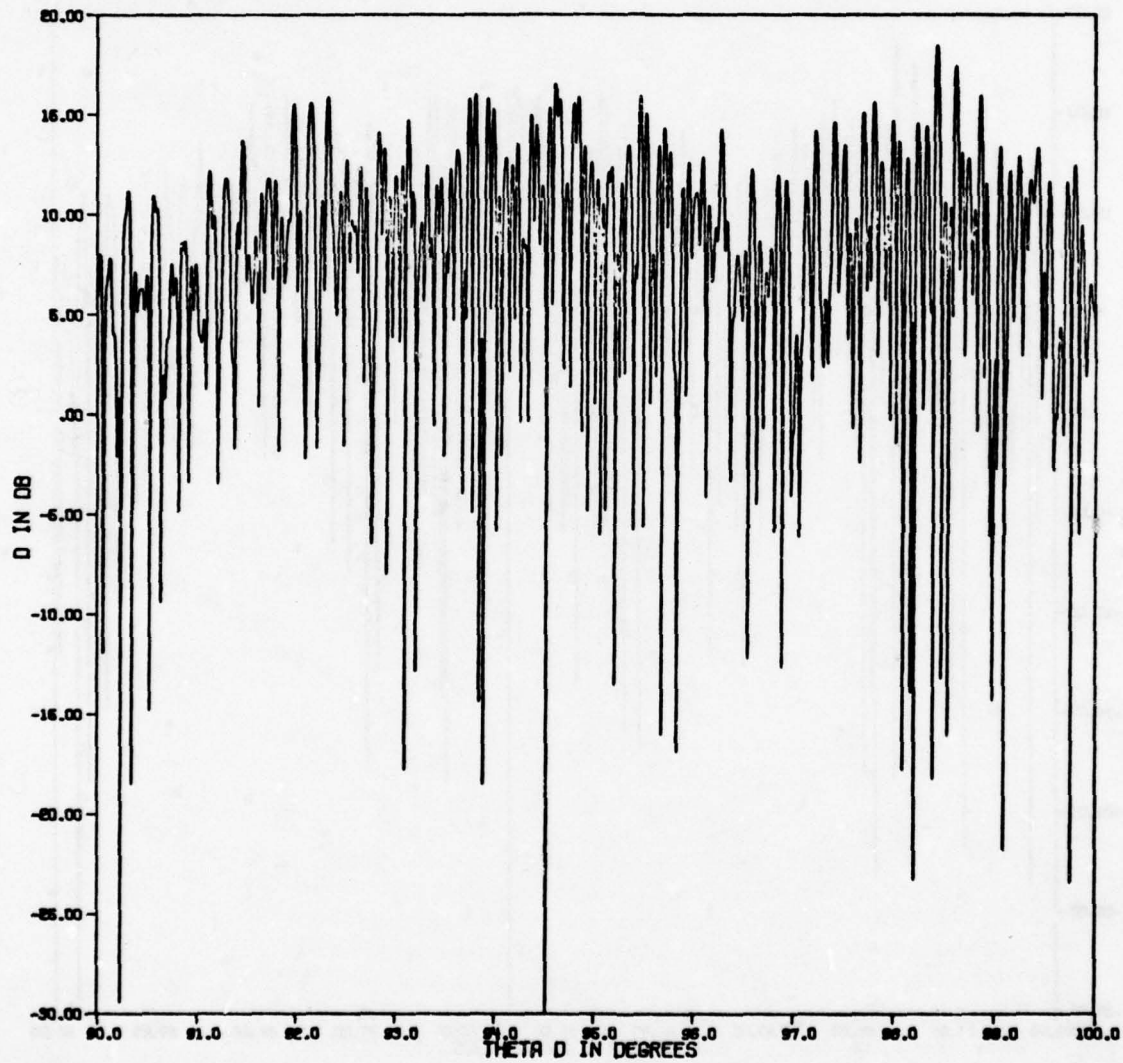


Figure 2-101. Power ratio versus viewing angle for 10-point target.

D VS THETA D. THETA E = THETA D
FREQUENCY = 10 GHZ
10 REFLECTING POINTS

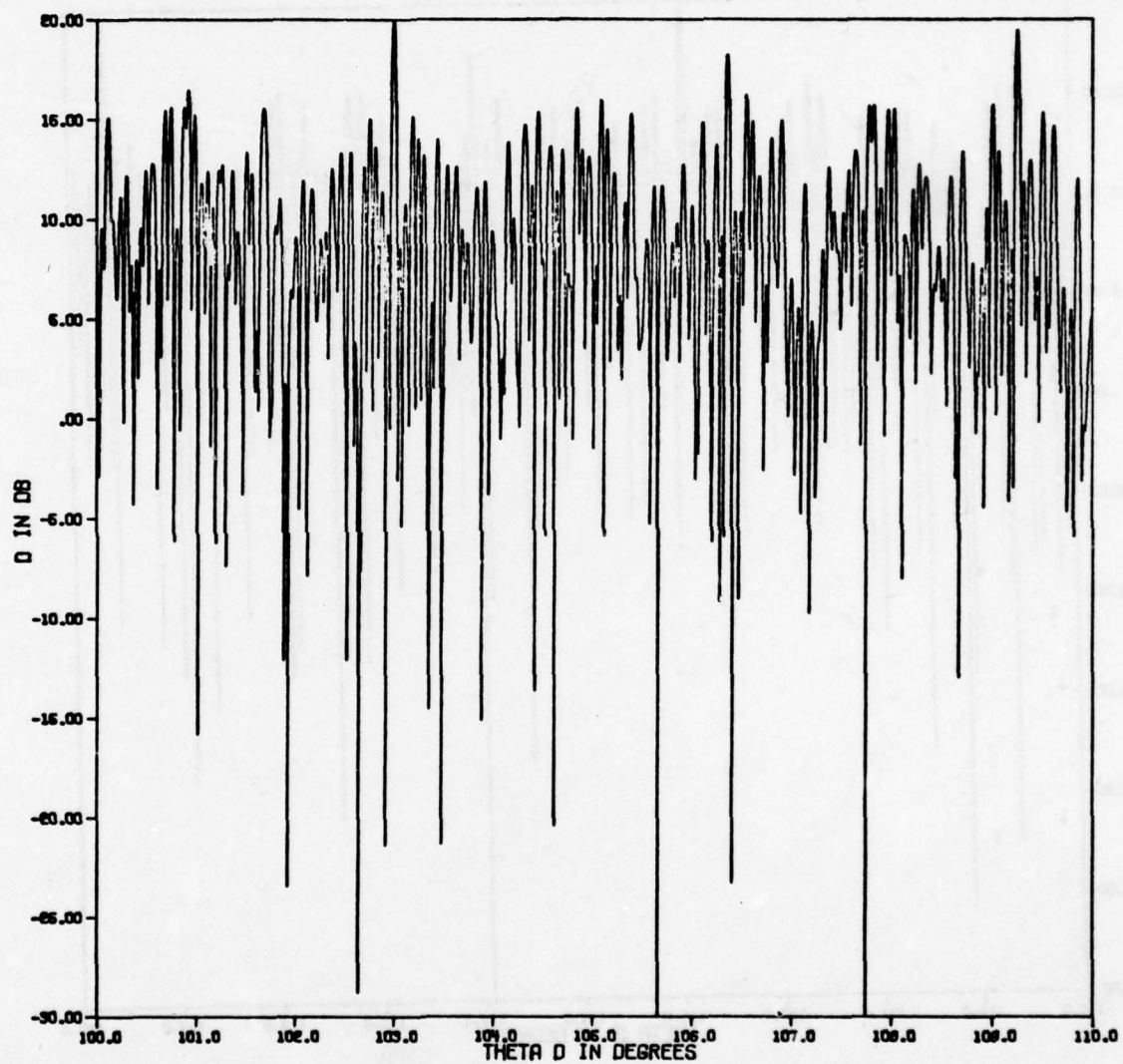


Figure 2-10j. Power ratio versus viewing angle for 10-point target.

D VS THETA D, THETA E = THETA D
FREQUENCY = 10 GHZ
10 REFLECTING POINTS

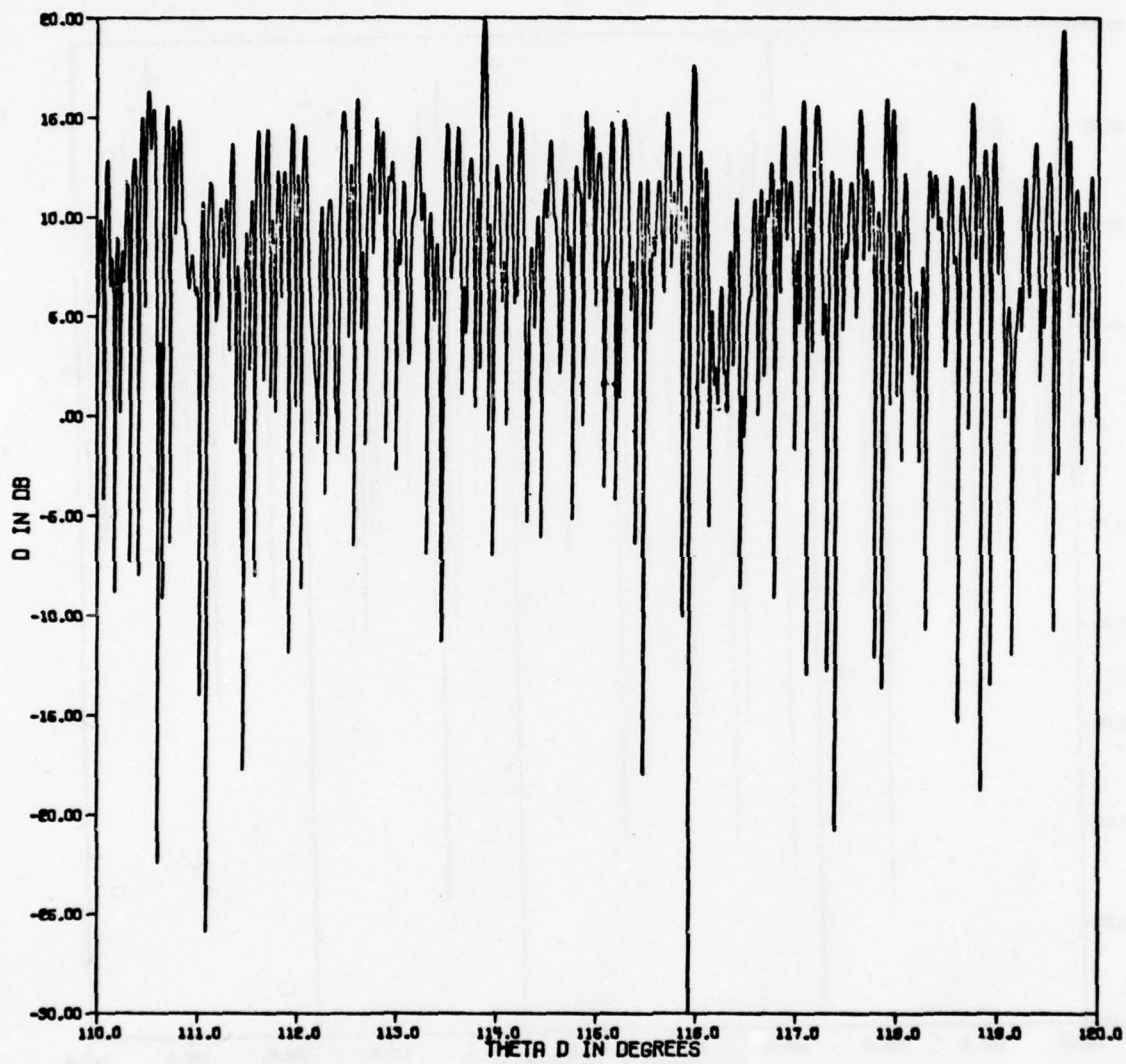


Figure 2-10k. Power ratio versus viewing angle for 10-point target.

D VS THETA D, THETA E = THETA D
FREQUENCY = 10 GHZ
10 REFLECTING POINTS

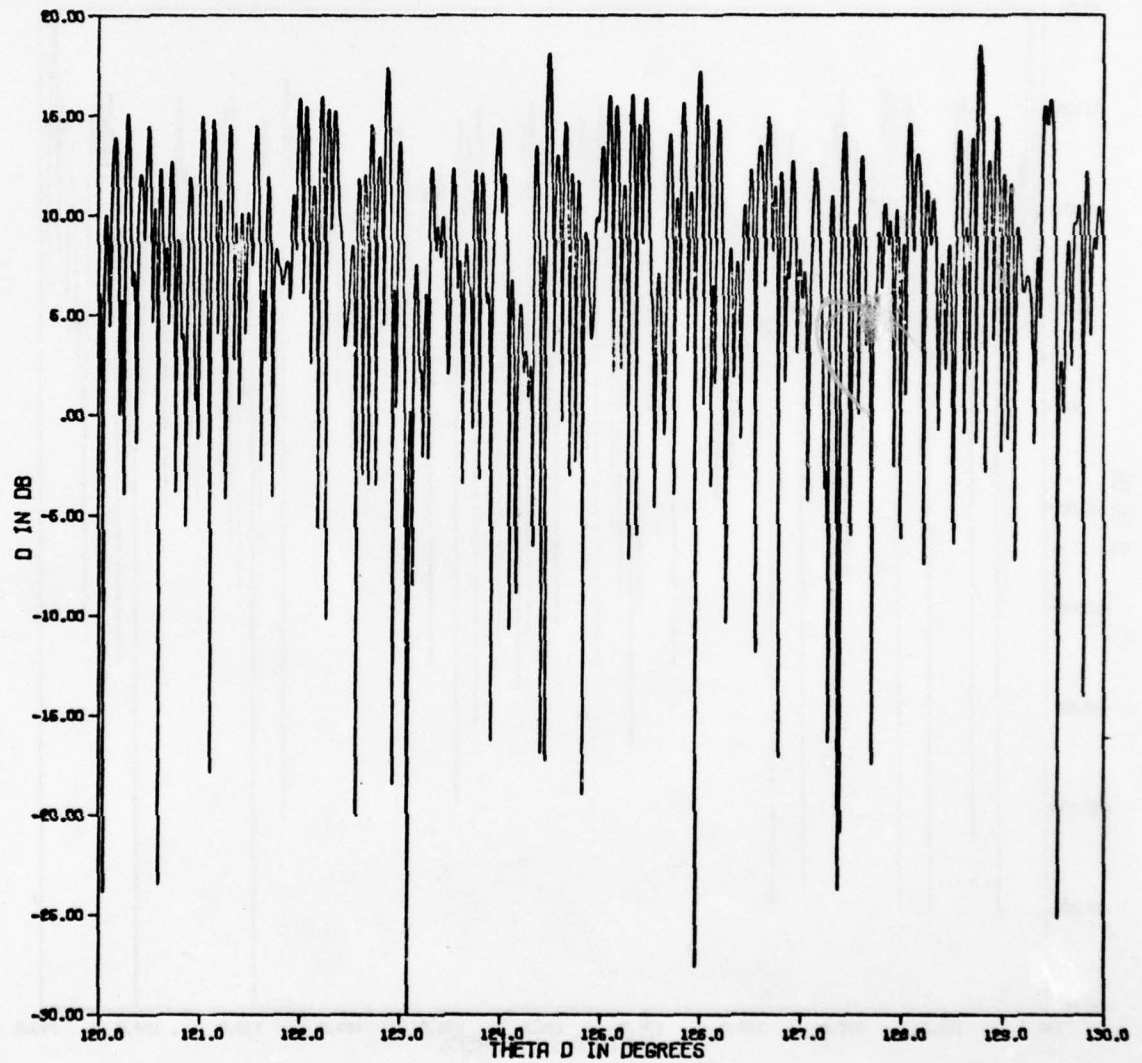


Figure 2-101. Power ratio versus viewing angle for 10-point target.

D VS THETA D, THETA E = THETA D
FREQUENCY = 10 GHZ
10 REFLECTING POINTS

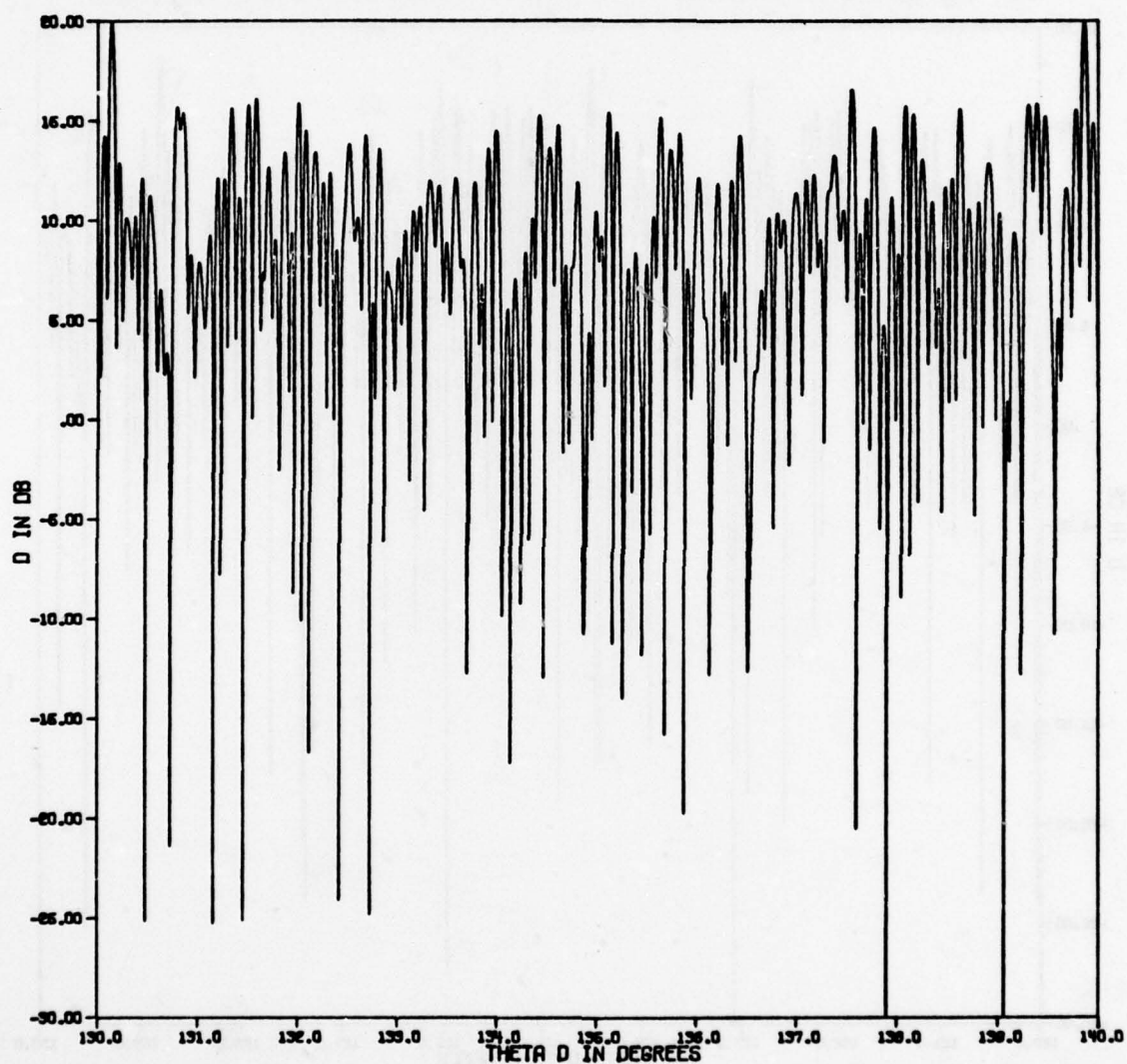


Figure 2-10m. Power ratio versus viewing angle for 10-point target.

D VS THETA D. THETA E = THETA D
FREQUENCY = 10 GHZ
10 REFLECTING POINTS

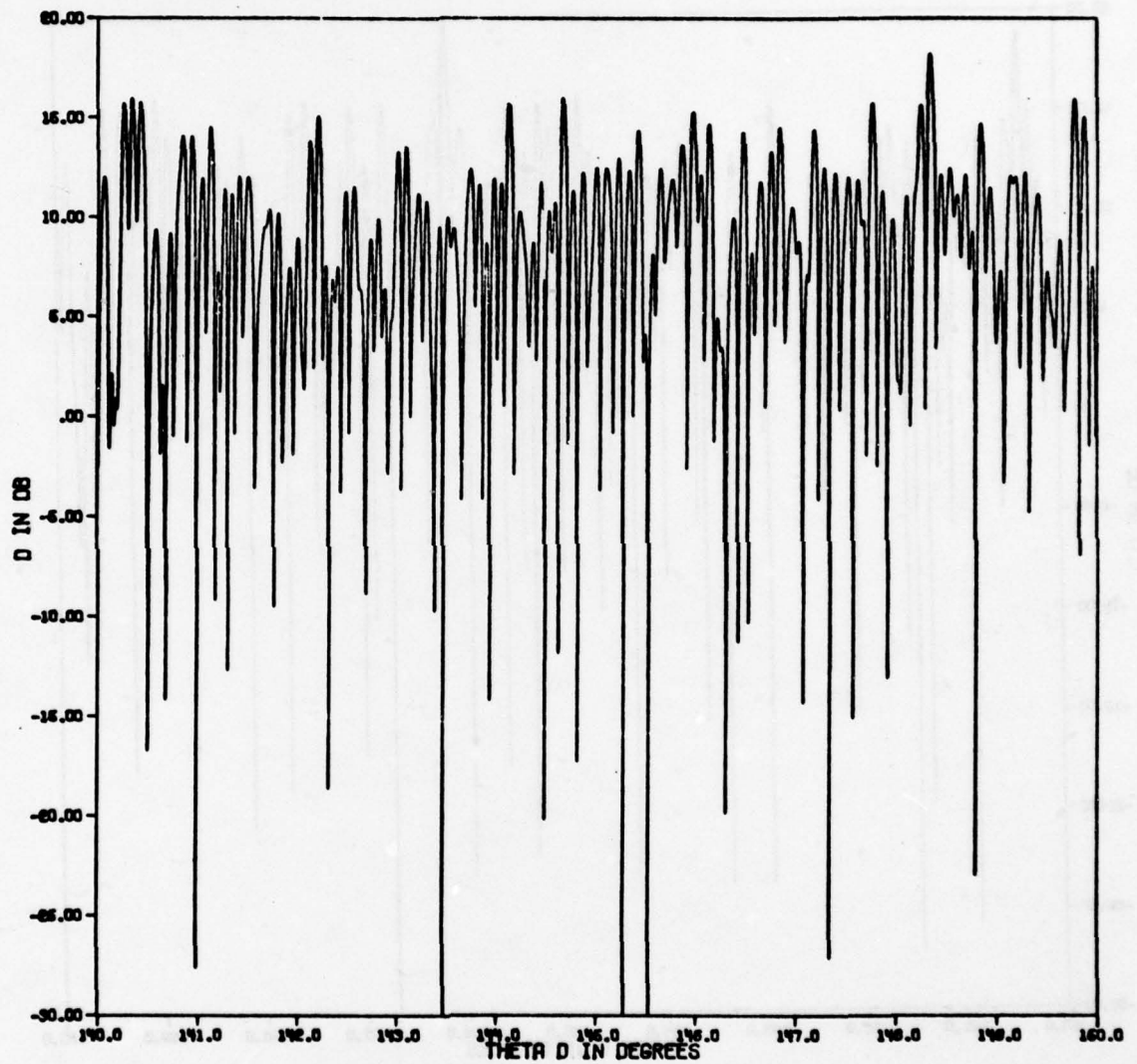


Figure 2-10n. Power ratio versus viewing angle for 10-point target.

D VS THETA D, THETA E = THETA D
FREQUENCY = 10 GHZ
10 REFLECTING POINTS

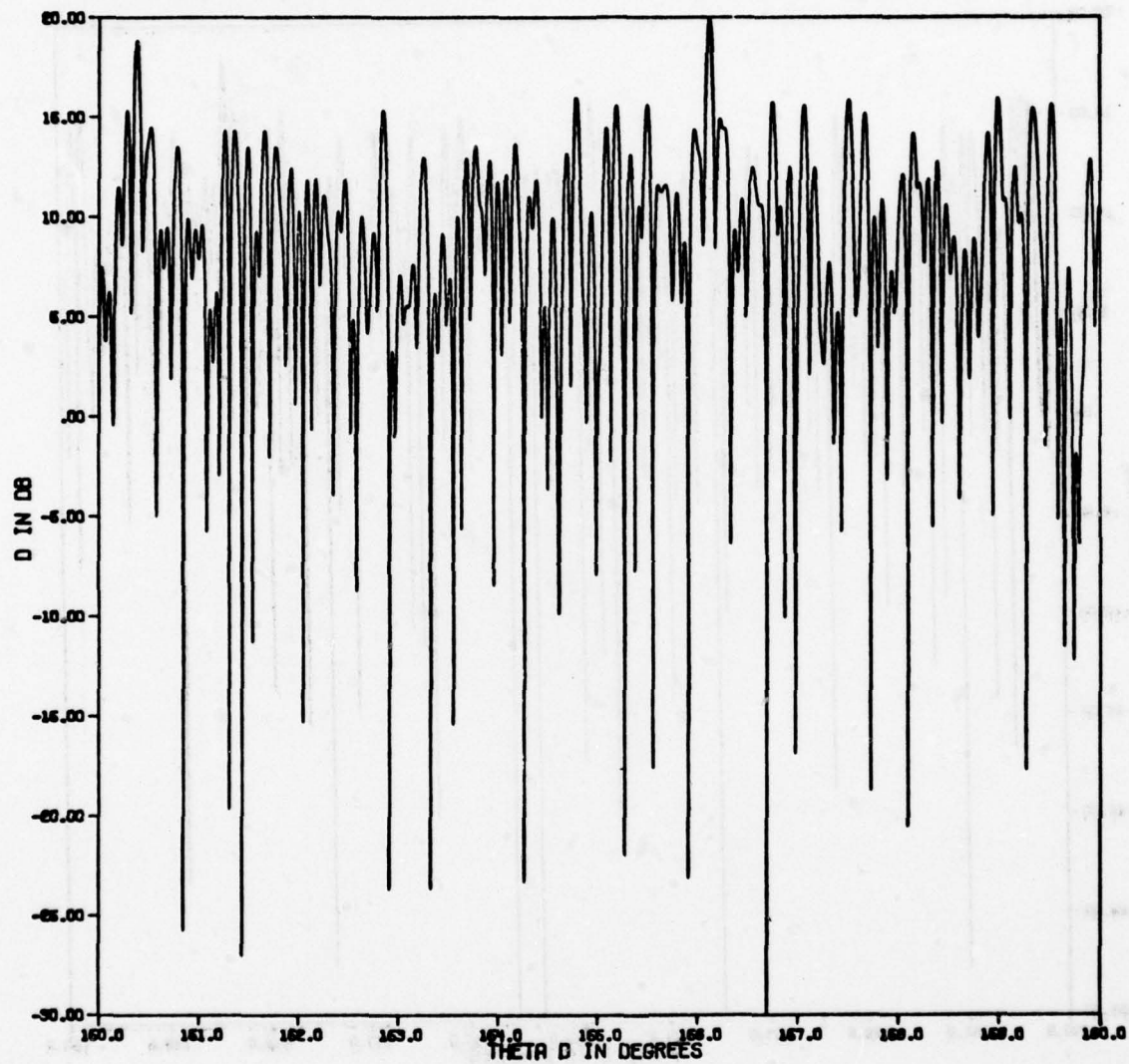


Figure 2-10o. Power ratio versus viewing angle for 10-point target.

D VS THETA D. THETA E = THETA D
FREQUENCY = 10 GHZ
10 REFLECTING POINTS

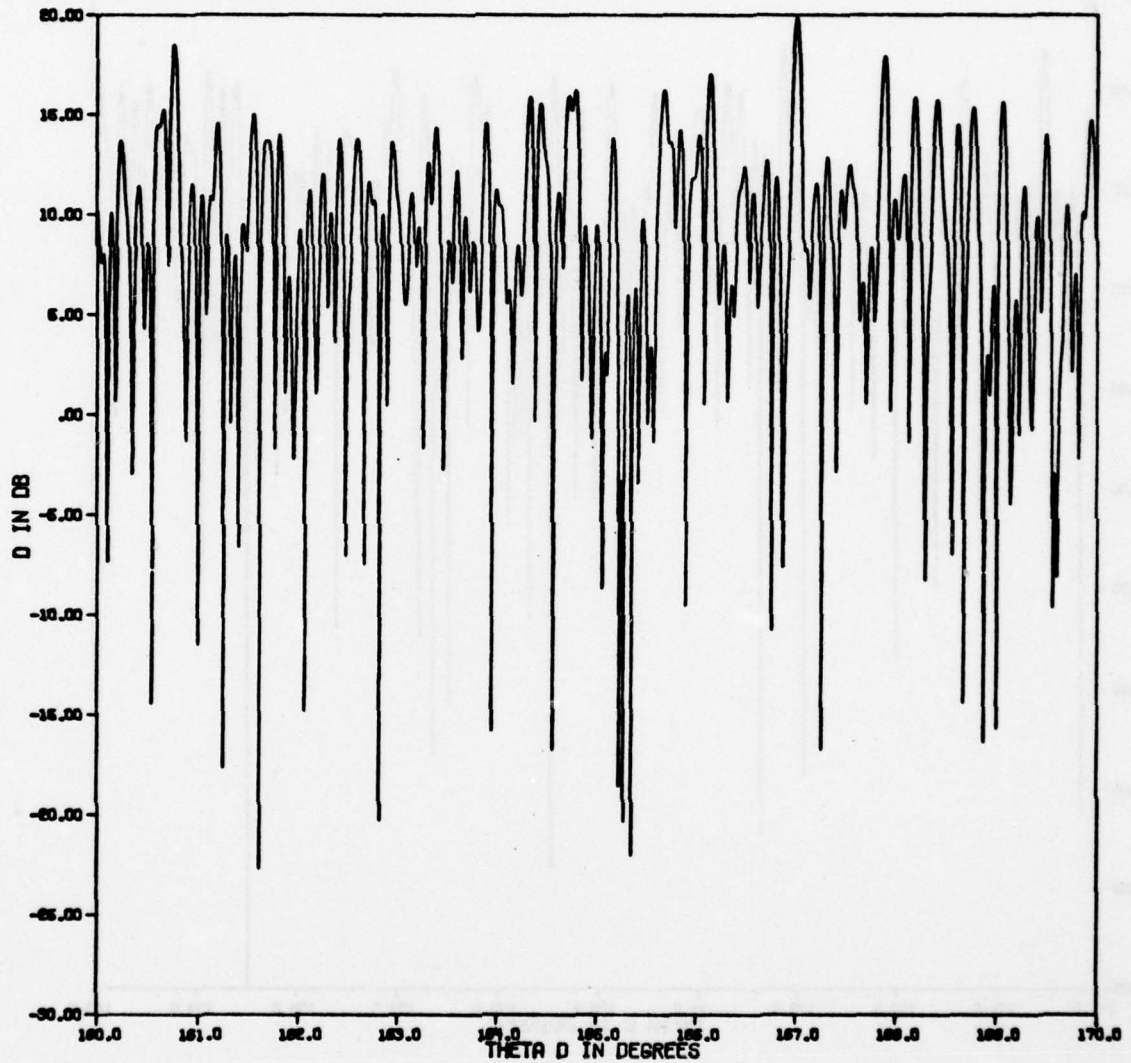


Figure 2-10p. Power ratio versus viewing angle for 10-point target.

D VS THETA D. THETA E = THETA D
FREQUENCY = 10 GHZ
10 REFLECTING POINTS

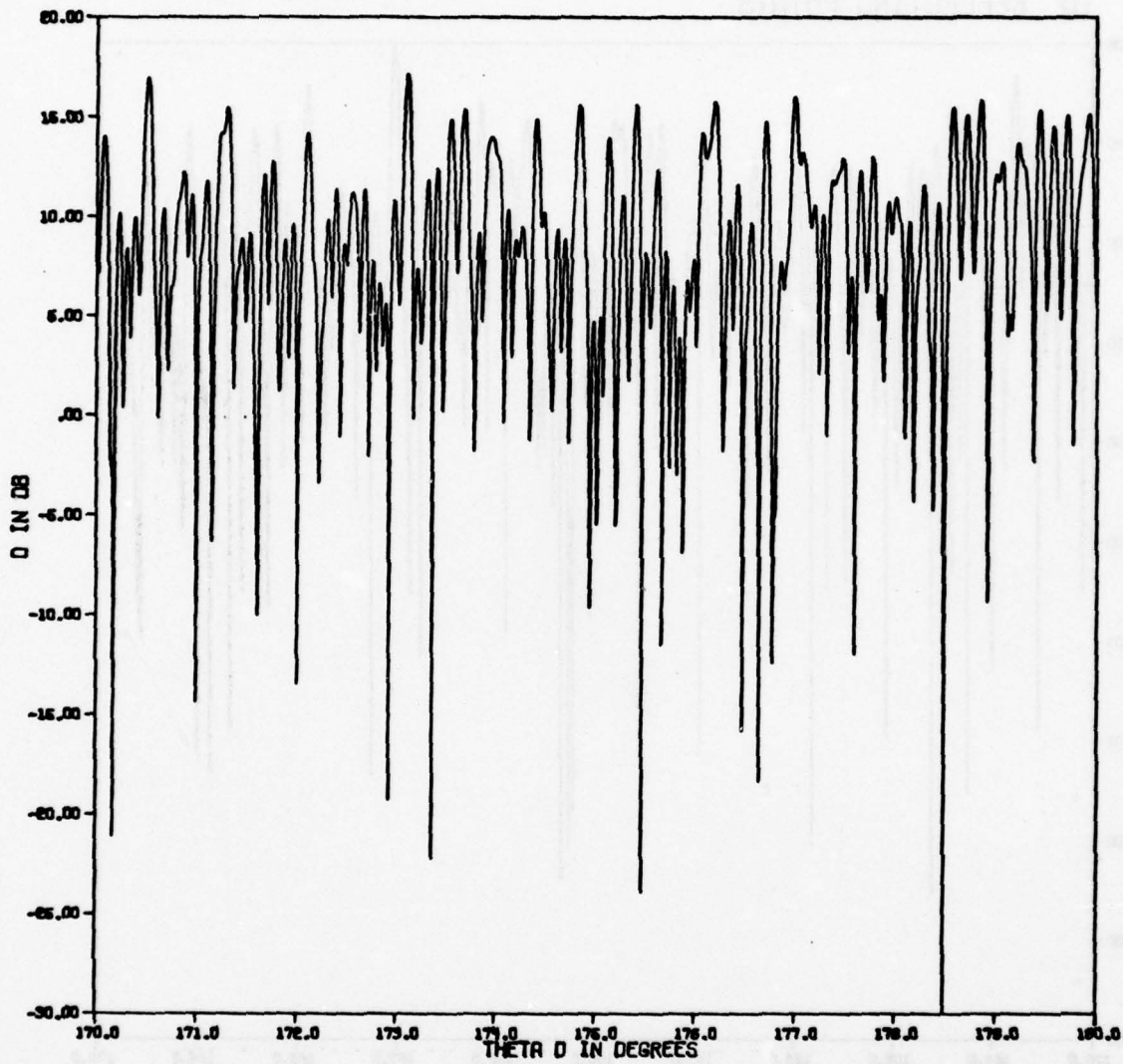


Figure 2-10q. Power ratio versus viewing angle for 10-point target.

do the maxima approach their limiting value of 20 dB; however, they generally are well above 10 dB.

2.2.3. Bistatic CW Signals

Assuming that a target is itself lossless it follows that all of the energy incident upon a target must be reradiated (i.e., scattered) in some direction. It is evident from Figures 2-6 through 2-10 that for many viewing angles and frequencies the power is not scattered back to the transmitter and therefore it must be reradiated in other directions. Figures 2-11a,b,c,d, 2-12a,b,c,d, and 2-13a,b,c,d show the bistatic power transfer function $|H(f)|^2$ as a function of viewing angle for frequencies $f = 1.04926419, 1.05991778, 4.49830053$ GHz, respectively. In each case the frequency was selected to correspond to a maximum near the extreme value for the backscattering case. The variations in amplitude with angle are of the same general nature as for the backscattering case. As would be expected, the maxima occur at different angular positions depending on the angle of incidence.

2.2.4. Pulse and Matched Filter Signals

Using as the transmitted signal a rectangular pulse with no carrier component, an energy ratio is obtained that is the maximum possible for any frequency. Use of this signal is equivalent to assuming that the returns from all scatterers add coherently; i.e., in phase. In this way, it is possible to obtain the upper bound on possible performance for any configuration. Figure 2-14, the energy ratio for the 10-point target as a function of viewing angle when five 1 ns pulses spaced 5 ns apart are employed. By comparison with Figures 1-14 and 1-15 it is seen that this is less effective than using a single pulse because of the many minima compared to the single pulse case.

MAG SQUARED OF H VS DETECTOR ANGLE
THETA E = 0 DEGREES
FREQUENCY = 1.04926419 GHZ
10 REFLECTING POINTS

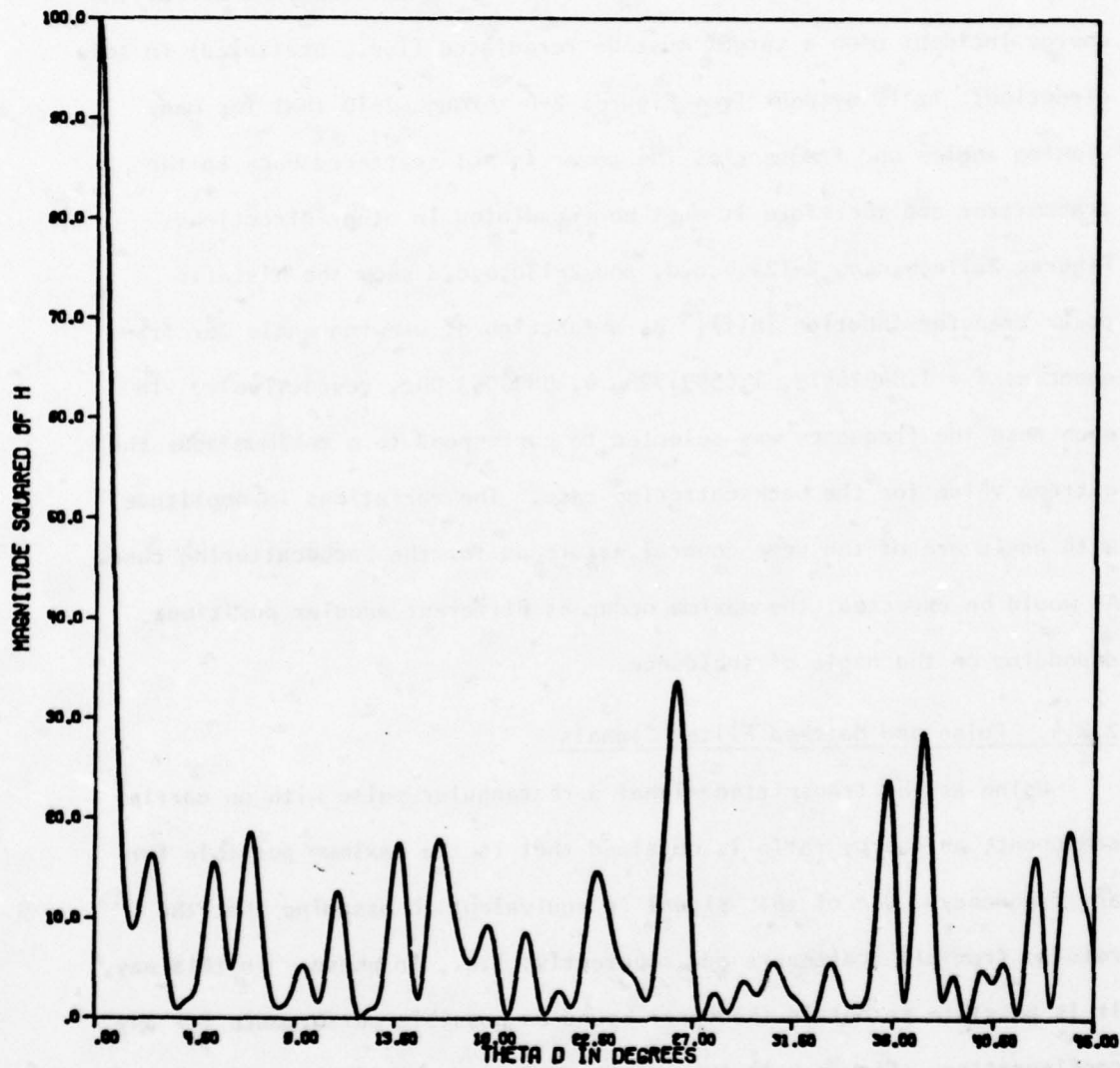


Figure 2-11a. Bistatic power transfer function versus viewing angle for 10-point target.

MAG SQUARED OF H VS DETECTOR ANGLE
THETA E = 0 DEGREES
FREQUENCY = 1.04926419 GHZ
10 REFLECTING POINTS

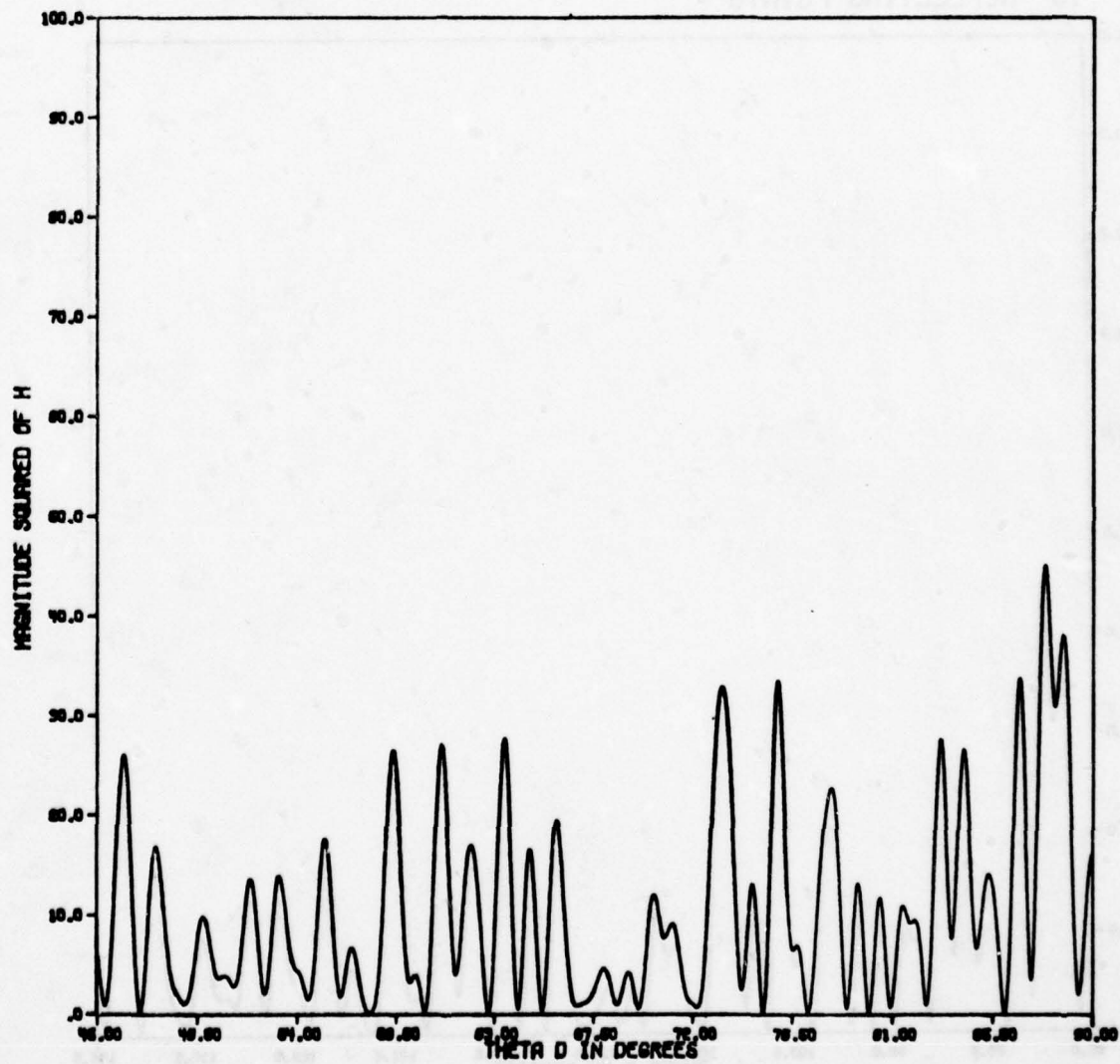


Figure 2-11b. Bistatic power transfer function versus viewing angle for 10-point target.

MAG SQUARED OF H VS DETECTOR ANGLE
THETA E = 0 DEGREES
FREQUENCY = 1.04926419 GHZ
10 REFLECTING POINTS

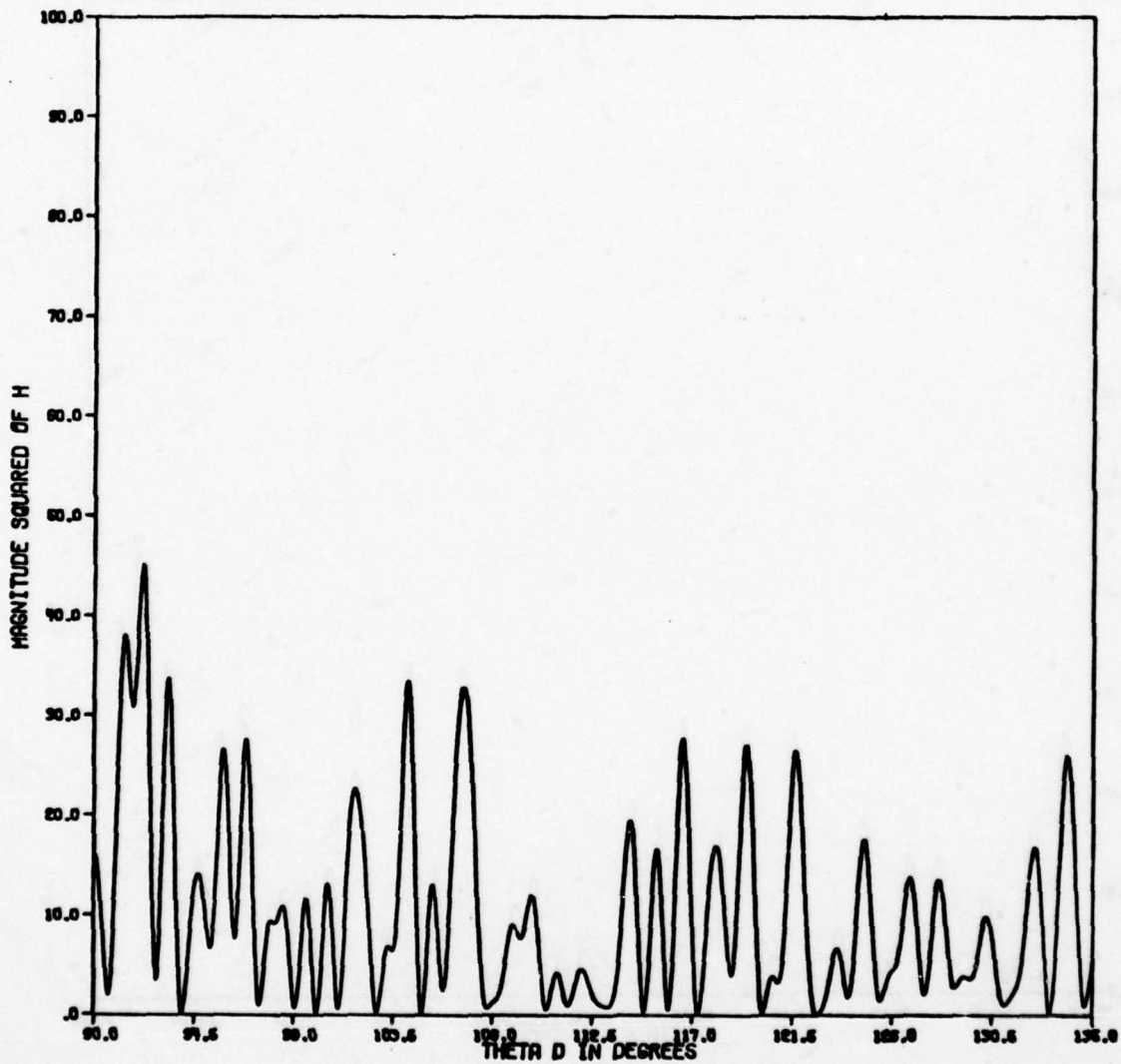


Figure 2-11c. Bistatic power transfer function versus viewing angle for 10-point target.

MAG SQUARED OF H VS DETECTOR ANGLE
THETA E = 0 DEGREES
FREQUENCY = 1.04926419 GHZ
10 REFLECTING POINTS

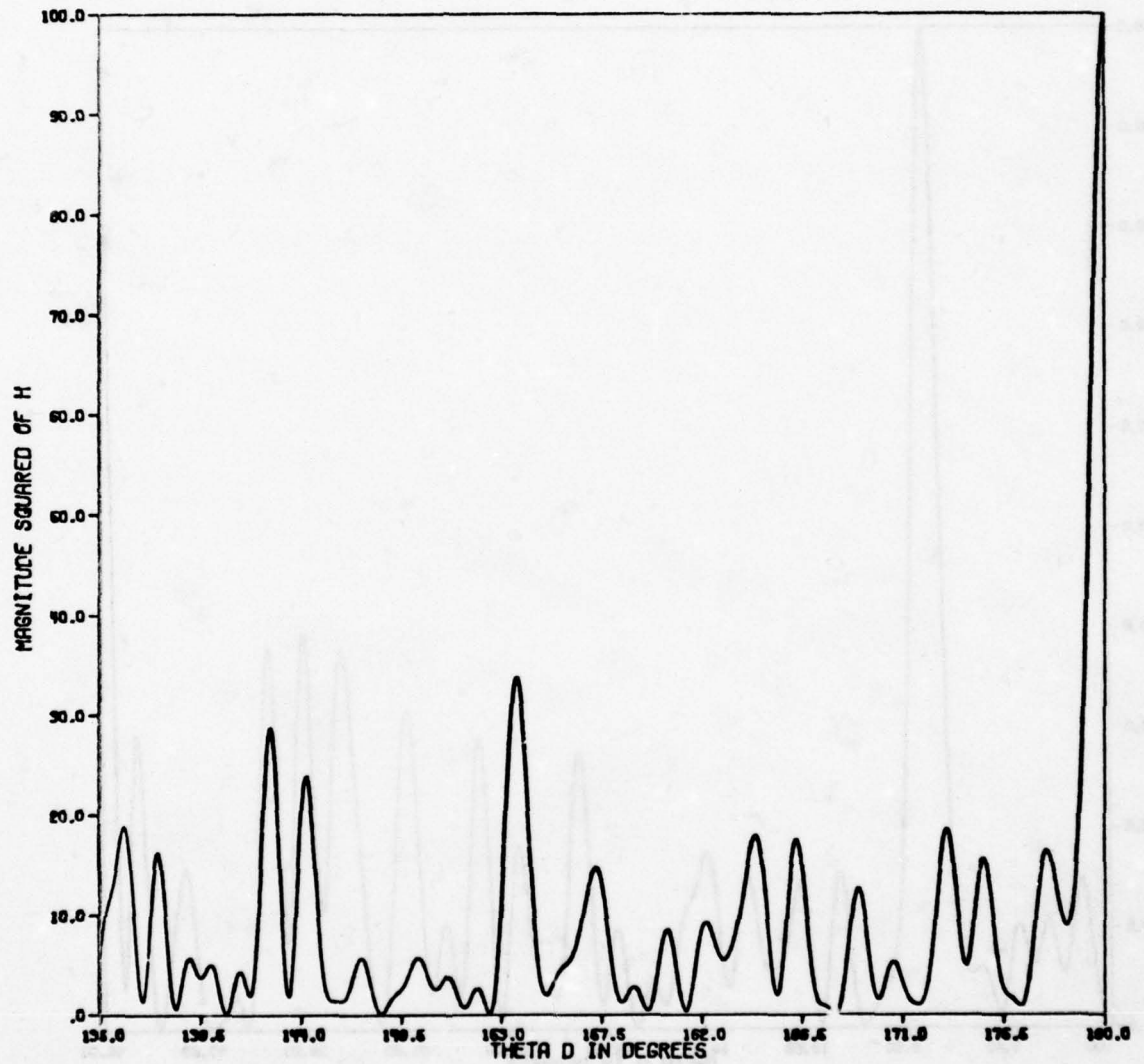


Figure 2-11d. Bistatic power transfer function versus viewing angle for 10-point target.

MAG SQUARED OF H VS DETECTOR ANGLE
THETA E = 45 DEGREES
FREQUENCY = 1.05991778 GHZ
10 REFLECTING POINTS

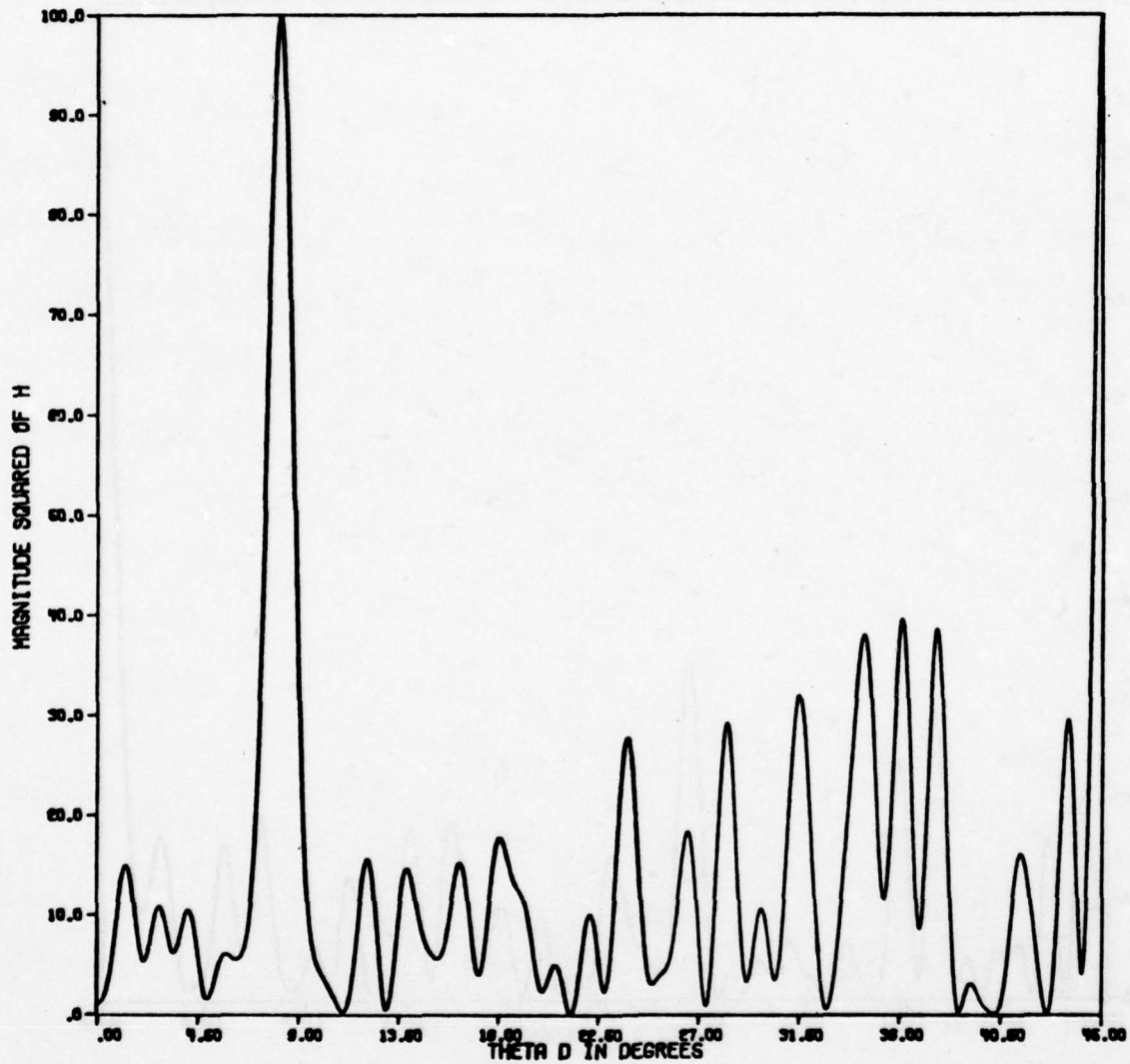


Figure 2-12a. Bistatic power transfer function versus viewing angle for 10-point target.

MAG SQUARED OF H VS DETECTOR ANGLE
THETA E = 45 DEGREES
FREQUENCY = 1.05991778 GHZ
10 REFLECTING POINTS

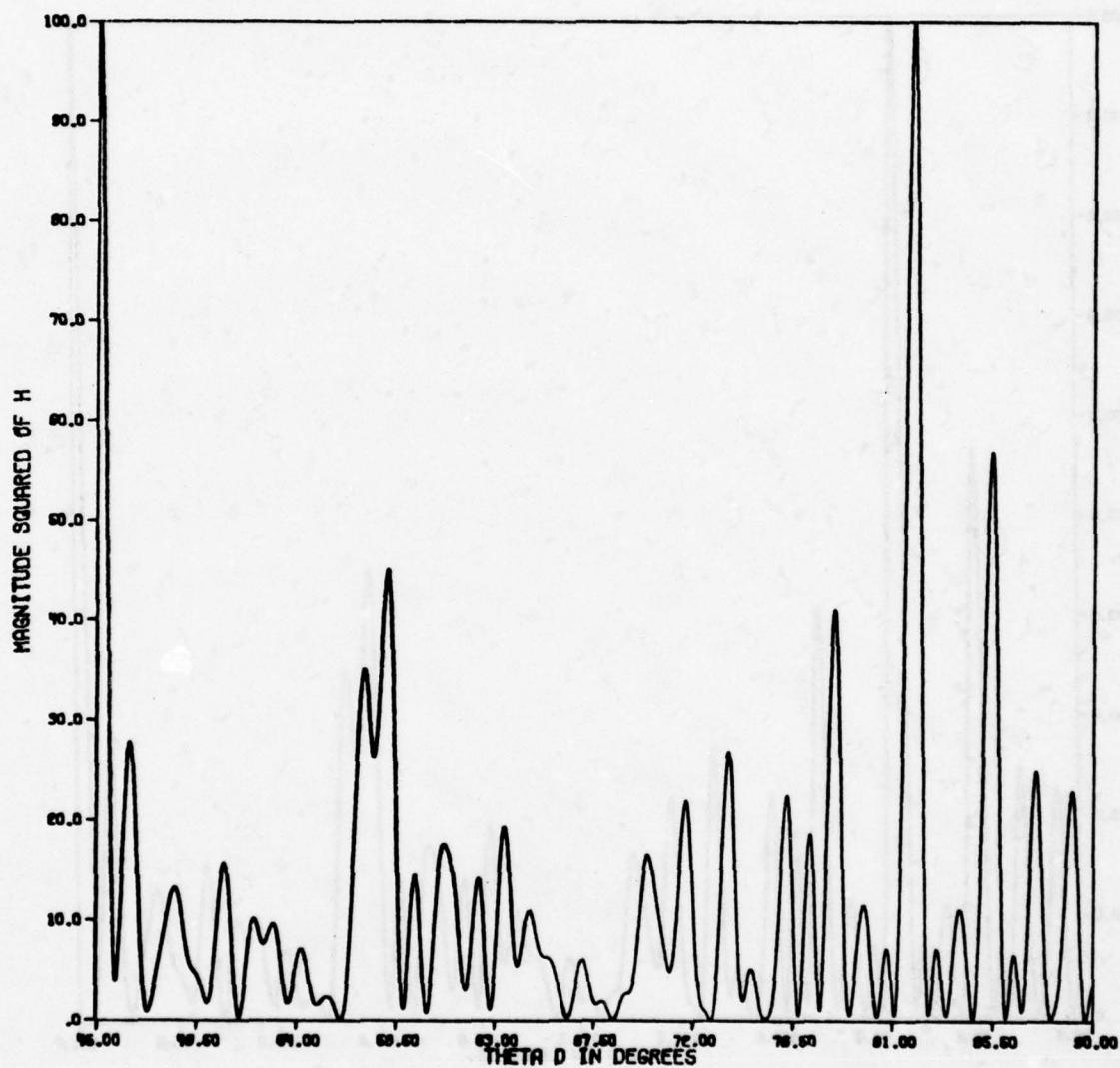


Figure 2-12b. Bistatic power transfer function versus viewing angle for 10-point target.

MAG SQUARED OF H VS DETECTOR ANGLE
THETA E = 45 DEGREES
FREQUENCY = 1.05991778 GHZ
10 REFLECTING POINTS

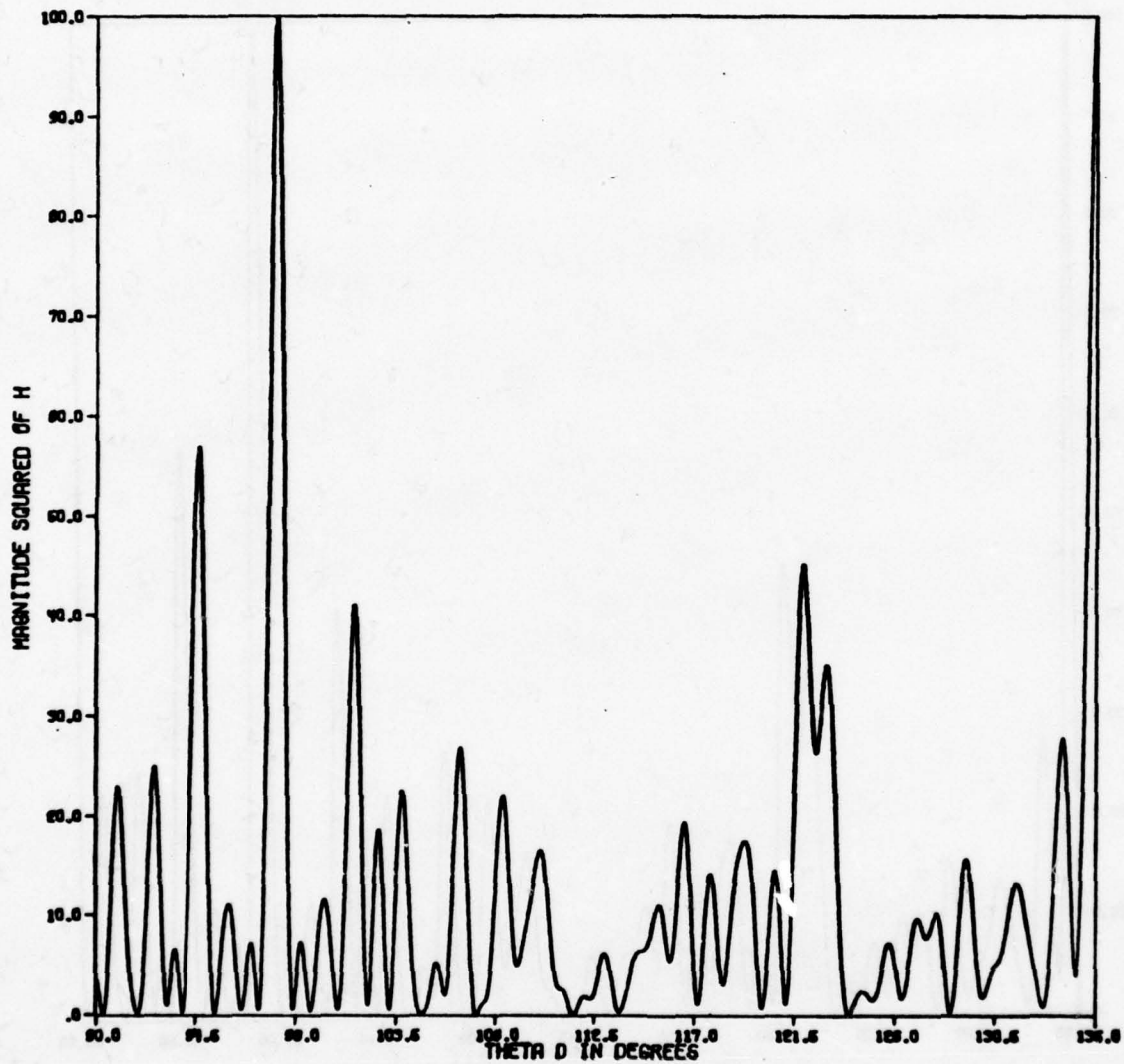


Figure 2-12c. Bistatic power transfer function versus viewing angle for 10-point target.

MAG SQUARED OF H VS DETECTOR ANGLE
THETA E = 45 DEGREES
FREQUENCY = 1.05991778 GHZ
10 REFLECTING POINTS

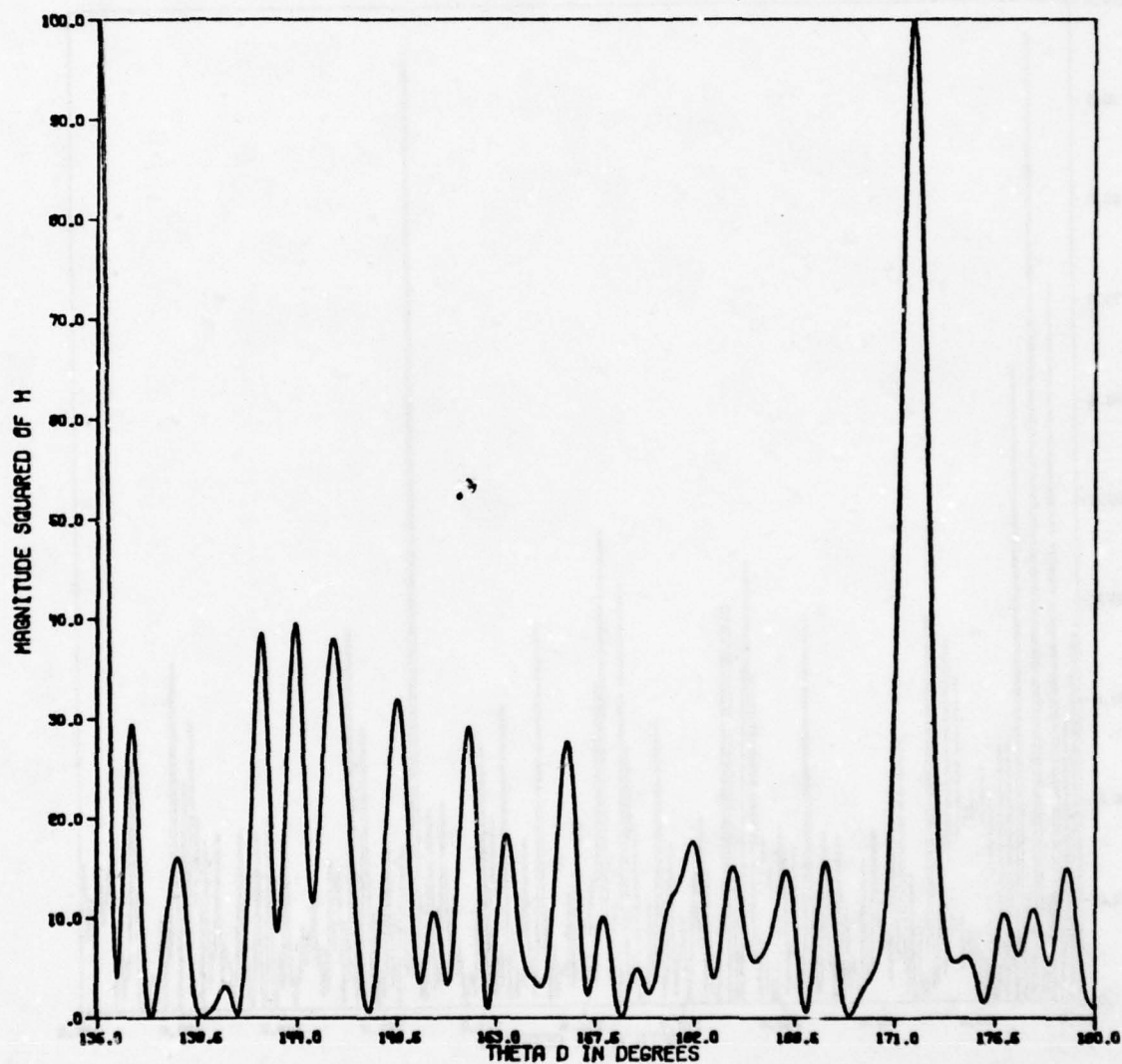


Figure 2-12d. Bistatic power transfer function versus viewing angle for 10-point target.

MAG SQUARED OF H VS DETECTOR ANGLE
THETA E = 60 DEGREES
FREQUENCY = 4.49830053 GHZ
10 REFLECTING POINTS

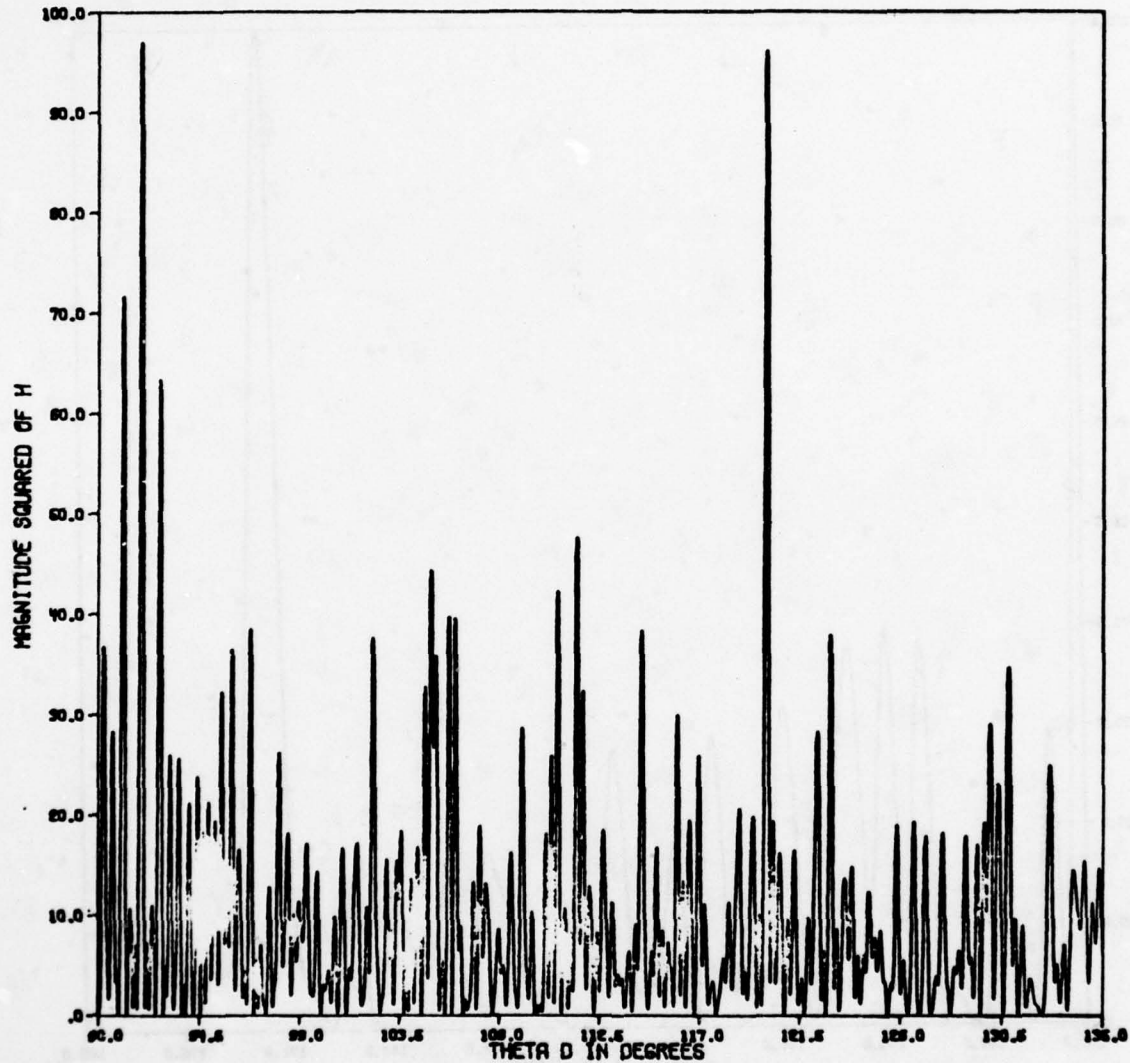


Figure 2-13a. Bistatic power transfer function versus viewing angle for 10-point target.

MAG SQUARED OF H VS DETECTOR ANGLE
THETA E = 60 DEGREES
FREQUENCY = 4.49830053 GHZ
10 REFLECTING POINTS

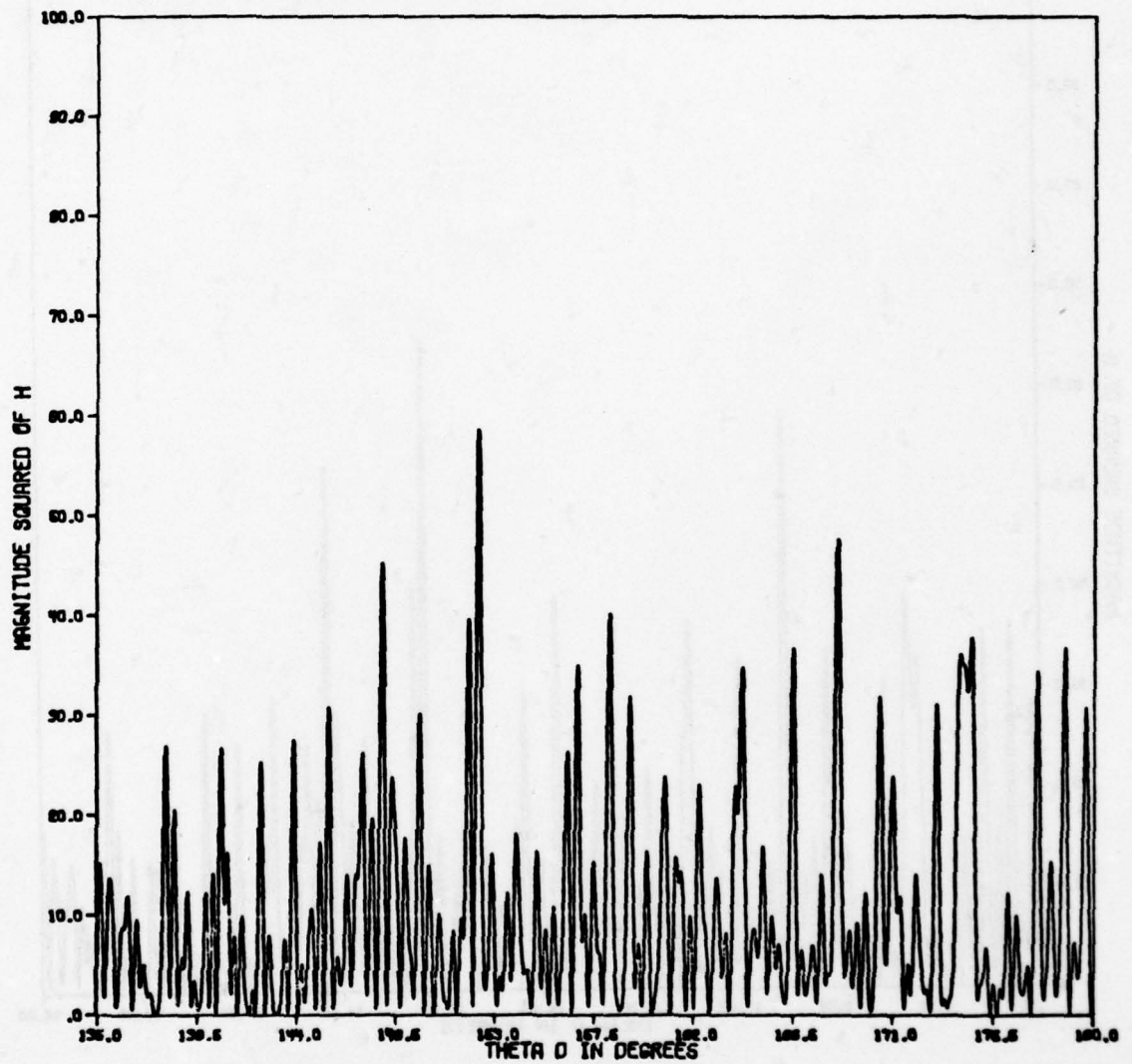


Figure 2-13b. Bistatic power transfer function versus viewing angle for 10-point target.

MAG SQUARED OF H VS DETECTOR ANGLE
THETA E = 60 DEGREES
FREQUENCY = 4.49830053 GHZ
10 REFLECTING POINTS

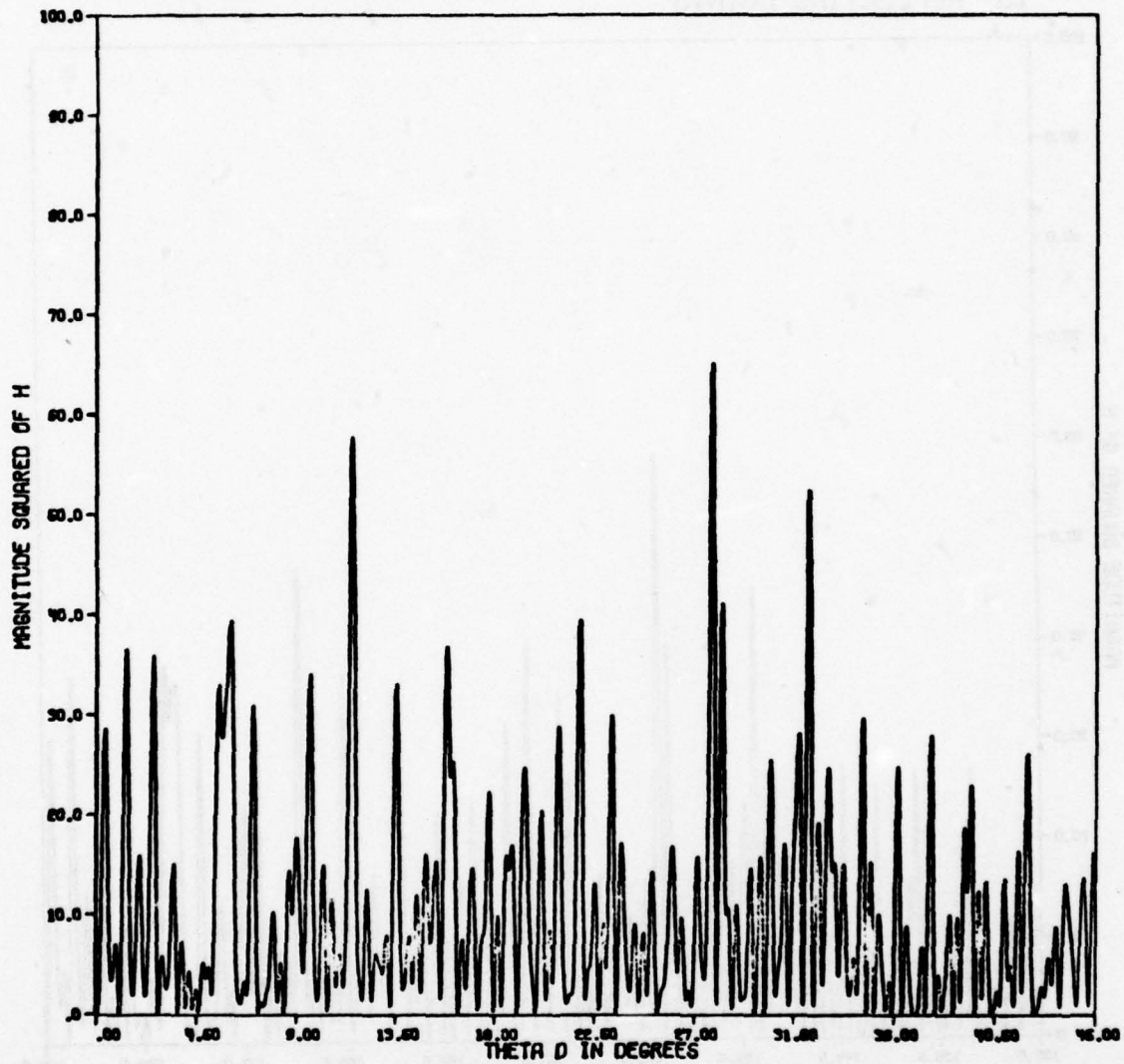


Figure 2-13c. Bistatic power transfer function versus viewing angle for 10-point target.

MAG SQUARED OF H VS DETECTOR ANGLE
THETA E = 60 DEGREES
FREQUENCY = 4.49830053 GHZ
10 REFLECTING POINTS

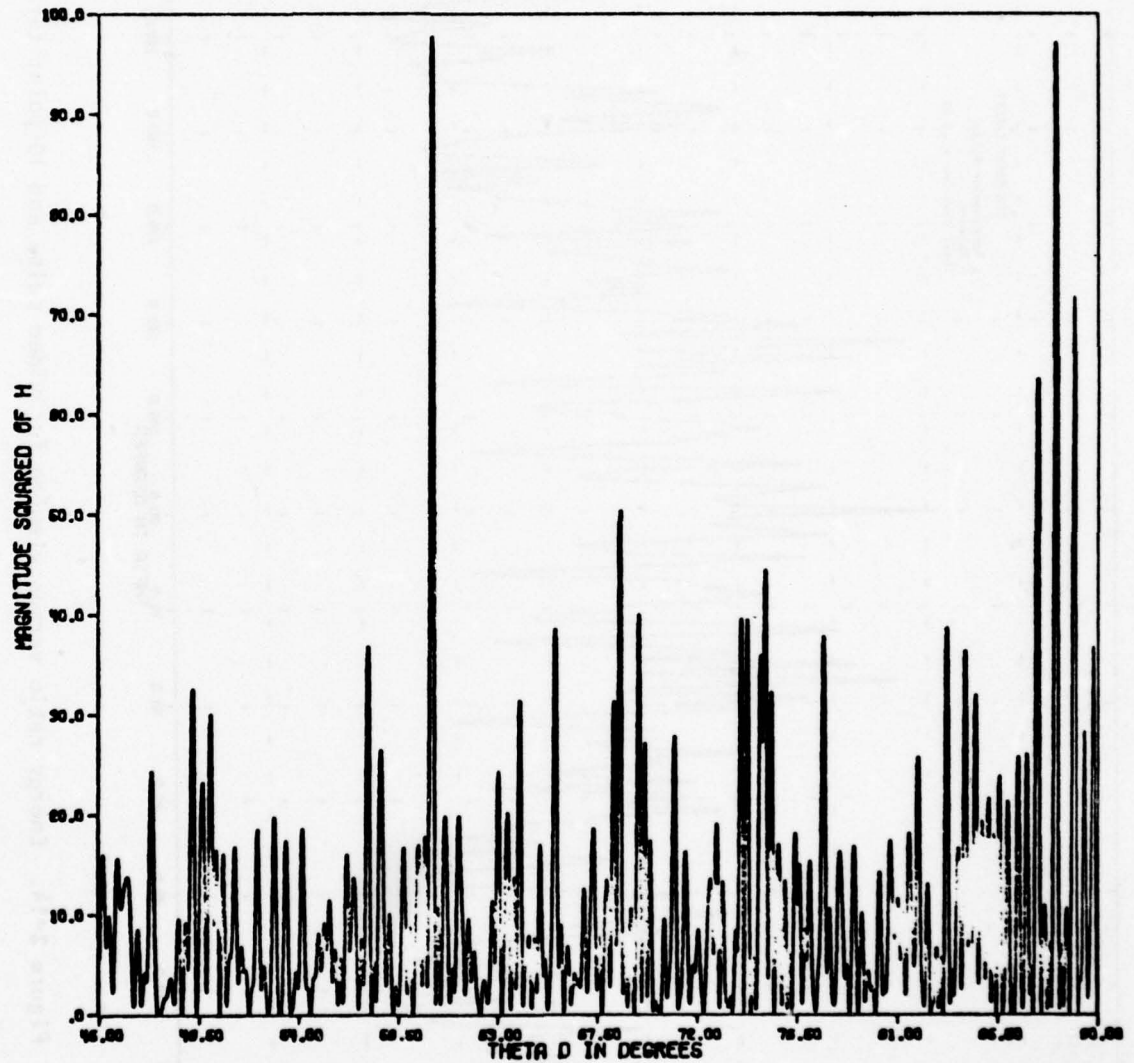


Figure 2-13d. Bistatic power transfer function versus viewing angle for 10-point target.

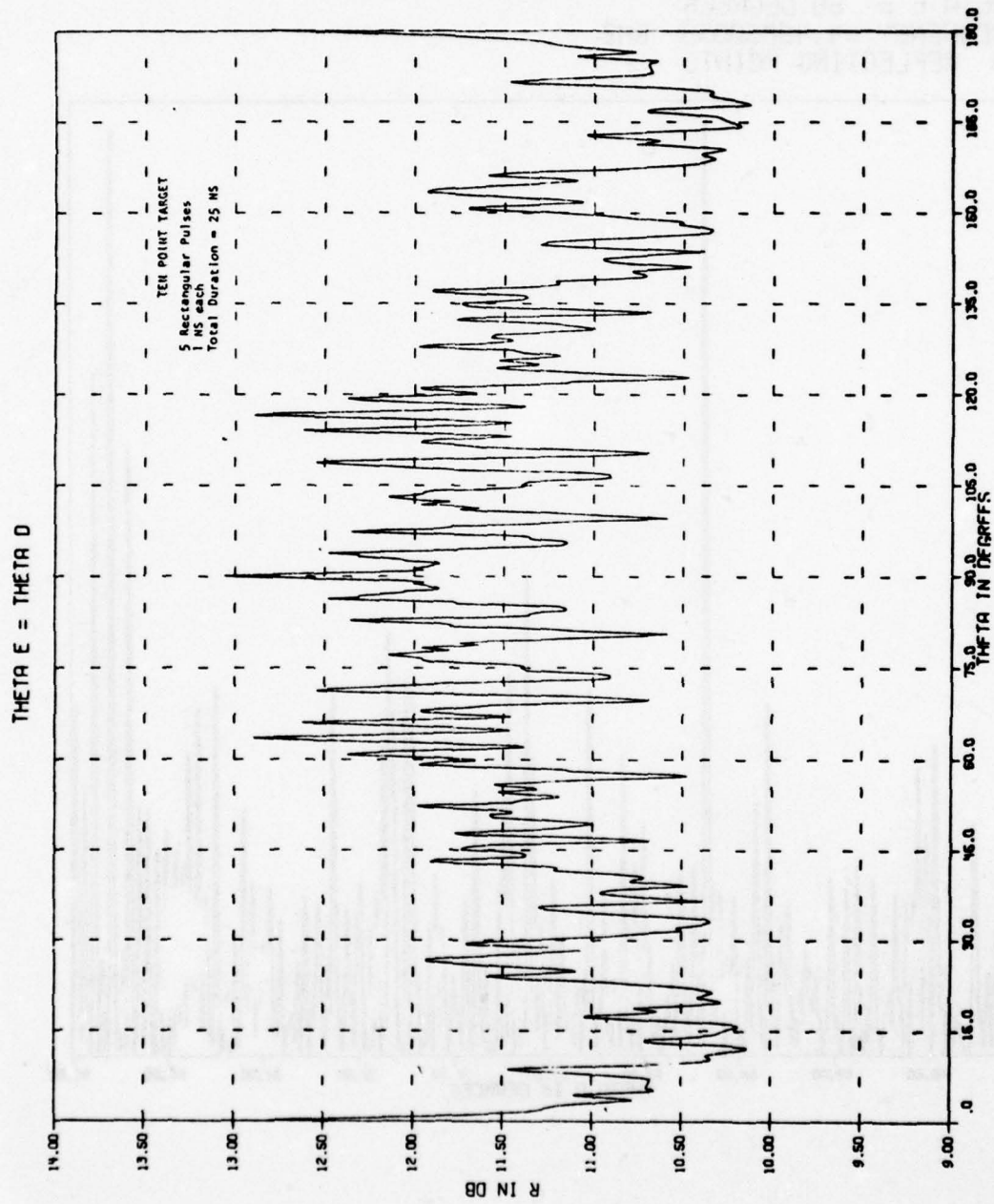


Figure 2-14. Energy ratio versus viewing for video pulse and 10-point target.

Figures 2-15a,b,c,d show the energy ratio for the matched filter signal as a function of θ_D in the vicinity of one of the maxima shown in Figure 1-17 and for four different pulse durations. It is clear from these figures that short pulse durations accentuate the sharpness of the response as a function of angle but do not give any increase in the maximum energy ratio.

2.2.5. RF Pulse Signals

Figure 2-16 shows the energy ratio as a function of viewing angle for the 10-point target illuminated by a 480 ns pulse at 1 GHz. The viewing angle ranges from 85° to 95° which encompasses a theoretical maximum which occurs at 90°. Figure 2-17 shows the same data for a frequency of 1.20306 GHz which is one of the frequencies for which $|H(f)|^2$ is a maximum as seen from Figure 2-6e. Because of the finite duration of the pulse, the full maximum is not reached; however, it comes within approximately 1 dB of the full maximum.

Figures 2-18a,b,c show the energy ratio for the 10-point target versus frequency for a 300 ns RF pulse at viewing angles of 90°, 89.9° and 89.5°, respectively. The high angular sensitivity of the target is clearly evident in these figures.

2.2.6. Simultaneous Angle and Frequency Variations

Figures 2-19, 2-20 and 2-21 show 3D plots of the CW power ratio for the 10-point target for simultaneous variations in both frequency and viewing angle. The discontinuous nature of the loci of maximum power ratios as discussed in connection with Figure 1-21 is also clearly evident in these figures.

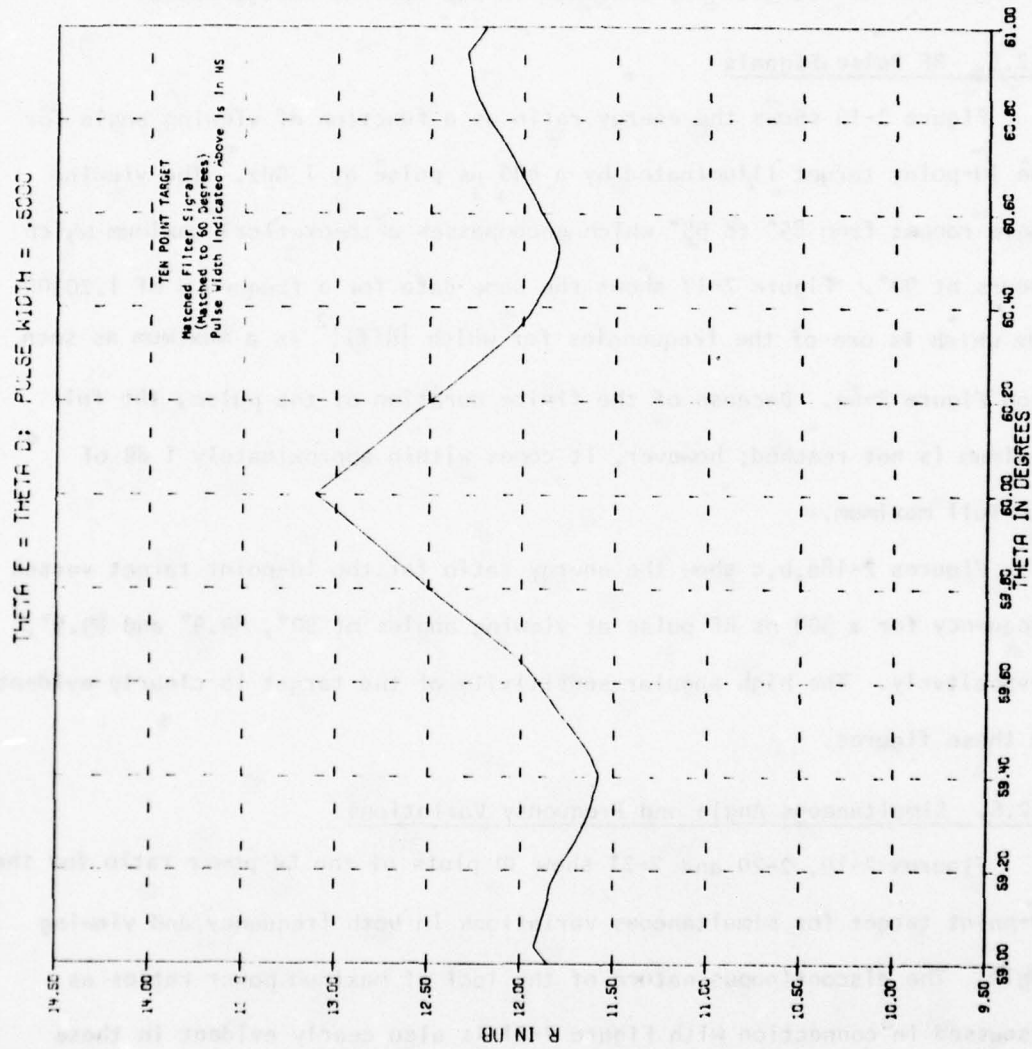


Figure 2-15a. Energy ratio versus viewing for video pulse and 10-point target.

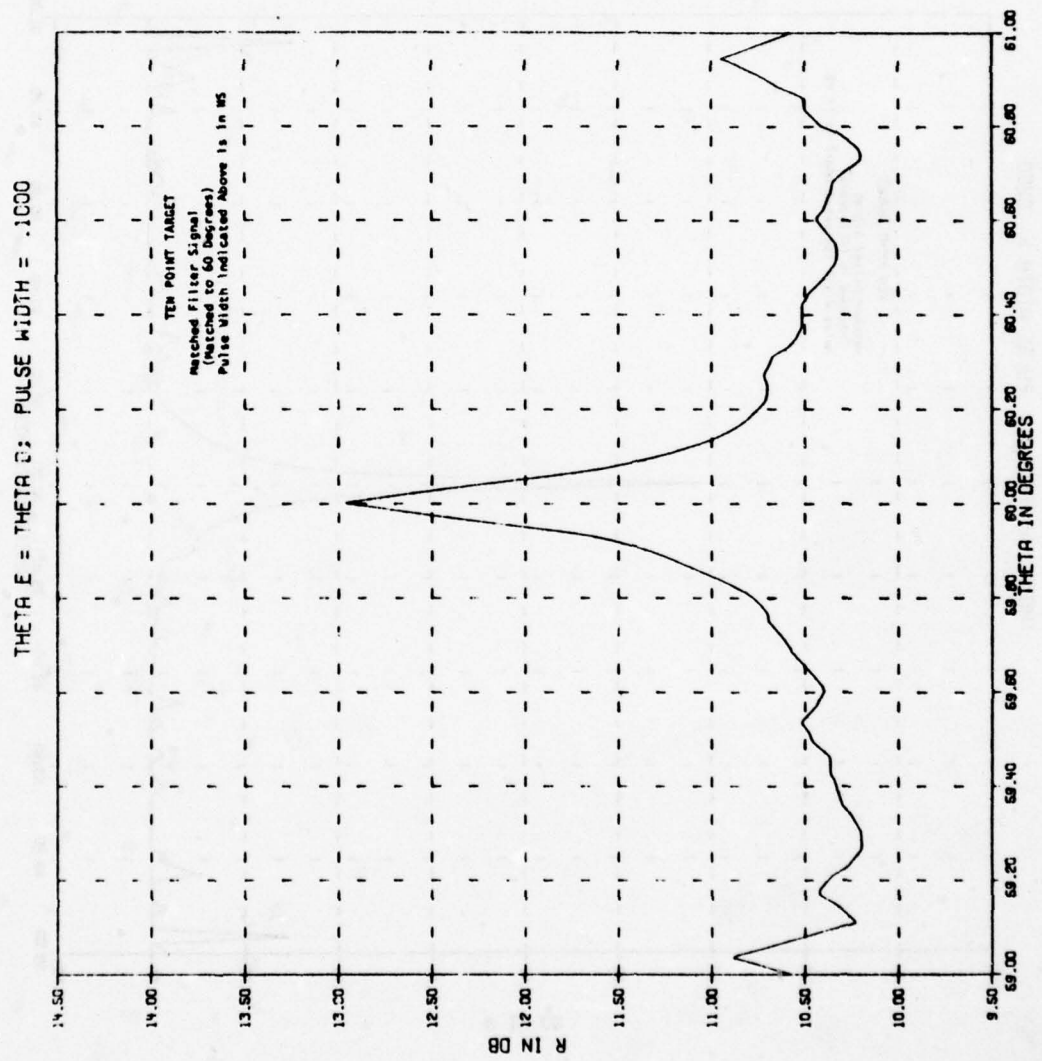


Figure 2-15b. Energy ratio versus viewing for video pulse and 10-point target.

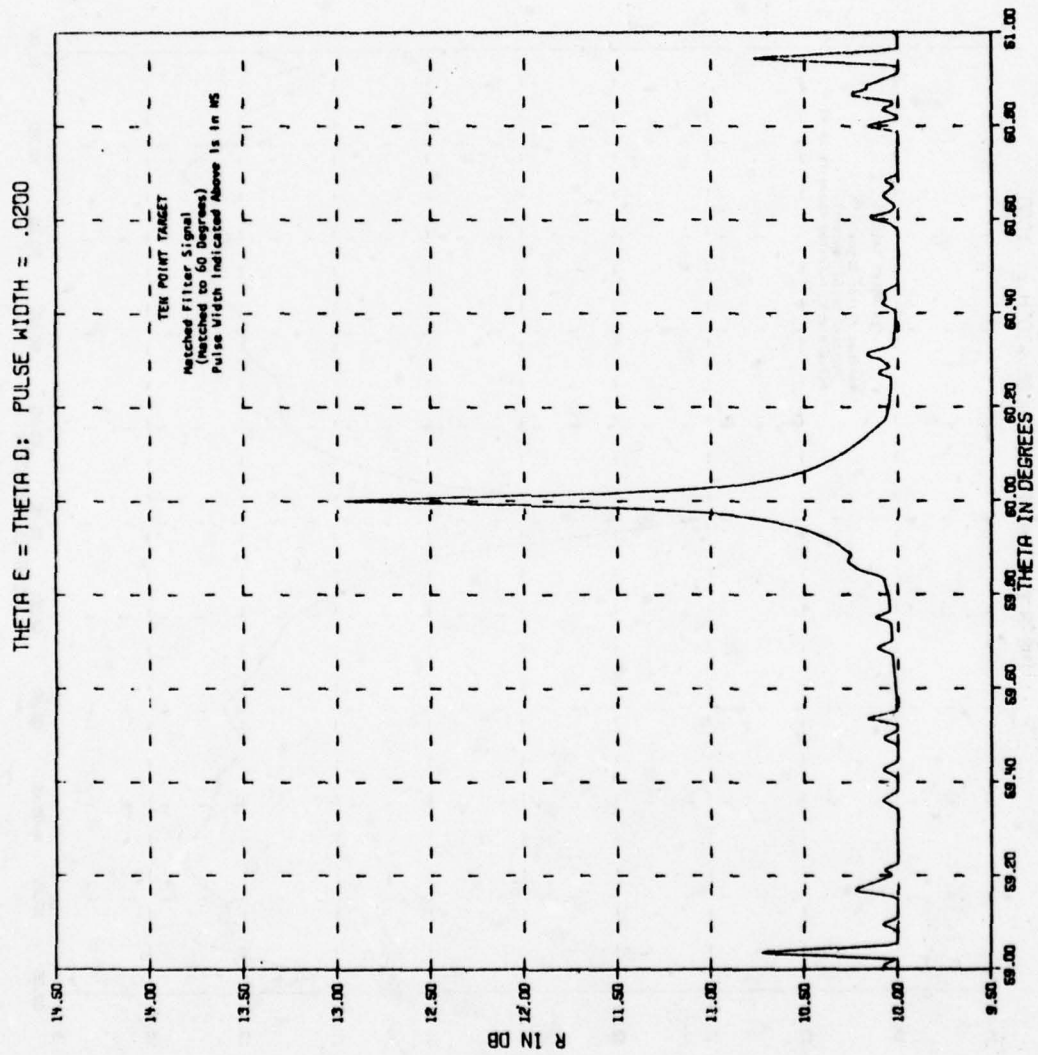


Figure 2-15c. Energy ratio versus viewing for video pulse and 10-point target.

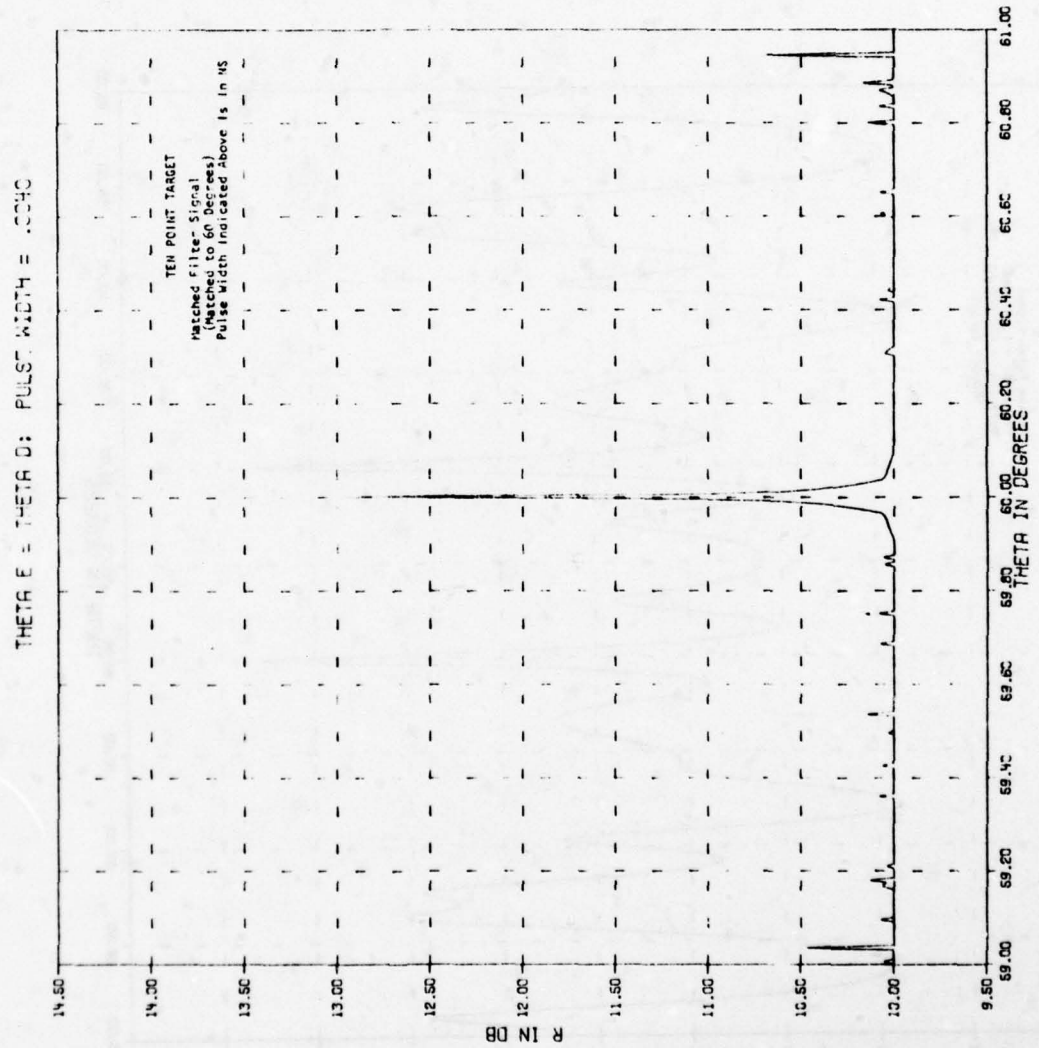


Figure 2-15d. Energy ratio versus viewing for video pulse and 10-point target.

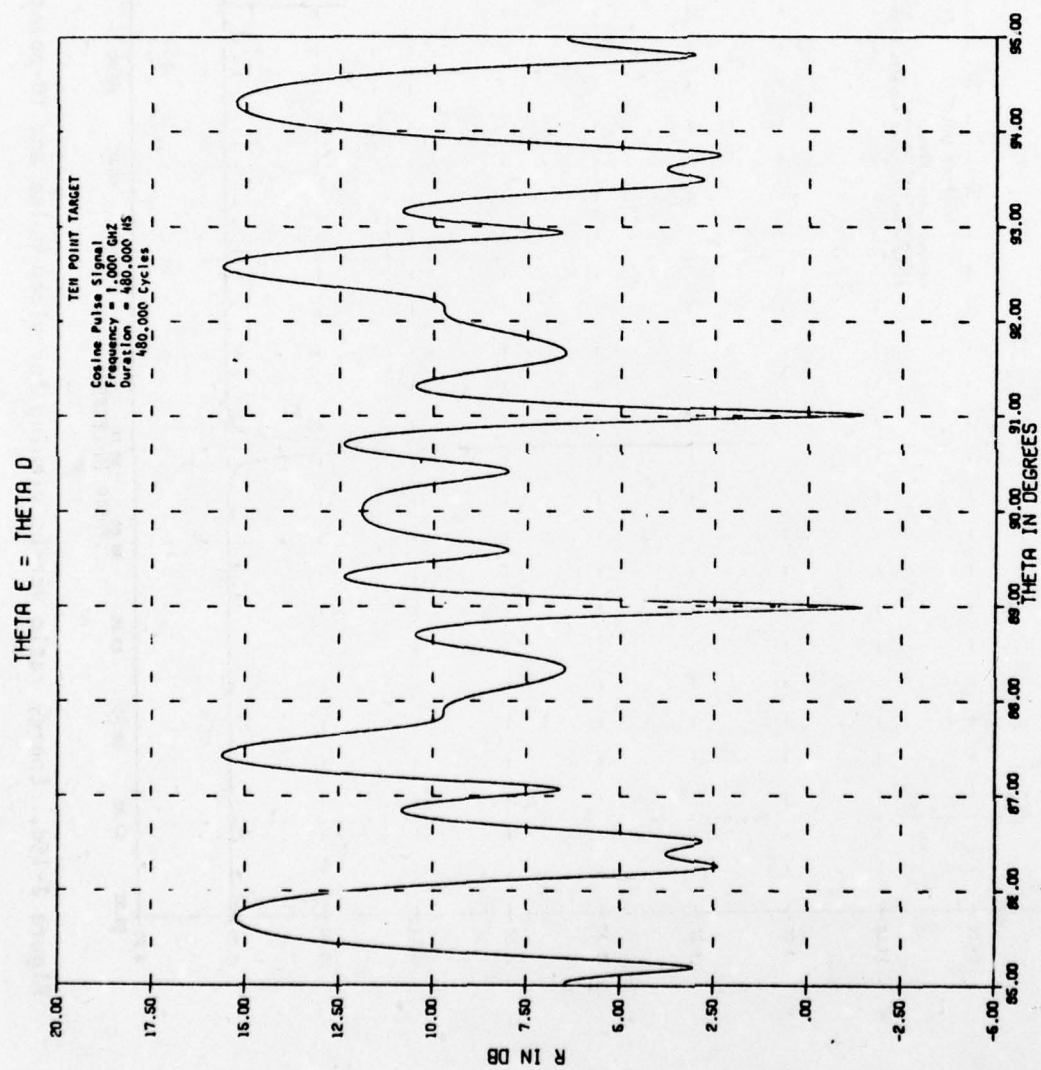


Figure 2-16. Energy ratio versus viewing angle for cosine pulse and 10-point target.

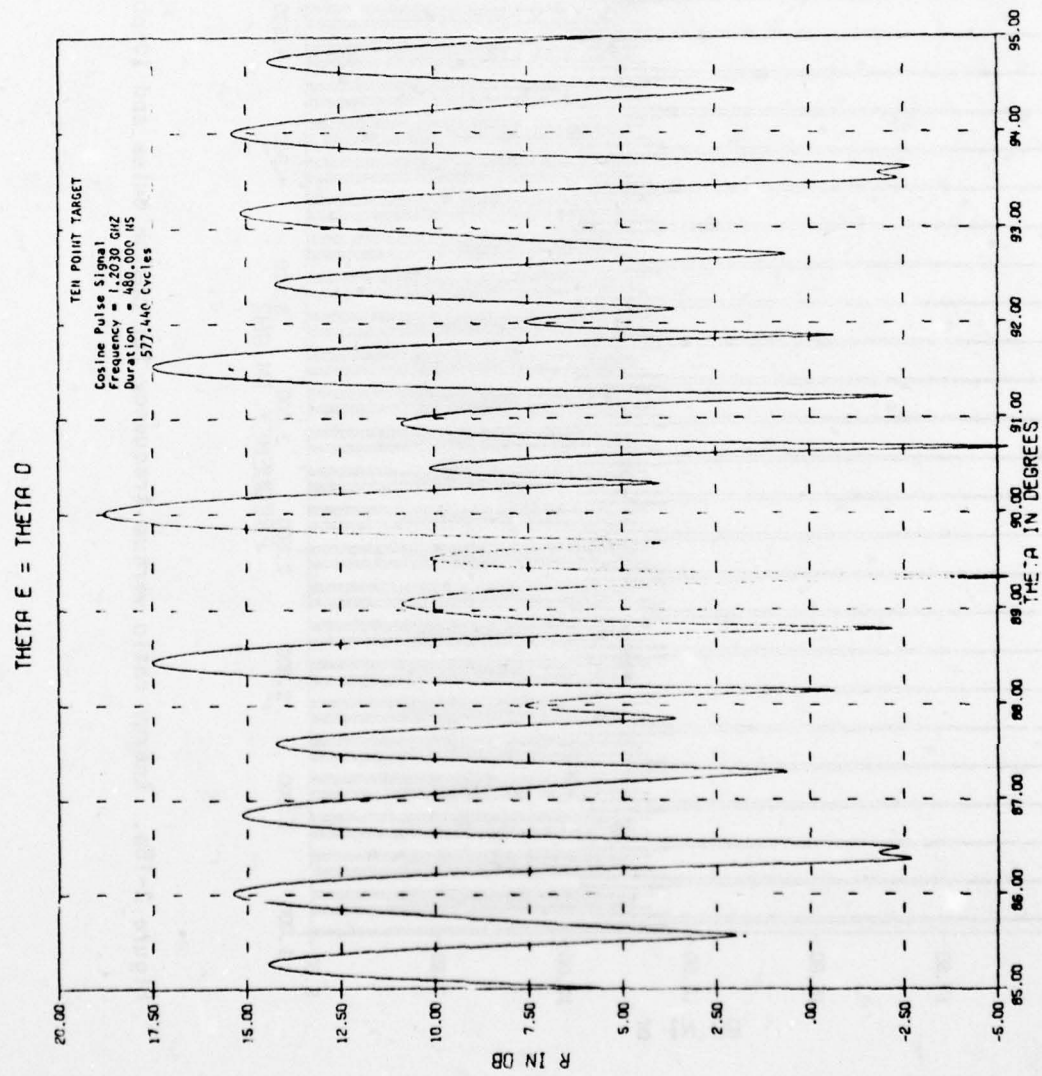


Figure 2-17. Energy ratio versus viewing angle for cosine pulse and 10-point target.

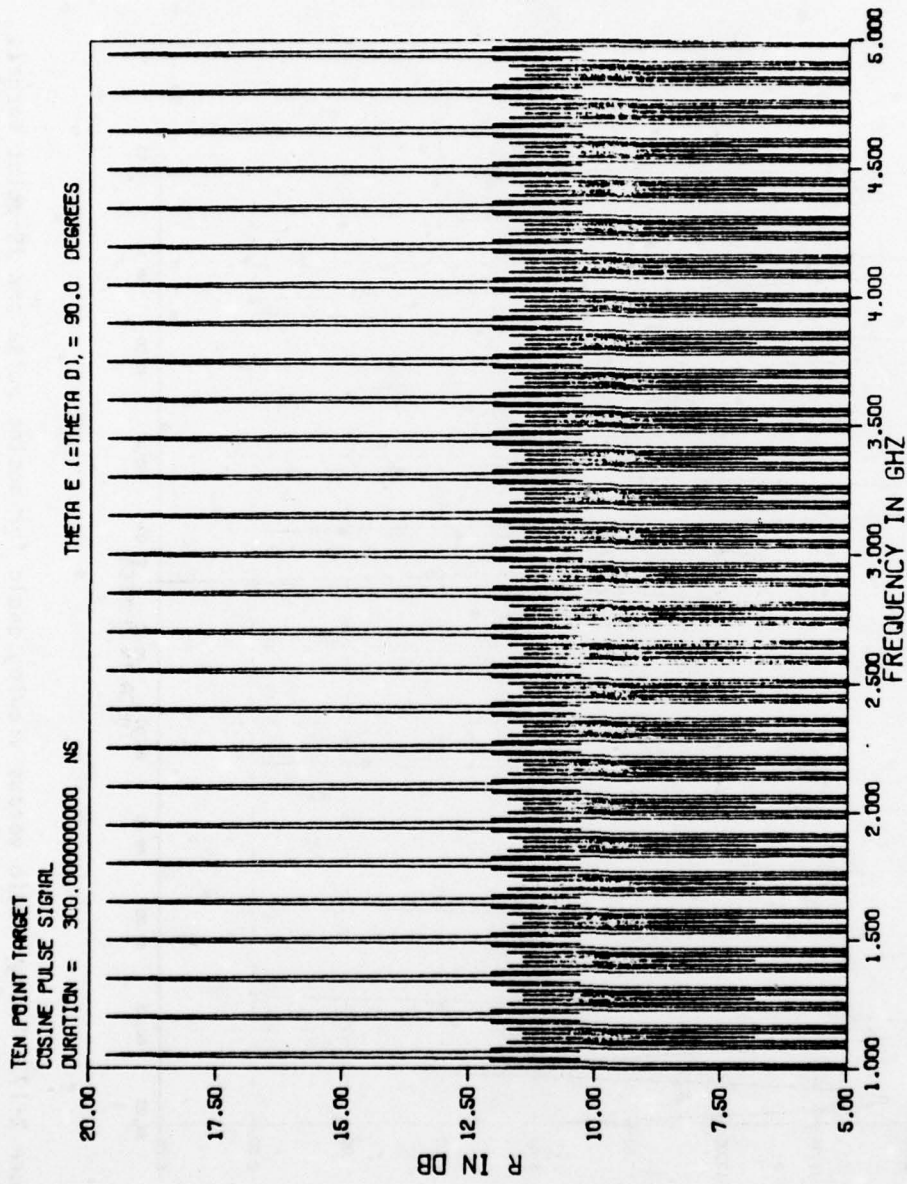


Figure 2-18a. Energy ratio versus frequency for cosine pulse and 10-point target.

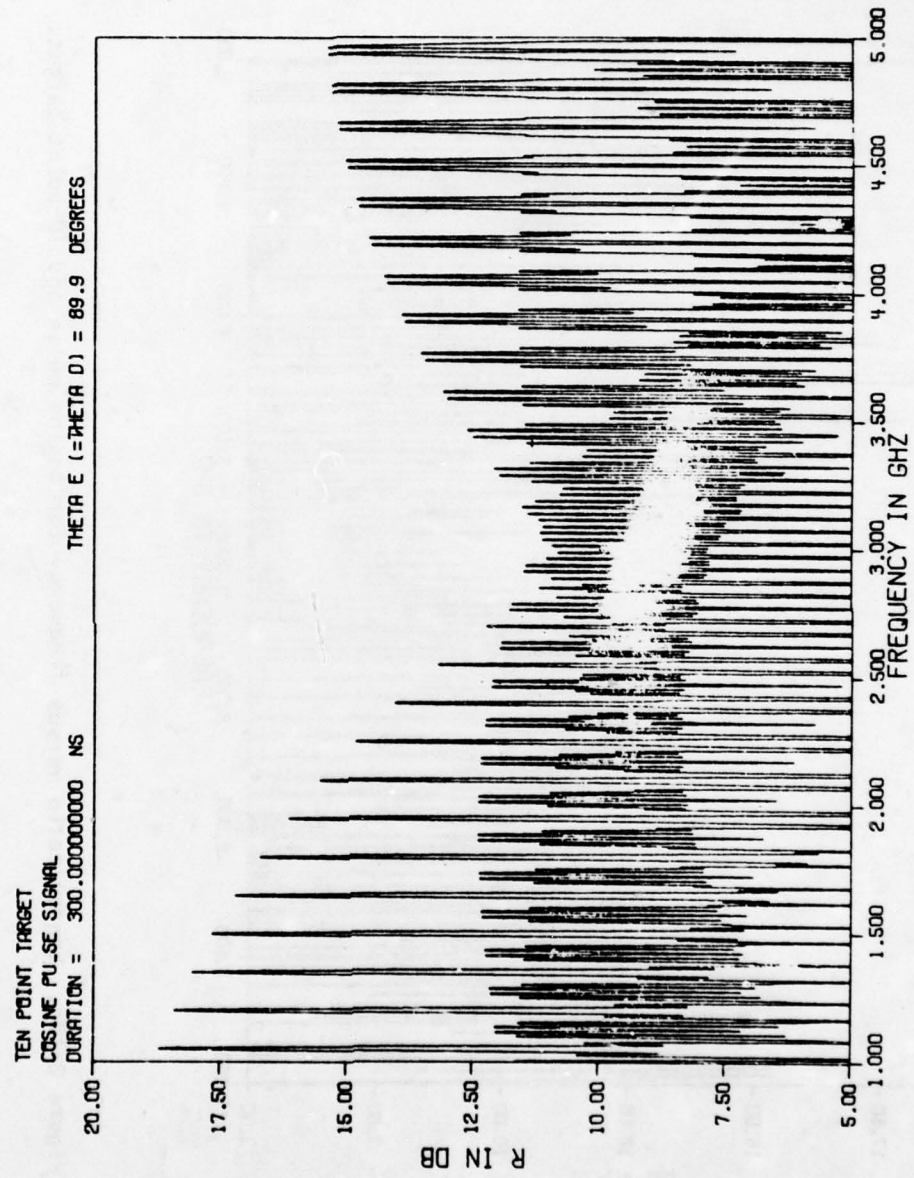


Figure 2-18b. Energy ratio versus frequency for cosine pulse and 10-point target.

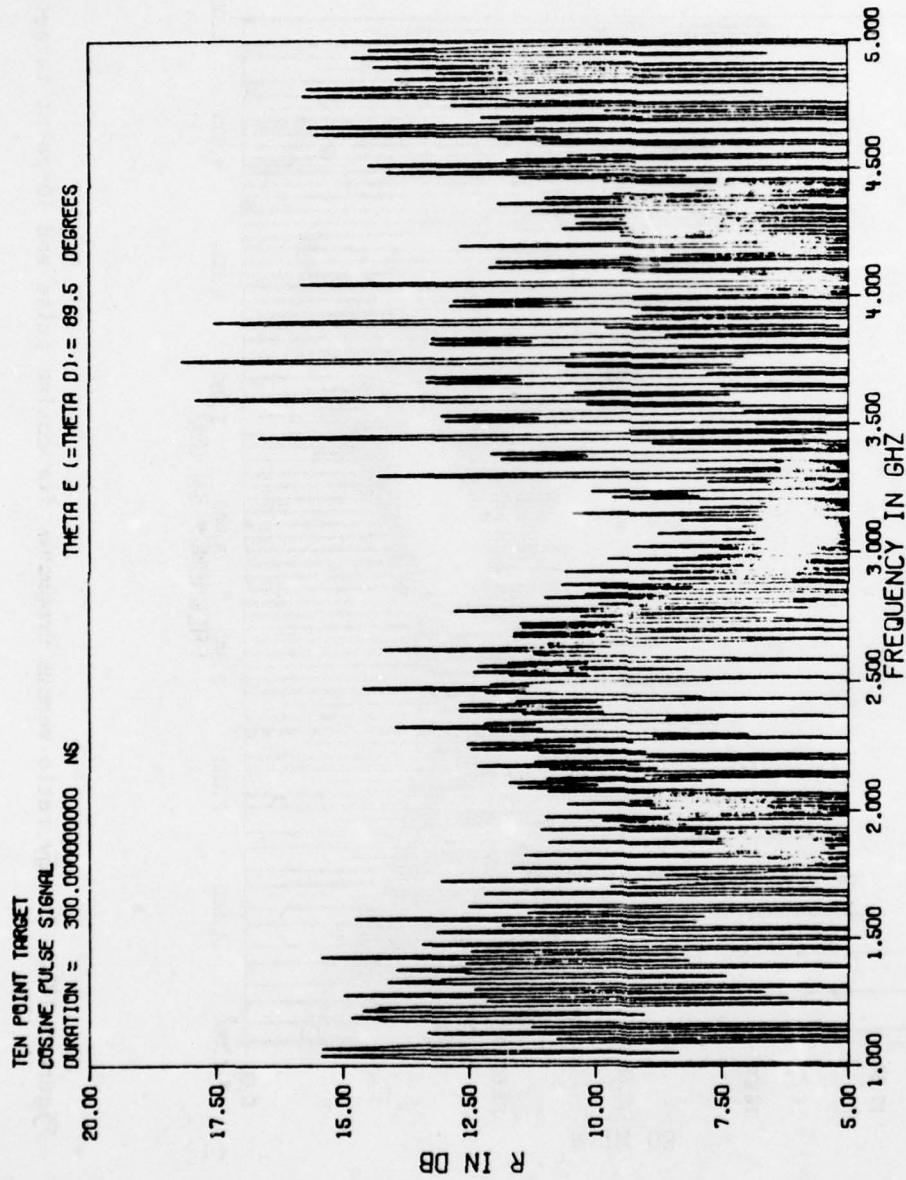


Figure 2-18c. Energy ratio versus frequency for cosine pulse and 10-point target.

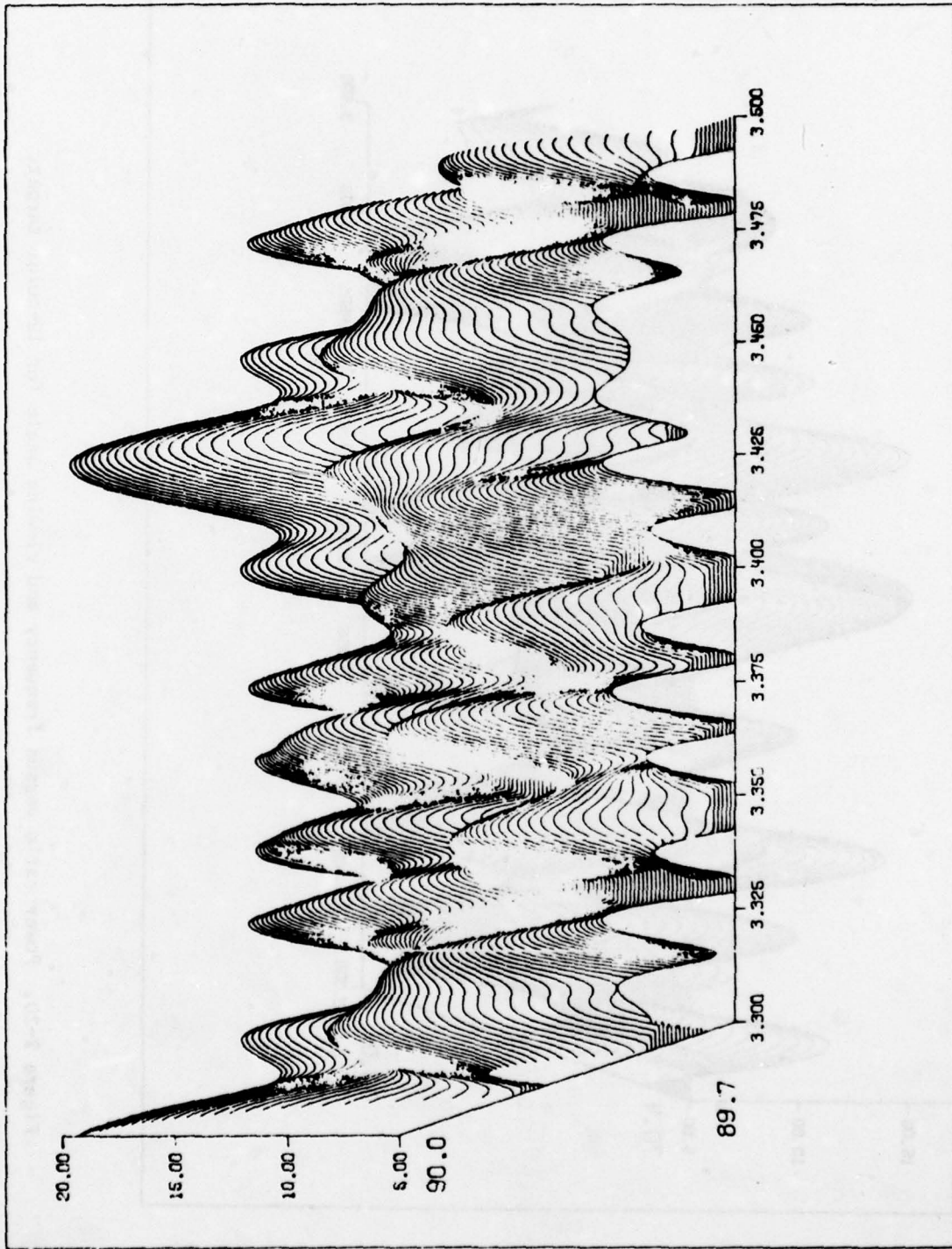


Figure 2-19. Power ratio versus frequency and viewing angle for 10-point target.

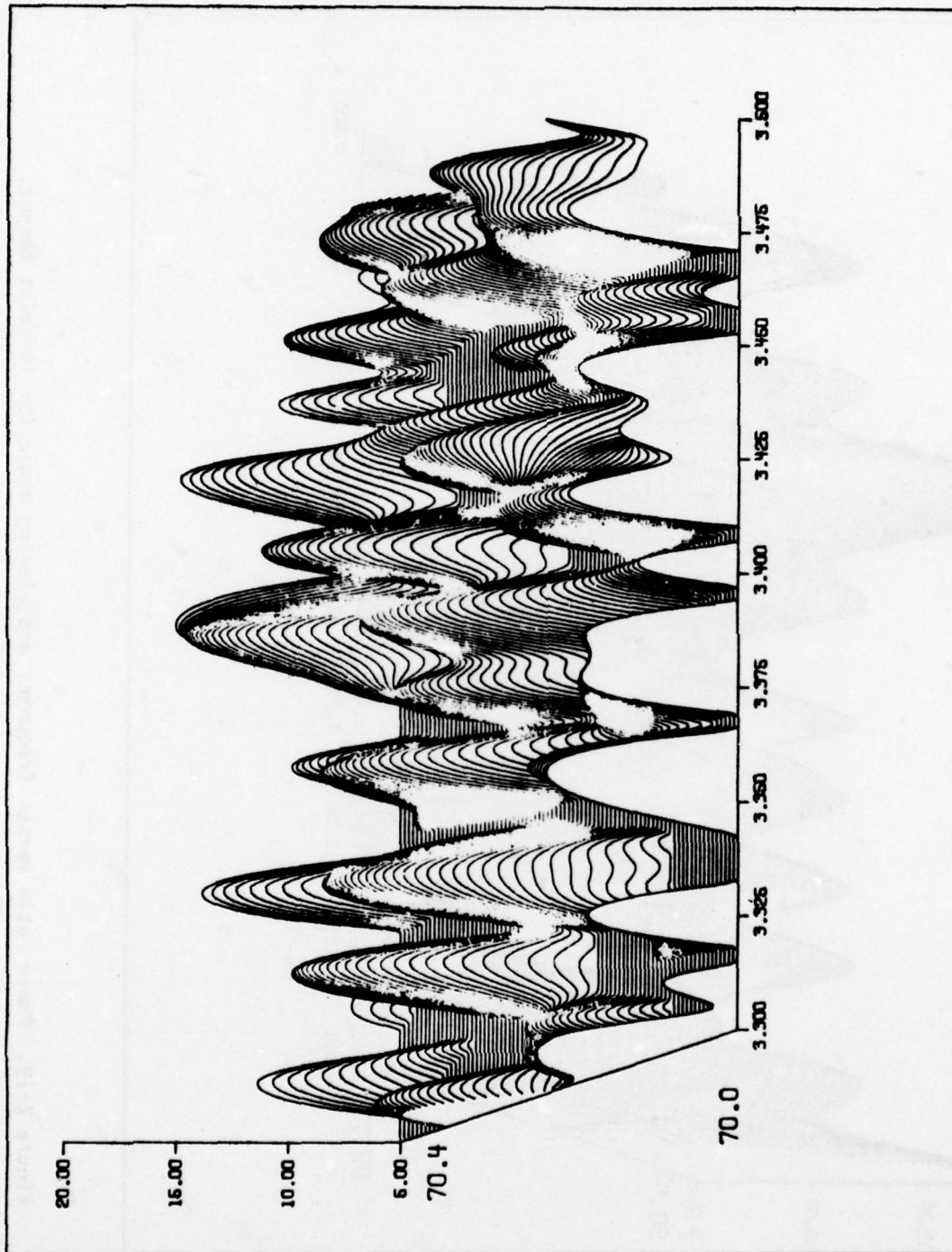


Figure 2-20. Power ratio versus frequency and viewing angle for 10-point target.

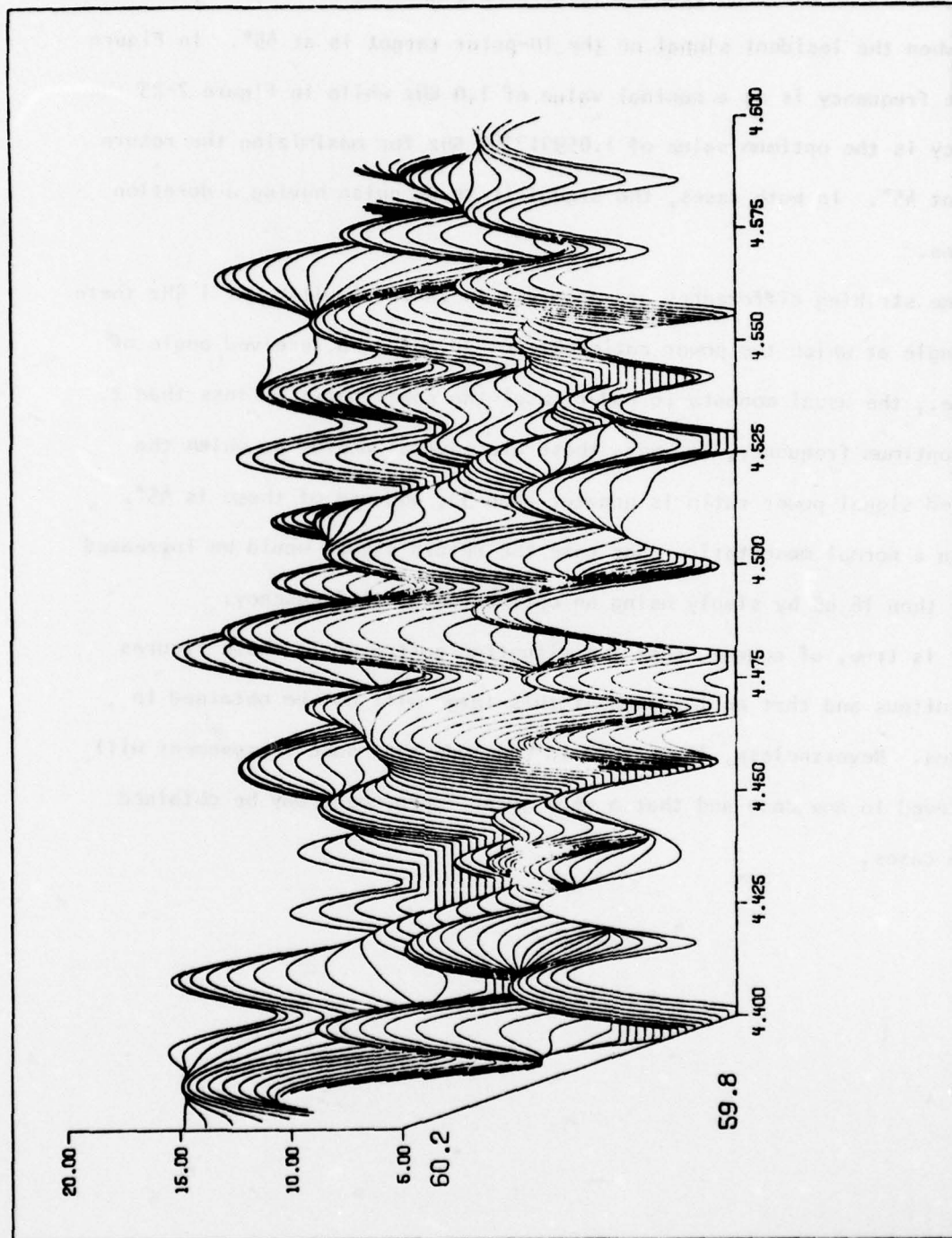


Figure 2-21. Power ratio versus frequency and viewing angle for 10-point target.

2.2.7. Comparison of Optimum and Non-Optimum Frequencies

Figures 2-22 and 2-23 show the scattered signal at all angles (in a 180° range) when the incident signal on the 10-point target is at 45° . In Figure 2-22 the frequency is at a nominal value of 1.0 GHz while in Figure 2-23 the frequency is the optimum value of 1.059917780 GHz for maximizing the return signal at 45° . In both cases, the signal is an RF pulse having a duration of 480 ns.

Some striking differences are apparent in these results. At 1 GHz there is no angle at which the power ratio exceeds 38 and at a received angle of 45° (i.e., the usual monostatic radar case) the power ratio is less than 2. At the optimum frequency, however, there are several angles at which the scattered signal power ratio is greater than 90, and one of these is 45° . Thus, in a normal monostatic radar case the return signal would be increased by more than 16 dB by simply using an optimum value of frequency.

It is true, of course, that the situation portrayed in these figures is fortuitous and that an improvement this large will not be obtained in all cases. Nevertheless, it is fair to conclude that some improvement will be achieved in any case and that a very great improvement may be obtained in some cases.

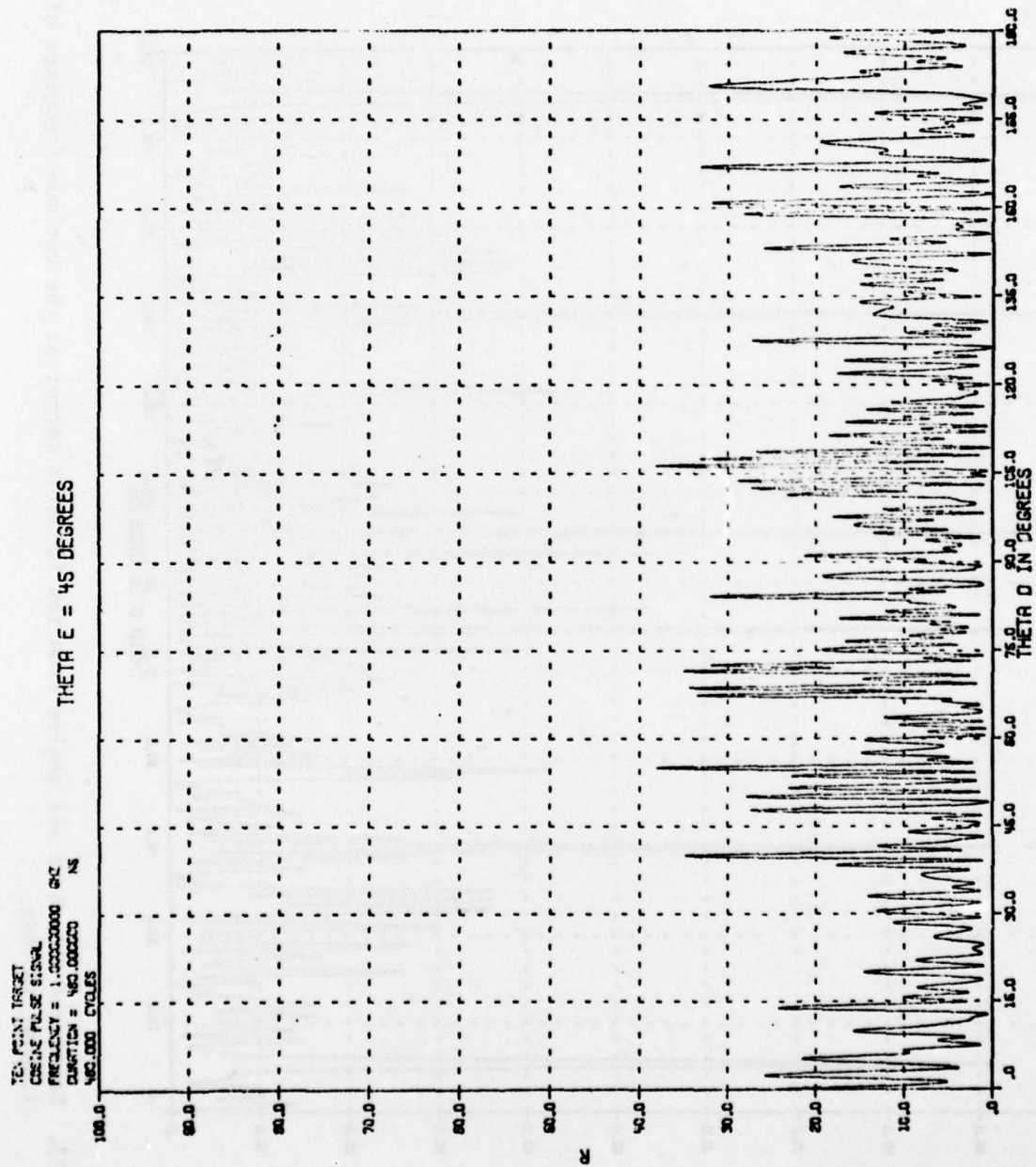


Figure 2-22. Scattered return at all angles from the 10-point target at 1 GHz.

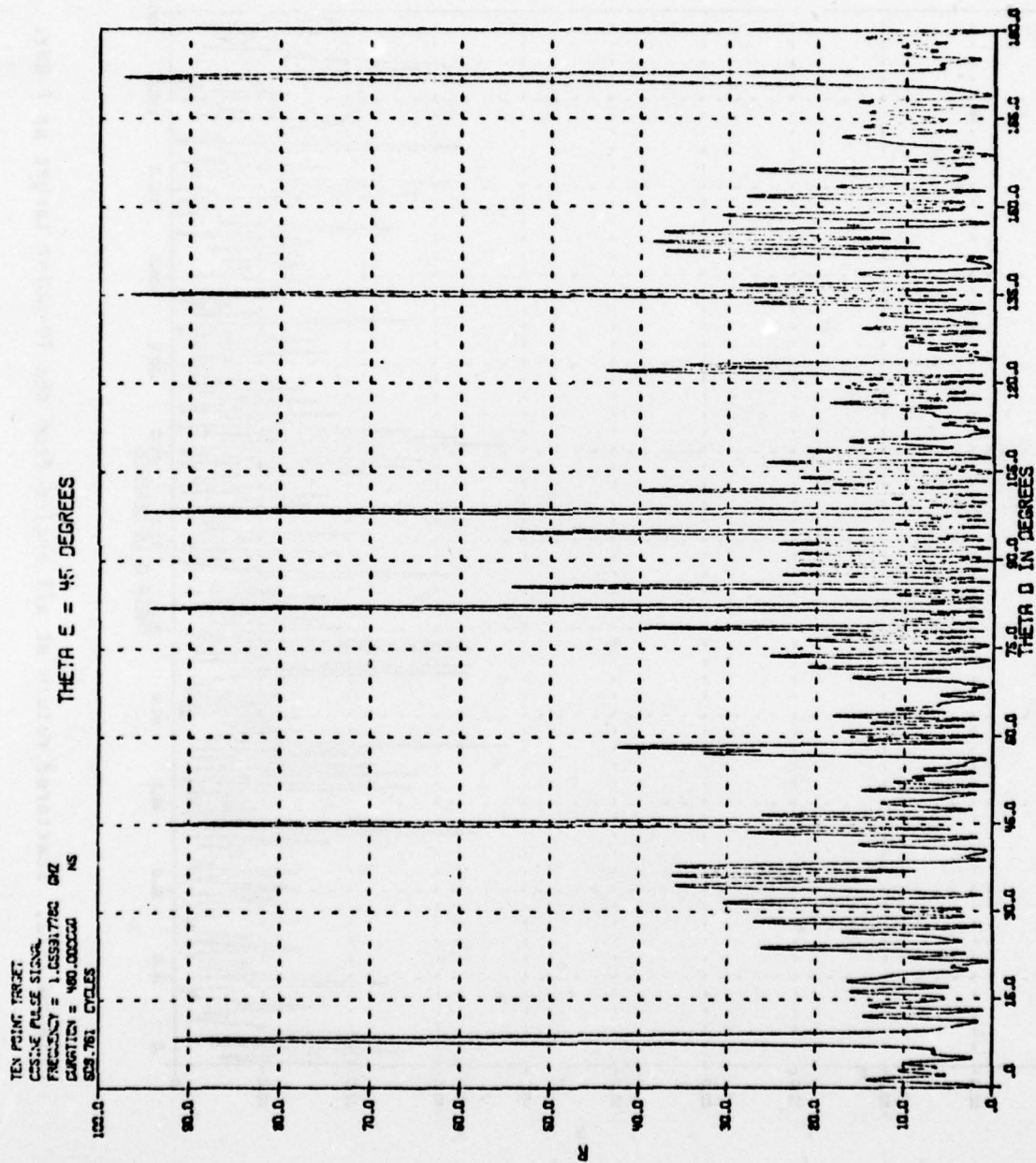


Figure 2-23. Scattered return at all angles from the 10-point target at the optimum frequency of 1.059917780 GHz.

3.1. CONCLUSIONS

The major conclusions may now be repeated and discussed in more detail and in a more quantitative manner.

Degree of Signal Enhancement. If a radar target has M predominant scatters with reflection coefficients of a_i , $i = 1, 2, \dots, M$, the maximum ratio of the reflected signal energy to the incident signal energy is

$$R_{\max} = \frac{M}{\left[\sum_{i=1}^M a_i \right]^2} \quad (2-70)$$

when coherent signal summation occurs. In the case of noncoherent signal summation, this ratio has an average value of

$$R_{\text{av}} = \sum_{i=1}^M a_i^2 \quad (2-71)$$

Thus, the factor by which the received signal energy may be increased is

$$F = \frac{R_{\max}}{R_{\text{av}}} = \frac{\frac{M}{\left[\sum_{i=1}^M a_i \right]^2}}{\sum_{i=1}^M a_i^2} \leq M \quad (2-72)$$

Optimum Signal Waveform. An explicit form for the optimum waveform for time-limited signals has not been found and it is conjectured that analytical solutions do not exist. A waveform that is optimum in some cases, and very nearly so in many cases, is the RF pulse with a rectangular envelope and a frequency that is one that is optimum for the steady-state sinusoid. Such a signal can be made more nearly optimum by making the pulse long compared to the duration of the target impulse response. More complex forms of signals, based on an orthonormal signal expansion, can also be found. These signals do not yield any significant improvement over RF pulses with a rectangular envelope operating at an optimum frequency. However, more research will be required to fully evaluate the performance of such waveforms -- particularly for short duration pulses.

Effect of Target Aspect Angle. The optimum frequency is a rapidly changing, and discontinuous, function of the angle of incidence. At some angles there may be no frequency within a reasonable range of frequencies at which near optimum results occur. Furthermore, as the frequency is increased in order to approach the theoretical maximum more clearly, the sensitivity of the response to aspect angle becomes even more severe.

3.2. RECOMMENDATIONS

The analytical results obtained in this study indicate that substantial enhancements of the radar cross-section occur for selected operating frequencies and/or target aspect angles. Although only simple target models were used in the analysis, the scattered signal was a very complex function of frequency, aspect angle and scatterer configuration, and a complete study could not be made in the available time. In order to more fully extend the understanding of the advantages of special signal design for scattering enhancement, it is recommended that the following additional work be carried out.

- 1) Continue the development of an optimum signal by way of the orthonormal expansion with the objective of more definitely proving or disproving the conjecture regarding the optimality of pulsed sinusoids.
- 2) Investigate more thoroughly the relationship between optimum frequencies and target aspect angle in order to evaluate the feasibility of adaptively determining the optimum frequencies from observed signals, or the feasibility of developing algorithms for making discontinuous changes in these frequencies as the need arises.
- 3) Determine the effects of doppler and target rotation on the relation of optimum frequencies to target aspect angle.
- 4) Investigate the use of wideband signals, or multiple frequency signals, as a means of identifying the optimum frequencies.
- 5) Investigate the use of multiple receivers, separated significantly in angle, and a single transmitter as a means of acquiring more information to optimize the signal.
- 6) Investigate the possibility of using the modulation induced on the received signal as a result of target motion to predict the optimum signal frequency.
- 7) Investigate the use of frequency modulated pulse trains to generate amplitude modulated return signals as a means of improving detectability and characterizing the target response function.